BIOCATALYSIS OF AROMATIC β-HYDROXY-α-AMINO ACIDS VIA REGIO- AND STEREOSELECTIVE AMINATION OF *TRANS*-3-ARYLGLYCIDATES USING A PHENYLALANINE AMINOMUTASE

By

Prakash Kumar Shee

A DISSERTATION

Submitted to
Michigan State University
in partial fulfillment of the requirements
for the degree of

Chemistry – Doctor of Philosophy

2020

ABSTRACT

BIOCATALYSIS OF AROMATIC β-HYDROXY-α-AMINO ACIDS VIA REGIO- AND STEREOSELECTIVE AMINATION OF *TRANS*-3-ARYLGLYCIDATES USING A PHENYLALANINE AMINOMUTASE

By

Prakash Kumar Shee

Biocatalytic process-development continues to advance toward discovering alternative transformation reactions to synthesize medicinally important molecules such as, β-hydroxy-α-amino acids. These bifunctional building blocks, a subclass of noncanonical amino acids, have two stereocenters and are valuable in the natural product, pharmaceutical, and agrochemical sectors.

Here, a 5-methylidene-3,5-dihydro-4*H*-imidazol-4-one (MIO)-dependent phenylalanine aminomutase from *Taxus canadensis* (*Tc*PAM) was repurposed to irreversibly biocatalyze an intermolecular amino group transfer regioselectively from (2*S*)-styryl-α-alanine to ring-substituted racemic *trans*-3-arylglycidates (i.e., cinnamate epoxides) to make the corresponding arylserines. The reaction scope of MIO-aminomutases, which primarily catalyze the reversible interconversion of α- and β-amino acids, can also catalyze the hydroamination of arylacrylates to form α- and β-amino acids. Here, we explore glycidates as a new class of substrates for the MIO-aminomutase family of enzymes. Racemic *trans*-3-arylglycidates were regio- and stereoselectively aminated to produce a mixture of *anti*-arylserine enantiomers predominantly. 3-Arylglycidates usually prefer nucleophilic attack at the benzylic C_β due to stabilization of the partial cationic properties (δ^+) at the C_β by the aryl ring, a stabilization that does not occur at C_α. *Tc*PAM catalysis, however, inverted this inherent nucleophilic regioselectivity by aminating at the C_α of *trans*-3-arylglycidates to make arylserine predominantly (97%) over aryl*iso*serine (3%). From among twelve substrates, the aminomutase ring-opened 3'-Cl-phenylglycidate to 3'-Cl-phenylserine 140 times faster than it opened the 4'-Cl-isomer, which was turned over slowest among all epoxides tested. GC/MS

analysis of chiral auxiliary derivatives of the biocatalyzed arylserine analogues showed that each product mixture contained (2*S*)+(2*R*)-*anti* and (2*S*)+(2*R*)-*syn* pairs with the *anti*-isomers predominating (~90:10 dr). Integrating the vicinal proton signals in the ^{1}H-NMR spectrum of the biocatalyzed arylserines and calculating the chemical shift difference (Δδ) between the *anti* and *syn* proton signals confirmed the diastereomeric ratios and relative stereochemistries. Application of a (2*S*)-threonine aldolase from *E. coli* further established the absolute stereochemistry of the chiral derivatives of the diastereomeric biocatalyzed products. The 2*R*:2*S* ratio for the biocatalyzed *anti*-isomers was highest (88:12) for 3'-NO_2-phenylserine and lowest (66:34) for 4'-F-phenylserine. This showed that the stereospecificity of *Tc*PAM is, in part, directed by the substituent-type on the arylglycidate analogue.

We also synthesized enantiopure 3-phenylglycidates and incubated them separately with *Tc*PAM. The absolute configurations of the biocatalyzed *anti*-phenylserine (major) and phenyl*iso*serine (minor) were evaluated to gain insights on the substrate specificity and selectivity of *Tc*PAM for aminating 3-phenylglycidate enantiomers. *Tc*PAM converted (2*S*,3*R*)-3-phenylglycidate to (2*S*)-*anti*-phenylserine predominantly (89%) and (2*R*,3*S*)-3-phenylglycidate to (2*R*)-*anti*-phenylserine (88%) over their antipodes with inversion of configuration at C_α in each case. Both glycidate enantiomers formed a small amount (~10%) of the *syn*-phenylserine with retention of configuration at the C_α. *Tc*PAM had a slight preference toward (2*S*,3*R*)-3-phenylglycidate, which was turned over (k_{cat} = 0.3 min^{-1}) 1.5 times faster than the (2*R*,3*S*)-glycidate (k_{cat} = 0.2 min^{-1}). The kinetics data showed that the amination of arylglycidate process follows a two-substrate ping-pong mechanism with competitive inhibition by the epoxide substrate at higher concentration.

I dedicate this dissertation to my parents for their countless sacrifices to fulfill my dream, my brother for taking all the blows up front and paving me a smoother road, and my sister for supporting me always. You all made it possible for me to become who I am today.

ACKNOWLEDGMENTS

Behind every doctorate, and every doctoral student, are people who played a vital role in guiding, inspiring, and supporting its recipient. While I cannot hope to thank everyone who contributed as professors, peers, or friends, I would, here, like to acknowledge those who have had among the most profound impacts upon my research and this dissertation.

I would first like to thank my advisor, Dr. Kevin D. Walker, for the extensive training, guidance, and support he provided throughout my stay at Michigan State University. Dr. Walker's encouragement and motivation, which extended far beyond the laboratory, helped me to grow as an independent researcher. This dissertation and its associated publications would not have been possible without Dr. Walker's support and insight. I am and will remain grateful for the integral, irreplaceable role Dr. Walker played in my academic development.

I am similarly thankful to the members of the graduate advisory committee: Prof. Xuefei Huang (second reader), Prof. James H. Geiger, Prof. John W. Frost, and Prof. Gary J. Blanchard. Prof. Huang mentored me throughout graduate school. I really appreciate his invaluable support during the final phase of my dissertation. Prof. Geiger, too, provided me with consistently engaging intellectual discussion and feedback, providing much-needed perspective on the structure and mechanism of our protein molecule. I am similarly indebted to Prof. Frost, whose inputs and guidance on the characterization of the enantiopure glycidols is greatly appreciated. I must also thank Prof. Blanchard, who offered me a doctoral position at Michigan State University. Prof. Blanchard has remained a stalwart ally in the many years since, and also wrote a number of recommendation letters that helped me obtain much-needed scholarships and funding.

Furthermore, I would like to extend my sincere appreciation both to Prof. A. Daniel Jones and his entire team at Mass Spectrometry and Metabolomics Core. Prof. Jones taught me all of the minute details and fine parameters of using complex mass spectrometry instruments. Prof. Jones was always available for discussions, and helped me troubleshoot a great many of the problems I experienced with LCMS or GCMS in my graduate life. The expertise I gained in his laboratory played a pivotal role in my pursuit of a career. I would like to thank Lijun Chen, Dr. Tony Schilmiller, and Dr. Casey Johnny for all the extensive training and enormous support during the frequent usage of the Mass Spectrometry.

At the MTR-NMR Facility, Dr. Daniel Holmes helped me develop a novel method to establish the relative stereoconfiguration of arylserine diastereomers. Dr. Holmes's assistance was crucial to the development of my dissertation. I cannot possibly overstate my thanks to Dr. Holmes for the multitude of suggestions and the guidance he offered in designing many key experiments.

I would like to recognize and thank Prof. Honggao Yan (BMB, MSU), whose collaboration helped deduce a kinetic equation for a two substrate ping-pong mechanism. This work provided substantial insight into my research. Prof. Yan's contribution added significant value to my work.

I would like to extent my sincere appreciation to Prof. Babak Borhan, who graciously shared his laboratory space and all the resources it encompasses. On countless occasions, I have set up moisture and temperature sensitive epoxidation reactions in the Borhan laboratory, and synthesized compounds of interest.

Prof. Robert E. Maleczka (Chair) was unerringly supportive. Near the end of my studies, he was actively involved in advocating for a safe return to research during the 2020 coronavirus outbreak. Without Prof. Maleczka's advocacy, it is likely I would have never been able to finish my research timely.

I would also, yet again, like to thank my mentors and peers in the Walker Laboratory. They are all, without exceptional, extremely resourceful professionals who made my doctoral candidacy a success. To Dr. Nishanka Dilini Ratnayake and Dr. Edith N. Onyeozili: I would like both of you to know that you are nothing short of amazing, and I am vastly grateful for your introduction to this research project. Furthermore, both of you made vital contributions to the initial stages of the project which undoubtedly laid the foundations for my dissertation. Dr. Ruth Njeri Muchiri: you treated me like an younger brother, and I am thankful for your mentorship and guidance. You were approachable and informative, and I truly enjoyed learning from and alongside you. Much of my time in the Walker Laboratory was spent with Dr. Tyler Walter, with whom I made many memories. I enjoyed my time at Michigan State with you, Dr. Walter, and must also thank you for the cultural education you imparted. It was, like so many other things you have done, par excellence. I wish you the best in all of your future endeavors. I would also like to thank Jean-Bosco Shingiro, Gayanthi Attanayake, and Aimen Al-Hilfi for making my last years at Michigan State even more memorable. You all made and fostered an accepting, friendly work environment. I hope for success for all of you in your continued research.

Many thanks to all of the fantastic undergraduates who worked with me at the Walker Laboratory. Of special note: Olivia, Brendyn, Lawrence, Shahrazad, Jeshua, Ciara, and Arianna. Not only were you all great partners in the laboratory, but you provided phenomenal technical support, too. Olivia: your contribution with the aldolase enzyme was highly significant to the shape and form of my dissertation. Thank you!

Alongside the Walker Laboratory, I vastly appreciate the current and past members of the Wulff, Borhan, Maleczka, Jackson, Weliky, Geiger and Smith groups for sharing their resources. I was always welcomed in your laboratories; your courtesy meant much, both in the provision of

resources and in the construction of my professional identity. Of the members of these groups, I would like to individually thank Wei, Xiaopeng, Yubai, Ruwanthi, Tayeb, Pengchao, Hadi Gholami, Ali Akbar, Debarshi, Soham, Ankush, James, Saeedeh, Dan, Arzoo, Badru-Dean, and Hadi Nayebi. I will, most certainly, miss sharing ideas with each of you, as well as your camaraderie.

At the institutional level, I remain indebted to the Department of Chemistry, the Department of Biochemistry and Molecular Biology, the Michigan State University College of Natural Sciences, and the Graduate School for providing me with assistantships and fellowships, all necessary for the continuation of my research and graduate life at Michigan State and in the United States.

To those of you overseas: I, too, remain as indebted to you as anyone else. My professors at the Indian Institute of Technology Bombay, and before that at Jadavpur University, sparked and fanned my passions for sciences. They brought me to Chemistry, and they helped fulfil my ambition of finding a high-quality doctoral program. I must particularly offer my never-ending thanks to Prof. Sambasivarao Kotha, who patiently guided me throughout my M.Sc. research project. Prof. Swadesh R. Roy Chowdhury, and Prof. Sanjay Bhar at Jadavpur University, believed in me from the beginnings of my higher education. They were moral bulwarks and educational champions, who lent me the very essential support I needed as an underprivileged student.

And, to my friends: you made my eight-year-long stay at Michigan State and in East Lansing a pleasure. Perhaps more importantly, you helped keep me sane! I, like most every other graduate student, had my hard times. You all made it possible to retain some energy, and to power through with a happy, still-intact soul. I love each of you with all my heart, and I accord special thanks to Dr. Dhritabrata Mandal, Dr. Saurja Dasgupta, Dr. Kalyan Santra, Dr. Krishnaja Duvvuri, Dr. Ananya Rakshit, Dr. Sanhita Sinharay, Dr. Tamal K. Ghosh, Dr. Anup Adhikari, Dr. Raza Haque,

Dr. Zakia Alavi, Dr. Ali Haque, Beena Haque, Dr. Abhishek Dutta Chuwdhury, Dr. Tarang Chugh, Yashesh Dhebar, George Kapali, Ryan Farrick, and (Dr.) Supriya Ghosh, for their constant love and support, intellectual input, and suggestions in writing this dissertation.

No amount of appreciation is enough for all the beautiful people who supported me selflessly during my undergraduate studies, when higher education seemed a scarcely-affordable dream. My sincere thanks and gratitude go to Mrs. Ajanta Sadhu (didi), Mr. Arindam Sadhu, Mr. Abhijit Sengupta (kaku), the Srijan Sujan family, and the late Mr. Gautam Sen. You all stood by me and believed in me when I desperately needed your love and support. You made me part of your families, and I could never have asked for me. I will always love each and every one of you, no matter the oceans now between us.

In my youth, too, I was also exceptionally fortunate to have a friend, a philosophic mentor, and a guide in Dr. Souvagya Biswas (Vagyo Da). He inspired me from my time at Jadavpur, and has motivated me ever since. He mentored me, and he treated me like a younger brother. Vagyo Da prepared me for every hurdle I could have faced as a young student, from the IIT entrance exam to the infamous GRE. Whatever I needed, he was able to help, from applications to universities abroad, to my first flight, graduate frustrations, job hunt, and thesis defense. You have long been my mentor, as well as a brother and there is nothing more I could ask of you that you did not offer. I will, most certainly, miss staying within an easy drive of your home.

Lastly, but never least, there is not a single chance I could have gotten to where I am now without the unconditional, unwavering support of my family. I owe every shred of my success to you. Maa and Baba: you raised me right, even though it meant making what must have been millions of sacrifices. Maa, you gave me my passion, the ability to dream beyond where I was. You showed me the power of education, and its rare ability to uplift the impoverished. And Baba,

while your love language was always silent, I never once questioned its presence. You worked, relentlessly and tirelessly, to raise three children, give them food, and the best education we could afford. You were generous with your family, and with all around you; I know, even at work, you never stopped thinking of ways to our obstacles. Even now, writing this, I still cannot imagine what strength it must have taken for you to do all that you did; you are my true hero, and my enduring inspiration. Maa and Baba, I cannot give enough words to appreciate your sacrifices, for myself, for my brother, and for my sister.

And it was my older brother, my Dada, who made our family's first foray into the sciences. You are the one who first lit my interest, and you are the reason I chose to pursue chemistry. I may have followed in your footsteps blindly for a time, but your wisdom and direction have given meaning to my professional life. I am forever grateful that you chose to take responsibility for my young life, to share your success, to help me grow in comfortable shade as you stood against and endured the worst of weather.

My sister, Mon, you supported me through my worst days when I was depressed and directionless. You never, not once, failed to brighten my day, to give me new resolve. Thank you for putting up with me and being my strongest supporter. I love you with all my heart.

Lastly, Boudi, my sister-in-law and Ryka, I am sorry that I lost so much time with our family while chasing my dream. Thank you for never making me question my path, for always making me smile whenever we talked. I hope, now that I am passing one stage of life for another, that I can make up for the years I have been gone.

All of you, my family: I would be nothing without your love, your protection, and guidance. I will love you always, no matter where I may be, no matter our separation, no matter this distance of necessity. Thank you.

TABLE OF CONTENTS

LIST OF TABLES xiv

LIST OF FIGURES xv

LIST OF SCHEMES xxvi

KEY TO ABBREVIATIONS xxvii

Chapter 1: Overview of Biocatalysis in Organic Chemistry and Pharmaceutical Industry 1
REFERENCES 13

Chapter 2: Biocatalysis of Arylserines and Arylisoserines using Phenylalanine Aminomutase from *Taxus canadensis* (*Tc*PAM) and 3-Arylglycidate Racemates. 20
2.1 Introduction 20
2.1.1 Aminomutases: Enzyme Class (EC) of 1,2-Amino Acid Isomerases 20
2.1.2 Mechanistic Diversity of Aminomutases 21
2.1.3 MIO-dependent Aminomutases 21
2.1.4 Overview of Aryl Amino Acid Aminomutases 23
2.1.5 MIO Function 24
2.1.6 Intramolecular and Intermolecular Mechanisms of MIO-Aminomutases 27
2.1.7 Arylserines and Arylisoserines 30
2.2 Experimental 36
2.2.1 Chemicals and Reagents 36
2.2.2 Instrumentation 37
2.2.3 General Procedure for the Syntheses of *trans*-3-Arylglycidate Analogues 37
2.2.4 Stereochemical Analysis of *trans*-3-Arylglycidates using GC/EI-MS. 41
2.2.5 Stability of Racemic Arylglycidates in Assay Buffer 42
2.2.6 Expression and Purification of *Tc*PAM. 43
2.2.7 Expression and Purification of (2*S*)-Threonine Aldolase (*ltaE*). 44
2.2.8 Control Assay Experiments: Activity of *Tc*PAM toward Arylglycidates 45
2.2.9 Biocatalysis of Arylserine and Arylisoserine with *Tc*PAM. 45
2.2.10 Measurement of Kinetic Parameters. 45
2.2.11 General Procedure for the Syntheses of Arylserines. 46
2.2.12 Establishing Relative Stereoconfiguration (*syn*/*anti*) of Arylserine Diastereomers using ^{1}H NMR Spectroscopy. 48
2.2.13 General Method for Derivatizing Arylserines with a Chiral Auxiliary. 48
2.2.14 (2*S*)-Threonine Aldolase catalyzed resolution of Arylserine Diastereomers 50
2.2.15 Computational Methods for Biomolecular Docking. 50
2.2.16 Calculation of Covalent van der Waals Volumes. 51
2.3 Results and Discussion 52
2.3.1 Synthesis and Characterization of the Racemic 3-Arylglycidate Substrates. 52
2.3.2 Separation of *trans*-3-Arylglycidate Enantiomers using a Chiral- GC/EI-MS 53
2.3.3 Hydrolysis of Arylglycidates in Assay Buffer 54

2.3.4 Control-Assay Experiments 56
2.3.5 Biocatalysis of Arylserines and Arylisoserines. 58
2.3.6 Synthesis of Arylserine Diastereomers. 60
2.3.7 Assessing the Regiochemistry of the *Tc*PAM-catalyzed Transamination Reaction. 61
2.3.8 Establishing Relative Stereoconfiguration of Arylserines by ^{1}H NMR Analysis. 63
2.3.9 Relative Stereochemistry of the *Tc*PAM Reaction by Chiral Auxiliary Derivatization. 66
2.3.10 Absolute Stereochemistry of the *Tc*PAM Reaction by Aldolase Resolution. 67
2.3.11 Epoxide Substrate Docking Model of *Tc*PAM. 69
2.3.12 Kinetics of Arylserine Biocatalysis. 73
2.3.13 Kinetics of Aryl*iso*serine Biocatalysis. 75
2.4 Conclusion 77
APPENDIX 80
REFERENCES 127

Chapter 3: Insight into the Mechanism of Regio- and Stereoselective Amination of Enantiopure 3-Phenylglycidate Isomers to Phenylserine by *Tc*PAM. 141
3.1 Introduction 141
3.2 Experimental 144
3.2.1 Chemicals and Reagents 144
3.2.2 Synthesis of (2*R*,3*R*)-3-Phenylglycidol (21a)[35] 144
3.2.3 Synthesis of (2*S*,3*S*)-3-Phenylglycidol (21b). 145
3.2.4 General Procedure to Characterize the Enantiomeric Excess of Glycidols (21a and 21b) 146
3.2.5 Synthesis of Potassium (2*S*,3*R*)-3-Phenylglycidate (14aa) from 21a. 146
3.2.6 Synthesis of Potassium (2*R*,3*S*)-3-Phenylglycidate (14ab) from 21b. 147
3.2.7 Enantiopurity of the Synthesized 3-Phenylglycidates. 147
3.2.8 Production of Phenylserine by *Tc*PAM Biocatalysis. 148
3.2.9 General Method for Chiral Auxiliary Derivatization of Phenylserines and Phenylisoserines. 148
3.2.10 Kinetic Analysis. 150
3.3 Results and Discussion 151
3.3.1 Synthesis of and Characterization of Enantioenriched 3-Phenylglycidate Substrates (14aa and 14ab). 151
3.3.2 Enantiopurity of the Synthesized 3-Phenylglycidate isomers (14aa and 14ab). 152
3.3.3 Glycidate Ring-Opening by *Tc*PAM Catalysis and Analysis of its Stereoselectivity. 153
3.3.4 Probing the Formation of the *Anti*- and *Syn*-Phenylserines using Computational Docking. 160
3.3.5 Proposed Mechanism and Derivation of the Kinetic Equation. 163
3.3.6 Kinetic Analyses. 167
3.4 Conclusion 171
3.5 Future Studies. 172
APPENDIX 176
REFERENCES 188

LIST OF TABLES

Table 1.1. Various Enzymatic Processes Involving Epoxides in Microorganisms..... 9

Table 2.1. Stereochemistry of β-Arylalanine Products Catalyzed by MIO-Dependent Aminomutases and Their Corresponding Biosynthetic Products. 26

Table 2.2. GC Oven Heating Parameters. 42

Table 2.3. Synthesis of 3-Arylglycidate Analogues[a] and Isolated Yields. 52

Table 2.4. Control Experiments. 56

Table 2.5. 500 MHz ^{1}H NMR data for the synthetic and biocatalyzed arylserine analogues (**15a**–**15l**) recorded in D_2O at pH 1.5. 64

Table 2.6. 500 MHz ^{1}H NMR data for the chemically synthesized arylserine analogues (**15a**–**15l**) recorded in D_2O at a pH range of 0-4.0. 65

Table 2.7. Kinetics of *Tc*PAM for Turnover of Arylglycidates (**14a**–**14l)** to Arylserines (**15a**–**15l**) and Arylisoserines (**16a–16l**). 74

Table 3.1. Kinetics of *Tc*PAM for turnover of 3-phenylglycidate enantiomers to phenylserine[a]. 171

LIST OF FIGURES

Figure. 1.1. Comparison of chemocatalytic and biocatalytic processes to sitagliptin. (A) Chemocatalytic synthesis of sitagliptin involves enamine (**2**) formation, followed by rhodium-catalyzed asymmetric hydrogenation at high pressure. (B) The biocatalytic route involves direct amination of prositagliptin ketone (**1**), followed by phosphate salt formation to yield enantiopure sitagliptin phosphate (Januvia™) (**4**). 5

Figure. 1.2. Different enzymatic routes toward the synthesis of the key side chain of Atorvastatin (**8**) (Lipitor®). These routes show a combination of KRED with a halohydrin dehalogenase (HHDH) (*Route I*, developed by Codexis), a nitrilase (*Route II*),[37] or an aldolase (*Route III*).[38] ... 7

Figure. 1.3. Pathway to acetoacetate from 1-propene in *Xanthobacter sp.* 11

Figure. 1.4. Partial biosynthesis of Taxol from (2*S*)-α-phenylalanine in *Taxus* plants. 12

Figure. 1.5. Biocatalysis of arylserine and arylisoserine analogues from *trans*-3-arylglycidates and (2*S*)-styryl-α-alanine (**12**) by using an MIO-aminomutase. The asterisks (*) identify a chiral center. 12

Figure. 2.1. 1,2-Amino group isomerization catalyzed by aminomutases. 20

Figure. 2.2. A) The mechanism of how the MIO forms from a conserved triad of active site residues. B) Reactions of the MIO moiety with nucleophiles from $NaBH_4$ or KCN resulted in the loss of aminomutase activity due to MIO- inactivation. 23

Figure. 2.3. The mechanism of MIO-aminomutase catalyzed reaction via an amino-alkylation intermediate to make a β-amino acid. *Route a*: the (3*S*)-β-arylalanine isomer is made via a pathway where the acrylate intermediate does not rotate before being re-aminated at the C_β. *Route b*: the (3*R*)-isomer via a pathway where the arylacrylate intermediate rotates inside the active site before being re-aminated at the C_β. 24

Figure. 2.4. Transaminase activity of *Tc*PAM with A) its natural substrate; B) surrogate (2*S*)-styryl-α-alanine. 27

Figure. 2.5. *Tch*PAM-catalyzed addition of ammonia to substituted arylacrylates. 28

Figure. 2.6. Proposed covalent binding of a 3-arylglycidate inhibitor in the *Sg*TAM active site A) Formation of a dihydroxy ether intermediate reported by Montanavon and co-workers.[17] B) Reinterpretation of bound intermediate as a β-hydroxy-α-amino adduct formed by MIO-NH_2 as informed by the proposed amino-linked adducts made in the *Pa*PAM crystal structures.[29] 30

Figure. 2.7. The occurrence of synthetic and biosynthetic β-phenyl-β-hydroxy-α-amino acid building blocks in bioactive compounds. Stereochemical designations listed in brackets [] are described in **Figure. 2.8**. 31

Figure. 2.8. Stereoisomerism convention for A) Arylserine, and B) Arylisoserine used herein. The equivalent, archaic designations for arylserine diastereomers are listed in brackets []. 32

Figure. 2.9. The occurrence of synthetic and biosynthetic α-hydroxy-β-amino acid building blocks in bioactive compounds. 33

Figure. 2.10. Various chemical synthetic strategies to synthesize β-hydroxy-α-amino acids: a). aza-Claisen rearrangement; b). proteinogenic amino acid derivatization; c). asymmetric hydrogenation; d). Strecker reaction; e). Sharpless aminohydroxylation and dihydroxylation reaction; f). Electrophilic amination; g). Mannich type reaction; h). Oxy-Michael addition; i). Asymmetric aldol condensation; and j). multicomponent reaction. 34

Figure. 2.11. Biocatalysis of arylserine and arylisoserine analogues from *trans*-3-arylglycidates and (2*S*)-styryl-α-alanine by using an MIO-aminomutase. The asterisk (*) indicates a chiral center. 36

Figure. 2.12. Enantiopurity of the synthetically derived methyl esters of A) 3-phenylglycidate (**14a**) (49:51), extracted ion *m*/*z* 121; B) 3-(3'-OCH_3-phenyl)glycidate (**14b**) (50:50), extracted ion *m*/*z* 151; C) (**14c**) 3-(3'-CH_3-phenyl)glycidate (**14c**) (49:51), extracted ion *m*/*z* 135; D) 3-(3'-F-phenyl)glycidate (**14d**) (50:50), extracted ion *m*/*z* 139; E) 3-(3'-Cl-phenyl)glycidate (**14e**) (50:50), extracted ion *m*/*z* 155; and F) 3-(3'-Br-phenyl)glycidate (**14f**) (50:50), extracted ion *m*/*z* 199 analyzed by chiral GC/EI-MS. The base peak ion was used for extracted-ion selection of the derivatives; partial chromatograms are shown. The ratio of each enantiomer is shown in parentheses. 53

Figure. 2.13. Enantiopurity of the synthetically derived methyl esters of G) 3-(3'-NO_2-phenyl)glycidate (**14g**) (47:53), extracted ion *m*/*z* 166; H) 3-(4'-NO_2-phenyl)glycidate (**14h**) (46:54), extracted ion *m*/*z* 166; I) 3-(4'-CH_3-phenyl)glycidate (**14i**) (50:50), extracted ion *m*/*z* 135; J) 3-(4'-F-phenyl)glycidate (**14j**) (50:50), extracted ion *m*/*z* 139; K) 3-(4'-Cl-phenyl)glycidate (**14k**) (47:53), extracted ion *m*/*z* 155; and L) 3-(4'-Br-phenyl)glycidate (**14l**) (50:50), extracted ion *m*/*z* 199.analyzed by chiral GC/EI-MS. The base peak ion was used for extracted-ion selection of the derivatives; partial chromatograms are shown. The ratio of each enantiomer is shown in parentheses. 54

Figure. 2.14. ^{1}H NMR of 3-phenylglycidate (**14a**) in deuterated Assay Buffer. A) NMR spectra were recorded at 15 min intervals starting from t_1 to t_7. At t_1 = 0 min and at t_7 = 90 min, the ratio of **14a**:dihydroxy product = 100:0, and B) NMR spectrum after storing the sample in deuterated Assay Buffer at ~25 °C for 1 week, the ratio of **14a**:dihydroxy product = 100:4. See Appendix for the associated ^{1}H NMR data for other arylglycidate analogues (**14b**-**14l**). 55

Figure. 2.15. Relative abundances of arylisoserine (**16b)** and arylserine (**15b**) products made from C_β- and C_α-amination, respectively, of 3-(3'-OCH_3-phenyl)glycidate (**14b**) (1 mM) when incubated with 2M NH_4OH and *Tc*PAM (100 µg/mL) (*top trace*) and without *Tc*PAM (*bottom trace*)..... 58

Figure. 2.16. Resonance and inductive stabilizations of the partial positive charge (δ^+) (due to bond polarization) at the C_β of arylglycidate substrates **14a**, **14b**, and **14i** assisted by the aryl-ring. For substrate **14h**, the electron-withdrawing NO_2 group resonance destabilizes the δ^+ at the

benzylic carbon (C_β), and the regioselectivity is reversed, directing an incoming nucleophile to attack at C_α preferentially. 59

Figure. 2.17. GC/EI-MS spectra of authentic A) (2*S*)+(2*R*)-*syn*-phenylserine from Sigma-Aldrich, B) phenylserine biocatalyzed from 3-phenylglycidate by *Tc*PAM catalysis (see **Figure. 2.19** for GC profiles), and of C) (2*R*,3*S*)-*syn*-phenylisoserine (see **Figure. 2.72** for GC profile). Each hydroxy amino acid was derivatized to its *O*-trimethylsilyl *N*-[(2*S*)-2-methylbutyryl] methyl ester. The molecular ion (M•+, *m*/*z* 351) was not observed for either analyte..... 62

Figure. 2.18. An expanded 500 MHz ^{1}H NMR of A) synthesized phenylserine (**15a**), and B) of **15a** containing authentic (*2S*)-*syn*-phenylserine recorded in D_2O at pH 1.5. Chemical shift values are listed vertically above each peak, and the relative area under each peak is listed horizontally next to each peak..... 63

Figure. 2.19. Gas-chromatography/mass spectrometry extracted-ion (*m*/*z* 179) chromatograms of A) synthesized phenylserine (**15a**), as shown in **Scheme 2.1B,** was derivatized with a chiral auxiliary as per **Scheme 2.1A**. Peaks at 7.95 min and 8.01 min correspond to (2*S*)+(2*R*)-*anti*-phenylserine isomers, and those at 8.10 and 8.13 min correspond to (2*S*)+(2*R*)-*syn*-phenylserine isomers; B) derivatized authentic (2*S*)+(2*R*)-*syn*-phenylserine racemate (Sigma-Aldrich, contains 13% (2*S*)+(2*R*)-*anti*-phenylserine as an impurity; C) chiral-auxiliary of biocatalyzed phenylserine made from the racemic 3-phenylglycidate. Biocatalyzed (2*S*)+(2*R*)-*syn*-phenylserine stereoisomers were also produced at ~9% (peaks at 8.10 and 8.13 min); and D) Extracted ion (*m*/*z* 179) chromatogram of derivatized phenylserine after treating with (2*S*)-TA for 15 min. 67

Figure. 2.20. Distribution of enantiomers (2*R*)-*anti* (gray bars) and (2*S*)-*anti* (black bars) in biocatalyzed products for the substituted phenylserine analogues. 68

Figure. 2.21. A) Lowest energy binding poses are shown of (2*S*,3*R*)-3-phenylglycidate ((2*S*,3*R*)-**14a**) (orange sticks) and (2*R*,3*S*)-3-phenylglycidate ((2*R*,3*S*)- **14a**) (light-gray sticks) at center of the image. The conformations are consistent with the active site of *Tc*PAM consisting of residues (shown as dark gray and yellow sticks), the catalytic Tyr80, a putative catalytic Tyr322 (light blue sticks), binding contact Arg325 (golden-rod sticks), and the methylidene imidazolone (MIO) moiety (green sticks). B) (2*S*,3*R*)- **14a** (orange sticks) and C) (2*R*,3*S*)- **14a** (light-gray sticks) are posed separately in the active site to highlight the nominal distances (<3.5 Å) that substituents on the aryl ring are from active site residues. Printed on the aryl ring, '*m*' designates *meta*-positions (equivalent to the 3'-designation used in the text), and '*p*' designates the *para*-position (equivalent to the 4'-designation used in the text) per ligand. Heteroatoms are colored red for oxygen and blue for nitrogen. The images were produced with UCSF Chimera,[136], and the docking conformations were generated with AutoDock Vina[127] from PDB code 3NZ4. Numbers are distances in Å. D) *Tc*PAM in complex with cinnamic acid, based on PDB codes 3NZ4 and 4CQ5. 70

Figure. 2.22. *a*) Rendering of the mechanism showing attack of the NH_2-MIO on the σ* antibonding orbital (gray lobe) at C_α for the C–O σ bond of (2*S*,3*R*)-**14a** to produce (2*R*)-*anti*-phenylserine. *b*) A double inversion-of-configuration mechanism is envisioned to access the minor *syn*-stereoisomer that proceeds through a putative lactone intermediate..... 71

Figure. 2.23. Various viewing angles centering on the surfaces of A) Leu104, B) Leu108, and C) Lys427 deep in the aryl binding pocket of *Tc*PAM (PDB code 3NZ4) with poses of the docked (2*S*,3*R*)-**14a** (orange sticks) and (2*R*,3*S*)-**14a** (light-gray sticks)..... 72

Figure. 2.24. SDS-PAGE gel of wild-type *Tc*PAM (82% pure) and (2*S*)-TA (99% pure) after Coomassie blue staining. Purity was estimated by a Kodak Gel Logic 100 Imaging System; *lane* 1: *Tc*PAM (10 µL of a 13.7 mg/mL solution); *lane* 2: *Tc*PAM (5 µL of a 13.7 mg/mL solution); *lane* 3: PageRuler © Prestained Ladder: MW (kDa) – 170, 130, 100, 70, 55, 40, 35, 25, 15; *lane* 4: (2*S*)-TA (10 µL of a 8.8 mg/mL solution); and *lane* 5: (2*S*)-TA (5 µL of a 8.8 mg/mL solution). 81

Figure. 2.25. ^{1}H NMR of 3-(3′-OCH_3-phenyl)glycidate (**14b**) in deuterated Assay Buffer. A) NMR spectra were recorded at 15 min intervals starting from t_1 to t_7. At t_1 = 0 min and at t_7 = 90 min, the ratio of **14b**:dihydroxy product = 100:0, and B) NMR spectrum after storing the sample in deuterated Assay Buffer at ~25 °C for 1 week, the ratio of **14b**:dihydroxy product = 100:3. . 82

Figure. 2.26. ^{1}H NMR of 3-(3′-CH_3-phenyl)glycidate (**14c**) in deuterated Assay Buffer. A) NMR spectra were recorded at 15 min intervals starting from t_1 to t_7. At t_1 = 0 min and at t_7 = 90 min, the ratio of **14c**:dihydroxy product = 100:7, and B) NMR spectrum after storing the sample in deuterated Assay Buffer at ~25 °C for 1 week, the ratio of **14c**:dihydroxy product = 100:12..... 83

Figure. 2.27. ^{1}H NMR of 3-(3′-F-phenyl)glycidate (**14d**) in deuterated Assay Buffer. A) NMR spectra were recorded at 15 min intervals starting from t_1 to t_7. At t_1 = 0 min and at t_7 = 90 min, the ratio of **14d**:dihydroxy product = 100:0, and B) NMR spectrum after storing the sample in deuterated Assay Buffer at ~25 °C for 1 week, the ratio of **14d**:dihydroxy product = 100:2. 84

Figure. 2.28. ^{1}H NMR of 3-(3′-Cl-phenyl)glycidate (**14e**) in deuterated Assay Buffer. A) NMR spectra were recorded at 15 min intervals starting from t_1 to t_7. At t_1 = 0 min and at t_7 = 90 min, the ratio of **14e**:dihydroxy product = 100:0, and B) NMR spectrum after storing the sample in deuterated Assay Buffer at ~25 °C for 1 week, the ratio of **14e**:dihydroxy product = 100:1..... 85

Figure. 2.29. ^{1}H NMR of 3-(3′-Br-phenyl)glycidate (**14f**) in deuterated Assay Buffer. A) NMR spectra were recorded at 15 min intervals starting from t_1 to t_7. At t_1 = 0 min and at t_7 = 90 min, the ratio of **14f**:dihydroxy product = 100:0, and B) NMR spectrum after storing the sample in deuterated Assay Buffer at ~25 °C for 1 week, the ratio of **14f**:dihydroxy product = 100:1. 86

Figure. 2.30. ^{1}H NMR of 3-(3′-NO_2-phenyl)glycidate (**14g**) in deuterated Assay Buffer. A) NMR spectra were recorded at 15 min intervals starting from t_1 to t_7. At t_1 = 0 min and at t_7 = 90 min, the ratio of **14g**:dihydroxy = 100:0, and B) ^{1}H NMR spectrum after storing the sample in deuterated Assay Buffer at ~25 °C for 1 week, the ratio of the ratio of **14g**:dihydroxy product = 100:2..... 87

Figure. 2.31. ^{1}H NMR of 3-(4′-NO_2-phenyl)glycidate (**14h**) in deuterated Assay Buffer. A) NMR spectra were recorded at 15 min intervals starting from t_1 to t_7. At t_1 = 0 min and t_7 = 90 min, the ratio of **14h**:dihydroxy product = 100:9, and B) NMR spectrum after storing the sample in deuterated Assay Buffer at ~25 °C for 1 week, the ratio of **14h**:dihydroxy product = 100:9. 88

Figure. 2.32. ^{1}H NMR of 3-(4′-CH_3-phenyl)glycidate (**14i**) in deuterated Assay Buffer. A) NMR spectra were recorded at 15 min intervals starting from t_1 to t_7. At t_1 = 0 min and at t_7 = 90 min, the

ratio of **14i**:dihydroxy product = 100:1, and B) NMR spectrum after storing the sample in deuterated Assay Buffer at ~25 °C for 1 week, the ratio of **14i**:dihydroxy product = 100:5. 89

Figure. 2.33. ^{1}H NMR of 3-(4′-F-phenyl)glycidate (**14j**) in deuterated Assay Buffer. A) NMR spectra were recorded at 15 min intervals starting from t_1 to t_7. At t_1 = 0 min and t_7 = 90 min, the ratio of **14j**:dihydroxy product = 100:4, and B) NMR spectrum after storing the sample in deuterated Assay Buffer at ~25 °C for 1 week, the ratio of **14j**:dihydroxy product = 100:7. 90

Figure. 2.34. ^{1}H NMR of 3-(4′-Cl-phenyl)glycidate (**14k**) in deuterated Assay Buffer. A) NMR spectra were recorded at 15 min intervals starting from t_1 to t_7. At t_1 = 0 min and t_7 = 90 min, the ratio of **14k**:dihydroxy product = 100:0, and B) NMR spectrum after storing the sample in deuterated Assay Buffer at ~25 °C for 1 week, the ratio of **14k**:dihydroxy product = 100:3. 91

Figure. 2.35. ^{1}H NMR of 3-(4′-Br-phenyl)glycidate (**14l**) in deuterated Assay Buffer. A) NMR spectra were recorded at 15 min intervals starting from t_1 to t_7. At t_1 = 0 min and t_7 = 90 min, the ratio of **14l**:dihydroxy product = 100:0, and B) NMR spectrum after storing the sample in deuterated Assay Buffer at ~25 °C for 1 week, the ratio of **14l**:dihydroxy product = 100:1. 92

Figure. 2.36. A) Relative abundances of arylisoserine (**16a)** and arylserine (**15a**) products made from C_β- and C_α-amination, respectively, of 3-phenylglycidate (**14a**) (1 mM) when incubated with 2M NH_4OH and *Tc*PAM (100 µg/mL) (*top trace*) and without *Tc*PAM (*bottom trace*). B) Relative abundances of arylisoserine (**16i)** and arylserine (**15i**) products made from C_β- and C_α-amination, respectively, of 3-(4'-CH_3-phenyl)glycidate (**14i**) (1 mM) when incubated with 2M NH_4OH and *Tc*PAM (100 µg/mL) (*top trace*) and without *Tc*PAM (*bottom trace*). C) Relative abundances of arylisoserine (**16h)** and arylserine (**15h**) products made from C_β- and C_α-amination, respectively, of 3-(4'-NO_2-phenyl)glycidate (**14h**) (1 mM) when incubated with 2M NH_4OH and *Tc*PAM (100 µg/mL) (*top trace*) and without *Tc*PAM (*bottom trace*)..... 93

Figure. 2.37. GC/EI-MS spectra of A) authentic (2*S*/2*R*)-*anti*-3′-OCH_3-phenylserine (**15b**) and B) 3′-OCH_3-phenylserine biocatalyzed from 3-(3′-OCH_3-phenyl)glycidate (**14b**) by *Tc*PAM catalysis. Each hydroxyamino acid was derivatized as their *O*-trimethylsilyl *N*-[(2*S*)-2-methylbutyryl] methyl ester. The molecular ion ($M^{\bullet+}$, *m*/*z* 381) was not observed for either analyte. 94

Figure. 2.38. GC/EI-MS spectra of A) authentic (2*S*/2*R*)-*anti*-3′-CH_3-phenylserine (**15c**) and B) 3′-CH_3-phenylserine biocatalyzed from 3-(3′-CH_3-phenyl)glycidate (**14c**) by *Tc*PAM catalysis. Each hydroxyamino acid was derivatized as their *O*-trimethylsilyl *N*-[(2*S*)-2-methylbutyryl] methyl ester. The molecular ion ($M^{\bullet+}$, *m*/*z* 365) was not observed for either analyte. 94

Figure. 2.39. GC/EI-MS spectra of A) authentic (2*S*/2*R*)-*anti*-3′-F-phenylserine (**15d**) and B) 3′-F-phenylserine biocatalyzed from 3-(3′-F-phenyl)glycidate (**14d**) by *Tc*PAM catalysis. Each hydroxyamino acid was derivatized as their *O*-trimethylsilyl *N*-[(2*S*)-2-methylbutyryl] methyl ester. The molecular ion ($M^{\bullet+}$, *m*/*z* 369) was not observed for either analyte. 95

Figure. 2.40. GC/EI-MS spectra of A) authentic (2*S*/2*R*)-*anti*-3′-Cl-phenylserine (**15e**) and B) 3′-Cl-phenylserine biocatalyzed from 3-(3′-Cl-phenyl)glycidate (**14e**) by *Tc*PAM catalysis. Each hydroxyamino acid was derivatized as their *O*-trimethylsilyl *N*-[(2*S*)-2-methylbutyryl] methyl ester. The molecular ion ($M^{\bullet+}$, *m*/*z* 385) was not observed for either analyte. 95

Figure. 2.41. GC/EI-MS spectra of A) authentic (2*S*/2*R*)-*anti*-3′-Br-phenylserine (**15f**) and B) 3′-Br-phenylserine biocatalyzed from 3-(3′-Br-phenyl)glycidate (**14f**) by *Tc*PAM catalysis. Each hydroxyamino acid was derivatized as their *O*-trimethylsilyl *N*-[(2*S*)-2-methylbutyryl] methyl ester. The molecular ion ($M^{\bullet+}$, *m*/*z* 429) was not observed for either analyte. 96

Figure. 2.42. GC/EI-MS spectra of A) authentic (2*S*/2*R*)-*anti*-3′-NO_2-phenylserine (**15g**) and B) 3′-NO_2-phenylserine biocatalyzed from 3-(3′-NO_2-phenyl)glycidate (**14g**) by *Tc*PAM catalysis. Each hydroxyamino acid was derivatized as their *O*-trimethylsilyl *N*-[(2*S*)-2-methylbutyryl] methyl ester. The molecular ion ($M^{\bullet+}$, *m*/*z* 396) was not observed for either analyte. 96

Figure. 2.43. GC/EI-MS spectra of A) authentic (2*S*/2*R*)-*anti*-4′-NO_2-phenylserine (**15h**) and B) 4′-NO_2-phenylserine biocatalyzed from 3-(4′-NO_2-phenyl)glycidate (**14h**) by *Tc*PAM catalysis. Each hydroxyamino acid was derivatized as their *O*-trimethylsilyl *N*-[(2*S*)-2-methylbutyryl] methyl ester. The molecular ion ($M^{\bullet+}$, *m*/*z* 396) was not observed for either analyte. 97

Figure. 2.44. GC/EI-MS spectra of A) authentic (2*S*/2*R*)-*anti*-4′-CH_3-phenylserine (**15i**) and B) 4′-CH_3-phenylserine biocatalyzed from 3-(4′-CH_3-phenyl)glycidate (**14i**) by *Tc*PAM catalysis. Each hydroxyamino acid was derivatized as their *O*-trimethylsilyl *N*-[(2*S*)-2-methylbutyryl] methyl ester. The molecular ion ($M^{\bullet+}$, *m*/*z* 365) was not observed for either analyte. 97

Figure. 2.45. GC/EI-MS spectra of A) authentic (2*S*/2*R*)-*anti*-4′-F-phenylserine (**15j**) and B) 4′-F-phenylserine biocatalyzed from 3-(4′-F-phenyl)glycidate (**14j**) by *Tc*PAM catalysis. Each hydroxyamino acid was derivatized as their *O*-trimethylsilyl *N*-[(2*S*)-2-methylbutyryl] methyl ester. The molecular ion ($M^{\bullet+}$, *m*/*z* 369) was not observed for either analyte. 98

Figure. 2.46. GC/EI-MS spectra of A) authentic (2*S*/2*R*)-*anti*-4′-Cl-phenylserine (**15k**) and B) 4′-Cl-phenylserine biocatalyzed from 3-(4′-Cl-phenyl)glycidate (**14k**) by *Tc*PAM catalysis. Each hydroxyamino acid was derivatized as their *O*-trimethylsilyl *N*-[(2*S*)-2-methylbutyryl] methyl ester. The molecular ion ($M^{\bullet+}$, *m*/*z* 385) was not observed for either analyte. 98

Figure. 2.47. GC/EI-MS spectra of A) authentic (2*S*/2*R*)-*anti*-4′-Br-phenylserine (**15l**) and B) 4′-Br-phenylserine biocatalyzed from 3-(4′-Br-phenyl)glycidate (**14l**) by *Tc*PAM catalysis. Each hydroxyamino acid was derivatized as their *O*-trimethylsilyl *N*-[(2*S*)-2-methylbutyryl] methyl ester. The molecular ion ($M^{\bullet+}$, *m*/*z* 429) was not observed for either analyte. 99

Figure. 2.48. Partial ^{1}H NMR (500 MHz, D_2O at pH 1.5) spectra of A) chemically synthesized phenylserine (**15a**) and B) biosynthetic phenylserine produced from phenylglycidate (**14a**) by *Tc*PAM. 100

Figure. 2.49. Partial ^{1}H NMR (500 MHz, D_2O at pH 1.5) spectra of A) chemically synthesized 3′-OCH_3-phenylserine (**15b**) and B) biosynthetic 3′-OCH_3-phenylserine produced from 3-(3′-OCH_3-phenyl)glycidate (**14b**) by *Tc*PAM. 101

Figure. 2.50. Partial ^{1}H NMR (500 MHz, D_2O at pH 1.5) spectra of A) chemically synthesized 3′-CH_3-phenylserine (**15c**) and B) biosynthetic 3′-CH_3-phenylserine produced from 3-(3′-CH_3-phenyl)glycidate (**14c**) by *Tc*PAM..... 102

Figure. 2.51. Partial ^{1}H NMR (500 MHz, D_2O at pH 1.5) spectra of A) chemically synthesized 3′-F-phenylserine (**15d**) and B) biosynthetic 3′-F-phenylserine produced from 3-(3′-F-phenyl)glycidate (**14d**) with *Tc*PAM. 103

Figure. 2.52. Partial ^{1}H NMR (500 MHz, D_2O at pH 1.5) spectra of A) chemically synthesized 3′-Cl-phenylserine (**15e**) and B) biosynthetic 3′-Cl-phenylserine produced from 3-(3′-Cl-phenyl)glycidate (**14e**) by *Tc*PAM..... 104

Figure. 2.53. Partial ^{1}H NMR (500 MHz, D_2O at pH 1.5) spectra of A) chemically synthesized 3′-Br-phenylserine (**15f**) and B) biosynthetic 3′-Br-phenylserine produced from 3-(3′-Br-phenyl)glycidate (**14f**) by *Tc*PAM. 105

Figure. 2.54. Partial ^{1}H NMR (500 MHz, D_2O at pH 1.5) spectra of A) chemically synthesized 3′-NO_2-phenylserine (**15g**) and B) biosynthetic 3′-NO_2-phenylserine produced from 3-(3′-NO_2-phenyl)glycidate (**14g**) by *Tc*PAM. 106

Figure. 2.55. Partial ^{1}H NMR (500 MHz, D_2O at pH 1.5) spectra of A) chemically synthesized 4′-NO_2-phenylserine (**15h**) and B) biosynthetic 4′-NO_2-phenylserine produced from 3-(4′-NO_2-phenyl)glycidate (**14h**) by *Tc*PAM. 107

Figure. 2.56. Partial ^{1}H NMR (500 MHz, D_2O at pH 1.5) spectra of A) chemically synthesized 4′-CH_3-phenylserine (**15i**) and B) biosynthetic 4′-CH_3-phenylserine produced from 3-(4′-CH_3-phenyl)glycidate (**14i**) by *Tc*PAM. 108

Figure. 2.57. Partial ^{1}H NMR (500 MHz, D_2O at pH 1.5) spectra of A) chemically synthesized 4′-F-phenylserine (**15j**) and B) biosynthetic 4′-F-phenylserine produced from 3-(4′-F-phenyl)glycidate (**14j**) by *Tc*PAM..... 109

Figure. 2.58. Partial ^{1}H NMR (500 MHz, D_2O at pH 1.5) spectra of A) chemically synthesized 4′-Cl-phenylserine (**15k**) and B) biosynthetic 4′-Cl-phenylserine produced from 3-(4′-Cl-phenyl)glycidate (**14k**) by *Tc*PAM. 110

Figure. 2.59. Partial ^{1}H NMR (500 MHz, D_2O at pH 1.5) spectra of A) chemically synthesized 4′-Br-phenylserine (**15l**) and B) biosynthetic 4′-Br-phenylserine produced from 3-(4′-Br-phenyl)glycidate (**14l**) by *Tc*PAM. 111

Figure. 2.60. GC/EI-MS extracted-ion chromatograms of biosynthetic arylserines derivatized as their *O*-trimethylsilyl *N*-[(2*S*)-2-methylbutyryl] methyl esters A) phenylserine (**15a**) (extracted ion *m*/*z* 179), B) 3′-OCH_3-phenylserine (**15b**) (extracted ion *m*/*z* 209), C) 3′-methylphenylserine (**15c**) (extracted ion *m*/*z* 193), D) 3′-F-phenylserine (**15d**) (extracted ion *m*/*z* 197), E) 3′-Cl-phenylserine (**15e**) (extracted ion *m*/*z* 213), and F) 3′-Br-phenylserine (**15f**) (extracted ion *m*/*z* 257)..... 112

Figure. 2.61. GC/EI-MS extracted-ion chromatograms of biosynthetic arylserines derivatized as their *O*-trimethylsilyl *N*-[(2*S*)-2-methylbutyryl] methyl esters G) 3′-NO_2-phenylserine (**15g**) (extracted ion *m*/*z* 224), H) 4′-NO_2-phenylserine (**15h**) (extracted ion *m*/*z* 224), I) 4′-CH_3-phenylserine (**15i**) (extracted ion *m*/*z* 193), J) 4′-F-phenylserine (**15j**) (extracted ion *m*/*z* 197), K) 4′-Cl-phenylserine (**15k**) (extracted ion *m*/*z* 213), and L) 4′-Br-phenylserine (**15l**) (extracted ion *m*/*z* 257)..... 113

Figure. 2.62. GC/EI-MS extracted-ion chromatograms of synthetic arylserines derivatized as their *O*-trimethylsilyl *N*-[(2*S*)-2-methylbutyryl] methyl ester before (*top trace*) and after 10-min treatment with (2*S*)-TA (*bottom trace*): A) 3′-OCH_3-phenylserine (**15b**) (extracted ion *m*/*z* 209), B) 3′-CH_3-phenylserine (**15c**) (extracted ion *m*/*z* 193), C) 3′-F-phenylserine (**15d**) (extracted ion *m*/*z* 197), D) 3′-Cl-phenylserine (**15e**) (extracted ion *m*/*z* 213), E) 3′-Br-phenylserine (**15f**) (extracted ion *m*/*z* 257), and F) 3′-NO_2-phenylserine (**15g**) (extracted ion *m*/*z* 224). 114

Figure. 2.63. GC/EI-MS extracted-ion chromatograms of synthetic arylserines derivatized as their *O*-trimethylsilyl *N*-[(2*S*)-2-methylbutyryl] methyl ester before (*top trace*) and after 10-min treatment with (2*S*)-TA (*bottom trace*): G) 4′-NO_2-phenylserine (**15h**) (extracted ion *m*/*z* 224); H) 4′-CH_3-phenylserine (**15i**) (extracted ion *m*/*z* 193), I) 4′-F-phenylserine (**15j**) (extracted ion *m*/*z* 197), J) 4′-Cl-phenylserine (**15k**) (extracted ion *m*/*z* 213) and K) 4′-Br-phenylserine (**15l**) (extracted ion *m*/*z* 257)..... 115

Figure. 2.64. Michaelis-Menten kinetics for the turnover of arylglycidate analogues (**14a**–**14f**) to their corresponding arylserines (**15a**–**15f**). 116

Figure. 2.65. Michaelis-Menten kinetics for the turnover of arylglycidate analogues (**14g**–**14l**) to their corresponding arylserines (**15g**–**15l**). 117

Figure. 2.66. Michaelis-Menten kinetics for the turnover of arylglycidate analogues (**14a**–**14f**) to their corresponding aryl*iso*serines (**16a**–**16f**). 118

Figure. 2.67. Michaelis-Menten kinetics for the turnover of arylglycidate analogues (**14g**–**14l**) to their corresponding arylisoserines (**16g**–**16l**)..... 119

Figure. 2.68. The six-hour time course for the conversion of four representative 3-arylglycidate racemates [3-phenylglycidate (**14a**) (●), 3′-F- (**14d**) (♦), 3′-Cl- (**14e**) (▲), and 4′-Cl- (**14k**) (■) phenylglycidate (each at 400 µM)] to their corresponding arylserines in assays containing *Tc*PAM (100 µg/mL), and (2*S*)-styryl-α-alanine (1 mM) in 50 mM NaH_2PO_4/Na_2HPO_4 (pH 8.0), n = 3. Arylserine production is shown as a percentage relative to the initial epoxide substrate concentration. These example epoxides were turned over by *Tc*PAM from fastest (3'-Cl) to slowest (4'-Cl). 120

Figure. 2.69. Lowest energy binding poses are shown of A) (2*R*,3*S*)-**14f**; B) (2*S*,3*R*)-**14f**; C) (2*R*,3*S*)-**14e**; D) (2*S*,3*R*)-**14e**; E) (2*R*,3*S*)-**14g**; F) (2*S*,3*R*)-**14g**; G) (2*R*,3*S*)-**14b**; and H) (2*S*,3*R*)-**14b**. 121

Figure. 2.70. Lowest energy binding poses are shown of A) (2*R*,3*S*)-**14l**; B) (2*S*,3*R*)-**14l**; C) (2*R*,3*S*)-**14k**; D) (2*S*,3*R*)-**14k**; E) (2*R*,3*S*)-**14h**; and F) (2*S*,3*R*)-**14h**. 122

Figure. 2.71. Putative binding pose of (2*S*,3*R*)-3-(3'-OCH_3-phenyl)glycidate (**14b**) in a conformation aligned for NH_2-MIO attack at C_β (labeled 'β') to make the arylisoserine (**16b**). C_α is labeled with 'α' for reference. 123

Figure. 2.72. GC/EI-MS extracted ion (*m*/*z* 106) chromatogram of authentic (2*R*,3*S*)-*syn*-phenylisoserine (**16a**) derivatized as its *O*-trimethylsilyl *N*-[(2*S*)-2-methylbutyryl] methyl ester (**18a**). 123

Figure. 2.73. LC-ESI-MS/MS spectra of A) authentic (2*R*,3*S*)-*syn*-phenylisoserine (**16a**) (structures of diagnostic fragment ions are shown and used to characterize the fragment ions of the biocatalyzed arylisoserine analogues (below). B) phenylisoserine (**16a**); C) 3'-OCH_3-phenylisoserine (**16b**); D) 3'-CH_3-phenylisoserine (**16c**); and E) 3'-F-phenylisoserine (**16d**) biocatalyzed by *Tc*PAM from the corresponding 3-arylglycidates. 124

Figure. 2.74. LC-ESI-MS/MS spectra of F) 3'-Cl-phenylisoserine (**16e**); G) 3'-Br-phenylisoserine (**16f**); H) 3'-NO_2-phenylisoserine (**16g**); I) 4'-NO_2-phenylisoserine (**16h**); J) 4'-CH_3-phenylisoserine (**16i**); and K) 4'-F-phenylisoserine (**16j**) biocatalyzed by *Tc*PAM from the corresponding 3-arylglycidates. 125

Figure. 2.75. LC-ESI-MS/MS spectra of L) 4'-Cl-phenylisoserine (**16k**) and M) 4'-Br-phenylisoserine (**16l**) biocatalyzed by *Tc*PAM from their corresponding 3-arylglycidates. 126

Figure. 3.1. A) Reactions catalyzed by MIO-dependent ammonia lyases (ALs) and aminomutases (AMs), making either the acrylate or β-amino acid from the corresponding α-amino acid. The MIO and aminated-MIO (NH_2-MIO) are shown. The asterisk (*) identifies an (*R*/*S*)-chiral center; B) Production of either enantiomer of α- and β-arylalanine using engineered PAL/PAM catalysis; C) PAM-mediated amine transfer from (*S*)-styryl-α-alanine to acrylate acceptors. D) Addition of ammonia and primary amines to mesaconate analogues using engineered methylaspartate ammonia lyase (MAL) to produce (2*S*)-*syn*-aspartate analogues. 142

Figure. 3.2. Chiral HPLC separation of A). (2*R*,3*R*)-3-phenylglycidol (**21a**), 92% *e.e.*; B) .(2*S*,3*S*)-3-phenylglycidol (**21b**), 90% *e.e*; and C) a co-injection of enantioenriched samples of **21a** and **21b**. 152

Figure. 3.3. Extracted ion (*m*/*z* 121) chromatogram of (A) racemic methyl 3-phenylglycidate (51:49), (B) methyl (2*S*,3*R*)-3-Phenylglycidate (4:96, 12.56 min), and (C) methyl (2*R*,3*S*)-3-Phenylglycidate (95:5, 12.37 min). 153

Figure. 3.4. Stereoisomerism convention for A) phenylserine, and B) phenylisoserine used herein. 154

Figure. 3.5. GC/EI-MS extracted-ion chromatograms with *m*/*z* 179 ion monitoring of A) phenylserine stereoisomers derivatized with a chiral auxiliary (cf. **Scheme 3.2A**). An earlier study[29] involving enzymatic resolution with (2*S*)-threonine aldolase confirmed that peaks at 8.88 min and 8.93 min correspond to chiral derivatives of (2*S*)-*anti*- and (2*R*)-*anti*-phenylserine isomers, respectively, and peaks at 9.02 and 9.05 min correspond to the chiral derivatives of (2*S*)-*syn*- and (2*R*)-*syn*-phenylserine isomers (cf. **Figure. 2.19**). Chiral derivatives of B) authentic (2*S*)-*syn*-phenylserine (Bachem); C) biocatalyzed phenylserine made from (2*S*,3*R*)-3-phenylglycidate (the (2*S*)-*anti*:(2*R*)-*anti*:(2*S*)-*syn* isomers are abundant at a relative ratio of 2:90:8); and D) biocatalyzed phenylserine made from (2*R*,3*S*)-3-phenylglycidate (the (2*S*)-*anti*:(2*R*)-*anti*:(2*R*)-*syn* isomers are abundant at a relative ratio of 76:15:9). 156

Figure. 3.6. GC/EI-MS extracted-ion chromatograms with *m*/*z* 106 ion monitoring of a chiral auxiliary derivative of A) authentic (2*R*,3*S*)-*syn*-phenylisoserine (Bachem); B) authentic (2*R*,3*R*)-*anti*-phenylisoserine (Chem Impex); C) *anti*-phenylisoserine enantiomers synthesized from authentic racemic 3-phenylglycidate;[42,43] D) (2*S*,3*S*)-*anti*-phenylisoserine synthesized from

(2*S*,3*R*)-3-phenylglycidate (**14aa**); E) (2*R*,3*R*)-*anti*-phenylisoserine made from (2*R*,3*S*)-3-phenylglycidate (**14ab**); F) biocatalyzed (2*S*,3*S*)-*anti*-phenylisoserine made from (2*S*,3*R*)-3-phenylglycidate substrate (**14aa**); and G) biocatalyzed (2*R*,3*R*)-*anti*-phenylisoserine made from (2*R*,3*S*)-3-phenylglycidate substrate (**14ab**). Note, isoserines in *Panels C, D,* and *E,* were made from the corresponding glycidates by nucleophilic addition of NH_4OH..... 158

Figure. 3.7. Absolute stereoconfiguration of biocatalyzed phenylserine produced from A) (2*S*,3*R*)-3-phenylglycidate (**14aa**); and B) (2*R*,3*S*)-3-phenylglycidate (**14ab**). Proposed mechanism for the formation of C) (2*S*)-*syn*-phenylserine from **14aa**; and D) (2*R*)-*syn*-phenylserine from **14ab** through intramolecular carboxylate assisted oxiranone formation followed by amination at C_α by MIO-NH_2. 159

Figure. 3.8. A) Lowest energy binding conformations of A) (2*S*,3*R*)-3-phenylglycidate (**14aa**) (light-grey sticks); and B) (*R*)-3-((*R*)-hydroxy(phenyl)methyl)oxiran-2-one (**22aa**) (light grey sticks) are shown at the center of the image inside the *Tc*PAM active site. The residues shown here include a catalytic Tyr80 (yellow sticks), a putative catalytic Tyr322 (yellow sticks), binding contact Arg325 (orange sticks), and the methylidene imidazolone (MIO) moiety (green sticks). Heteroatoms are colored red for oxygen and blue for nitrogen. The images were produced with UCSF Chimera,[45] and the docking conformations were generated with AutoDock Vina[44] from *Tc*PAM crystal structure (PDB code 3NZ4). 162

Figure. 3.9. A) Lowest energy binding conformations of A) (2*R*,3*S*)-3-phenylglycidate (**14ab**) (light-grey sticks); and B) (*R*)-3-((*R*)-hydroxy(phenyl)methyl)oxiran-2-one (**22ab**) (light grey sticks) are shown at the center of the image inside the *Tc*PAM active site. The residues shown here include a catalytic Tyr80 (yellow sticks), a putative catalytic Tyr322 (yellow sticks), binding contact Arg325 (orange sticks), and the methylidene imidazolone (MIO) moiety (green sticks). Heteroatoms are colored red for oxygen and blue for nitrogen. The images were produced with UCSF Chimera,[45] and the docking conformations were generated with AutoDock Vina[44] from *Tc*PAM crystal structure (PDB code 3NZ4). 163

Figure. 3.10. Modified Michaelis-Menten plots for the turnover of A) (2*S*,3*R*)-3-phenylglycidate (**14aa**); and B) (2*R*,3*S*)-3-phenylglycidate (**14ab**) to their corresponding phenylserine at fixed concentration of the 3-phenylglycidate enantiomer. Double reciprocal Lineweaver-Burk plot of C) (2*S*,3*R*)-3-phenylglycidate (**14aa**); and D) (2*R*,3*S*)-3-phenylglycidate (**14ab**) to their corresponding phenylserine at fixed concentration of 3-phenylglycidate enantiomer [100 μM (■), 500 μM (●), 1000 μM (▲), and 2500 μM (▼)].E) Secondary plot of $Vmaxapp$ (calculated from each plot of **Figure. 3.10**A vs [**14aa**]; and F) Secondary plot of $vmaxapp$ (calculated from each plot of **Figure. 3.10**B vs [**14ab**] to calculate the true K_M of the glycidate substrates. 170

Figure. 3.11. Partial ^{1}H NMR (500 MHz, $CDCl_3$) spectra of (2*R*,3*R*)-3-Phenylglycidol (**21a**). 177

Figure. 3.12. Partial ^{13}C NMR (126 MHz, $CDCl_3$) spectra of (2*R*,3*R*)-3-Phenylglycidol (**21a**). 178

Figure. 3.13. Partial ^{1}H NMR (500 MHz, $CDCl_3$) spectra of (2*S*,3*S*)-3-Phenylglycidol (**21b**). 179

Figure. 3.14. Partial ^{13}C NMR (126 MHz, $CDCl_3$) spectra of (2*S*,3*S*)-3-Phenylglycidol (**21b**). 180

Figure. 3.15. Partial ^{1}H NMR (500 MHz, D_2O) spectra of Potassium (2*S*,3*R*)-3-Phenylglycidate (**14aa**). 181

Figure. 3.16. Partial ^{13}C NMR (126 MHz, D_2O) spectra of Potassium (2*S*,3*R*)-3-Phenylglycidate (**14aa**). 182

Figure. 3.17. Partial ^{1}H NMR (500 MHz, D_2O) spectra of Potassium (2*R*,3*S*)-3-Phenylglycidate (**14ab**). 183

Figure. 3.18. Partial ^{13}C NMR (126 MHz, D_2O) spectra of Potassium (2*R*,3*S*)-3-Phenylglycidate (**14ab**). 184

Figure. 3.19. GC/EI-MS spectra of A) authentic (2*R*,3*S*)-*syn*-phenylisoserine from Bachem (**6b**); B) authentic (2*R*,3*R*)-*anti*-phenylisoserine from ChemImpex C) derivatized *anti*-phenylisoserine enantiomers produced from authentic racemic 3-phenylglycidate; and D). derivatized (2*S*,3*S*)-*anti*-phenylisoserine (**16ac**) made from (2*S*,3*R*)-3-phenylglycidate (**14aa**) and NH_4OH. Each hydroxyamino acid was derivatized as their *O*-trimethylsilyl *N*-[(2*S*)-2-methylbutyryl] methyl ester. The molecular ion ($M^{\bullet+}$, *m*/*z* 351) was not observed. 185

Figure. 3.20. GC/EI-MS spectra of A) derivatized (2*R*,3*R*)-*anti*-phenylisoserine (**16ad**) made from (2*R*,3*S*)-3-phenylglycidate (**14ab**) and NH_4OH B) biocatalyzed (2*S*,3*S*)-*anti*-phenylisoserine (**16ac**) made from (2*S*,3*R*)-3-phenylglycidate (**14aa**) by *Tc*PAM; and C) biocatalyzed (2*R*,3*R*)-*anti*-phenylisoserine (**16ad**) made from (2*R*,3*S*)-3-phenylglycidate (**14ab**) by *Tc*PAM. Each hydroxyamino acid was derivatized as their *O*-trimethylsilyl *N*-[(2*S*)-2-methylbutyryl] methyl ester. The molecular ion ($M^{\bullet+}$, *m*/*z* 351) was not observed. 186

Figure. 3.21. Gas-chromatography/mass spectrometry extracted-ion chromatograms with *m*/*z* 336 ion monitoring of derivatized *anti*-phenylserine and *anti*-phenylisoserine enantiomers produced from NH_4OH assisted ring opening of authentic racemic 3-phenylglycidate. Peaks at 8.84 min and 8.90 min correspond to racemic *anti*-phenylserine (18%) produced from amination at the C_α, and peaks at 9.33 min and 9.41 min correspond to racemic *anti*-phenylisoserine produced from the amination at C_β. 187

LIST OF SCHEMES

Scheme 2.1. A) *Tc*PAM was incubated with (2*S*)- styryl-α-alanine (**12**) (1 mM) and separately with each *trans*-3-phenylglycidate racemate (**14a**–**14l**). Step *a*) *i) Tc*PAM (1.7 mg/mL) in Assay Buffer, 2 min pre-equilibration, **14a**–**14l** (10 mM), 29 °C, 4 h. Step *b*) Derivatization of putative phenylserines and phenylisoserines using a chiral auxiliary for stereoisomeric resolution. *i*) (2*S*)-2-Methylbutyric anhydride, pyridine, rt, 20 min; *ii*) 6 M HCl, pH 2; *iii*) CH_2N_2, EtOAc/MeOH (3:1 *v*/*v*), rt, 15 min; and *iv*) chlorotrimethylsilane, pyridine, CH_2Cl_2, rt, 15 min. *Insets*: stereoisomerism of (2*R*,3*S*)-*syn*-phenylisoserine. B) Synthesis of the stereoisomers of phenylserine analogues from glycine and a substituted benzaldehyde. a) step *i*) triethylamine, *n*-BuOH and H_2O, 12 h, rt; step *ii*) 6 M HCl, pH 2; and step *iii*) $NaHCO_3$, pH 6. 60

Scheme 3.1. Synthesis of (2*S*,3*R*)-3-phenylglycidate (**14aa**) and (2*R*,3*S*)-3-phenylglycidate (**14ab**). a) (–)-DET, Ti(O*i*-Pr)$_4$, *t*-BuOOH, 4 Å MS, CH_2Cl_2, 16 h, –30 °C; a′) (+)-DET, Ti(O*i*-Pr)$_4$, *t*-BuOOH, 4 Å MS, CH_2Cl_2, 16 h, –30 °C; b) *i*) $RuCl_3$, $NaIO_4$, $NaHCO_3$, $CH_3CN/CCl_4/H_2O$, rt, 72 h.; *ii*) $KHCO_3$, acetone/H_2O, 0 °C, 1h. 151

Scheme 3.2. Chiral auxiliary derivatization of A) authentic phenylserine diastereomers; and B) phenylisoserine diastereomers comprising (2*S*,3*S*)-*anti*-(**16ac**), (2*R*,3*R*)-*anti*-(**16ad**), and (2*R*,3*S*)-*syn*-phenylisoserine (**16ab**). Derivatization was performed using (a) (*i*) (2*S*)-2-Methylbutyric anhydride, pyridine, rt, 15 min; (*ii*) 6 M HCl, pH 2; (*iii*) CH_2N_2, EtOAc/MeOH (3:1 v/v), rt, 10 min; and (*iv*) chlorotrimethylsilane, pyridine,CH_2Cl_2, rt, 15 min.; and (b) 2 M aq. NH_4OH, rt, 1h. 155

Scheme 3.3. Proposed mechanism of phenylserine biocatalysis. The pathway constituting E→Q depicts the two-substrate ping-pong mechanism where (2*S*)-styryl-α-alanine acts as the amino group donor. The pathway involving E→EB shows the competitive substrate inhibition at higher concentration (>1000 μM) of 3-phenylglycidate. *Inset 1* shows the scheme of a typical ping-pong mechanism. 164

KEY TO ABBREVIATIONS

n-BuOH: *n*-Butanol

CCl_4: Carbon tetrachloride

$CDCl_3$: Deuterated chloroform

CH_2Cl_2: Dichloromethane

CH_2N_2: Diazomethane

CO_2: Carbon dioxide

D_2O: Deuterium oxide

DMSO: Dimethyl sulfoxide

DNA: Deoxyribonucleic acid

DOPS: (2*S*,3*R*)-3,4-Dihydroxyphenylserine

E. coli: *Escherichia coli*

EDTA: Ethylenediaminetetraacetic acid

EPA: Environmental Protection Agency

ESI: Electrospray ionization

EtOAc: Ethyl acetate

EtOH: Ethanol

GC/EI-MS: Gas chromatography electron ionization mass spectrometry

GDH: Glucose dehydrogenase

H_2O: Water

HIV: Human immunodeficiency virus

HCl: Hydrochloric acid

HHDH: Halohydrin dehalogenase

HRMS: High resolution mass spectrometry

IPTG: Isopropyl-β-D-thiogalactopyranoside

KCN: Potassium cyanide

KOH: Potassium hydroxide

KRED: Ketoreductase

LB: Lysogeny broth

LC/ESI/MS: Liquid-chromatography electrospray ionization mass spectrometry

LC/ESI/MRM: Liquid-chromatography electrospray ionization multiple reaction monitoring

$MgSO_4$: Magnesium Sulfate

MIO: 4-methylidene-1*H*-imidazol-5(4*H*)-one

Na_2EDTA: Disodium ethylenediaminetetraacetate

Na_2HPO_4: Disodium hydrogen phosphate

$NaBH_4$: Sodium borohydride

NaCl: Sodium chloride

$NaHCO_3$: Sodium bicarbonate

NaH_2PO_4: Sodium dihydrogen phosphate

NCL: Native Chemical Ligation

NH_4OH: Ammonium hydroxide

NMR: Nuclear Magnetic Resonance

OD: Optical density

PAL: Phenylalanine ammonia lyase

PAM: Phenylalanine aminomutase

PCR: Polymerase chain reaction

PDB: Protein data bank

PLP: Pyridoxal-5′-phosphate

SAM: *S*-adenosyl methionine

SDS-PAGE: Sodium dodecyl sulfate-polyacrylamide gel electrophoresis

TA: Threonine aldolase

TAM: Tyrosine aminomutase

TOF: Time of flight

UCSF: University of California-San Francisco

WWTP: Wastewater treatment plants

Chapter 1: Overview of Biocatalysis in Organic Chemistry and Pharmaceutical Industry

Biocatalysis is defined as the use of living systems or their parts, such as isolated enzymes and microbial-whole cells, to speed up the chemical synthesis of organic compounds.[1] Biocatalytic processes are gradually appearing as an appealing technological alternative in the pharmaceutical industry due to the excellent chemo-, regio-, and stereoselectivity that biocatalysis offers over classical organic synthesis. Such catalysis often avoids using scarce metals, protecting group manipulations, and environmentally hazardous conditions, and involve milder conditions in water at room temperature, higher atom economy, and greener methods.[2]

The Development of Biocatalysis: Its Beginning to Current State of the Art

Humans have been using enzymes for centuries in fermentation to produce cheese, vinegar, and alcoholic beverages. In the modern era, it was the pioneering work of Louis Pasteur on separating a racemic mixture of ammonium tartrate using a culture of the fungus *Penicillium glaucum* that set the first milestone in biocatalysis.[3] Pasteur provided the first application of enzyme-catalyzed kinetic resolution, which is now a widely exercised technique in academia and industry. After this landmark research, biocatalysis advanced in the 20th century, when scientists learned how to use whole-cell cultures, cell extracts, or partially purified enzymes in various biocatalytic processes to make commodity chemicals.[4-8]

Biocatalysis in Its First Wave. Techniques for the isolation and purification of enzymes were subsequently optimized in the mid-20th century. These purified enzyme preparations were used in stereoselective transformations of non-natural substrates and highlight the first wave of biocatalysis.[2,7] Some notable examples include employing a plant extract for the biocatalysis of (*R*)-(+)-mandelonitrile from benzaldehyde and hydrogen cyanide,[4] hydroxylating steroids within

microbial cell hosts,[8] converting glucose to the sweeter fructose isomer using a glucose isomerase,[9] and producing β-lactam antibiotics on an industrial-scale using penicillin G acylase.[10]

Biocatalysis in Its Second Wave. However, the major limitation in enzyme-catalyzed processes until the end of the 1970s was obtaining sufficient enzyme quantities for industrial purposes.[7] Conventional enzyme preparation methods relied on isolating native enzymes from the natural host, such as from microorganisms, insects, plants, or mammalian species.[11] Typically, these native enzymes were present in small amounts, making their application in biocatalysis intractable. With the advent of recombinant DNA technology, enzymes could be overexpressed efficiently in non-native host organisms in a laboratory or industrial setting, marking the second wave of biocatalysis.[1] During this phase, structure-based protein engineering technologies expanded the substrate scope of enzymes and made it possible to biocatalyze a wide variety of non-natural products that could be used as intermediates in chemical synthesis or as final products.[7,11] Notable examples of these biocatalytic transformations include lipase-catalyzed resolution of 3-phenylglycidate esters in the synthesis of the drug diltiazem (used to lower blood pressure),[12] carbonyl-reductase catalyzed synthesis of enantiomerically pure ethyl (*S*)-4-chloro-3-hydroxybutanoate to synthesize statins drugs to lower cholesterol,[13] and nitrile hydratase catalyzed industrial production of acrylic acid and methacrylic acid for the polymer industry.[14]

Biocatalysis in Its Third Wave. The third and the most significant wave of biocatalysis accelerated the speed of biocatalytic optimizations through directed evolution approaches initiated in the mid and late 1990s and is still currently used.[15,16] The *in vitro* molecular biology methods were modeled on Darwinian evolution to rapidly and broadly modify the intrinsic structural and catalytic properties of an enzyme. This Darwinian approach includes random amino acid modification by altering the cDNA encoding the enzyme.[15,16] This technique uses error-prone PCR

or gene shuffling, followed by transforming the cDNA into an expression vector and subcloning in an expression host. The resulting cDNA libraries within these hosts are separately expressed and screened for mutant enzymes with improved thermal and operational stability, and broader substrate acceptance and selectivity, often uninformed by a crystal structure.[11] Industrial-scale biocatalysis primarily focused on ketoreductases (KREDs), hydrolases, cofactor generation, and protein stability in organic solvents.[11,15,16]

As a result of the biocatalysis advancements, remarkable new capabilities and properties were introduced into enzymes, such as accepting previously inert substrates. For example, a KRED from *Microbacterium campoquemadoensis* was engineered to turn over methyl (*E*)-2-(3-(3-(2-(7-chloroquinolin-2-yl)vinyl)phenyl)-3-oxopropyl)benzoate on the biosynthetic pathway of Montelukast,[17] and a transaminase from *Arthrobacter sp.* was modified to accept the substrate prositagliptin on the biosynthetic pathway of sitagliptin.[18,19] Another example includes changing the properties of a sesquiterpene synthase to biosynthesize different sesquiterpenes in *Nicotiana tabacum*[20] by diverting the amino acid metabolism pathway to produce branched-chain alcohols for biofuels.[21] Valuable biotechnological and bioinformatics tools emerged during the third wave of biocatalysis that advanced gene synthesis and sequence analysis, protein engineering technologies (including directed evolution), and computer-based modeling and docking methods. Before this biotechnological windfall, enzymatic processes were designed to offset the limitation in stability and reactivity of the enzymes used, but currently the enzymes are engineered and chosen from a smarter library of variants, suitable for the process specifications.[1,11,15]

The third wave of biocatalysis significantly helped to generalize and widen the use of biocatalysis over the past few decades by complementing synthetic organic chemistry transformations in the pharmaceutical, agrochemical, materials, polymers, food, and fine-chemical

sectors.[7,11,22-24] The pharmaceutical industry has seen a remarkable application of biocatalytic processes.[25] The directed-evolution approach has been successfully commercialized by many companies like Codexis, Merck, Pfizer, and Arch Pharm Labs Limited.[2,11] A notable example includes the development of a biocatalytic route for the commercial production of the antidiabetic compound sitagliptin, which was previously synthesized chemically and marketed as Januvia® (**4**), by Merck. Januvia® was the first marketed antihyperglycemic drug for Type 2 diabetes mellitus and the most widely marketed dipeptidyl peptidase-4 inhibitor worldwide, reaching sales of $6.36 billion in 2014 and expected to reach $7.53 billion in 2020.[26-28] It was only second to insulin glargine amongst the antidiabetics.[11,27]

The first chemical synthesis of sitagliptin was achieved through asymmetric hydrogenation of an enamine (**2**) moiety, derived from prositagliptin (**1**), using a rhodium-based chiral catalyst (Rh-[Josiphos]) under high pressure (250 psi) (**Figure. 1.1A**). This process suffered from inadequate stereoselectivity (97%) for pharmaceutical standards, and the final product was contaminated with rhodium salts, requiring further purification steps at the expense of yield to increase the enantiomeric excess and purity.[29]

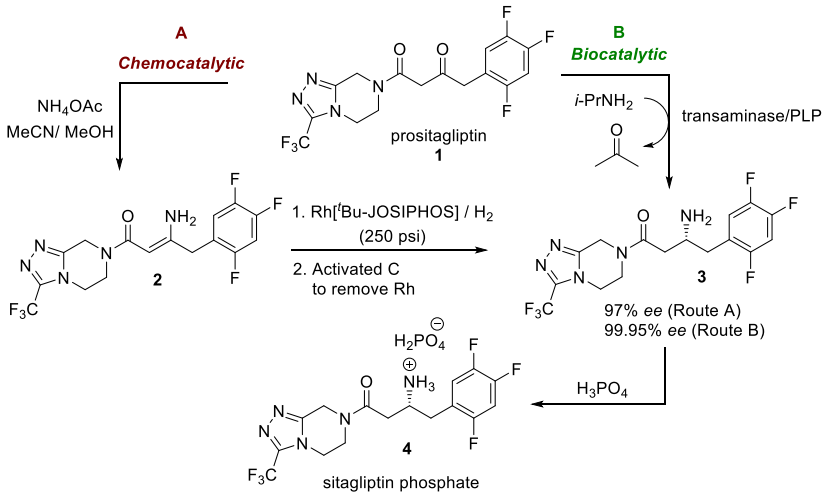

Figure. 1.1. Comparison of chemocatalytic and biocatalytic processes to sitagliptin. (A) Chemocatalytic synthesis of sitagliptin involves enamine (**2**) formation, followed by rhodium-catalyzed asymmetric hydrogenation at high pressure. (B) The biocatalytic route involves direct amination of prositagliptin ketone (**1**), followed by phosphate salt formation to yield enantiopure sitagliptin phosphate (Januvia™) (**4**).

Scientists at Merck and Codexis have recently used a bioengineering approach to rationally design an (*R*)-selective transaminase (ATA-117) and optimize its properties for improved efficiency in sitagliptin manufacturing (**Figure. 1.1B**).[18] ATA-117, a homolog of an enzyme from *Arthrobacter sp*., was initially active only toward methyl and other small cyclic ketones.[30,31] A combination of computational modeling and site-saturation mutagenesis was used to create a larger active site that could bind and turn over a truncated methyl ketone analogue similar to prositagliptin. These efforts resulted in marginal activity, only 4% turnover from 10 g/L enzyme and 2 g/L prositagliptin substrate loading. After 11 rounds of directed evolution and high throughput screening, the best ATA-117 variant was found to catalyze the transaminase reaction with 99.95% e.e. After 27 mutations, the final ATA-117 variant (6 g/L enzyme loading) was capable of converting 200 g/L prositagliptin ketone to sitagliptin in 50% DMSO with a 92% assay yield.[18] In comparison with the Rh-catalyzed process, this biocatalytic route produced sitagliptin with a 13% increase in overall yield, a 53% increase in productivity, and a 19% reduction in total

waste resulting in the elimination of heavy metals and a reduction in total manufacturing cost.[18] This process received the Presidential Green Chemistry Challenge Award (Greener Reaction Conditions Award) from the U.S. Environmental Protection Agency (EPA) in 2010.

Another representative example is the multi-ton scale Codexis protocol of ethyl (*R*)-4-cyano-3-hydroxybutyrate (**7**), a key molecule constituting the side chain of atorvastatin (Lipitor®) (**8**). The cholesterol-lowering drug Lipitor® had global sales of $11.9 billion in 2010. Due to a high demand of **7** for the synthesis of Atorvastatin (estimated to be more than 100 metric tons), it was desirable to minimize the hazardous waste produced and cost involved while maintaining or improving the purity.[32] KREDs and other enzymes were thoroughly investigated to make the chiral intermediates involved in the synthesis of Atorvastatin and other statin analogs. Seven enzymatic processes were developed to vary the KRED properties to obtain the intermediate they were producing on the synthetic pathway (**Figure. 1.2**).[7]

The Codexis protocol (**Figure. 1.2**, Route I) employed a KRED-based reduction of **5** in combination with an NADP-dependent glucose dehydrogenase (GDH) for cofactor regeneration. This reduction produced **6** with 96% isolated yield and 99.5% e.e. The next step was catalyzed by a halohydrin dehalogenase (HHDH) that typically eliminates halides from a vicinal haloalcohol via an epoxide ring.[33,34] HHDH substrate selectivity was honed by directed evolution and could substitute the chloro functional group with a cyano to produce **7**. Codexis was awarded the U.S. Environmental Protection Agency's Presidential Green Chemistry Challenge Award in 2006 for this process.[35] The three-enzyme biocatalytic protocol used milder conditions to produce **7**. The enzymatic process was more favorable to a previously reported chemical synthesis that involved an S_N2 replacement of the halogen with cyanide in alkaline medium (pH 10) at high temperature

(80 °C). These conditions generated many byproducts because both **6** and **7** were not stable in alkaline solution.

The enzymes KRED and HHDH used in the commercial biocatalytic approach to **7** initially showed low activity, significant product inhibition, and poor stability under the operating condition.[27] After *in vitro* optimization through enzyme evolution using gene shuffling techniques resulted in an overall process where the volumetric productivity per mass catalyst load of the cyanation process was improved by ~2500 fold, a 14-fold reduction in reaction time, a 7-fold increase in substrate loading, a 25-fold reduction in enzyme load, and a 50% increase in isolated yield compared to the synthetic route.[32,36]

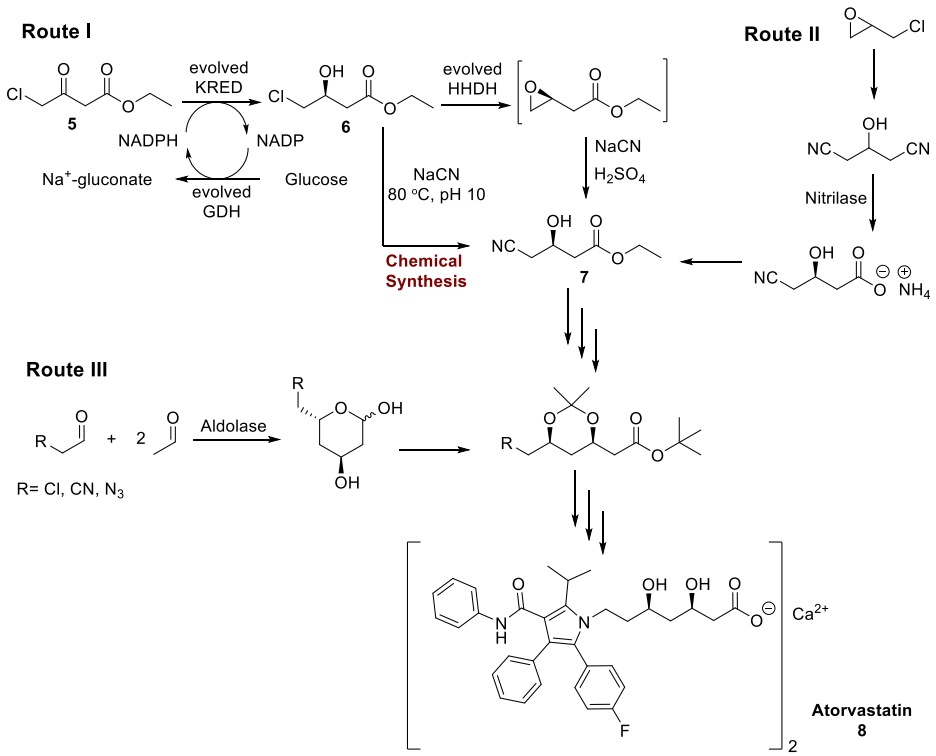

Figure. 1.2. Different enzymatic routes toward the synthesis of the key side chain of Atorvastatin (**8**) (Lipitor®). These routes show a combination of KRED with a halohydrin dehalogenase (HHDH) (*Route I*, developed by Codexis), a nitrilase (*Route II*),[37] or an aldolase (*Route III*).[38]

Biocatalysis is no longer limited to the niches of small-molecule synthesis and application within the pharmaceutical industry. This field of biochemistry has evolved as a desirable

alternative for the ever-increasing demand for renewable energy sources and chemical feedstocks.[25] Recent advancements in laccase-mediated grafting of biopolymers, for example, lignocelluloses, cellulose, and chitosan have the potential to provide environmentally benign alternatives for the wood, textile, and paper industry.[39] Enzymes also have been used successfully as an enhancer in the biodegradation of synthetic polymers in the wastewater system.[40] Hydrolases from wastewater microorganisms were employed to breakdown poly(oxyethylene terephthalate) polymers *in vitro* and under realistic Waste Water Treatment Plants (WWTP) conditions.

Biocatalysis in Its Fourth Wave. The fourth wave of biocatalysis is ongoing. This phase includes a multidisciplinary approach of combining molecular genetics, metagenomics, and bioinformatics tools to discover and even synthesize novel enzymes that did not previously exist in nature. These techniques are combined with the development of multi-enzyme cascade reactions, immobilization methods, and microreactor technologies.[41,42] In fourth-wave biocatalysis, the target enzyme has been through iterative mutations and is often significantly modified compared to the wild type, containing only 10-20% of the wild type residues. As an example, a protein with 300 amino acids has 20^{300} possible sequence combinations of the 20 natural amino acids. The daunting scope of enzyme variants cannot be achieved only using random mutagenesis and high-throughput screening approaches. While the field of *de novo* enzymes is emerging as an exciting alternative in recent years, the resulting enzymes typically have much lower efficiency than what can be achieved from directed evolution techniques.[43,44] In the future, the advances of the fourth wave of biocatalysis need to merge the empirical random mutagenesis data with advanced computational tools to design operation and functional biocatalysts. These two approaches will bode well for managing the large data sets generated across multiple protein evolution projects and will enhance the predictability of machine learning algorithms.

The Application of Epoxides in Biocatalysis

This thesis uses glycidate (epoxide) substrates in an aminotransferase reaction to make stereoisomers of arylserines and arylisoserines; thus, it is fitting to provide a brief overview of the application of epoxides in biocatalysis. Epoxides play a vital role in the biocatalysis of value-added chemicals and pharmaceuticals due to the intrinsic reactivity of the epoxide ring.[45,46] Enzymes that catalyze regio- and stereoselective ring-opening of epoxides include epoxide hydrolases (EHs), halohydrin dehalogenases (HHDHs), glutathione *S*-transferases, and CoM-transferases (**Table 1.1**).[46] Epoxide hydrolases use water as the nucleophile to catalyze the hydrolysis of epoxides to the corresponding diols. The stereoselectivity of epoxide hydrolases can thus also be used for kinetic resolution of racemic epoxide substrates, producing a chiral 1,2-dihydroxy compound while leaving the unreactive epoxide intact.

Table 1.1. Various Enzymatic Processes Involving Epoxides in Microorganisms.

Enzyme	Accepted nucleophile(s)	Example of product(s)
Epoxide hydrolase	H_2O	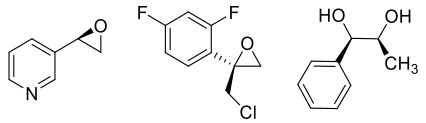
Halohydrin dehalogenase	Cl^-, Br^-, I^-, CN^-, OCN^-, SCN^-, N_3^-, NO_2^-, HCO_2^-	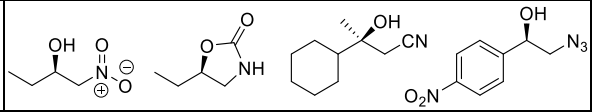
Glutathione-*S*-transferase	GSH, Cys	
CoM-transferase	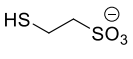	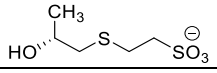

HHDHs are bacterial enzymes involved in the biodegradation of xenobiotic halogenated compounds. They catalyze the reversible dehalogenation of vicinal haloalcohols through intramolecular substitution of a halogen atom to yield an epoxide and halide.[33,46] HHDHs exhibit high regio- and enantioselectivity toward aliphatic and aromatic vicinal haloalcohols, and thus are employed in the production of enantiopure epoxides as well as their ring-opened products.[34,47]

HHDH from *Agrobacterium radiobacter* (*Ar*HHDH) is the best-studied enzyme in this group and is reported to catalyze the epoxide ring-opening reaction with a range of ionic and non-ionic nucleophiles with high enantiomeric excess and high yields.[48,49] The non-halide nucleophiles accepted by the *Ar*HHDH are ambidentate anions with a linear shape that binds inside the tunnel-shaped active site. For example, while HHDHs generally do not accept $–NH_2$ (or NH_3) with sp^3 (tetrahedral) hybridized orbital geometry as a nucleophile, HHDHs can tolerate linear azido nucleophiles to make an azido alcohol from a haloalcohol. The reduction of the azido group accessed the amino alcohols indirectly.[50]

Several other enzymes involved in the microbial conversion of epoxides are also reported in the literature. Glutathione *S*-transferases (GSH) are associated with the detoxification of compounds by their signature tripeptide glutathione (γ-Glu-Cys-Gly) that employs the catalytic thiol group of cysteine, followed by further metabolization.[51,52] Two distinct mechanisms are found for the metabolism of epoxides by glutathione; the most common one involves hydrogen bonding of the thiol group of glutathione to suitable groups of the enzyme, making it more nucleophilic. Alternatively, complexation of the epoxide substrate by metal ion like Mn (II) makes it more electrophilic, facilitating the nucleophilic attack by the glutathione thiol. The complete role of GSH in epoxide metabolism is not yet known.

Epoxides are also common intermediates in the biodegradation of alkenes in bacteria like *Rhodococcus rhodochrous* and *Xanthobacter sp.* where short-chain aliphatic alkenes such as ethylene, propylene, or 1-butene are epoxidized using NADH-dependent monooxygenases. The epoxide then gets carboxylated by CO_2 to form a β-keto acid as the final product by a process catalyzed by a four-component, multi-enzyme system (**Figure. 1.3**). The epoxide is opened by a cofactor M (CoM, 2-mercapto-1-ethyl sulfonate) dependent transferase (**Table 1.1**).[45,53]

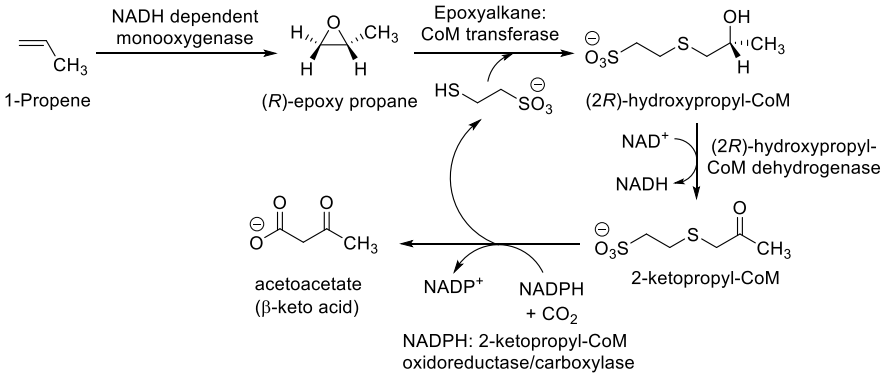

Figure. 1.3. Pathway to acetoacetate from 1-propene in *Xanthobacter sp.*

Biocatalytic Transformations of Epoxide by an Aminotransfer Reaction (Thesis Work).

This thesis describes research done with variously substituted epoxides, 3-arylglycidates. These glycidates are regio- and stereoselectively aminated by employing a phenylalanine aminomutase (PAM) biocatalyst and (2*S*)-styryl-α-alanine as an NH_2 donor to produce *anti*-arylserines as the major products. Phenylalanine aminomutases (PAMs) are responsible for the isomerization of α-phenylalanine to β-phenylalanine.[54] In *Taxus* plants, *Tc*PAM catalyzes the conversion of (2*S*)-α-phenylalanine (**9**) to (3*R*)-β-phenylalanine (**10**), which is the biosynthetic precursor of the phenylisoserinyl side chain of anticancer drug Taxol (**11**) (**Figure. 1.4**).[55-57] The excellent product enantioselectivity (99.9 % e.e.) and broad substrate scope of *Tc*PAM make it an attractive biocatalyst for β-phenylalanine production.[58]

In earlier work, (2*S*)-styryl-α-alanine was used as a non-natural substrate to achieve aminotransferase activity using *Tc*PAM, transferring an amino group from (2*S*)-styryl-α-alanine to exogenously supplied acrylate moieties to make α- and β-amino acids.[59]

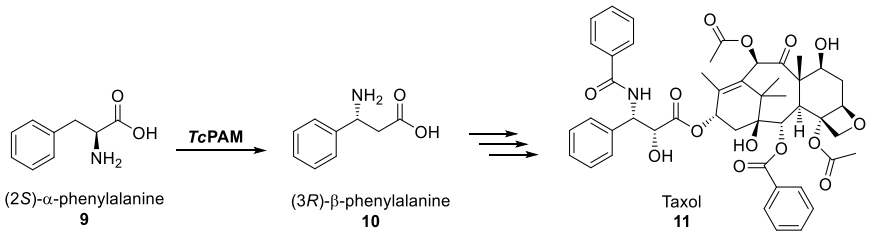

Figure. 1.4. Partial biosynthesis of Taxol from (2*S*)-α-phenylalanine in *Taxus* plants.

In this work, a new class of acceptor molecules, 3-arylglycidates, were successfully transaminated using (2*S*)-styryl-α-alanine (**12**) and *Tc*PAM to produce arylserines and arylisoserines (**Figure. 1.5**).[60] Arylserine and arylisoserine scaffolds are found in clinically significant antibiotics, including vancomycin and its analogues,[61,62] ristocetin from *Amycolatopsis* and teicoplanins from *Actinoplanes*,[63] chloramphenicol from *Streptomyces*,[64] katanosin depsipeptides from *Cytophaga* and *Lysobacter* bacteria,[65] and the antineoplastic agent paclitaxel from *Taxus spp.* and its analogues.[57,66] Given the beneficial pharmacological, chemical, and physical properties of these aromatic hydroxy amino acids, there is considerable interest in making these bifunctional molecules either synthetically, biocatalytically, or by a combination of both approaches.

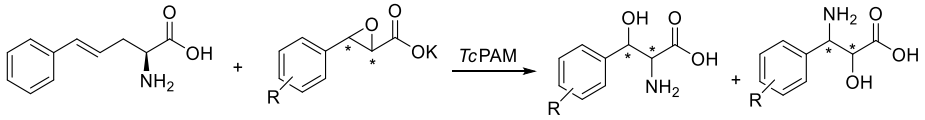

Figure. 1.5. Biocatalysis of arylserine and arylisoserine analogues from *trans*-3-arylglycidates and (2*S*)-styryl-α-alanine (**12**) by using an MIO-aminomutase. The asterisks (*) identify a chiral center.

REFERENCES

REFERENCES

1. Arnold, F. H. (2001) Combinatorial and Computational Challenges for Biocatalyst Design, *Nature 409*, 253-257.

2. Truppo, M. D. (2017) Biocatalysis in the Pharmaceutical Industry: The Need for Speed, *ACS Med. Chem. Lett. 8*, 476-480.

3. Pasteur, L. (1858) Mémoire Sur La Fermentation De L'acide Tartrique., *C. R. Acad. Sci. 46*, 615-618.

4. Rosenthaler, L. (1908) Durch Enzyme Bewirkte Ssymmetrische Synthesen, *Biochem. Z 14*, 238-253.

5. Drauz, K., Gröeger, H., and May, O. (2012) Enzyme Catalysis in Organic Synthesis a Comprehensive Handbook, Third, completely revised and enlarged edition / ed., pp 3 volumes (lii, 1985 pages), Wiley-VCH,, Weinheim, Germany.

6. Ortiz de Montellano, P. R. (2005) *Cytochrome P450 : Structure, Mechanism, and Biochemistry*, Third edition. ed., Kluwer Academic/Plenum Publishers, New York.

7. Bornscheuer, U. T., Huisman, G. W., Kazlauskas, R. J., Lutz, S., Moore, J. C., and Robins, K. (2012) Engineering the Third Eave of Biocatalysis, *Nature 485*, 185-194.

8. Sedlaczek, L., and Smith, L. L. (1988) Biotransformations of Steroids, *Crit. Rev. Biotechnol. 7*, 187-236.

9. Jensen, V. J., and Rugh, S. (1987) [33] Industrial-Scale Production and Application of Immobilized Glucose Isomerase In *Methods Enzymol.*, Vol. 136, pp 356-370, Academic Press.

10. Bruggink, A., Roos, E. C., and de Vroom, E. (1998) Penicillin Acylase in the Industrial Production of β-Lactam Antibiotics, *Org. Process Res. Dev. 2*, 128-133.

11. Reetz, M. T. (2013) Biocatalysis in Organic Chemistry and Biotechnology: Past, Present, and Future, *J. Am. Chem. Soc. 135*, 12480-12496.

12. Matsumae, H., Furui, M., and Shibatani, T. (1993) Lipase-Catalyzed Asymmetric Hydrolysis of 3-Phenylglycidic Acid Ester, the Key Intermediate in the Synthesis of Diltiazem Hydrochloride, *J. Ferment. Bioeng. 75*, 93-98.

13. Ye, Q., Ouyang, P., and Ying, H. (2011) A Review—Biosynthesis of Optically Pure Ethyl (*S*)-4-Chloro-3-Hydroxybutanoate Ester: Recent Advances and Future Perspectives, *Appl. Microbiol. Biotechnol. 89*, 513-522.

14. Nagasawa, T., Nakamura, T., and Yamada, H. (1990) Production of Acrylic Acid and Methacrylic Acid Using *Rhodococcus rhodochrous* J1 Nitrilase, *Appl. Microbiol. Biotechnol. 34*, 322-324.

15. Arnold, F. H. (2015) The Nature of Chemical Innovation: New Enzymes by Evolution, *Q. Rev. Biophys. 48*, 404-410.

16. Denard, C. A., Ren, H., and Zhao, H. (2015) Improving and Repurposing Biocatalysts via Directed Evolution, *Curr. Opin. Chem. Biol. 25*, 55-64.

17. Liang, J., Lalonde, J., Borup, B., Mitchell, V., Mundorff, E., Trinh, N., Kochrekar, D. A., Nair Cherat, R., and Pai, G. G. (2010) Development of a Biocatalytic Process as an Alternative to the (−)-DIP-Cl-Mediated Asymmetric Reduction of a Key Intermediate of Montelukast, *Org. Process Res. Dev. 14*, 193-198.

18. Savile, C. K., Janey, J. M., Mundorff, E. C., Moore, J. C., Tam, S., Jarvis, W. R., Colbeck, J. C., Krebber, A., Fleitz, F. J., Brands, J., Devine, P. N., Huisman, G. W., and Hughes, G. J. (2010) Biocatalytic Asymmetric Synthesis of Chiral Amines from Ketones Applied to Sitagliptin Manufacture, *Science 329*, 305-309.

19. Desai, A. A. (2011) Sitagliptin Manufacture: A Compelling Tale of Green Chemistry, Process Intensification, and Industrial Asymmetric Catalysis, *Angew. Chem. Int. Ed. 50*, 1974-1976.

20. O'Maille, P. E., Malone, A., Dellas, N., Andes Hess, B., Smentek, L., Sheehan, I., Greenhagen, B. T., Chappell, J., Manning, G., and Noel, J. P. (2008) Quantitative Exploration of the Catalytic Landscape Separating Divergent Plant Sesquiterpene Synthases, *Nat. Chem. Biol. 4*, 617-623.

21. Atsumi, S., Hanai, T., and Liao, J. C. (2008) Non-Fermentative Pathways for Synthesis of Branched-Chain Higher Alcohols As Biofuels, *Nature 451*, 86-89.

22. Turner, N. J., and Truppo, M. D. (2013) Biocatalysis Enters a New Era, *Curr. Opin. Chem. Biol. 17*, 212-214.

23. Bezborodov, A. M., and Zagustina, N. A. (2016) Enzymatic Biocatalysis in Chemical Synthesis of Pharmaceuticals (Review), *Appl. Biochem. Microbiol. 52*, 237-249.

24. Griengl, H., Schwab, H., and Fechter, M. (2000) The Synthesis of Chiral Cyanohydrins by Oxynitrilases, *Trends Biotechnol. 18*, 252-256.

25. Pollard, D. J., and Woodley, J. M. (2007) Biocatalysis for Pharmaceutical Intermediates: The Future Is Now, *Trends Biotechnol. 25*, 66-73.

26. Alcántara, C. M., and Alcántara, A. R. (2018) Biocatalyzed Synthesis of Antidiabetic Drugs: A Review, *Biocatal. Biotransform. 36*, 12-46.

27. Alcántara, A. R. (2017) Biotransformations in Drug Synthesis : A Green and Powerful Tool for Medicinal Chemistry, *J. Med. Chem. Drug Des. 1*, 1-7.

28. da Rocha Fernandes, J., Ogurtsova, K., Linnenkamp, U., Guariguata, L., Seuring, T., Zhang, P., Cavan, D., and Makaroff, L. E. (2016) IDF Diabetes Atlas Estimates of 2014 Global Health Expenditures on Diabetes, *Diabetes Res. Clin. Pract. 117*, 48-54.

29. Hansen, K. B., Hsiao, Y., Xu, F., Rivera, N., Clausen, A., Kubryk, M., Krska, S., Rosner, T., Simmons, B., Balsells, J., Ikemoto, N., Sun, Y., Spindler, F., Malan, C., Grabowski, E. J. J., and Armstrong, J. D. (2009) Highly Efficient Asymmetric Synthesis of Sitagliptin, *J. Am. Chem. Soc. 131*, 8798-8804.

30. Truppo, M. D., Turner, N. J., and Rozzell, J. D. (2009) Efficient Kinetic Resolution of Racemic Amines Using a Transaminase in Combination With an Amino Acid Oxidase, *Chem. Commun.*, 2127-2129.

31. Koszelewski, D., Clay, D., Rozzell, D., and Kroutil, W. (2009) Deracemisation of α-Chiral Primary Amines by a One-Pot, Two-Step Cascade Reaction Catalysed by ω-Transaminases, *Eur. J. Org. Chem. 2009*, 2289-2292.

32. Ma, S. K., Gruber, J., Davis, C., Newman, L., Gray, D., Wang, A., Grate, J., Huisman, G. W., and Sheldon, R. A. (2010) A Green-by-Design Biocatalytic Process for Atorvastatin Intermediate, *Green Chem. 12*, 81-86.

33. Hasnaoui-Dijoux, G., Majerić Elenkov, M., Lutje Spelberg, J. H., Hauer, B., and Janssen, D. B. (2008) Catalytic Promiscuity of Halohydrin Dehalogenase and its Application in Enantioselective Epoxide Ring Opening, *ChemBioChem 9*, 1048-1051.

34. Lutje Spelberg, J. H., Tang, L., van Gelder, M., Kellogg, R. M., and Janssen, D. B. (2002) Exploration of the Biocatalytic Potential of a Halohydrin Dehalogenase Using Chromogenic Substrates, *Tetrahedron Asymmetry 13*, 1083-1089.

35. Ritter, S. K. (2006) GOING GREEN KEEPS GETTING EASIER, *Chem. Eng. News 84*, 24-27.

36. Pilar, H., Vittorio, P., María, J. H., and Andres, R. A. (2014) Biocatalysis in the Pharmaceutical Industry. A Greener Future, *Curr. Green Chem. 1*, 155-181.

37. Bergeron, S., Chaplin, D. A., Edwards, J. H., Ellis, B. S. W., Hill, C. L., Holt-Tiffin, K., Knight, J. R., Mahoney, T., Osborne, A. P., and Ruecroft, G. (2006) Nitrilase-Catalysed Desymmetrisation of 3-Hydroxyglutaronitrile: Preparation of a Statin Side-Chain Intermediate, *Org. Process Res. Dev. 10*, 661-665.

38. Greenberg, W. A., Varvak, A., Hanson, S. R., Wong, K., Huang, H., Chen, P., and Burk, M. J. (2004) Development of an Efficient, Scalable, Aldolase-Catalyzed Process for Enantioselective Synthesis of Statin Intermediates, *Proc. Natl. Acad. Sci. U S A 101*, 5788.

39. Slagman, S., Zuilhof, H., and Franssen, M. C. R. (2018) Laccase-Mediated Grafting on Biopolymers and Synthetic Polymers: A Critical Review, *ChemBioChem 19*, 288-311.

40. Haernvall, K., Zitzenbacher, S., Biundo, A., Yamamoto, M., Schick, M. B., Ribitsch, D., and Guebitz, G. M. (2018) Enzymes as Enhancers for the Biodegradation of Synthetic Polymers in Wastewater, *ChemBioChem 19*, 317-325.

41. Poppe, L., and Vértessy, B. G. (2018) The Fourth Wave of Biocatalysis Emerges— The 13th International Symposium on Biocatalysis and Biotransformations, *ChemBioChem 19*, 284-287.

42. Kries, H., Blomberg, R., and Hilvert, D. (2013) *De Novo* Enzymes by Computational Design, *Curr. Opin. Chem. Biol. 17*, 221-228.

43. Obexer, R., Pott, M., Zeymer, C., Griffiths, A. D., and Hilvert, D. (2016) Efficient Laboratory Evolution of Computationally Designed Enzymes With Low Starting Activities Using Fluorescence-Activated Droplet Sorting, *Protein Eng. Des. Sel. 29*, 355-366.

44. Garrabou, X., Verez, R., and Hilvert, D. (2017) Enantiocomplementary Synthesis of γ-Nitroketones Using Designed and Evolved Carboligases, *J. Am. Chem. Soc. 139*, 103-106.

45. de Vries, E. J., and Janssen, D. B. (2003) Biocatalytic Conversion of Epoxides, *Curr. Opin. Biotechnol. 14*, 414-420.

46. Nestl, B. M., Hammer, S. C., Nebel, B. A., and Hauer, B. (2014) New Generation of Biocatalysts for Organic Synthesis, *Angew. Chem. Int. Ed. 53*, 3070-3095.

47. Lutje Spelberg, J. H., Tang, L., Kellogg, R. M., and Janssen, D. B. (2004) Enzymatic Dynamic Kinetic Resolution of Epihalohydrins, *Tetrahedron Asymmetry 15*, 1095-1102.

48. de Jong, R. M., Tiesinga, J. J. W., Rozeboom, H. J., Kalk, K. H., Tang, L., Janssen, D. B., and Dijkstra, B. W. (2003) Structure and Mechanism of a Bacterial Haloalcohol Dehalogenase: A New Variation of the Short-Chain Dehydrogenase/Reductase Fold Without an NAD(P)H Binding Site, *The EMBO Journal 22*, 4933-4944.

49. de Jong, R. M., Tiesinga, J. J. W., Villa, A., Tang, L., Janssen, D. B., and Dijkstra, B. W. (2005) Structural Basis for the Enantioselectivity of an Epoxide Ring Opening Reaction Catalyzed by Halo Alcohol Dehalogenase HheC, *J. Am. Chem. Soc. 127*, 13338-13343.

50. Lutje Spelberg, J. H., van Hylckama Vlieg, J. E. T., Tang, L., Janssen, D. B., and Kellogg, R. M. (2001) Highly Enantioselective and Regioselective Biocatalytic Azidolysis of Aromatic Epoxides, *Org. Lett. 3*, 41-43.

51. Anderson, M. E. (1998) Glutathione: An Overview of Biosynthesis and Modulation, *Chem. Biol. Interact. 111-112*, 1-14.

52. Laughlin, L. T., Bernat, B. A., and Armstrong, R. N. (1998) Mechanistic Imperative for the Evolution of a Metalloglutathione Transferase of the Vicinal Oxygen Chelate Superfamily, *Chem. Biol. Interact. 111-112*, 41-50.

53. Clark, D. D., Allen, J. R., and Ensign, S. A. (2000) Characterization of Five Catalytic Activities Associated with the NADPH:2-Ketopropyl-coenzyme M [2-(2-Ketopropylthio)ethanesulfonate] Oxidoreductase/Carboxylase of the *Xanthobacter* Strain Py2 Epoxide Carboxylase System, *Biochemistry 39*, 1294-1304.

54. Wu, B., Szymański, W., Heberling, M. M., Feringa, B. L., and Janssen, D. B. (2011) Aminomutases: Mechanistic Diversity, Biotechnological Applications and Future Perspectives, *Trends Biotechnol. 29*, 352-362.

55. Feng, L., Wanninayake, U., Strom, S., Geiger, J., and Walker, K. D. (2011) Mechanistic, Mutational, and Structural Evaluation of a *Taxus* Phenylalanine Aminomutase, *Biochemistry 50*, 2919-2930.

56. Walker, K. D., and Floss, H. G. (1998) Detection of a Phenylalanine Aminomutase in Cell-Free Extracts of *Taxus brevifolia* and Preliminary Characterization of Its Reaction, *J. Am. Chem. Soc. 120*, 5333-5334.

57. Walker, K. D., Klettke, K., Akiyama, T., and Croteau, R. (2004) Cloning, Heterologous Expression, and Characterization of a Phenylalanine Aminomutase Involved in Taxol Biosynthesis, *J. Biol. Chem. 279*, 53947-53954.

58. Klettke, K. L., Sanyal, S., Mutatu, W., and Walker, K. D. (2007) β-Styryl- and β-Aryl-β-Alanine Products of Phenylalanine Aminomutase Catalysis, *J. Am. Chem. Soc. 129*, 6988-+.

59. Wanninayake, U., Deporre, Y., Ondari, M., and Walker, K. D. (2011) (*S*)-Styryl-α-Alanine Used to Probe the Intermolecular Mechanism of an Intramolecular MIO-Aminomutase, *Biochemistry 50*, 10082-10090.

60. Shee, P. K., Ratnayake, N. D., Walter, T., Goethe, O., Onyeozili, E. N., and Walker, K. D. (2019) Exploring the Scope of an α/β-Aminomutase for the Amination of Cinnamate Epoxides to Arylserines and Arylisoserines, *ACS Catal. 9*, 7418-7430.

61. Evans, D. A., Wood, M. R., Trotter, B. W., Richardson, T. I., Barrow, J. C., and Katz, J. L. (1998) Total Syntheses of Vancomycin and Eremomycin Aglycons, *Angew. Chem. Int. Ed. 37*, 2700-2704.

62. Rao, A. V. R., Gurjar, M. K., Reddy, K. L., and Rao, A. S. (1995) Studies Directed Toward the Synthesis of Vancomycin and Related Cyclic Peptides, *Chem. Rev. 95*, 2135-2167.

63. Hughes, C. S., Longo, E., Phillips-Jones, M. K., and Hussain, R. (2017) Characterisation of the Selective Binding of Antibiotics Vancomycin and Teicoplanin by the VanS Receptor Regulating Type a Vancomycin Resistance in the Enterococci, *Biochim. Biophys. Acta Gen. Subj. 1861*, 1951-1959.

64. Fraunfelder, F. W., and Fraunfelder, F. T. (2013) Restricting Topical Ocular Chloramphenicol Eye Drop Use in the United States. Did We Overreact?, *Am. J. Ophthalmol. 156*, 420-422.

65. Goldstein, D. S. (2006) L-Dihydroxyphenylserine (L-DOPS): A Norepinephrine Prodrug, *Cardiovasc. Drug Rev. 24*, 189-203.

66. Gueritte-Voegelein, F., Guenard, D., Lavelle, F., Le Goff, M. T., Mangatal, L., and Potier, P. (1991) Relationships Between the Structure of Taxol Analogs and Their Antimitotic Activity, *J. Med. Chem. 34*, 992-998.

Chapter 2: Biocatalysis of Arylserines and Arylisoserines using Phenylalanine Aminomutase from *Taxus canadensis* (*Tc*PAM) and 3-Arylglycidate Racemates.

2.1 Introduction

2.1.1 Aminomutases: Enzyme Class (EC) of 1,2-Amino Acid Isomerases

Isomerases (EC 5) are a general class of enzymes that convert a molecule from one isomer to another.[1] The intermolecular isomerase (EC 5.4) family has enzymes that promote the transfer of an acyl-, phospho-, amino-, hydroxy- or other functional group from one position of a molecule to another.[2] Aminomutases (AMs) (EC 5.4.3) are a subclass of enzymes that catalyze reversible cross-exchange of an amino group and a proton on vicinal carbons of a substrate (**Figure. 2.1**).[3]

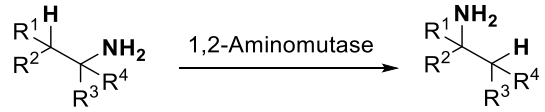

Figure. 2.1. 1,2-Amino group isomerization catalyzed by aminomutases.

The AM family has gained much attention due to the application of the biocatalysts in the synthesis of medicinally important molecules.[4] This family is comprised of lysine 2,3- (EC 5.4.3.2),[5,6] β-lysine 5,6- (EC 5.4.3.3),[7-9] D-lysine 5,6- (EC 5.4.3.4),[10,11] D-ornithine 4,5- (EC 5.4.3.5),[12,13] tyrosine 2,3- (EC 5.4.3.6),[14-20] leucine 2,3- (EC 5.4.3.7),[21,22] glutamate-1-semialdehyde 2,1- (EC 5.4.3.8),[23,24] glutamate 2,3- (EC 5.4.3.9),[25] and phenylalanine (EC 5.4.3.10[26,27] and 5.4.3.11[28,29]) aminomutases. A 2-*aza*-L-tyrosine 2,3-aminomutase was discovered, and based on amino acid sequence homology, likely belongs to EC 5.4.3-K21227.[30] The catalytic properties of these

aminomutases make them attractive for synthetic applications because of their regio- and enantioselectivity, and potential for the preparation of valuable non-natural β-amino acids.[3]

2.1.2 Mechanistic Diversity of Aminomutases

Aminomutases use various cofactors to catalyze the vicinal exchange of the amino group and proton in a molecule. The aminomutase reaction mechanism can be classified into a homolytic or heterolytic pathway. The mechanisms of lysine 2,3-,[5,6] β-lysine 5,6-,[7-9] D-lysine 5,6-,[10,11] D-ornithine 4,5-,[12,13] leucine 2,3-,[21,22] and glutamate 2,3-aminomutases[25] involve radical intermediates, and thus follow a homolytic pathway. These enzymes use either *S*-adenosyl methionine (SAM), pyridoxal 5′-phosphate (PLP), and a $[4Fe\text{-}4S]^{+}$ (iron-sulfur) cluster or adenosylcobalamin (vitamin B12) and PLP as cofactors. Tyrosine 2,3-[14-20] and phenylalanine aminomutases[26-29] catalyze their isomerization reaction using the heterolytic pathway to break and make bonds and require a 4-methylidene-1*H*-imidazol-5(4*H*)-one (MIO) catalytic group made by the backbone residues in the active site.

2.1.3 MIO-dependent Aminomutases

The MIO-dependent aminomutases catalyze the isomerization of α/β-amino acid via a heterolytic mechanism.[27,31] In 1998, Walker and coworkers reported on the activity of an aminomutase in the cell-free extracts from *Taxus brevifolia* plant tissue.[26] It was the first-ever reported aminomutase from a higher plant and also the first phenylalanine aminomutase from any source. It catalyzed the conversion of (2*S*)-α-phenylalanine to (3*R*)-β-phenylalanine *en route* to the biosynthesis of anti-cancer drug Taxol.[26] It was shown that the intramolecular isomerization proceeded with retention of configuration at the C_{β}, which was different from single-electron transfer mechanisms used by microbial aminomutases characterized at the time. However, no claims were made that the AM from *T. brevifolia* was MIO-dependent.

Five years after the discovery of the *T. brevifolia* aminomutase activity, Christenson and coworkers discovered a novel MIO-dependent tyrosine aminomutase from *Streptomyces globisporus* (*Sg*TAM) that showed high homology with a histidine ammonia lyase from *Streptomyces griseus* (39% identity and 56% similarity)[32] and a phenylalanine ammonia lyase from *Streptomyces maritimus* (38% identity and 56% similarity).[33] Each of these MIO-dependent enzymes has the signature Ala-Ser-Gly motif that is the origin of this MIO-moiety in the active site. *Sg*TAM converts (2*S*)-α-tyrosine to (3*S*)-β-tyrosine during the biosynthesis of enediyne antitumor antibiotic C-1027.[31] The MIO-moiety was previously identified by X-ray crystallographic analysis of a histidine ammonia lyase from *Pseudomonas putida* (EC 4.3.1.3), [34] and the Ala-Ser-Gly residues were proposed to cyclize and form the MIO-group autocatalytically through sequential condensation reactions (**Figure. 2.2**A). Based on previous studies that verified the function of the MIO,[35-37] *Sg*TAM was incubated with $NaBH_4$ (10 mM) or KCN (2 mM). These nucleophilic reactants abrogated the aminomutase activity by fouling the reactivity of the MIO, as the nucleophile acceptor (**Figure. 2.2**B). Additionally, mutation of the serine residue (S153A) of the MIO triad decreased the *Sg*TAM activity by 340-fold. This analogous mutation in other MIO-dependent enzymes also reduced the activity.[31] These results suggested that *Sg*TAM relied on a catalytic MIO-moiety.

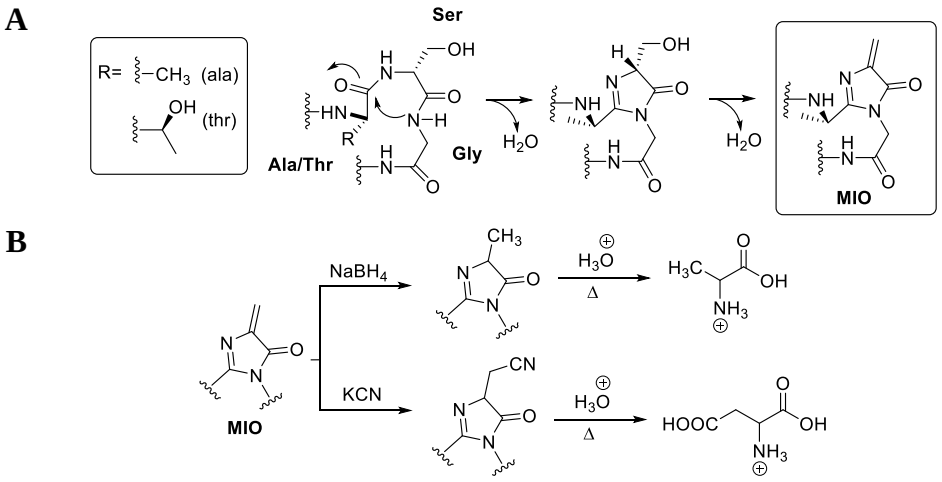

Figure. 2.2. A) The mechanism of how the MIO forms from a conserved triad of active site residues. B) Reactions of the MIO moiety with nucleophiles from $NaBH_4$ or KCN resulted in the loss of aminomutase activity due to MIO- inactivation.

In 2004, a random sequencing of a cDNA library derived from *Taxus cuspidata* cells that provided them several of the twelve defined genes of Taxol biosynthesis, including a PAM.[38] A gene cloning method was used to acquire a phenylalanine ammonia lyase (PAL)-like sequence from the *Taxus cuspidata* cDNA library and expressed in *Escherichia coli*.[27] The expressed enzyme was confirmed as an AM that was identical to the recombinant AM from *Taxus chinensis* acquired earlier by reverse genetic approach.[39] This PAM from *Taxus sp.* (*Tc*PAM) contained the signature ASG motif in the active site, identifying the mutase as MIO-dependent.[27] Both plant *Tc*PAM and bacterial *Sg*TAM form their MIO by condensation of the Ala-Ser-Gly residues,[26,31] while the aminomutase from *Pantoea agglomerans* (*Pa*PAM) uses a *Thr*-Ser-Gly sequence.[28]

2.1.4 Overview of Aryl Amino Acid Aminomutases

MIO-dependent aminomutases have been discovered on various biosynthetic pathways (**Table 2.1**). The mutases isomerize (2*S*)-α-amino acids to non-proteinogenic β-amino acids by intramolecular 2,3-amino group transfer. *Tc*PAM and *Pa*PAM catalyze the production of β-phenylalanine on the pathways to Taxol and the antibiotic andrimid, respectively.[27,40] The bacterial *Sg*TAM is on the biosynthetic pathway to the antitumor antibiotic C-1027, and a TAM from

Chondromyces cracatus (*Cc*TAM) produces β-tyrosine on the pathway to cytotoxic chondramides.[18] Other instances of TAMs include *Os*TAM from rice (*Oryza sativa*),[16] MdpC4 TAM from *Actinomadura madurae* on the pathway to the antitumor and antibiotic maduropeptin,[41] *Mf*TAM from *Myxococcus fulvus* and *Mx*TAM from *Myxococcus sp.* are involved in the biosynthesis of myxovalargin,[19] and KedY4 from *Streptoalloteichus sp.* Lies on the pathway to the antitumor and antibiotic kedarcidin.[30] KedY4 stereoselectively catalyzes the conversion of (2*S*)-α-2-aza-tyrosine to (3*R*)-β-2-aza-tyrosine, and it is also the first MIO-dependent aminomutase to accept a heteroaromatic amino acid as a substrate.[30]

2.1.5 MIO Function

The electrophilic methylidene group of MIO gets *N*-alkylated transiently by the α-amino group of the substrate (**Figure. 2.3**). The resulting *N*-alkylated ammonium group is then displaced as an MIO-NH_2 adduct with simultaneous removal of H_β by a catalytic Tyr residue.

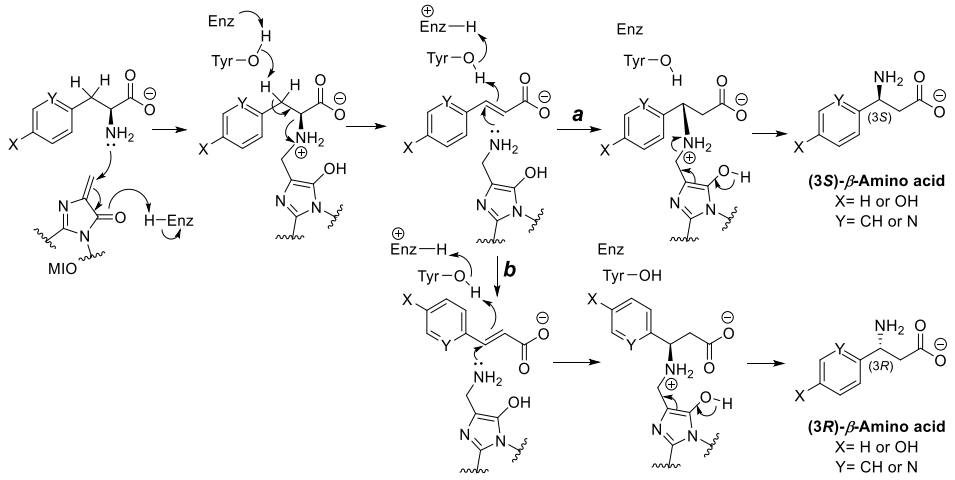

Figure. 2.3. The mechanism of MIO-aminomutase catalyzed reaction via an amino-alkylation intermediate to make a β-amino acid. *Route a*: the (3*S*)-β-arylalanine isomer is made via a pathway where the acrylate intermediate does not rotate before being re-aminated at the C_β. *Route b*: the (3*R*)-isomer via a pathway where the arylacrylate intermediate rotates inside the active site before being re-aminated at the C_β.

This elimination reaction produces an arylacrylate intermediate, which is released in the lyase reaction, yet primarily serves as a scaffold for stereospecific amination at C_β to produce β-amino acids. For example, *Tc*PAM, *Cc*TAM, and *Os*TAM catalyze the (3*R*)-β-amino acid from the (2*S*)-α-amino acid. On this pathway, the arylacrylate intermediate is proposed to rotate in the active site before β-amination, resulting in the delivery of the amine group to the *re*-face of the arylacrylate to produce the (3*R*)-β-isomer (**Figure. 2.3**).

The stereoconfigurations of the final biocatalyzed products and the migratory groups (NH_2 and H) have been studied extensively for both phenylalanine- (PAMs) and tyrosine aminomutases (TAMs) (**Table 2.1**). These enzymes can be categorized based on the absolute configuration of the biocatalyzed β-amino acid. *Sg*TAM[31] and *Pa*PAM[40] produce (3*S*)-β-arylalanines, while *Tc*PAM[42] and *Cc*TAM[18] catalyze the formation of (3*R*)-β-enantiomer. However, TAMs exhibit less enantioselectivity compared to the PAMs. TAMs produce one enantiomer of the β-amino acid under kinetic control, but the opposite enantiomer is also produced when equilibrium is reached after prolonged incubation of the enzyme with the substrate.[19,31] As an example, *Sg*TAM produces (3*S*)-β-tyrosine as the major product initially. As the reaction proceeds, the 3*R*:3*S* ratio approaches 1:1 after prolonged incubation likely due to the partial inversion and retention of stereoconfiguration pathways used by TAMs.[3,18,31,43] By comparison, *Cc*TAM produces a mixture of (3*R*)-β-tyrosine (90%) and (3*S*)-β-tyrosine (10%) initially, and the 3*R*:3*S* ratio of the mixture reached 85:15 as the reaction reached equilibrium.[14] The product distribution of *Cc*TAM also varies with pH, At pH 7, the 3*R*:3*S* ratio was at 83:17, and then changed to 73:27 at pH 9. *Os*TAM from rice plants, however, has better enantioselectivity among the TAMs and makes (3*R*)-β-tyrosine predominantly (97%) with 3% (3*S*)-β-enantiomer, the 97:3 *R*:*S* was kept over a pH range from 7-10 over 24 h incubation.

Table 2.1. Stereochemistry of β-Arylalanine Products Catalyzed by MIO-Dependent Aminomutases and Their Corresponding Biosynthetic Products.

Enzyme	Substrate	Product	Configuration at C_α and C_β	Biosynthetic product
Phenylalanine Aminomutase (*Taxus sp.*)	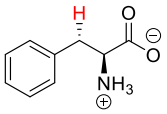 (2*S*)-α-phenylalanine	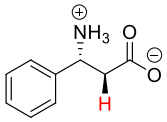 (3*R*)-β-phenylalanine	Retention	Anti-cancer Taxol
Phenylalanine Aminomutase (*Pantoea agglomerans*)	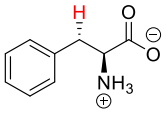 (2*S*)-α-phenylalanine	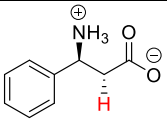 (3*S*)-β-phenylalanine	Unknown	Antibiotic andrimid
Tyrosine Aminomutase (*Streptomyces globisporus*)	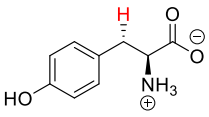 (2*S*)-α-tyrosine	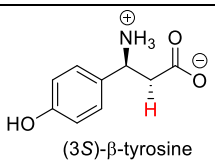 (3*S*)-β-tyrosine	Inversion	Antitumor antibiotic C-1027
		1:1 (3*S*):(3*R*)-β-tyrosine at equilibrium	Inversion and retention	
Tyrosine Aminomutase (*Chondromyces cracatus*)	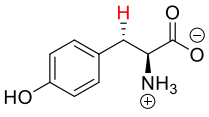 (2*S*)-α-tyrosine	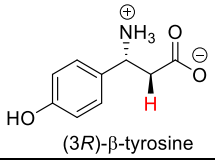 (3*R*)-β-tyrosine	Retention	Cytotoxic chondramides
		6:1 (3*R*):(3*S*)-β-tyrosine at equilibrium	Inversion and retention	
Tyrosine Aminomutase (*Oryza sativa*)	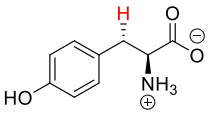 (2*S*)-α-tyrosine	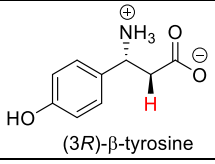 (3*R*)-β-tyrosine	Retention	Unknown
Tyrosine Aminomutase (*Actinomadura madurae*)	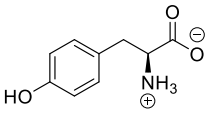 (2*S*)-α-tyrosine	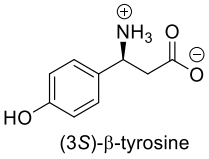 (3*S*)-β-tyrosine	Unknown	Antitumor antibiotic maduropeptin
Tyrosine Aminomutase (*Myxococcus sp.*)				Bacterial protein biosynthesis inhibitor myxovalargin
2-Aza-tyrosine Aminomutase (*Streptoalloteichus sp.*)	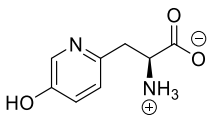 (2*S*)-2-aza-tyrosine	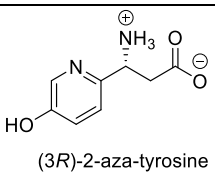 (3*R*)-2-aza-tyrosine	Unknown	Antitumor antibiotic kedarcidin

Thus, TAMs catalyze the isomerization reaction with both inversion and retention of configuration at the α- and β-carbons giving mixtures of enantiomers for the product. By contrast, PAMs are highly enantioselective (>99.9%), and thus are projected to be more suitable for applications in

scalable biocatalytic production of enantiopure β-arylalanines as synthetic building block for pharmaceuticals.[44-49]

2.1.6 Intramolecular and Intermolecular Mechanisms of MIO-Aminomutases

2.1.6.1 Transaminase Studies of *Tc*PAM Using (2*S*)-Styryl-α-alanine as Amine Donor

*Tc*PAM catalyzes the formation of (3*R*)-β-phenylalanine with intramolecular exchange of the α-amino group and the *pro*-(3*S*)-proton with retention-of-configuration at both the reaction termini.[42,50] *Tc*PAM was co-incubated with both [^{15}N]-(*S*)-*α*-phenylalanine and [ring,3-$^{2}H_6$]-(*E*)-cinnamate, and there was 97% incorporation of the [^{15}N]amino group intramolecularly into (*R*)-*β*-phenylalanine. However, a small amount (3%) of [^{15}N,$^{2}H_6$]-*β*-phenylalanine also formed due to intermolecular amine transfer from the crossover reaction (**Figure. 2.4**A).[50] This discovery set up the platform for exploring further transaminase studies with *Tc*PAM. Various non-natural amino acids were tested as the initial amine donor substrate and (2*S*)-styryl-α-alanine was found to be 1.5 times faster than the natural substrate (2*S*)-α-phenylalanine, and *Tc*PAM predominantly catalyzed the formation of (2*E*,4*E*)-styrylacrylate (99%) with only 1% β-aminated product.

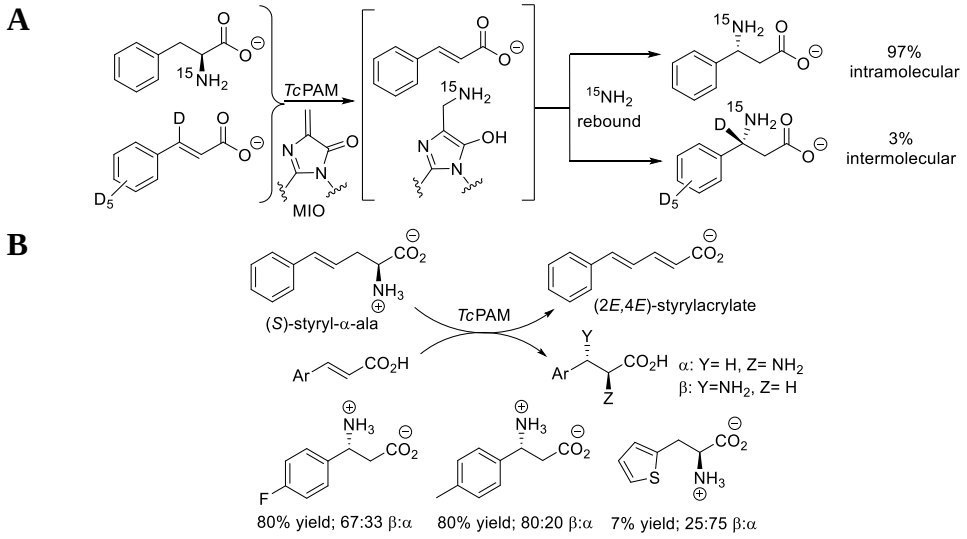

Figure. 2.4. Transaminase activity of *Tc*PAM with A) its natural substrate; B) surrogate (2*S*)-styryl-α-alanine.

Later, in a burst phase kinetics study, *Tc*PAM was shown to transfer the amino group from (2*S*)-styryl-α-alanine, employed as a surrogate substrate, to exogenously supplied arylacrylates via an MIO-NH_2 adduct.[51] The transaminase function of *Tc*PAM catalyzed efficient intermolecular exchange of the amino group to make a mixture of α- and β-amino acids (**Figure. 2.4**B).[50,51]

2.1.6.2 Transaminase Studies employing Ammonium Hydroxide as the Amine Donor

In 2009, an alternate route to make enantiopure α- and β-amino acids from the amination of arylacrylates, catalyzed by a PAM from *Taxus chinensis* (*Tch*PAM).[49] An aqueous solution of ammonia (NH_4OH, 6 M, pH 10) was used as the amino group source, in which a series of arylacrylates with electron-donating and electron-withdrawing substituents on the aryl ring were incubated with *Tch*PAM. The arylacrylates were converted to their corresponding α- or β-amino acids (**Figure. 2.5**). The regioselectivity of the α:β-amination ratios varied from 99:1 (for 2′-Br) to 9:91 (for 4′-*i*-Pr); however, typically more evenly distributed mixtures of α- and β-amino acids were formed from most of the other acrylate substrates. Active site mutagenesis (Q319M) on *Tch*PAM improved the regioselectivity toward β-amination from 35:65 to 9:91 α- to β-amination (for 4′-fluoro-cinnamate), and thus, enantioenriched β-amino acids were biocatalyzed from arylacrylates through one-step ammonia addition (**Figure. 2.5**).[52,53]

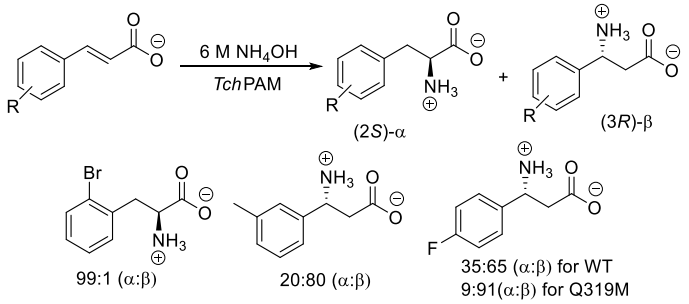

Figure. 2.5. *Tch*PAM-catalyzed addition of ammonia to substituted arylacrylates.

2.1.6.3 Employing Epoxides (Glycidates) as Amino Group Acceptors in MIO-Catalysis

In an earlier study, a covalently trapped 3-phenylglycidate (i.e., cinnamate epoxide) was seen in the active site of *Sg*TAM crystal (PDB: 2RJR), which helped dissect its mechanism.[17] The trapped glycidate formed a presumed phenylpropan-3-ol covalently attached to the MIO via an ether linkage.[17] The authors assumed the crystallization media contained no exogenous amino group resources, and thus, the MIO was armed as HO-MIO by the addition of water. This modified MIO was deemed the source of the ether-linked enzyme/substrate adduct. The ability of *Sg*TAM to trap a glycidate hinted that the reaction pathway for any MIO-enzyme should be aborted theoretically by covalent inhibition by a glycidate substrate (**Figure. 2.6**A). It is interesting to note that the crystal structures of an MIO-dependent *Pa*PAM solved in a subsequent study showed dual occupancy of α- and β-phenylalanines (the natural substrate and product, respectively) covalently linked to the MIO moiety. [29] The latter study demonstrated that residual ammonia remained in the buffer after enzyme purification through affinity chromatography, likely coming from the Lysogeny Buffer (LB) used to grow the bacteria in which *Tc*PAM was overexpressed. Dialyzed *Tc*PAM enzyme preparations were incubated in assays buffers containing cinnamate with the trace concentration of ammonia (NH_4OH) found in commercial LB media remaining after enzyme affinity chromatography. The trace ammonia was sufficient for *Tc*PAM to convert cinnamate to α- and β-phenylalanine.[29] Thus, we reinterpreted the covalently-linked structures of *Sg*TAM to be a β-hydroxy-α-amino adduct (**Figure. 2.6B**), rather than a dihydroxy ether intermediate attached to the MIO (**Figure. 2.6A**).[17]

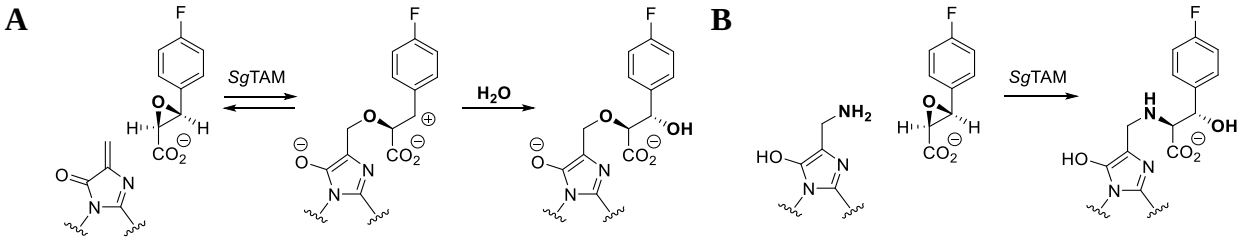

Figure. 2.6. Proposed covalent binding of a 3-arylglycidate inhibitor in the *Sg*TAM active site A) Formation of a dihydroxy ether intermediate reported by Montanavon and co-workers.[17] B) Reinterpretation of bound intermediate as a β-hydroxy-α-amino adduct formed by MIO-NH_2 as informed by the proposed amino-linked adducts made in the *Pa*PAM crystal structures.[29]

Encouraged by the intermolecular mechanism of *Tc*PAM and our reinterpretation of the chemistry of MIO enzymes with epoxides, we hypothesized that 3-arylglycidates could be potential amine acceptors during the transamination reaction catalyzed by *Tc*PAM. Here, we describe a new application for the *Tc*PAM catalyst to transfer an amino group to various ring-substituted 3-arylglycidates to make arylserines (major) and arylisoserines (minor).

2.1.7 Arylserines and Arylisoserines

2.1.7.1 Importance and Occurrence in Medicinally Active Compounds

Nonproteinogenic amino acids are a specialized class of organic compounds that often have intrinsic biological activity.[3,54-56] More frequently, these vital amino acids are found in peptides with antiviral,[57] antitumor,[58] anti-inflammatory,[59] or immunosuppressive[60] activities. β-Hydroxy-α-amino acids reside in an important subclass of nonproteinogenic amino acids, including arylserines, hydroxyaspartic acid, and hydroxyleucine. These bifunctional compounds introduce two chiral centers when used as biomolecular building blocks. Incorporation of unique stereochemistry into the residues of peptide chains can change their properties by, for example, increasing the stability against peptidases and prolonging bioavailability.[61-63] Further, β-hydroxy-α-amino acid scaffolds (**Figure. 2.7**) are found in clinically significant antibiotics, including glycopeptide vancomycin and its analogues, ristocetin from *Amycolatopsis*[64,65] and teicoplanins

from *Actinoplanes*,[66] the phenylpropanoid chloramphenicol from *Streptomyces*,[67] and katanosin depsipeptides from *Cytophaga* and *Lysobacter* bacteria.[68,69] The pentapeptide gymnangiamide from marine hydroid *Gymnangium regae* shows anticancer activity.[70] (2*S*,3*R*)-3,4-Dihydroxyphenylserine (DOPS, Droxidopa) is used for hypotension and as a Parkinsonian therapeutic,[71-73] while *N*-arylsulfonyl derivatives of phenylserine ethyl esters function as non-steroidal anti-inflammatory drugs.[74]

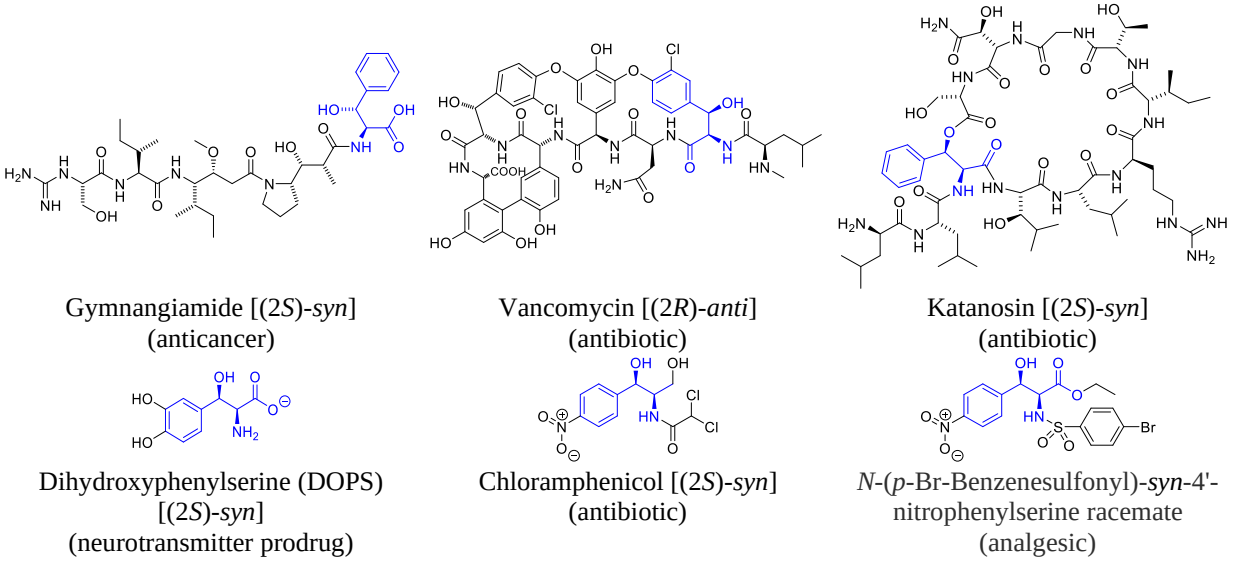

Gymnangiamide [(2*S*)-*syn*] (anticancer)

Vancomycin [(2*R*)-*anti*] (antibiotic)

Katanosin [(2*S*)-*syn*] (antibiotic)

Dihydroxyphenylserine (DOPS) [(2*S*)-*syn*] (neurotransmitter prodrug)

Chloramphenicol [(2*S*)-*syn*] (antibiotic)

N-(*p*-Br-Benzenesulfonyl)-*syn*-4'-nitrophenylserine racemate (analgesic)

Figure. 2.7. The occurrence of synthetic and biosynthetic β-phenyl-β-hydroxy-α-amino acid building blocks in bioactive compounds. Stereochemical designations listed in brackets [] are described in **Figure. 2.8**.

β-Hydroxy-α-amino acids have also been used recently in protein synthesis by chemical ligation at N-terminal serine and threonine sites, and this technique can likely be expanded to incorporate other non-proteinogenic β-hydroxy amino acids.[75] Additionally, an attractive subclass of non-natural heterocyclic β-hydroxy-α-amino acid amides are drug leads for their analgesic and immunostimulant activities.[76-79]

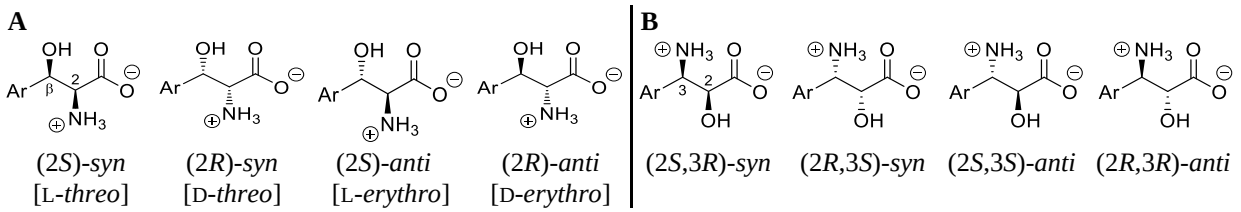

Figure. 2.8. Stereoisomerism convention for A) Arylserine, and B) Arylisoserine used herein. The equivalent, archaic designations for arylserine diastereomers are listed in brackets [].

Similarly, the interest in α-hydroxy-β-amino acids has grown significantly in recent years, stemming partly from their abundance in biologically active molecules such as bestatin,[80] edeine,[81] tatumine,[82] and microginin,[83] and also due to the use of these *iso*-amino acids to synthesize protease inhibitors (**Figure. 2.9**).[84] Prominent members of this class of compounds include isoserine,[85] isothreonine,[86] 3-amino-2-hydroxydecanoic acid,[87] 3-amino-2-hydroxy-4-phenylbutyric acid[88] and 3-phenylisoserine.[89] Paclitaxel (Taxol®), has been a widely used drug in taxane chemotherapy since its FDA approval in 1992, contains a (2*R*,3*S*)-3-phenylisoserine side chain (**Figure. 2.9**). It is the drug of choice for certain types of ovarian and breast cancers as it blocks the microtubule disassembly.[90-96] An analogue, docetaxel (Taxotere®), is used in metastatic breast cancer, ovarian and lung cancer, and also AIDS related Kaposi's sarcoma.[97-100] Cabazitaxel (Jevtana®) is potent newer generation taxane used against castration resistant prostate cancer.[101-103] Other instances of molecules containing a phenylisoserine moiety include (–)-cytoxazone, which is a potent, synthetic chemotherapeutic agent for atopic dermatitis and asthma,[104,105] and a lactarius sesquiterpene, modified synthetically with a phenylisoserine side chain, has antiviral, cytotoxic, and anti-proliferative properties (**Figure. 2.9**).[106,107]

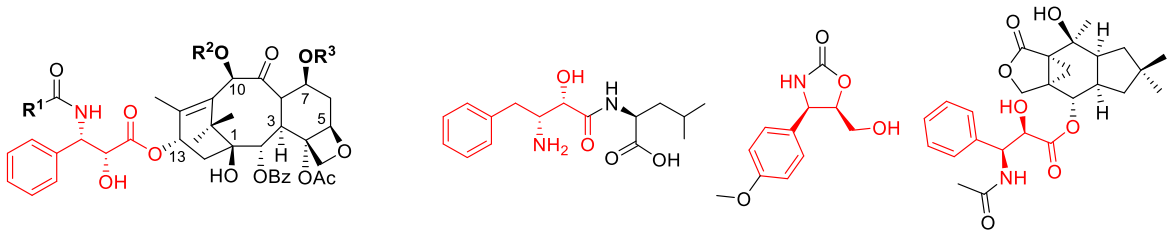

Paclitaxel: R^1 = Ph, R^2 = Ac, R^3 = H
Docetaxel:R^1 = *t*-BuO, R^2 = H, R^3 = H
Cabazitaxel:R^1 = *t*-BuO, R^2 = CH_3, R^3 = CH_3
(Anticancer)

Bestatin
(Protease inhibitor)

(–)-Cytoxazone
(Antibiotic)

Lactarius sesquiterpene
(Antiviral, Cytotoxic)

Figure. 2.9. The occurrence of synthetic and biosynthetic α-hydroxy-β-amino acid building blocks in bioactive compounds.

2.1.7.2 Current Methods for the Chemical Synthesis of Arylserine

Given the beneficial pharmacological, chemical, and physical properties of a compound containing β-hydroxy-α-amino acids, there is considerable interest in making these bifunctional scaffolds by synthetic approaches or in combination with biocatalytic routes.[79,108,109] Various synthetic strategies have been used to control the regio- and stereochemistry of β-hydroxy-α-amino acids, including asymmetric aldol condensation, oxy-Michael addition, electrophilic amination, aminohydroxylation of alkenes, and aza-Claisen rearrangement(**Figure. 2.10**).[71,110-113]

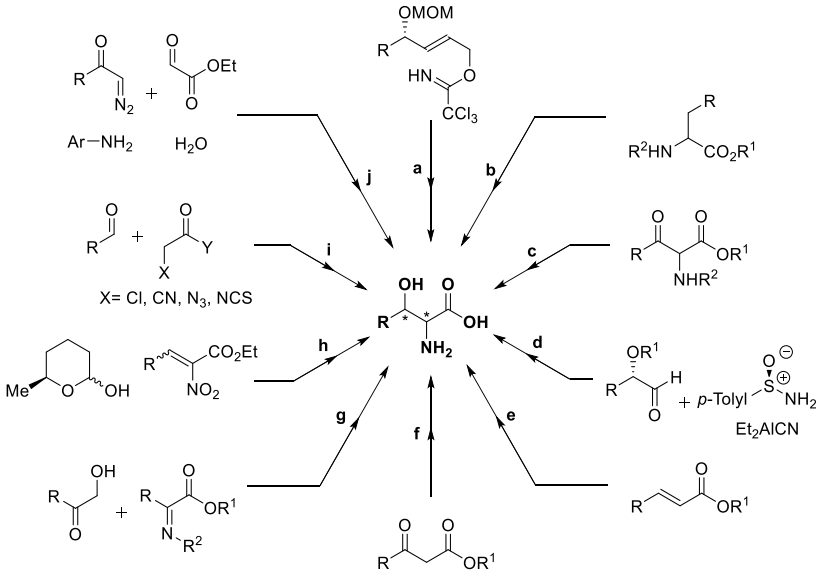

Figure. 2.10. Various chemical synthetic strategies to synthesize β-hydroxy-α-amino acids: a). aza-Claisen rearrangement; b). proteinogenic amino acid derivatization; c). asymmetric hydrogenation; d). Strecker reaction; e). Sharpless aminohydroxylation and dihydroxylation reaction; f). Electrophilic amination; g). Mannich type reaction; h). Oxy-Michael addition; i). Asymmetric aldol condensation; and j). multicomponent reaction.

Several of these methods incorporate protecting group manipulations to direct regiochemistry, add a functionalized chiral auxiliary to incorporate stereogenic centers, or apply heavy-metal catalysts to promote the reactions. These synthetic approaches are often highly efficient and stereoselective, but chemical manufacturers observe that these routes often violate green chemistry principles through the generation of heavy-metal waste, poor atom economy built on the synthesis of intricate chiral-ligand catalysts, and frequently fall short as sustainable methods.[114-116]

2.1.7.3 Current methods for the Biocatalysis of Arylserines

Biocatalysis is emerging as a valuable complementary tool for organic chemists to access regio- and stereocontrolled chemical transformations that otherwise use complex synthetic chiral ligands and often proceed through multiple steps in conventional methods.[115,117-119] Biocatalytic routes towards (2*S*)+(2*R*)-(*syn*/*anti*)-β-hydroxy-α-amino acids (**Figure. 2.8**) mixtures regularly use threonine aldolases (TAs).[120] TAs are divided into two groups depending on the (*R*)- or (*S*)-stereochemistry

at the C_α of threonine, where the amino group is attached. While the substrate specificity of TAs depends on the glycine donor substrate, they have broad specificity for the aldehyde, including non-natural aryl aldehydes when used to produce arylserines.[121] TAs are divided further into four subgroups, depending on the stereochemistry at the C_β of threonine where the hydroxyl group is attached. High-specificity (2*S*)-*syn*-TAs make only (2*S*)-*syn*-threonines, (2*S*)-*anti*-TAs are stereoselective for (2*S*)-*anti*-threonines, while low-specificity (2*S*)-TAs make a mixture of (2*S*)-*syn*- and (2*S*)-*anti*-threonines. Only low-specificity (2*R*)-TAs are known and make mixtures of (2*R*)-*syn*- and (2*R*)-*anti*-threonines.[109]

TA specificity is also used in industrial chemical processes for enantiospecific enzyme resolution to cleave (via a retro-aldol reaction) one enantiomer of a *syn*- or *anti*-β-hydroxy-α-amino acid pair.[109] This process stereospecifically enriches one stereoisomer over the other in a mixture. For example, a low specificity (2*R*)-TA stereospecifically catalyzed the retro-aldol cleavage of the (2*R*)-isomer in a (2*S*)+(2*R*)-*syn*-racemate to resolve the intact (2*S*)-*syn*-(3',4'-methylenedioxy)phenylserine enantiomer, a precursor of the therapeutic drug (2*S*)-*syn*-DOPS (L-DOPS).[122]

2.1.7.4 Biocatalysis of Arylserine and Arylisoserine using a MIO-Aminomutase

In this work, we used an irreversible, TA-*independent* biocatalytic method employing a repurposed 5-methylidene-3,5-dihydro-4*H*-imidazol-4-one (MIO)-dependent phenylalanine aminomutase (*Tc*PAM)[27,46,123] to make various ring-substituted phenylserines. *Tc*PAM converts (*2S*)-α-phenylalanine to (*3R*)-β-phenylalanine on the biosynthetic pathway to paclitaxel (Taxol). The inherent transaminase activity of this α/β-amino acid isomerase,[50,124] was repurposed to transfer an amino group from a surrogate donor substrate (*2S*)-styryl-α-alanine to various ring-

substituted *trans*-3-arylglycidates to make different arylserine and arylisoserine analogues (**Figure. 2.11**).

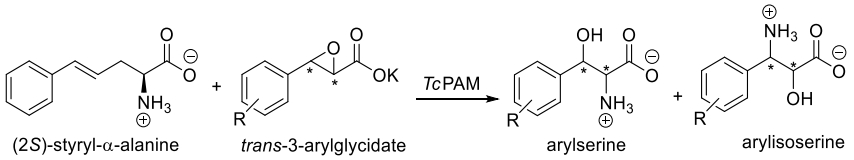

Figure. 2.11. Biocatalysis of arylserine and arylisoserine analogues from *trans*-3-arylglycidates and (2*S*)-styryl-α-alanine by using an MIO-aminomutase. The asterisk (*) indicates a chiral center.

To our surprise, in an initial pilot study, when the unsubstituted *trans*-3-phenylglycidate was incubated with *Tc*PAM, the amino group was transferred at the C_α forming β-hydroxy-α-amino acid phenylserine. Encouraged by this preliminary data, we hypothesized that the electronic effects of the substituents on the aromatic ring of 3-phenylglycidates would impact the regioselectivity of the amino group transfer. This exploration is the first instance of using an aminomutase to biocatalyze pharmaceutically and industrially important hydroxy amino acids.

2.2 Experimental

2.2.1 Chemicals and Reagents

trans-Cinnamic acid, *trans*-3-methoxycinnamic acid, *trans*-3-methylcinnamic acid, *trans*-3-fluorocinnamic acid, *trans*-3-chlorocinnamic acid, *trans*-3-bromocinnamic acid, *trans*-3-nitrocinnamic acid, *trans*-4-fluorocinnamic acid, *trans*-4-chlorocinnamic acid, *trans*-4-bromocinnamic acid, *trans*-4-nitrocinnamic acid, oxone monopersulfate, sodium phosphate monobasic, sodium phosphate dibasic heptahydrate, benzaldehyde, 3-methylbenzaldehyde, 3-methoxybenzaldehyde, 3-fluorobenzaldehyde, 3-chlorobenzaldehyde, 3-bromobenzaldehyde, 3-nitrobenzaldehyde, 4-methylbenzaldehyde, 4-fluorobenzaldehyde, 4-chlorobenzaldehyde, 4-bromobenzaldehyde, 4-nitrobenzaldehyde, *rac*-(2*S*+2*R*)-*syn*-phenylserine, pyridoxal-5′-phosphate, chlorotrimethylsilane, and (2*S*)-(+)-methylbutyric anhydride were purchased from

Millipore-Sigma (Burlington, MA). *trans*-4-Methylcinnamic acid and 1,1,1-trifluoroacetone were purchased from Oakwood Chemical (Estill, SC). (2*S*)-Styryl-α-alanine and L-3-bromo-α-phenylalanine was purchased from Chem Impex (Wood Dale, IL). (2*S*)-*syn*-Phenylserine and (2*R*,3*S*)-phenylisoserine hydrochloride was purchased from Bachem (Torrance, CA). All chemicals were used without further purification unless noted.

2.2.2 Instrumentation

A gas chromatograph (6890N, Agilent) coupled with a mass selective detector (5973 *inert*, Agilent) operated in electron impact mode (70 eV ionization voltage) was used for the analysis of derivatized amino acids. The instrument was equipped with a capillary GC column (30 m × 0.25 mm × 0.25 uM; HP-5MS; J & W Scientific) with He as the carrier gas (flow rate, 1 mL/min). The injector port (at 250 °C) was set to splitless injection mode. A 1-uL aliquot of each sample was injected using an Agilent 7683 auto-sampler (Agilent, Atlanta, GA). A capillary GC column (25 m × 0.25 mm × 0.39 mm; CP-Chirasil-Dex CB, thickness 0.25 µm; Agilent Technologies, Santa Clara, CA) was used for the analysis of methyl-3-arylglycidates. All ^{1}H (500 MHz) and ^{13}C NMR (126 MHz) spectra were recorded using a Varian superconducting NMR-spectrometer using standard acquisition parameters. LC/ESI/MSMS analyses were recorded with a Xevo G2-XS QTof (Waters, Milford, MA), and LC/ESI by MRM spectral data was acquired on a Xevo TQ-S (Waters, Milford, MA) instrument.

2.2.3 General Procedure for the Syntheses of *trans*-3-Arylglycidate Analogues

The racemic arylglycidates were synthesized according to a procedure described previously.[125] In a 50-mL single-necked round-bottomed flask, a stirred slurry of a *trans*-aryl acrylic acid analogue (**13a-13l**) (0.75 mmol) in acetone (515 µL, 7.5 mmol) was treated first with sodium bicarbonate (3.3 mmol) and then with dropwise addition of water (515 µL). To the resulting thick

mixture, a solution of oxone monopersulfate (1.4 mmol, contains 1.8 equiv of $KHSO_5$) in 0.4 mM Na_2EDTA solution (1.6 mL) was added dropwise for 1 h while the temperature was kept at ~25 °C and the pH at 7.5. The mixture was then stirred an additional 6 h and cooled to –5 °C. The reaction was acidified to pH 2 (12 M HCl) and mixed with ethyl acetate (5 mL) with rapid stirring. The mixture was then filtered and extracted with ethyl acetate (3 × 50 mL). The combined organic fractions were washed with saturated NaCl, dried over anhydrous $MgSO_4$, filtered, and concentrated under vacuum. After all the solvent was removed, each *trans*-aryl glycidic acid analog was isolated as an oily residue. The oily residue was dissolved in ethanol (EtOH) (1 mL), cooled on ice, and treated with a solution of KOH (3.6 mmol) dissolved in EtOH (1 mL). The resulting thick slurry was filtered, and the residue was washed with EtOH and then dried under vacuum to provide the potassium 3-arylglycidates as a racemic mixture.

Potassium 3-phenylglycidate (14a). By following the general procedure, 420 mg (88% yield) of **14a** was made. ^{1}H NMR (500 MHz, D_2O): δ 7.41 (dd, *J* = 7.8, 5.7 Hz, 3H), 7.37–7.33 (m, 2H), 3.97 (d, *J* = 2.1 Hz, ^{1}H), 3.56 (d, *J* = 2.2 Hz, ^{1}H). ^{13}C NMR (126 MHz, CD_3OD) δ 175.56, 135.77, 129.14, 128.93, 126.20, 59.04, 57.66. HRMS (ESI-TOF) *m*/*z*: $[M - K]^-$ calcd for $C_9H_7O_3$ 163.0395; Found 163.0398.

Potassium 3-(3'-OCH_3-phenyl)glycidate (14b). Conversion of the 3'-OCH_3-cinnamate starting material was incomplete, yielding a mixture of glycidate and cinnamate at 88:12 (**14b**:**13b**). Following the general procedure yielded 264 mg of **14b** (41%). ^{1}H NMR (500 MHz, DMSO-d_6) δ 7.23 (t, *J* = 7.9 Hz, 1H), 6.86 – 6.76 (m, 3H), 3.73 (s, 3H), 3.68 (d, *J* = 2.0 Hz, 1H), 3.00 (d, *J* = 2.0 Hz, 1H). ^{13}C NMR (126 MHz, DMSO-d_6) δ 169.42, 140.21, 129.47, 117.96, 113.55, 110.75, 60.99, 55.58, 55.04. HRMS (ESI-TOF) *m*/*z*: $[M - K]^-$ calcd for $C_{10}H_9O_4$ 193.0501; Found 193.0504.

Potassium 3-(3'-CH_3-phenyl)glycidate (14c). By following the general procedure, 240 mg (78% yield) of **14c** was made. ^{1}H NMR (500 MHz, DMSO-d_6) δ 7.20 (dd, J = 7.5 Hz, ^{1}H), 7.09 (d, J = 7.5 Hz, ^{1}H), 7.02 (d, J = 8.3 Hz, 2H), 3.70 (d, J = 2.0 Hz, ^{1}H), 3.09 (d, J = 2.0 Hz, ^{1}H), 2.25 (s, 3H). ^{13}C NMR (126 MHz, DMSO-d_6) δ 171.86, 138.45, 138.05, 129.47, 129.08, 126.88, 123.59, 60.45, 56.60, 21.57. HRMS (ESI-TOF) m/z: [M – K]$^-$ calcd for $C_{10}H_9O_3$ 177.0552; Found 177.0551.

Potassium 3-(3'-F-phenyl)glycidate (14d). By following the general procedure, 300 mg (63% yield) of **14d** was made; ^{1}H NMR (500 MHz, DMSO-d_6) δ 7.39 – 7.27 (m, ^{1}H), 7.14 – 6.98 (m, 3H), 3.79 (d, J = 1.7 Hz, ^{1}H), 3.14 (d, J = 2.0 Hz, ^{1}H). ^{13}C NMR (126 MHz, DMSO-d_6) δ 170.90, 163.80, 141.40, 131.03, 122.54, 115.26, 112.88, 60.70, 55.68. HRMS (ESI-TOF) m/z: [M – K]$^-$ calcd for $C_9H_6O_3F$ 181.0301; Found 181.0302.

Potassium 3-(3'-Cl-phenyl)glycidate (14e). By following the general procedure, 760 mg (86% yield) of **14e** was made; ^{1}H NMR (500 MHz, DMSO-d_6) δ 7.37 – 7.31 (m, 2H), 7.29 (s, ^{1}H), 7.22 (d, J = 6.8 Hz, ^{1}H), 3.75 (d, J = 2.1 Hz, ^{1}H), 3.01 (d, J = 2.1 Hz, ^{1}H). ^{13}C NMR (126 MHz, DMSO-d_6) δ 168.83, 141.28, 133.17, 130.23, 127.64, 125.41, 124.41, 61.29, 54.80. HRMS (ESI-TOF) m/z: [M – K]$^-$ calcd for $C_9H_6O_3Cl$ 197.0005; Found 197.0009.

Potassium 3-(3'-Br-phenyl)glycidate (14f). By following the general procedure, 960 mg (91% yield) of **14f** was made; ^{1}H NMR (500 MHz, DMSO-d_6) δ 7.51 – 7.40 (m, 2H), 7.27 (m, 2H), 3.74 (d, J = 6.6 Hz, ^{1}H), 3.01 (d, J = 6.5 Hz, ^{1}H). ^{13}C NMR (126 MHz, DMSO-d_6) δ 169.21, 141.95, 130.95, 130.93, 128.71, 125.21, 122.14, 61.74, 55.14. HRMS (ESI-TOF) m/z: [M – K]$^-$ calcd for $C_9H_6O_3Br$ 240.9500; Found 240.9501.

Potassium 3-(3'-NO_2-phenyl)glycidate (14g). By following the general procedure, 262 mg (57% yield) of **14g** was made; ^{1}H NMR (500 MHz, DMSO-d_6) δ 8.16 – 8.10 (m, ^{1}H), 8.06 (t, J = 2.0 Hz,

^{1}H), 7.76 – 7.70 (m, ^{1}H), 7.63 (t, *J* = 7.9 Hz, ^{1}H), 3.93 (d, *J* = 2.0 Hz, ^{1}H), 3.06 (d, *J* = 2.1 Hz, ^{1}H). ^{13}C NMR (126 MHz, DMSO-d_6) δ 168.37, 147.96, 141.18, 132.33, 129.94, 122.56, 120.17, 61.63, 54.49. HRMS (ESI-TOF) *m*/*z*: $[M - K]^-$ calcd for $C_9H_6NO_5$ 208.0246; Found 208.0247.

Potassium 3-(4'-NO$_2$-phenyl)glycidate (14h). 1,1,1-Trifluoroacetone (1.8 equiv) was used instead of acetone and the reaction was stirred for 24 h after the addition of oxone. Yield: 154 mg of **14h** (28%); ^{1}H NMR (500 MHz, DMSO-d_6) δ 8.18 (d, *J* = 8.7 Hz, 2H), 7.53 (d, *J* = 8.8 Hz, 2H), 3.90 (d, *J* = 2.0 Hz, ^{1}H), 3.04 (d, *J* = 2.0 Hz, ^{1}H). ^{13}C NMR (126 MHz, DMSO-d_6) δ 168.27, 146.95, 146.72, 126.81, 123.54, 61.91, 54.66. HRMS (ESI-TOF) *m*/*z*: $[M - K]^-$ calcd for $C_9H_6NO_5$ 208.0246; Found 208.0249.

Potassium 3-(4'-CH$_3$-phenyl)glycidate (14i). Following the general procedure yielded 320 mg of **14i** (68%). ^{1}H NMR (500 MHz, DMSO-d_6) δ 7.15 – 7.09 (m, 4H), 3.71 (d, *J* = 2.0 Hz, ^{1}H), 3.15 (d, *J* = 1.7 Hz, ^{1}H), 2.23 (s, 3H). ^{13}C NMR (126 MHz, DMSO-d_6) δ 173.13, 138.94, 134.85, 130.17, 126.88, 60.33, 57.18, 21.69. HRMS (ESI-TOF) *m*/*z*: $[M - K]^-$ calcd for $C_{10}H_9O_3$ 177.0552; Found 177.0549.

Potassium 3-(4'-F-phenyl)glycidate (14j). Following the general procedure yielded 426 mg of **14j** (91%); ^{1}H NMR (500 MHz, DMSO-d_6) δ 7.28 (dd, *J* = 8.7, 5.5 Hz, 2H), 7.13 (t, *J* = 8.9 Hz, 2H), 3.76 (d, *J* = 2.0 Hz, ^{1}H), 3.14 (d, *J* = 2.1 Hz, ^{1}H). ^{13}C NMR (126 MHz, DMSO-d_6) δ 172.14, 161.82, 134.24, 128.77, 128.70, 116.24, 116.07, 60.45, 56.22. HRMS (ESI-TOF) *m*/*z*: $[M - K]^-$ calcd for $C_9H_6O_3F$ 181.0301; Found 181.0301.

Potassium 3-(4'-Cl-phenyl)glycidate (14k). Following the general procedure yielded 137 mg of **14k** (86%); ^{1}H NMR (500 MHz, DMSO-d_6) δ 7.45 (d, *J* = 8.5 Hz, 2H), 7.39 (d, *J* = 8.5 Hz, 2H), 4.16 (d, *J* = 1.8 Hz, ^{1}H), 3.66 (d, *J* = 1.8 Hz, ^{1}H). HRMS (ESI-TOF) *m*/*z*: $[M - K]^-$ calcd for $C_9H_6O_3Cl$ 197.0005; Found 197.0007.

Potassium 3-(4'-Br-phenyl)glycidate (14l). Following the general procedure yielded 1.2 g of **14l** (64%); ^{1}H NMR (500 MHz, DMSO-d_6) δ 7.48 (d, J = 8.1 Hz, 2H), 7.19 (d, J = 8.0 Hz, 2H), 3.76 (d, J = 2.0 Hz, ^{1}H), 3.17 (d, J = 2.0 Hz, ^{1}H). ^{13}C NMR (126 MHz, DMSO-d_6) δ 173.02, 137.42, 132.53, 129.12, 122.52, 60.46, 56.71. HRMS (ESI-TOF) m/z: $[M - K]^-$ calcd for $C_9H_6O_3Br$ 240.9500; Found 240.9503.

2.2.4 Stereochemical Analysis of *trans*-3-Arylglycidates using GC/EI-MS.

Each potassium 3-arylglycidate (0.05 mmol), suspended in 1 mL H_2O, was titrated with 6 N HCl (pH 3). The resulting aryl glycidic acids were extracted into ethyl acetate (2 mL), and the organic solution was treated with diazomethane (0.9 equiv) dissolved in ether. The organic solvent was evaporated to 100 μL, and an aliquot (1 μL) was injected on the gas chromatography/electron-impact mass spectrometry (GC/EI-MS).

Chiral GC/EI-MS analysis was performed on an Agilent 6890N gas chromatograph equipped with a capillary GC column (25 m × 0.25 mm × 0.39 mm; CP-Chirasil-Dex CB, thickness 0.25 μm; Agilent Technologies, Santa Clara, CA) with He as the carrier gas (flow rate, 1 mL/min). The injector port (at 250 °C) was set to splitless injection mode. A 1-uL aliquot of each sample was injected using an Agilent 7683 auto-sampler (Agilent, Atlanta, GA). Various GC heating gradients were used to elute each of the epoxide racemates from the column (**Table 2.2**). Mass spectra were recorded in the mass range of 50 – 400 m/z to analyze the analogues of methyl 3-arylglycidate (**Figure. 2.12** and **Figure. 2.13**).

Table 2.2. GC Oven Heating Parameters.

Glycidate	GC/EI-MS conditions
14a, **14i**	Initial column temperature started at 70 °C, then increased at 40 °C/min to 95 °C with a 7 min hold, ramped at 10 °C/min to 150 °C, then increased by 30 °C/min to 175 °C, and returned to 70 °C over 3 min.
14b	Initial column temperature started at 70 °C, then increased at 40 °C/min to 90 °C with a 10 min hold, ramp at 8 °C/min to 150 °C and held for 8.5 min, then increased by 20 °C/min to 180 °C, and returned to 70 °C over 3 min.
14c	Initial column temperature started at 70 °C, then increased at 40 °C/min to 90 °C with a 7 min hold, ramp at 10 °C/min to 140 °C, then increased by 30 °C/min to 170 °C, and returned to 70 °C over 3 min.
14d, **14j**	Initial column temperature started at 70 °C, then increased at 40 °C/min to 95 °C with an 8 min hold, ramp at 10 °C/min to 140 °C, then increased by 30 °C/min to 180 °C, and returned to 70 °C over 3 min.
14e	Initial column temperature started at 70 °C, then increased at 40 °C/min to 95 °C with a 10 min hold, then ramp at 8 °C/min to 150 °C, then increased by30 °C/min to 180 °C, and returned to 70 °C over 3 min.
14f, **14l**	Initial column temperature started at 70 °C, then increased at 40 °C/min to 90 °C with a 5 min hold, ramp at 10 °C/min to 150 °C and held for 7 min, then increased by 20 °C/min to 180 °C, and returned to 70 °C over 3 min.
14g, **14h**	Initial column temperature started at 70 °C, then increased at 40 °C/min to 95 °C with a 15 min hold, then ramp at 8 °C/min to 150 °C with a 10 min hold, then increased by 10 °C/min to 185 °C, and returned to 70 °C over 3 min.
14k	Initial column temperature started at 70 °C, then increased at 40 °C/min to 90 °C with a 2 min hold, then ramp at 10 °C/min to 150 °C with a 7 min hold, then increased by 20 °C/min to 180 °C, and returned to 70 °C over 3 min.

2.2.5 Stability of Racemic Arylglycidates in Assay Buffer

The water in Assay Buffer (20 mL, 50 mM NaH_2PO_4/Na_2HPO_4, pH 8.0, 0% glycerol) was evaporated under a stream of nitrogen gas, D_2O (20 mL) was added and then evaporated to replace the exchangeable protons with deuterons. This deuteron-for-proton exchange was repeated to depress the HDO signal in the ^1H NMR spectrum, and the concentrated buffer was dissolved in D_2O to achieve a final concentration was 50 mM phosphates. Each glycidate substrate (**14a-14l**) was dissolved separately in the deuterated Assay Buffer and analyzed in a time course ^1H NMR experiment. Spectra were recorded every 15 min, starting from $t_1 = 0$ min to $t_7 = 90$ min to monitor the formation of dihydroxy products resulting from ring-opening of the epoxides. After this 90 min

time course, the samples were then stored inside the NMR tube at ~25 °C for 7 days, and the quality of the sample was assessed by ^{1}H NMR (**Figure. 2.14**).

2.2.6 Expression and Purification of *Tc*PAM.

The *tcpam* cDNA (codon-optimized for expression in bacteria) was previously ligated into the expression vector pET28a(+),[27] and the recombinant-plasmid encoded an N-terminal His_6 tag. *Escherichia coli* BL21(DE3) cells, transformed to express *Tc*PAM, were grown at 37 °C for 12 h in 150 mL of Lysogeny broth (LB). Separate aliquots (25 mL) of this inoculum culture were then added to each of six 1-L cultures of LB supplemented with kanamycin (50 μg/mL). The cells were incubated at 37 °C until OD_{600} = 0.7. Isopropyl-β-D-thiogalactopyranoside (IPTG, 500 μM) was added to the cultures with expression conducted at 16 °C for 16 h. The cells were harvested by centrifugation at 4,650*g* (15 min), and the pellets were diluted in resuspension buffer (100 mL of 50 mM sodium phosphate containing 5% (v/v) glycerol and 300 mM NaCl, pH 8.0). The cells were then lysed by brief sonication [one 10-s burst at 60% power with a 20-s rest interval for 20 cycles on a Misonix Sonicator (Danbury, CT)]. The cellular debris was removed by centrifugation at 27,200*g* (20 min) followed by high-speed centrifugation at 142,000*g* (90 min) to remove light membrane debris. The resultant crude aminomutase in the soluble fraction was purified by nickel-nitrilotriacetic acid affinity chromatography according to the protocol described by the manufacturer (Invitrogen, Carlsbad, CA); *Tc*PAM eluted in 50 mL of 250 mM imidazole dissolved in resuspension buffer. Fractions containing active soluble *Tc*PAM (76.5 kDa) were combined and loaded onto a size-selective centrifugal filtration unit (30,000 NMWL, Millipore Sigma, Burlington, MA). The protein solution was concentrated and diluted over several cycles until the imidazole and salt concentrations were <1 μM, and the final volume was 1 mL (~14 mg of *Tc*PAM). The quantity of *Tc*PAM was measured using a Nanodrop spectrophotometer

(ThermoFisher Scientific, Waltham, MA), and the purity (82%) was assessed by SDS-PAGE with Coomassie Blue staining using Kodak Gel Logic 100 Imaging System (version 3.6.3) to integrate the relative intensities of the scanned protein bands.

2.2.7 Expression and Purification of (2*S*)-Threonine Aldolase (*ltaE*).

A cDNA (from *E. coli*, accession number: P75823) encoding a low specificity (2*S*)-threonine aldolase (*ltaE*) was ligated into a pET28a(+) vector, encoding an appended N-terminal His_6-tag, to make a recombinant plasmid (designated as pKDW014_lsTA) was purchased from GenScript (Piscataway, NJ). *Escherichia coli* BL21(DE3) cells were then transformed with pKDW014_lsTA to overexpress the *ltaE* gene by standard protocols (Millipore Sigma, Burlington, MA). Transformed bacteria were used to inoculate LB (100 mL) and grown at 37 °C for 12 h. Separate aliquots (15 mL) of this inoculum culture were added to each of three 1-L cultures of LB supplemented with kanamycin (50 μg/mL). The cells were incubated at 37 °C until OD_{600}= 0.6, and IPTG (100 μM) was added to induce expression at 16 °C for 16 h. The cells were harvested by centrifugation at 4,650*g* (15 min), and the pellets were diluted in resuspension buffer (at pH 7.0) containing 10 μM PLP and 300 mM NaCl. The cells were then lysed by brief sonication [one 10-s burst at 60% power with a 20-s rest interval for 20 cycles on a Misonix Sonicator], and the cellular debris was removed by centrifugation at 27,200*g* (20 min) followed by high-speed centrifugation at 142,000*g* (90 min) to remove light membrane debris. The clarified lysate containing crude (2*S*)-TA in the soluble fraction was purified by nickel-nitrilotriacetic acid affinity chromatography according to the protocol described by the manufacturer (Invitrogen, Carlsbad, CA); (2*S*)-TA was eluted in 50 mL of 250 mM imidazole. Fractions containing active soluble (2*S*)-TA (36.5 kDa) were combined and loaded onto a size-selective centrifugal filtration unit (15,000 NMWL, Millipore Sigma). The protein solution was concentrated and diluted over several cycles

until the imidazole and salt concentrations were <1 μM, and the final volume was 1 mL. The concentration of (2*S*)-TA was measured (8.8 mg/mL) using a Nanodrop spectrophotometer (ThermoFisher Scientific). The purity (99%) was assessed by SDS-PAGE with Coomassie Blue staining using a Kodak Gel Logic 100 Imaging System (version 3.6.3) to integrate the relative intensities of the scanned protein bands.

2.2.8 Control Assay Experiments: Activity of *Tc*PAM toward Arylglycidates

3-(3'-Methoxyphenyl)glycidate (**14b**) was used as a representative substrate in the control assays that contained all the necessary components for an operational assay except either the amine group donor [(2*S*)-styryl-α-alanine (1 mM) or NH_4OH (2 M)] or the enzyme was omitted. Each assay was analyzed using a liquid-chromatography electrospray-ionization and analyzed by a multiple reaction monitoring (LC/ESI-MRM) method.

2.2.9 Biocatalysis of Arylserine and Arylisoserine with *Tc*PAM.

A solution of (2*S*)-styryl-α alanine (**12**) (1 mM) in Assay Buffer (50 mM NaH_2PO_4/Na_2HPO_4 buffer, pH 8.0, 5% glycerol) was preincubated with *Tc*PAM (100 μg/mL) for 2 min. 3-Arylglycidate (**14a−14l**) (1 mM) was added to the solution, and the assay was mixed at 31 °C on a rocking shaker for 2.5 h. The reaction was then stopped with 10% formic acid to adjust the pH to 3.0, and 3'-bromo-α-phenylalanine (50 nM) was added as an internal standard. This reaction mixture was analyzed by LC/ESI-MRM method.

2.2.10 Measurement of Kinetic Parameters.

The steady-state enzyme kinetic constants were calculated by varying each arylglycidate substrate from 25 μM and increasing the concentration in intervals up to 1000 μM in triplicate assays containing *Tc*PAM (100 μg/mL) and (2*S*)-styryl-α alanine (**12**) (1 mM). The reactions were terminated with 10% formic acid (pH 3.0), and 3'-bromo-α-phenylalanine (50 nM) was added as

an internal standard. The resultant ring-opened biocatalyzed products without, derivatization, were quantified by LC/ESI-MRM. The apparent kinetic parameters for the production of arylserine and arylisoserine (k_{cat}^{Ser}, k_{cat}^{Iso}, K_{M}) were calculated by non-linear regression with Origin Pro 9.0 software (Northampton, MA), using the Michaelis-Menten equation: $v_o = [E_o]k_{cat}/(K_M + [S])$.

2.2.11 General Procedure for the Syntheses of Arylserines.

The arylserine analogues were synthesized according to a procedure described previously.[126] Triethylamine (22 mmol) was added to a solution of glycine (5 mmol) in water (4 mL). To this solution, an aryl aldehyde (**19a-19l**) (10 mmol) was added dropwise over 15 min, and the mixture was stirred for 12 h at ~25 °C. The color of the reaction mixture gradually changed from clear and colorless to yellow-brown. *n*-Butanol (3 mL) was added, and the triethylamine was evaporated under vacuum. The butanolic solution was diluted with water (3 mL), and the mixture was acidified to pH 2 with HCl (6 M). The acidified solution was stirred at ~25 °C for 3 h and partitioned against ethyl acetate (2 × 5 mL) to remove the unreacted aryl aldehyde. The aqueous layer was separated and neutralized to pH 6.0 with a saturated $NaHCO_3$ solution to precipitate the arylserine. The mixture was stirred for 1 h at 0 °C, and the arylserine product was washed with water (3 mL) and dried under vacuum to yield the mixture of arylserine diastereomers.

Phenylserine (15a). ^{1}H NMR (500 MHz, D_2O, pH 1.5) *anti*-isomer δ 7.50 – 7.36 (m, 5H), 5.37 (d, *J* = 4.2 Hz, ^{1}H), 4.33 (d, *J* = 4.2 Hz, ^{1}H). *syn*-isomer δ 7.50 – 7.36 (m, 5H), 5.41 (d, *J* = 4.0 Hz, ^{1}H), 4.24 (d, *J* = 4.0 Hz, ^{1}H). *anti*:*syn* = 75:25.

3′-OCH$_3$-phenylserine (15b). ^{1}H NMR (500 MHz, D_2O, pH 1.5) *anti*-isomer δ 7.47 – 6.88 (m, 4H), 5.36 (d, *J* = 4.0 Hz, ^{1}H), 4.36 (d, *J* = 4.0 Hz, ^{1}H). *syn*-isomer δ 7.47 – 6.88 (m, 4H), 5.41 (d, *J* = 3.7 Hz, ^{1}H), 4.27 (d, *J* = 3.7 Hz, ^{1}H). *anti*:*syn* = 71:29.

3′-CH_3-phenylserine (15c). ^{1}H NMR (500 MHz, D_2O, pH 1.5) *anti*-isomer δ 7.38 – 7.16 (m, 4H), 5.33 (d, *J* = 4.2 Hz, ^{1}H), 4.33 (d, *J* = 4.2 Hz, ^{1}H). *syn*-isomer δ 7.38 – 7.16 (m, 4H), 5.37 (d, *J* = 4.0 Hz, ^{1}H), 4.23 (d, *J* = 4.0 Hz, ^{1}H). *anti*:*syn* = 68:32.

3′-F-phenylserine (15d). ^{1}H NMR (500 MHz, D_2O, pH 1.5) *anti*-isomer δ 7.50 – 7.09 (m, 4H), 5.39 (d, *J* = 4.0 Hz, ^{1}H), 4.38 (d, *J* = 3.9 Hz, ^{1}H), *syn*-isomer δ 7.50 – 7.09 (m, 4H), 5.45 (d, *J* = 3.7 Hz, ^{1}H), 4.29 (d, *J* = 3.7 Hz, ^{1}H). *anti*:*syn* = 71:29.

3′-Cl-phenylserine (15e). ^{1}H NMR (500 MHz, D_2O, pH 1.5) *anti*-isomer δ 7.46 – 7.26 (m, 4H), 5.35 (d, *J* = 4.0 Hz, ^{1}H), 4.32 (d, *J* = 3.9 Hz, ^{1}H), *syn*-isomer δ 7.46 – 7.26 (m, 4H), 5.39 (d, *J* = 3.9 Hz, ^{1}H), 4.22 (d, *J* = 3.9 Hz, ^{1}H). *anti*:*syn* = 97:3.

3′-Br-phenylserine (15f). ^{1}H NMR (500 MHz, D_2O, pH 1.5) *anti*-isomer δ 7.69 – 7.30 (m, 4H), 5.36 (d, *J* = 4.0 Hz, ^{1}H), 4.33 (d, *J* = 4.0 Hz, ^{1}H). *syn*-isomer δ 7.69 – 7.30 (m, 4H), 5.40 (d, *J* = 3.9 Hz, ^{1}H), 4.23 (d, *J* = 3.9 Hz, ^{1}H). *anti*:*syn* = 58:42.

3′-NO_2-phenylserine (15g). ^{1}H NMR (500 MHz, D_2O, pH 1.5) *anti*-isomer 8.31 – 7.65 (m, 4H), 5.50 (d, *J* = 3.7 Hz, ^{1}H), 4.42 (d, *J* = 3.7 Hz, ^{1}H). *syn*-isomer δ 8.37 – 7.68 (m, 4H), 5.54 (d, *J* = 3.8 Hz, ^{1}H), 4.32 (d, *J* = 3.9 Hz, ^{1}H). *anti*:*syn* = 96:4.

4′-NO_2-phenylserine (15h). ^{1}H NMR (500 MHz, D_2O, pH 1.5) *anti*-isomer ^{1}H NMR 8.26 (d, *J* = 8.8 Hz, 2H), 7.63 (d, *J* = 9.0 Hz, 2H), 5.49 (d, *J* = 3.6 Hz, ^{1}H), 4.43 (d, *J* = 3.6 Hz, ^{1}H). *syn*-isomer δ 8.29 (d, *J* = 8.8 Hz, 2H), 7.70 (d, *J* = 9.0 Hz, 2H), 5.55 (d, *J* = 3.9 Hz, ^{1}H) 4.33 (d, *J* = 3.8 Hz, ^{1}H). *anti*:*syn* = 83:17.

4′-CH_3-phenylserine (15i). ^{1}H NMR (500 MHz, D_2O, pH 1.5) *anti*-isomer δ 7.34 – 7.24 (m, 4H), 5.33 (d, *J* = 4.2 Hz, ^{1}H), 4.34 (d, *J* = 4.3 Hz, ^{1}H). *syn*-isomer δ 7.34 – 7.24 (m, 4H), 5.37 (d, *J* = 4.1 Hz, ^{1}H), 4.25 (d, *J* = 4.1 Hz, ^{1}H). *anti*:*syn* = 72:28.

4′-F-phenylserine (15j). ^{1}H NMR (500 MHz, D_2O, pH 1.5) *anti*-isomer δ 7.50 – 7.38 (m, 4H), 7.18 (qd, *J* = 8.9, 2.1 Hz, 4H), 5.41 (d, *J* = 4.0 Hz, ^{1}H), 5.37 (d, *J* = 4.2 Hz, ^{1}H), 4.35 (d, *J* = 4.2 Hz, ^{1}H), 4.26 (d, *J* = 4.0 Hz, ^{1}H). *anti*:*syn* = 52:48.

4′-Cl-phenylserine (15k). ^{1}H NMR (500 MHz, D_2O, pH 1.5) *anti*-isomer δ 7.49 – 7.37 (m, 4H), 5.36 (d, *J* = 4.0 Hz, ^{1}H), 4.34 (d, *J* = 4.1 Hz, ^{1}H). *syn*-isomer δ 7.49 – 7.37 (m, 4H), 5.40 (d, *J* = 4.0 Hz, ^{1}H), 4.24 (d, *J* = 4.0 Hz, ^{1}H). *anti*:*syn* = 45:55.

4′-Br-phenylserine (15l). ^{1}H NMR (500 MHz, D_2O, pH 1.5) *anti*-isomer δ 7.68 – 7.31 (m, 4H), 5.38 (d, *J* = 4.0 Hz, ^{1}H), 4.38 (d, *J* = 4.0 Hz, ^{1}H). *syn*-isomer δ 7.68 – 7.31 (m, 4H), 5.42 (d, *J* = 4.0 Hz, ^{1}H), 4.28 (d, *J* = 4.0 Hz, ^{1}H). *anti*:*syn* = 58:42.

2.2.12 Establishing Relative Stereoconfiguration (*syn*/*anti*) of Arylserine Diastereomers using ^{1}H NMR Spectroscopy.

A ^{1}H NMR-based method was developed to characterize the relative stereoconfiguration (*syn* vs *anti*) of arylserine diastereomers without further chemical derivatization. A mixture of chemically synthesized arylserine diastereomers (**15a**-**15l**) (0.17 mmol) was dissolved in D_2O (700 µL). ^{1}H NMR spectra were recorded in triplicate studies for a range of pH varying from 4.0-1.0 at every 0.5 pH interval. HCl (6 M) was added dropwise to adjust the pH, which was measured using Taylor colorpHast® pH test strips 0-6 (Millipore-Sigma (Burlington, MA). Chemical shifts (δ) for H_α and H_β, coupling constant between H_α and H_β ($^3J_{H_\alpha\text{-}H_\beta}$), and the chemical shift difference between H_α and H_β doublets (Δδ) were measured from ^{1}H NMR analyses.

2.2.13 General Method for Derivatizing Arylserines with a Chiral Auxiliary.

A mixture of all four diastereomers of arylserine (**15a**-**15l**) (0.21 mmol) was dissolved in Assay Buffer (1 mL). To this solution were added pyridine (50 µL, 0.62 mmol) and (*2S*)-2-methylbutyric anhydride (60 µL, 0.30 mmol), and the reaction mixture was stirred for 20 min at ~25 °C. The

solution was adjusted to pH 2 (6 M HCl) to quench the reaction, and the *N*-protected arylserine was extracted with ethyl acetate (2 mL). The organic layer was separated and evaporated under a stream of nitrogen gas, and the resultant residue was dissolved in 3:1 EtOAc/MeOH (v/v) (1 mL). Diazomethane in diethyl ether was added dropwise to obtain the methyl ester, and the solvent was removed under a stream of nitrogen gas. The resulting methyl ester was dissolved in dichloromethane (1 mL) to which pyridine (100 µL, 1.24 mmol) and chlorotrimethylsilane (150 µL, 1.18 mmol) were added, and the solution was stirred for 15 min at ~25 °C. The reaction was quenched with water (1 mL), and the organic fraction was separated and analyzed by gas chromatography coupled with electron-impact mass spectrometry (GC/EI-MS).

GC/EI-MS analysis was performed on an Agilent 6890N gas chromatograph equipped with a capillary GC column (30 m × 0.25 mm × 0.25 uM; HP-5MS; J & W Scientific) with He as the carrier gas (flow rate, 1 mL/min). The injector port (at 250 °C) was set to splitless injection mode. A 1-uL aliquot of each sample was injected using an Agilent 7683 autosampler (Agilent, Atlanta, GA). Initial column temperature started at 50 °C, and it was increased at 50 °C/min to 150 °C, then increased by 20 °C/min to 200 °C. It was then ramped at 10 °C/min to 225 °C, with a 5-min hold, and finally increased by 25 °C/min to 250 °C. For 3′-NO_2- (**15g**) and 4′-NO_2-phenylserines (**15h**) initial column temperature started at 50 °C, and it was increased at 50 °C/min to 225 °C, with a 9-min hold. It was again ramped at 1 °C/min to 228 °C, and finally increased by 60 °C/min to 250 °C. The gas chromatograph was coupled to a mass-selective detector (Agilent, 5973 *inert*) operated in electron impact mode (70 eV ionization voltage). All spectra were recorded in the mass range of 50 – 400 *m*/*z* (except 50 – 450 *m*/*z* for **15f** and **15l**) to analyze the hydroxy amino acids derivatized as their *O*-trimethylsilyl *N*-[(2*S*)-2-methylbutyryl] methyl esters.

2.2.14 (2*S*)-Threonine Aldolase catalyzed resolution of Arylserine Diastereomers

A low specificity (2*S*)-threonine aldolase (TA) expressed from *Escherichia coli* was used to catalyze the retro-aldol cleavage of arylserine diastereomers and help assign the absolute stereoconfigurations. This enzyme catalyzes reversible diastereoselective retro aldol cleavage of (2*S*)-*syn*- and (2*S*)-*anti*-arylserine, selectively from a mixture of all four diastereomers, to produce aryl aldehyde and glycine. A mixture of all four diastereomers of arylserine (**15a**-**15l**) (0.21 mmol) and pyridoxal-5′-phosphate (PLP, 1 mM) was dissolved in Assay Buffer (910 µL). To this solution (2*S*)-TA (1 mg, 8.72 mg/mL) was added, and the reaction mixture was incubated at 31 °C. Aliquots were withdrawn at 0, 10, 20, and 40 min for **15a**-**15l** to assess the timeframe of the steady-state turnover. Each aliquot was derivatized according to the procedure described in **Scheme 2.1A** to convert them to their corresponding *O*-trimethylsilyl *N*-[(2*S*)-2-methylbutyryl] methyl esters, and analyzed by GC/EI-MS to determine that (2*S*)-TA was at steady state during the 10-min incubation.

2.2.15 Computational Methods for Biomolecular Docking.

Docking of the *trans*-3-arylglycidate enantiomers was performed using AutoDock Vina (version 1.1.2)[127] and AutoDock Tools (version 4.2.6).[128] The *trans*-cinnamate ligands and water molecules were first removed from the crystal structure of *Taxus canadensis* phenylalanine aminomutase (*Tc*PAM; PDB code: 3NZ4). Then the (2*R*,3*S*)- and (2*S*,3*R*)-3-arylglycidate ligands (**14a**–**14l**) and enzyme files were converted to the .pdbqt file format using the AutoDock Tools software to make them compatible with AutoDock Vina. An empty grid was created to define the binding site where the ligands would be docked in the *Tc*PAM active site. AutoDock Vina provided 9 orientations for each of the docked epoxides into the active site of *Tc*PAM. The lowest energy

(i.e., apparent highest affinity) and logically docked orientation for each epoxide enantiomer was chosen.

2.2.16 Calculation of Covalent van der Waals Volumes.

The molecular volumes of the substituents on the aryl carboxylate substrates were estimated as Connolly solvent-excluded volume[129] using Chem3D Ultra software (ver. 63.0, Perkin Elmer) and a probe radius of 0.2 Å. The volume of a phenyl radical was subtracted from the estimated volume of a phenyl attached to a substituent. The geometries of polyatomic substituents such as CH_3, OCH_3, NO_2 attached to phenyl were MM2 energy minimized using the default parameters of the Chem3D Ultra software.

2.3 Results and Discussion

2.3.1 Synthesis and Characterization of the Racemic 3-Arylglycidate Substrates.

Various commercially available aryl acrylic acids (**13a**–**13l**) were oxidized with Murray's reagent to synthesize the corresponding ring-substituted 3-arylglycidates (**14a**–**14l**) as their racemates (**Table 2.3**).[125] The enantiomeric ratios of each racemate methyl ester were ~1:1 by chiral GC/EI-MS analysis (**Figure. 2.12** and **Figure. 2.13**). Trifluoroacetone was used instead of acetone to modify Murray's reagent and oxidize the less reactive NO_2-cinnamate analogues to epoxides **14g** and **14h**. The 3-(4'-OCH_3-phenyl)glycidate rapidly hydrolyzed to the dihydroxy compound under these reaction conditions and thus could not be tested in this study.

Table 2.3. Synthesis of 3-Arylglycidate Analogues[a] and Isolated Yields.

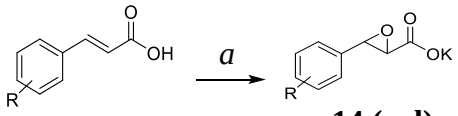

13 (a–l) **14 (a–l)**

Entry	R	Time (h)	Yield (%)	Entry	R	Time (h)	Yield (%)
14a	H	2	88	**14g**	3′-NO_2	24	30
14b	3′-OCH_3	24	41[b]	**14h**	4′-NO_2	24	28
14c	3′-CH_3	2	78	**14i**	4′-CH_3	24	68
14d	3′-F	12	63	**14j**	4′-F	16	91
14e	3′-Cl	2	86	**14k**	4′-Cl	16	86
14f	3′-Br	2	91	**14l**	4′-Br	6	64

[a]Step *i)* $NaHCO_3$, acetone (or 1,1,1-trifluoroacetone), H_2O (Murray′s reagent) (or $NaHCO_3$, $CF_3C(O)CH_3$, H_2O when R = NO_2); step *ii)* oxone in 0.4 mM EDTA, 2-24 h, 25 °C*;* and step *iii)* KOH in EtOH. [b]The product was an 88:12 mixture of compounds **14b** and **13b**, respectively.

2.3.2 Separation of *trans*-3-Arylglycidate Enantiomers using a Chiral- GC/EI-MS

The synthesized arylglycidate analogues were found to be racemic (**Figure. 2.12** and **Figure. 2.13**).

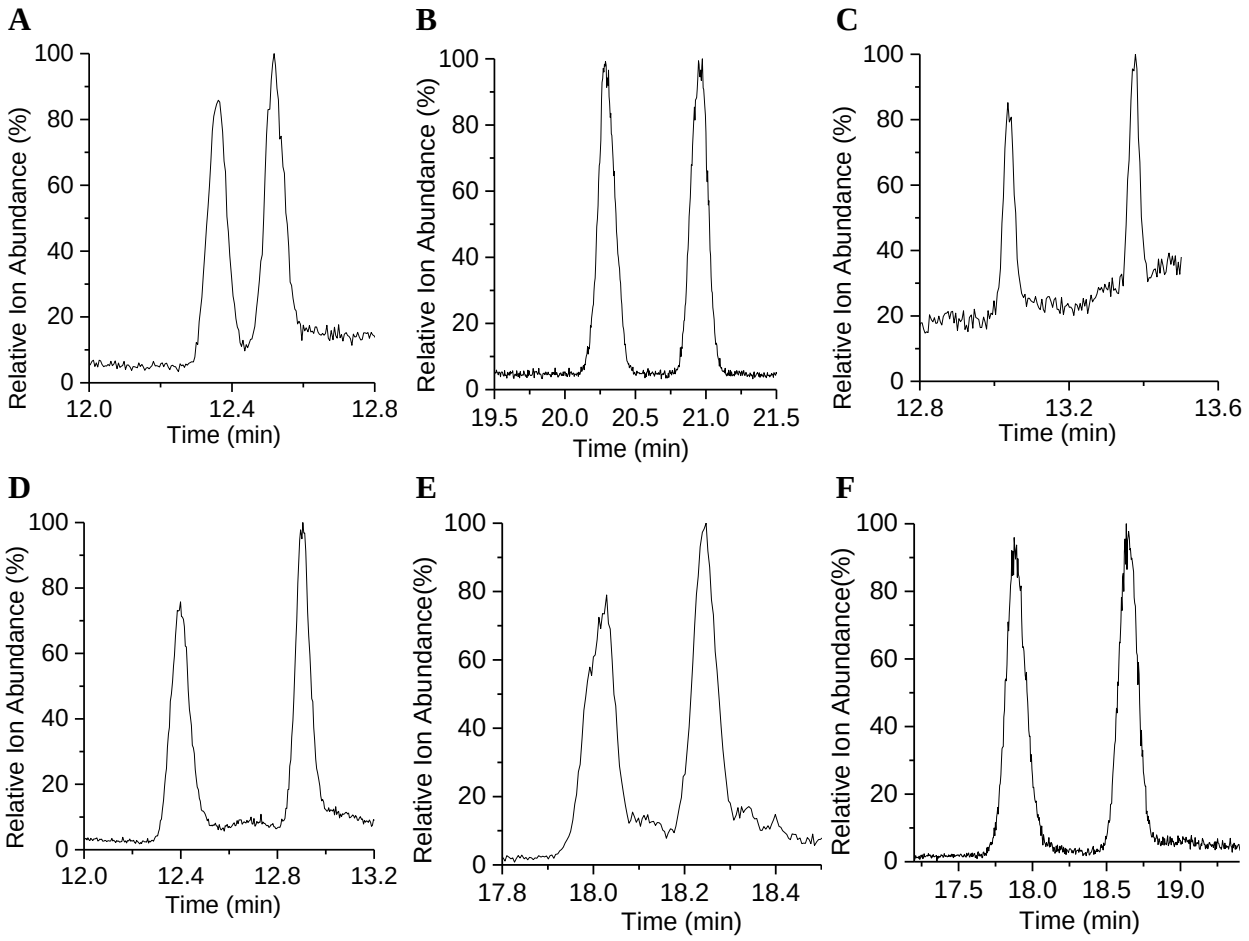

Figure. 2.12. Enantiopurity of the synthetically derived methyl esters of A) 3-phenylglycidate (**14a**) (49:51), extracted ion *m*/*z* 121; B) 3-(3'-OCH_3-phenyl)glycidate (**14b**) (50:50), extracted ion *m*/*z* 151; C) (**14c**) 3-(3'-CH_3-phenyl)glycidate (**14c**) (49:51), extracted ion *m*/*z* 135; D) 3-(3'-F-phenyl)glycidate (**14d**) (50:50), extracted ion *m*/*z* 139; E) 3-(3'-Cl-phenyl)glycidate (**14e**) (50:50), extracted ion *m*/*z* 155; and F) 3-(3'-Br-phenyl)glycidate (**14f**) (50:50), extracted ion *m*/*z* 199 analyzed by chiral GC/EI-MS. The base peak ion was used for extracted-ion selection of the derivatives; partial chromatograms are shown. The ratio of each enantiomer is shown in parentheses.

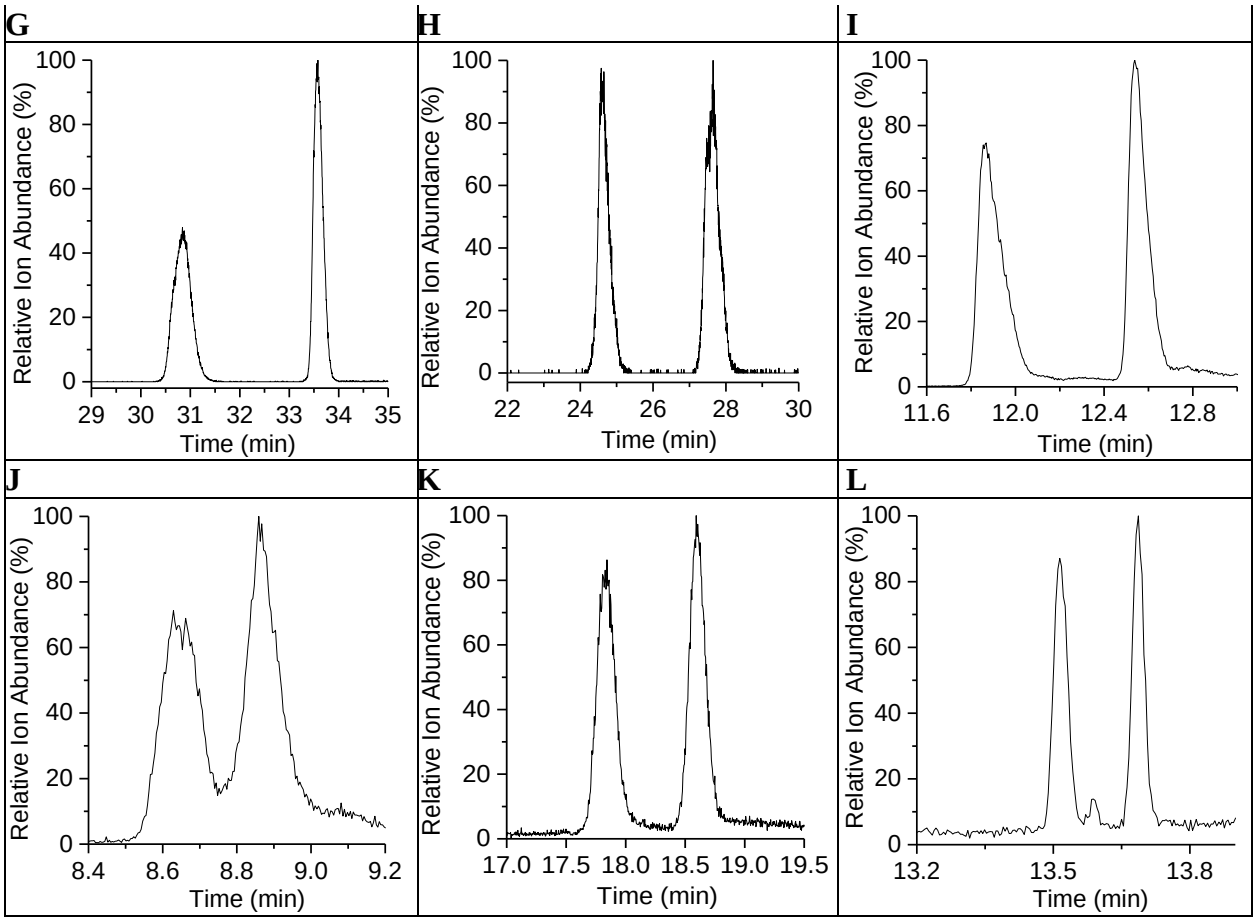

Figure. 2.13. Enantiopurity of the synthetically derived methyl esters of G) 3-(3'-NO_2-phenyl)glycidate (**14g**) (47:53), extracted ion *m*/*z* 166; H) 3-(4'-NO_2-phenyl)glycidate (**14h**) (46:54), extracted ion *m*/*z* 166; I) 3-(4'-CH_3-phenyl)glycidate (**14i**) (50:50), extracted ion *m*/*z* 135; J) 3-(4'-F-phenyl)glycidate (**14j**) (50:50), extracted ion *m*/*z* 139; K) 3-(4'-Cl-phenyl)glycidate (**14k**) (47:53), extracted ion *m*/*z* 155; and L) 3-(4'-Br-phenyl)glycidate (**14l**) (50:50), extracted ion *m*/*z* 199.analyzed by chiral GC/EI-MS. The base peak ion was used for extracted-ion selection of the derivatives; partial chromatograms are shown. The ratio of each enantiomer is shown in parentheses.

2.3.3 Hydrolysis of Arylglycidates in Assay Buffer

Racemic 3-arylglycidates (**14a**-**14l**) were stable in Assay Buffer up to 90 min, and there was no significant hydrolysis of the epoxide ring after 1 week in Assay Buffer for most of the glycidates (**Figure. 2.14**). However, **14a**, **14c**, and **14i** showed a slight (~5%) conversion to the dihydroxy product after one week of incubation. These results suggested that the 3-arylglycidate substrates are stable in the Assay Buffer during the amination reaction catalyzed by *Tc*PAM.

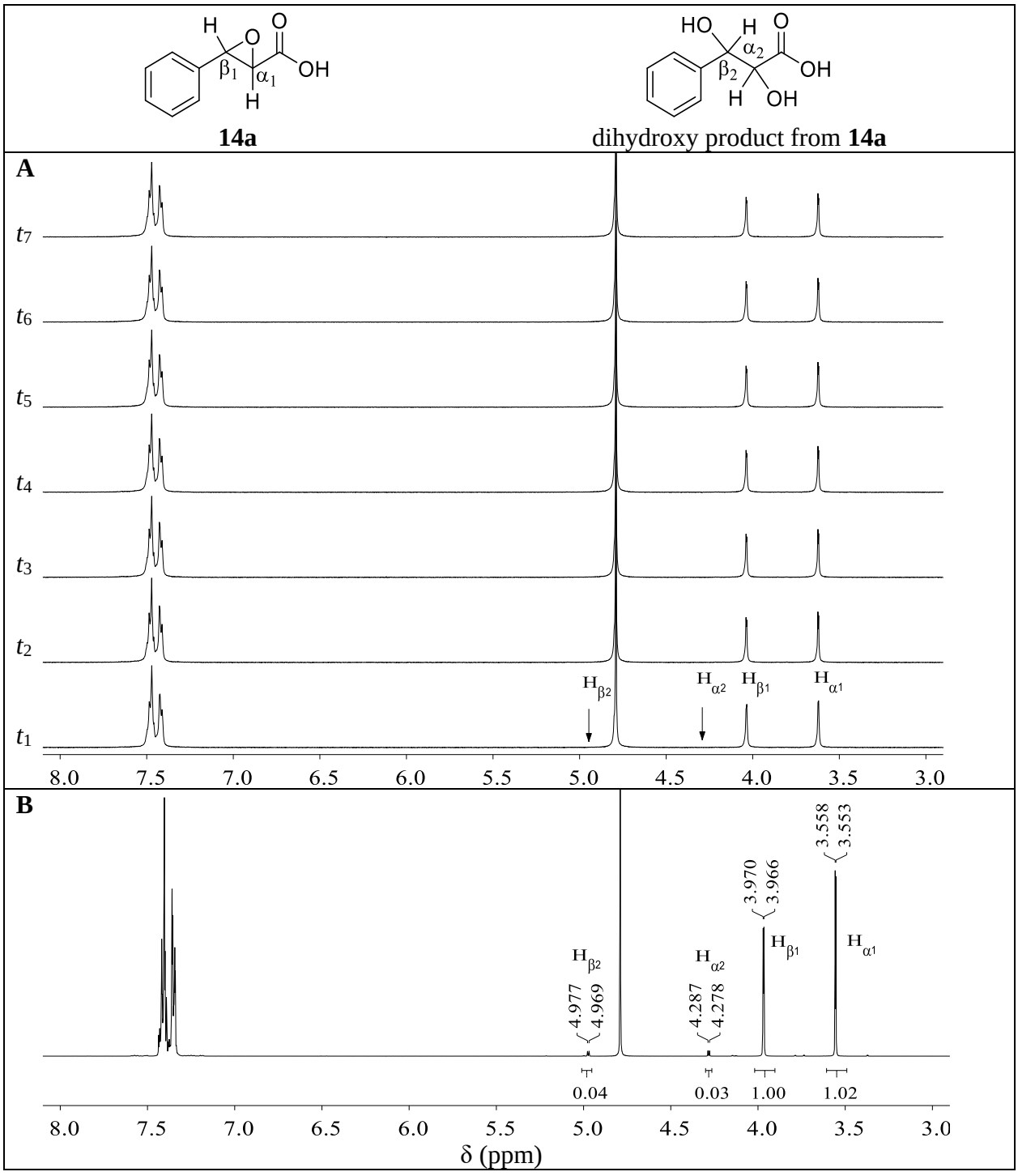

Figure. 2.14. ^{1}H NMR of 3-phenylglycidate (**14a**) in deuterated Assay Buffer. A) NMR spectra were recorded at 15 min intervals starting from t_1 to t_7. At t_1 = 0 min and at t_7 = 90 min, the ratio of **14a**:dihydroxy product = 100:0, and B) NMR spectrum after storing the sample in deuterated Assay Buffer at ~25 °C for 1 week, the ratio of **14a**:dihydroxy product = 100:4. See Appendix for the associated ^{1}H NMR data for other arylglycidate analogues (**14b**-**14l**).

2.3.4 Control-Assay Experiments

Table 2.4. Control Experiments.

Experiment (Exp)	NH_4OH (1 mM)	NH_4OH (2 M)	(2S)-styryl-α-alanine (**12**) (1 mM)	3-(3'-OCH_3-phenyl)glycidate (**14b**) (1mM)	*Tc*PAM (100 µg/mL)	3'-OCH_3-phenylserine (**15b**) produced (µM)	3'-OCH_3-phenylisoserine (**16b**) produced (µM)
1	–	–	–	+	+	0.05	0.02
2	–	–	+	+	+	31	11
3	+	–	–	+	+	0.06	0.02
4	+	–	–	+	–	0.03	0.01
5	–	+	–	+	+	17	230
6	–	+	–	+	–	16	250

In a pilot study that helped guide our kinetic analyses in our earlier published work[48] and later in this Chapter 2: for the substrate 3-(3'-OCH_3-phenyl)glycidate (**14b**), we observed that *Tc*PAM turned over **14b** to the highest proportion of isoserine (37%) relative to the serine isomer (63%) compared to the other glycidate substrates used in the study. We theorized that this higher isoserine proportioning likely resulted from nonenzymatic amination of the glycidate at the more electropositive C_β. Thus, **14b** was used as the model substrate in the control experiments to assess the contribution of nonenzymatic amination of the glycidates to the isoserine/serine distribution compared to that made from *Tc*PAM-catalyzed amination.

Experiment 1 (Exp-1), containing *Tc*PAM and the glycidate substrate **14b**, was incubated without an amine source, and a small amount of the hydroxy amino acids (~0.07 µM) was detected. Exp-3 was identical to Exp-1, except it contained 1 mM NH_4OH as the amine source, yet made a similarly low quantity of hydroxy amino acids (~0.08 µM) as in Exp-1. These experiments

suggested that the supplemental 1 mM NH_4OH did not improve enzyme turnover of the glycidate to its hydroxy amino acids compared to when the assay only had residual ammonia likely coming from the buffer containing the purified enzyme.[29] Control Exp-4, containing 1 mM NH_4OH yet no *Tc*PAM biocatalyst, contained a similar quantity of hydroxy amino acids (~0.04 μM), as in Exp-1 and Exp-3. The small amount of hydroxy amino acids from **14b** purportedly developed from occasional nonenzymatic epoxide-ring opening by the NH_4OH. Control Exp-5 (with biocatalyst) and 6 (without biocatalyst) were incubated with **14b** and 2 M NH_4OH as the amine source (**Table 2.4**). A mixture of serine **15b** and isoserine **16b** products, at 247 μM were measured in Exp-5 and at 266 μM in Exp-6, were similar and showed that at an elevated concentration of NH_4OH in the buffer, nonenzymatic ammonia-assisted ring-opening of the epoxide occurs predominantly. The conditions for control Exp-5 and Exp-6 were repeated for other glycidate substrates (**14a**, **14i**, and **14h**), and their product distributions were similar (**Figure. 2.36** in **Appendix**)

To summarize, Exp-3 and Exp-4 are identical to Exp-5 and Exp-6, respectively, except that the former two assays contain 1 mM NH_4OH, making trace amounts of products and the latter two 2 M NH_4OH, making >200 uM of products. Therefore, from these control experiments, we concluded that when the NH_4^+ salts are over 1 mM, the arylglycidates are aminated nonenzymatically. These results also informed us that the typical 6 M NH_4^+ salts used in earlier studies by other groups needed to stimulate an MIO-dependent enzyme to aminate arylacrylates[46,49,52] should be avoided while introducing glycidates as substrates.

The results of the preceding control assays informed us on Exp-2 that contained all the necessary components yet included 1 mM (2*S*)-styryl-α-alanine as the amine source to ensure the NH_4^+ salts in solution was <1 mM. In control Exp-2, **14b** was converted to serine **15b** and isoserine **16b** (~42 μM combined, 74% serine; 26% isoserine) by *Tc*PAM-catalyzed amination. The result

of the control experiments using **14b** helped us design an operational transamination assay that was driven by enzyme catalysis and not by an uncatalyzed side reaction to convert arylglycidates to hydroxy/amino-3-arylpropanoates.

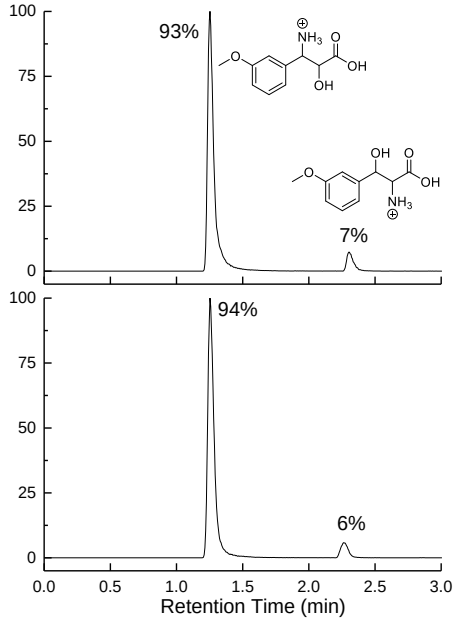

Figure. 2.15. Relative abundances of arylisoserine (**16b)** and arylserine (**15b**) products made from C_β- and C_α-amination, respectively, of 3-(3'-OCH_3-phenyl)glycidate (**14b**) (1 mM) when incubated with 2M NH_4OH and *Tc*PAM (100 µg/mL) (*top trace*) and without *Tc*PAM (*bottom trace*).

2.3.5 Biocatalysis of Arylserines and Arylisoserines.

Each arylglycidate substrate was incubated separately with the amine donor (2*S*)-styryl-α-alanine (**12**) and *Tc*PAM[51] at pH 8.0 to make the ring-opened hydroxy amino acids, arylserines, and arylisoserines. (2*S*)-Styryl-α-alanine (**12**) was used to aminate the MIO moiety of *Tc*PAM instead of 6 M ammonium salts at pH 9 used in several previous studies to convert various cinnamates to α- and β-amino acids.[46,49,53] Further, as we showed in this thesis through control experiments, an earlier study also demonstrated that high concentrations of ammonia nonenzymatically convert arylglycidates by nearly exclusive amination at the benzylic carbon (C_β) to arylisoserine.[130] The selective synthetic amination of arylglycidates at C_β is directed by the

ability of the benzylic functional group to resonance stabilize the δ^+ formed in the transition state (**Figure. 2.16**). This electronic-based regioselectivity would therefore be sensitive to the electronic effects of substituents on the aryl ring. Control experiments (with or without the *Tc*PAM catalyst) in this study showed that after incubating 2 M NH_4OH in 50 mM phosphate buffer, pH 8 for 2.5 h with the 3-arylglycidate substrate bearing a mesomerically electron-withdrawing 4'-NO_2 (**14h**), the amination reaction yielded a ~40:60 mixture of isoserine to serine, with the latter predominating (**Figure. 2.15**A). The 4'-NO_2 group ($\sigma_{4'\text{-}NO_2}$ = 0.78) (where σ is the Hammett substituent constant)[131] is positioned to pull electron density of the epoxide oxygen toward C_β, polarize the C_α–O bond, and thus encourage nucleophilic amination at C_α to form mostly arylserines as observed (**Figure. 2.16**). By contrast, 3-phenylglycidate (**14a**) ($\sigma_{[H]}$ = 0.0) and its 3'-OCH_3 (**14b**) ($\sigma_{[3'\text{-}OCH_3]}$ = 0.12) and 4'-CH_3 (**14i**) ($\sigma_{[4'\text{-}CH_3]}$ = -0.17) analogues have similar electronic influence on the epoxide ring opening. Substrates **14a**, **14b**, and **14i** favored intrinsic amination at C_β to form the corresponding arylisoserines at ≥93% compared to the lesser amount of arylserine when incubated with 2 M NH_4OH (**Figure. 2.15**), as observed in earlier synthetic studies.[130,132] Thus, (2*S*)- styryl-α-alanine (**12**) was chosen as a milder amine source to dissect the regiochemistry and stereoselectivity of *Tc*PAM transamination catalysis.

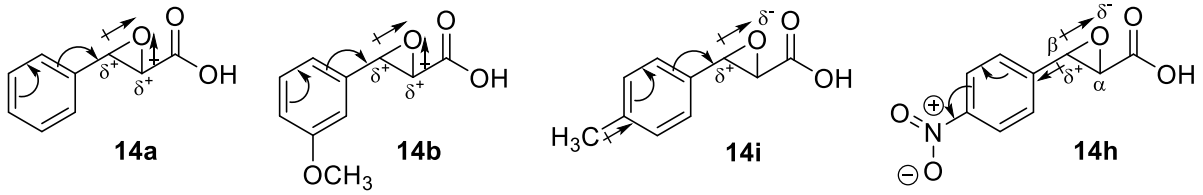

Figure. 2.16. Resonance and inductive stabilizations of the partial positive charge (δ^+) (due to bond polarization) at the C_β of arylglycidate substrates **14a**, **14b**, and **14i** assisted by the aryl-ring. For substrate **14h**, the electron-withdrawing NO_2 group resonance destabilizes the δ^+ at the benzylic carbon (C_β), and the regioselectivity is reversed, directing an incoming nucleophile to attack at C_α preferentially.

2.3.6 Synthesis of Arylserine Diastereomers.

Various ring-substituted arylserine analogues (**15a**–**15l**) were synthesized using the aldol condensation reaction between the corresponding aryl aldehyde (**19a**–**19l**) and glycine (**Scheme 2.1B**). *anti*-Arylserine was formed predominantly over their *syn*-isomers. The *anti*:*syn* ratio varied from 97:3 (for 3′-Cl) to 45:55 (for 4′-Cl). This gave access to all possible stereoisomers of arylserines (**Figure. 2.8**A) which were later used as synthetic standards to characterize the biocatalyzed arylserines formed from 3-arylglycidates and *Tc*PAM.

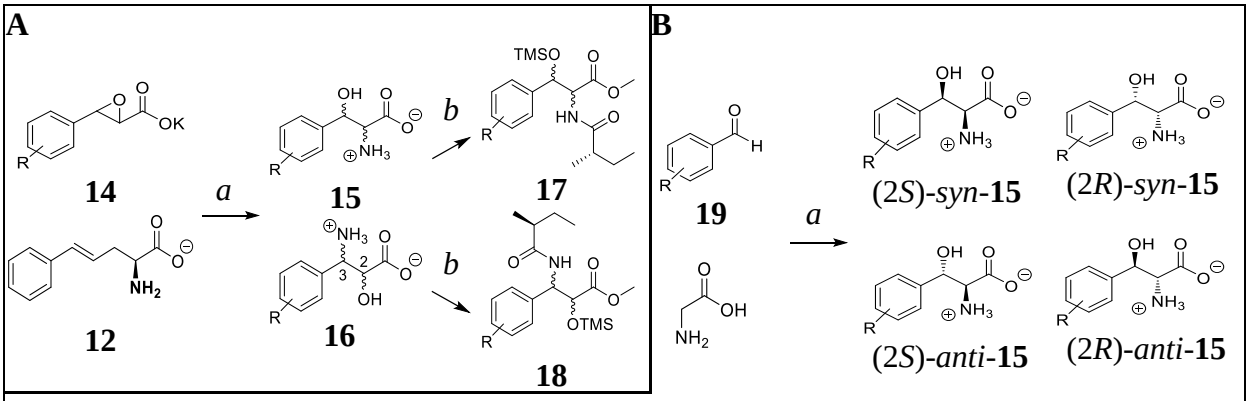

Entry	R	*anti*:*syn*	Entry	R	*anti*:*syn*
15a	H	75:25	**15g**	3′-NO_2	96:4
15b	3′-OCH_3	71:29	**15h**	4′-NO_2	83:17
15c	3′-CH_3	68:32	**15i**	4′-CH_3	72:28
15d	3′-F	71:29	**15j**	4′-F	52:48
15e	3′-Cl	97:3	**15k**	4′-Cl	45:55
15f	3′-Br	58:42	**15l**	4′-Br	58:42

Scheme 2.1. A) *Tc*PAM was incubated with (2*S*)- styryl-α-alanine (**12**) (1 mM) and separately with each *trans*-3-phenylglycidate racemate (**14a**–**14l**). Step *a*) *i) Tc*PAM (1.7 mg/mL) in Assay Buffer, 2 min pre-equilibration, **14a**–**14l** (10 mM), 29 °C, 4 h. Step *b*) Derivatization of putative phenylserines and phenylisoserines using a chiral auxiliary for stereoisomeric resolution. *i*) (2*S*)-2-Methylbutyric anhydride, pyridine, rt, 20 min; *ii*) 6 M HCl, pH 2; *iii*) CH_2N_2, EtOAc/MeOH (3:1 *v*/*v*), rt, 15 min; and *iv*) chlorotrimethylsilane, pyridine, CH_2Cl_2, rt, 15 min. *Insets*: stereoisomerism of (2*R*,3*S*)-*syn*-phenylisoserine. B) Synthesis of the stereoisomers of phenylserine analogues from glycine and a substituted benzaldehyde. a) step *i*) triethylamine, *n*-BuOH and H_2O, 12 h, rt; step *ii*) 6 M HCl, pH 2; and step *iii*) $NaHCO_3$, pH 6.

2.3.7 Assessing the Regiochemistry of the *Tc*PAM-catalyzed Transamination Reaction.

The regiochemistry and relative stereochemistry of the mutase amination reaction were assigned by derivatizing the products made from biocatalysis. For example, authentic racemic (2*S*)+(2*R*)-*syn*-phenylserine [(2*S*)+(2*R*)-*syn*-**15a**] and (2*R*,3*S*)-*syn*-phenylisoserine [(2*R*,3*S*)-*syn*-**16a**] standards (**Figure. 2.8**) were converted to their *O*-trimethylsilyl *N*-[(2*S*)-2-methylbutyryl] methyl esters (**Scheme 2.1A**).

The diagnostic fragment ions shown in the GC/EI-MS profile for the derivatized authentic phenylserine racemate were identical to those of the biocatalyzed phenylserine diastereomers yet distinct from those of the (2*R*,3*S*)-*syn*-phenylisoserine ((2*R*,3*S*)-*syn*-**16a**) standard derivatized identically (**Figure. 2.17**). GC/EI-MS fragmentation of the other biocatalytically made phenylserine analogues (**15a**–**15l**) was identical to the ion profiles of the corresponding synthetic phenylserine analogues derivatized identically (See Appendix).

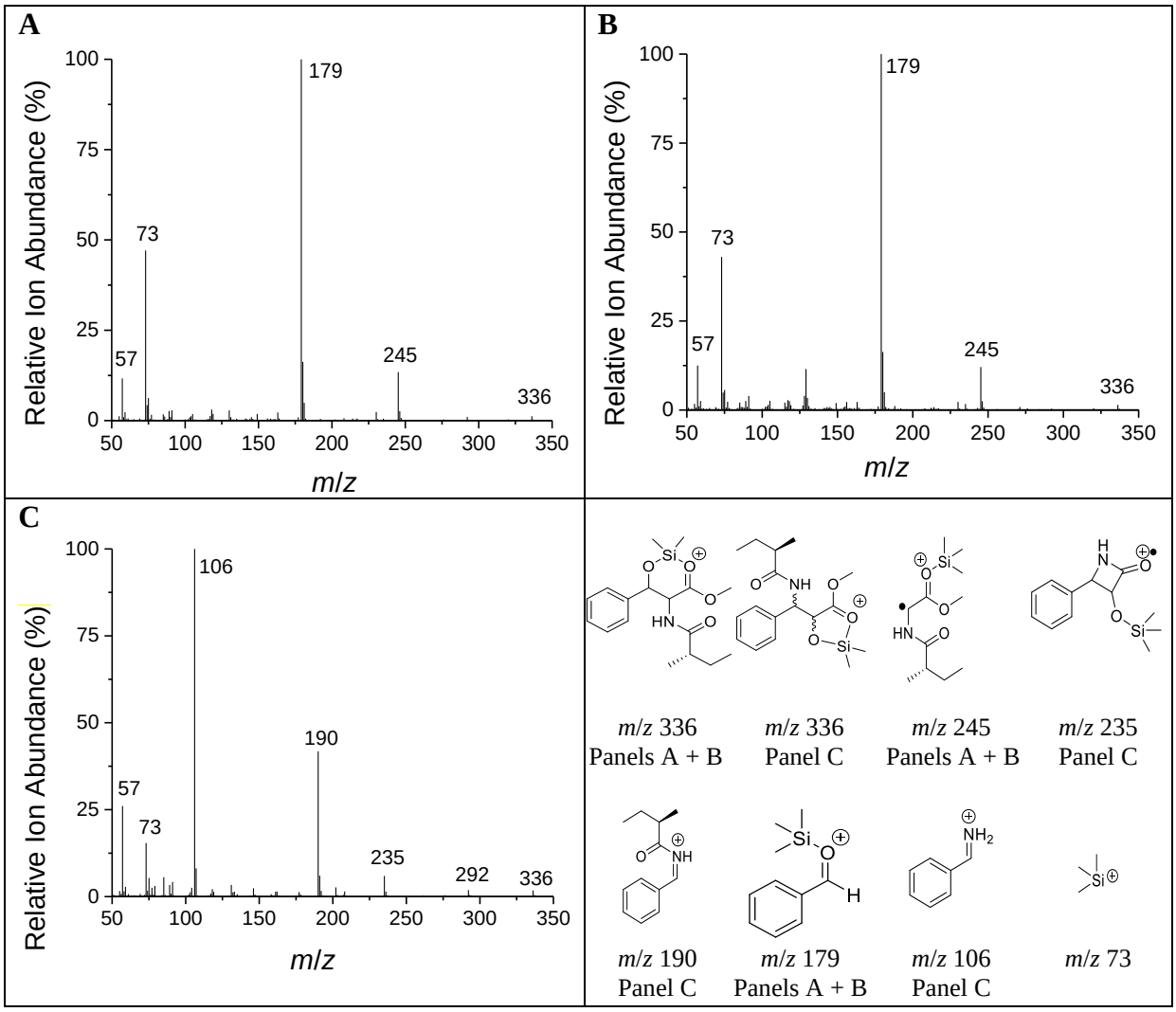

Figure. 2.17. GC/EI-MS spectra of authentic A) (2*S*)+(2*R*)-*syn*-phenylserine from Sigma-Aldrich, B) phenylserine biocatalyzed from 3-phenylglycidate by *Tc*PAM catalysis (see **Figure. 2.19** for GC profiles), and of C) (2*R*,3*S*)-*syn*-phenylisoserine (see **Figure. 2.72** for GC profile). Each hydroxy amino acid was derivatized to its *O*-trimethylsilyl *N*-[(2*S*)-2-methylbutyryl] methyl ester. The molecular ion (M•+, *m*/*z* 351) was not observed for either analyte.

*Tc*PAM could theoretically transfer the amino group to either C_α or C_β of the glycidate substrate to make phenylserine or phenylisoserine, respectively. We hypothesized that the aryl ring alone and the electronics of the substituents attached to it would differentially affect the reactivity at C_β toward nucleophilic amination, as they did in our control experiments. However, the regiochemical analysis showed that regardless of the electronic nature of the substituent attached to the aryl ring, *Tc*PAM aminated predominantly at C_α to open the 3-arylglycidates.

2.3.8 Establishing Relative Stereoconfiguration of Arylserines by ^{1}H NMR Analysis.

A ^{1}H NMR method was developed to establish the relative *syn*/*anti*-stereoconfigurations of the four synthesized arylserine diastereomers. The coupling constants for the vicinal protons (H_α and H_β) were similar ($^3J_{H_\alpha\text{-}H_{\beta(anti)}}$ and $^3J_{H_\alpha\text{-}H_{\beta(syn)}} \approx 4$ Hz) for the underivatized synthetic *anti*- and *syn*-phenylserine diastereomers (**15a**). Thus, differences in H_α and H_β coupling constants could not be used to distinguish the *anti*- and *syn*-diastereomers, as done in another study.[133] Thus, a small amount of authentic (2*S*)+(2*R*))-*syn*-phenylserine racemate was added to the synthesized mixture of *anti*- and *syn*-phenylserine diastereomers (**Figure. 2.18**A). The ^{1}H NMR of the "spiked" sample showed a relative increase of the doublet pair ("outer doublets") at δ 4.23 and δ 5.41 (**Figure. 2.18**B).

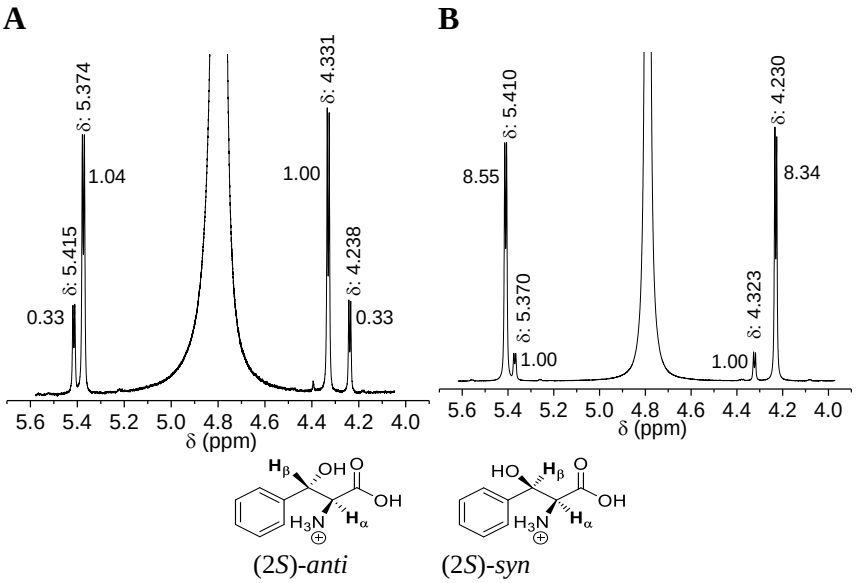

Figure. 2.18. An expanded 500 MHz ^{1}H NMR of A) synthesized phenylserine (**15a**), and B) of **15a** containing authentic (*2S*)-*syn*-phenylserine recorded in D_2O at pH 1.5. Chemical shift values are listed vertically above each peak, and the relative area under each peak is listed horizontally next to each peak.

The chemical shift difference (Δδ) of 1.15 ppm at pH 1.5 for the "outer doublets" assigned these signals to the *syn*-phenylserine enantiomers. The "inner doublets" at δ 4.33 and δ 5.37 ($\Delta\delta_{anti}$ = 1.04 ppm, pH 1.5) were thus assigned to the *anti*-phenylserine enantiomers. We used the trends in

the Δδ values to assign the relative *anti*/*syn*-stereochemistries and *anti*:*syn* ratios of the remaining synthetic and biocatalyzed arylserine analogues without derivatization.

Each chemically synthesized and biocatalyzed arylserine analogue was dissolved separately in D_2O at pH 1.5 and analyzed by ^1H NMR. The $\Delta\delta_{syn}$ (~1.15 ppm, pH 1.5) of the "outer doublets" was consistently larger than the ($\Delta\delta_{anti}$) (~1.05 ppm, pH 1.5) for the "inner doublets" (**Table 2.5** and **Figure. 2.48**–**Figure. 2.59**).

Table 2.5. 500 MHz ^1H NMR data for the synthetic and biocatalyzed arylserine analogues (**15a**–**15l**) recorded in D_2O at pH 1.5.

	R	$^3J_{H_\alpha\text{-}H_\beta}$ *anti* (Hz)	$^3J_{H_\alpha\text{-}H_\beta}$ *syn* (Hz)	$\Delta\delta_{anti}$[b] (ppm)	$\Delta\delta_{syn}$[b] (ppm)	$^3J_{H_\alpha\text{–}H_\beta}$ biocatalyzed (Hz)	$\Delta\delta_{biocatalyzed}$ (ppm)	*anti*:*syn*[c] (NMR)[a]	*anti*:*syn*[c] (GC-MS)
15a	H	4.0	4.0	**1.04**	1.17	4.0	**1.05**	93:7	91:9
15b	3′-OCH_3	4.0	4.0	**1.02**	1.15	4.0	**1.02**	100:0	95:5
15c	3′-CH_3	4.0	4.0	**1.00**	1.14	4.0	**1.01**	100:0	96:4
15d	3′-F	4.0	4.0	**1.02**	1.16	4.0	**1.04**	98:2	95:5
15e	3′-Cl	4.0	4.0	**1.03**	1.18	4.0	**1.01**	91:9	94:6
15f	3′-Br	4.0	4.0	**1.02**	1.17	4.0	**1.02**	93:7	92:8
15g	3′-NO_2	4.0	4.0	**1.08**	1.21	3.5	**1.08**	93:7	92:8
15h	4′-NO_2	3.5	4.0	**1.06**	1.22	4.0	**1.09**	97:3	96:4
15i	4′-CH_3	4.0	4.0	**1.00**	1.13	4.0	**0.99**	100:0	95:5
15j	4′-F	4.0	4.0	**1.03**	1.16	4.0	**1.03**	93:7	97:3
15k	4′-Cl	4.0	4.0	**1.03**	1.16	4.0	**1.00**	100:0	91:9
15l	4′-Br	4.0	4.0	**1.00**	1.13	4.0	**0.98**	100:0	95:5

[a]"0" indicates that the *syn*-isomer was below the limits of detection of the NMR (at ~100 nmol). [b]$\Delta\delta_{anti}$ and $\Delta\delta_{syn}$ values for the synthetic phenylserine analogues. [c]*anti*:*syn* ratio for the biocatalyzed arylserine analogues. n = 3. Standard error < 1%.

The NMR analysis substantiated that *Tc*PAM aminated the epoxide substrates predominantly at C_α to produce *anti*-arylserine analogues as the major product, regardless of the substituent on the aryl ring. A smaller amount (≤9%) of the *syn*-phenylserines was also made (See Appendix **Figure. 2.48**–**Figure. 2.59**).

Table 2.6. 500 MHz ^{1}H NMR data for the chemically synthesized arylserine analogues (**15a**–**15l**) recorded in D_2O at a pH range of 0-4.0.

Entry	R	pH	$^3J_{H_\alpha\text{-}H_\beta}$ (*anti*) (Hz)	$^3J_{H_\alpha\text{-}H_\beta}$ (*syn*) (Hz)	$\Delta\delta_{anti}{}^b$ (ppm)	$\Delta\delta_{syn}{}^b$ (ppm)
15a	H	4.0	4.0	4.0	1.26	1.37
		3.0	4.0	4.0	1.23	1.34
		1.5	4.0	4.0	1.05	1.18
		1.0	4.0	4.0	0.99	1.13
15b	3′-OCH_3	2.0	4.0	4.0	1.03	1.16
		1.5	4.0	4.0	1.01	1.14
15c	3′-CH_3	2.0	4.0	4.0	1.02	1.16
		1.5	4.0	4.0	1.00	1.14
15d	3′-F	3.0	4.0	4.0	1.22	1.34
		2.5	4.0	4.0	1.22	1.34
		1.5	4.0	4.0	1.02	1.16
15e	3′-Cl	3.5	4.0	4.5	1.24	1.36
		3.0	4.0	4.5	1.23	1.36
		2.0	4.0	4.5	1.08	1.22
		1.5	4.0	4.0	1.03	1.18
15f	3′-Br	3.5	4.0	4.5	1.23	1.36
		3.0	4.0	4.5	1.23	1.35
		2.0	4.0	4.0	1.12	1.24
		1.5	4.0	4.0	1.02	1.17
		1.0	4.0	4.0	0.97	1.12
15g	3′-NO_2	3.5	3.5	4.5	1.31	1.40
		3.0	3.5	4.5	1.30	1.40
		1.5	4.0	4.0	1.08	1.21
15h	4′-NO_2	3.0	3.5	4.0	1.27	1.40
		2.5	3.5	4.0	1.26	1.39
		1.5	3.5	4.0	1.06	1.22
15i	4′-CH_3	2.5	4.0	4.0	1.05	1.17
		1.5	4.0	4.0	1.00	1.13
15j	4′-F	2.0	4.0	4.0	1.10	1.22
		1.5	4.0	4.0	1.03	1.16
15k	4′-Cl	3.5	4.0	4.5	1.25	1.36
		3.0	4.0	4.5	1.25	1.36
		1.5	4.0	4.0	1.03	1.16
15l	4′-Br	1.5	4.0	4.0	1.00	1.13
		1.0	4.0	4.0	0.94	1.09

2.3.9 Relative Stereochemistry of the *Tc*PAM Reaction by Chiral Auxiliary Derivatization.

An orthogonal GC/MS separation method was used to verify the relative stereoconfiguration of the biocatalyzed arylserines assigned earlier in this study by a ^{1}H NMR method. The chiral *N*-(*S*)-methylbutyryl-*O*-trimethylsilyl methyl ester derivatization of the arylserines described herein were extended to a diastereomeric mixture of synthesized (2*S*)+(2*R*)-*syn*-**15a** and (2*S*)+(2*R*)-*anti*-**15a** (**Figure. 2.19**A), commercial-grade (2*S*)+(2*R*)-*syn*-**15a** (**Figure. 2.19**B), and **15a** biocatalyzed by *Tc*PAM from the racemic 3-phenylglycidate (**14a**) (**Figure. 2.19**C) (**Scheme 2.1A**). GC/MS profiles for the *N*,*O*-derivatives of the commercial (2*S*)+(2*R*)-*syn*-phenylserine had major peaks at retention times 8.10 min and 8.13 min (**Figure. 2.19**B) and thus established the stereochemistry of the later-eluting isomeric pair in the mixture. The retention times of these most abundant peaks in the commercial sample matched those of the lower abundant peaks for the derivatized isomers in the synthetic **15a** sample (**Figure. 2.19**A). The derivatized enantiomers in the phenylserine diastereomeric mixtures eluting at 7.95 min and 8.01 min were therefore assigned as (2*S*)+(2*R*)-*anti*-phenylserine (**Figure. 2.19**).

In summary, the derivatives of the *anti*-phenylserine enantiomers eluted first, and the *syn*-phenylserine enantiomers eluted later from the GC/MS. In the biocatalyzed sample, *Tc*PAM diastereoselectively turned over the racemate of phenylglycidate to a mixture of (2*R*)+(2*S*)-*anti*-phenylserines with one enantiomer predominating (**Figure. 2.19**C). The arylserines made from glycidates **14b**–**14l** by *Tc*PAM catalysis were derivatized to **17b**–**17l** and analyzed by GC/MS to assign the relative stereochemistries (**Figure. 2.60** and **Figure. 2.61**). The biocatalyzed products contained (2*R*)+(2*S*)-*anti*-arylserines as the major stereoisomers, with one enantiomer predominating, while the (2*R*)+(2*S*)-*syn*-arylserines were minor, at ≤9% relative abundance (**Table 2.5**).

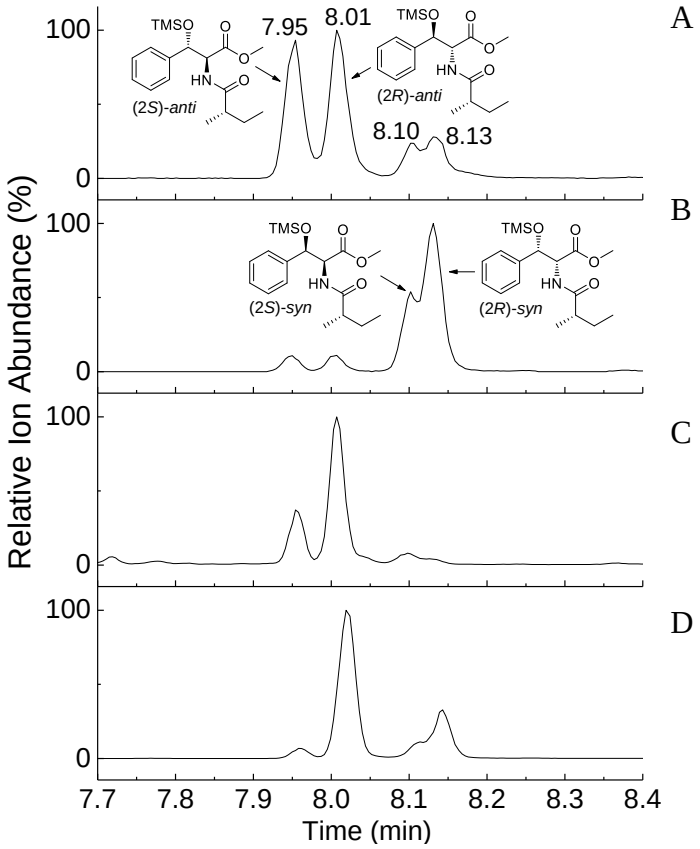

Figure. 2.19. Gas-chromatography/mass spectrometry extracted-ion (*m*/*z* 179) chromatograms of A) synthesized phenylserine (**15a**), as shown in **Scheme 2.1B,** was derivatized with a chiral auxiliary as per **Scheme 2.1A**. Peaks at 7.95 min and 8.01 min correspond to (2*S*)+(2*R*)-*anti*-phenylserine isomers, and those at 8.10 and 8.13 min correspond to (2*S*)+(2*R*)-*syn*-phenylserine isomers; B) derivatized authentic (2*S*)+(2*R*)-*syn*-phenylserine racemate (Sigma-Aldrich, contains 13% (2*S*)+(2*R*)-*anti*-phenylserine as an impurity; C) chiral-auxiliary of biocatalyzed phenylserine made from the racemic 3-phenylglycidate. Biocatalyzed (2*S*)+(2*R*)-*syn*-phenylserine stereoisomers were also produced at ~9% (peaks at 8.10 and 8.13 min); and D) Extracted ion (*m*/*z* 179) chromatogram of derivatized phenylserine after treating with (2*S*)-TA for 15 min.

2.3.10 Absolute Stereochemistry of the *Tc*PAM Reaction by Aldolase Resolution.

To assess which enantiomer was biocatalyzed more abundantly among the (2*R*)+(2*S*)-*anti*-arylserines, we used a low specificity (2*S*)-threonine aldolase (TA) from *E. coli*.[134] This enzyme resolution step cleaved the (2*S*)-*anti* diastereomers into a benzaldehyde moiety and glycine, resolving the synthesized (2*R*)-*anti*-hydroxy amino acid diastereomers. Each stereoisomeric mixture of synthesized arylserine (entries **15a**–**15l**) was treated with (2*S*)-TA. Aliquots were withdrawn at 15 min under steady-state enzymatic turnover to measure the relative abundances of

the arylserine diastereomers. The remaining arylserine stereoisomers were treated sequentially with (2*S*)-2-methylbutyric anhydride, diazomethane, and chlorotrimethylsilane.

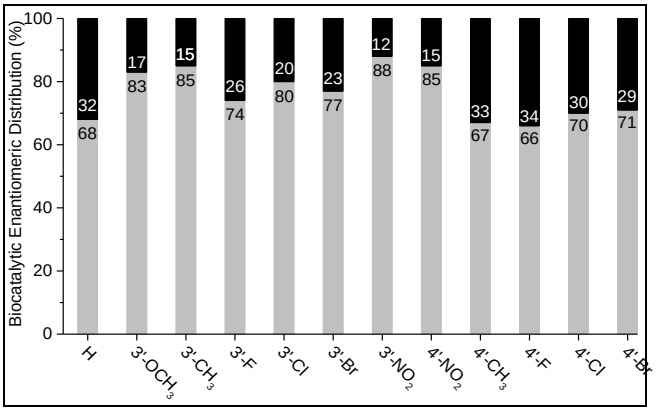

Figure. 2.20. Distribution of enantiomers (2*R*)-*anti* (gray bars) and (2*S*)-*anti* (black bars) in biocatalyzed products for the substituted phenylserine analogues.

GC/EI-MS analysis of each derivatized arylserine showed that the peak corresponding to the (2*S*)-*anti* isomer diminished relative to that for the (2*R*)-enantiomer (see **Figure. 2.19**D and **Figure. 2.62**–**Figure. 2.63**). We could then assign the 2*R*-*anti* and 2*S*-*anti*-isomers of each arylserine and calculate the 2*R*:2*S*-*anti* ratios of the biocatalyzed arylserines (**Figure. 2.20**). The 2*R*:2*S*-*anti* ratios for the biocatalyzed arylserines ranged from 66:34 (4'-F-phenylserine, **15j**) to 88:12 (3'-NO_2-phenylserine, **15g**) with the (2*R*)-*anti* isomer predominating (**Figure. 2.20**). The 2*R*:2*S* ratios for each *syn*-biocatalyzed product could not be calculated accurately because of their ~10-fold lower abundance than the *anti*-isomers and poorer resolution on the GC/MS (see **Figure. 2.19**B as an example). The *anti*:*syn* ratios calculated from the abundance of derivatized biocatalyzed arylserines determined by GC/MS analysis agreed with those calculated by the ^{1}H NMR method for the underivatized biocatalytically made arylserines (**Table 2.5**). There was no clear trend that explained how a combination of substituent electronic effects, position, and sterics influenced the *R*:*S* ratios of the arylserines made.

2.3.11 Epoxide Substrate Docking Model of *Tc*PAM.

We used solved structures of *Tc*PAM in complex with cinnamic acid (PDB code: 3NZ4 and 4CQ5) to help interpret whether the proposed dockings of 3-arylglycidate analogues in the *Tc*PAM active site by the AutoDock program were reasonable. The 3-phenylglycidate enantiomers, (2*S*,3*R*)-**14a** and (2*R*,3*S*)-**14a**, docked in the crystal structure of the TcPAM active site (**Figure. 2.21**A −**C**) were consistent with the conformation of the naturally occurring cinnamate intermediate in the crystal structure (**Figure. 2.21**D); the carboxylate group pointed toward Arg325, and the aryl binding region comprised key residues Ile431, Leu108, Leu104, and Leu227 (**Figure. 2.21**B and C). Docking poses suggest that (2*S*,3*R*)-**14a** yields the (2*R*)-*anti*-phenylserine (**Figure. 2.22**). The *anti*-stereochemistry of the arylserine products follows a mechanism proceeding through backside nucleophilic (S_N2) attack by the NH_2 group at C_α of the epoxide ring. The docked conformation of (2*S*,3*R*)-**14a** places the epoxide oxygen 2.7 Å from the catalytic Tyr80 of *Tc*PAM. Tyr80 normally functions as a general acid/base during the natural α- to β-phenylalanine isomerase reaction catalyzed by *Tc*PAM. Here, we believe Tyr80 also serves as a general acid to promote protonation-initiated epoxide opening during amination by the NH_2-MIO.

Conversely, the docked (2*R*,3*S*)-**14a** enantiomer is poised for making the (2*S*)-*anti*-arylserine. The oxirane oxygen of (2*R*,3*S*)-**14a** sits 2.9 Å from Tyr322 that has been identified as a key residue involved in forming the MIO moiety and keeping the NH_2-MIO adduct deprotonated so that it functions as a nucleophile during the normal *Tc*PAM-catalyzed isomerase reaction (**Figure. 2.21**A).[135] *Tc*PAM likely uses Tyr322 effectively as a surrogate general acid for protonation-initiated epoxide opening during amination by the NH_2-MIO of (2*R*,3*S*)-**14a**.

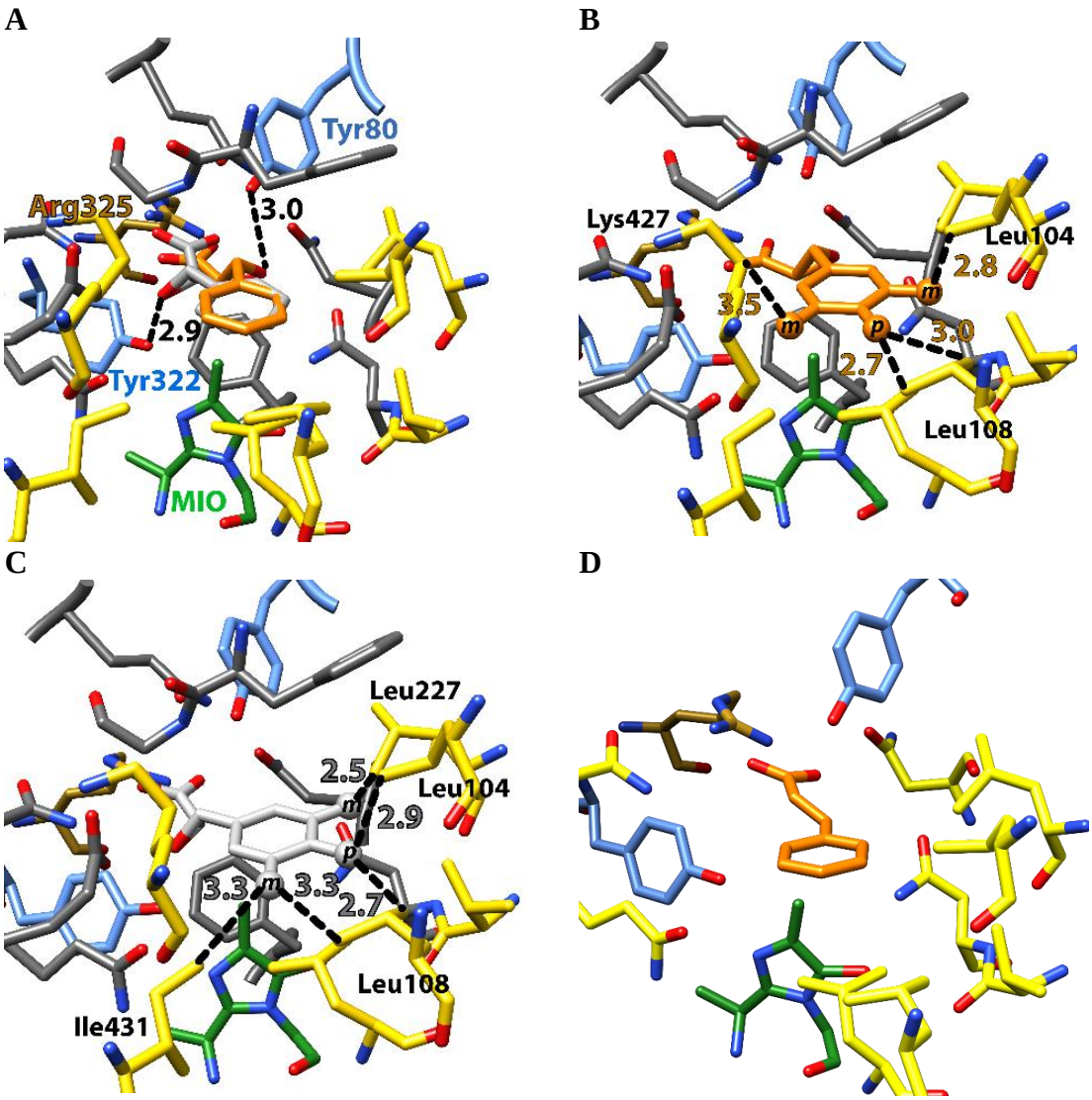

Figure. 2.21. A) Lowest energy binding poses are shown of (2*S*,3*R*)-3-phenylglycidate ((2*S*,3*R*)-**14a**) (orange sticks) and (2*R*,3*S*)-3-phenylglycidate ((2*R*,3*S*)- **14a**) (light-gray sticks) at center of the image. The conformations are consistent with the active site of *Tc*PAM consisting of residues (shown as dark gray and yellow sticks), the catalytic Tyr80, a putative catalytic Tyr322 (light blue sticks), binding contact Arg325 (golden-rod sticks), and the methylidene imidazolone (MIO) moiety (green sticks). B) (2*S*,3*R*)- **14a** (orange sticks) and C) (2*R*,3*S*)- **14a** (light-gray sticks) are posed separately in the active site to highlight the nominal distances (<3.5 Å) that substituents on the aryl ring are from active site residues. Printed on the aryl ring, '*m*' designates *meta*-positions (equivalent to the 3'-designation used in the text), and '*p*' designates the *para*-position (equivalent to the 4'-designation used in the text) per ligand. Heteroatoms are colored red for oxygen and blue for nitrogen. The images were produced with UCSF Chimera,[136], and the docking conformations were generated with AutoDock Vina[127] from PDB code 3NZ4. Numbers are distances in Å. D) *Tc*PAM in complex with cinnamic acid, based on PDB codes 3NZ4 and 4CQ5.

In this study, the *syn*-arylserine isomers were made at low levels compared to the *anti*-isomers for each arylglycidate analogues, and their resolution as chiral derivatives on GC/MS was poor; thus, accurate measurements of the ratio of the *syn*-enantiomers could not be made. The (2*R*)- and (2*S*)-*anti*- arylserine isomers are made through S_N2 attack by the amino group on the σ* antibonding orbital of C_α–O bond of the (2*S*,3*R*)- and (2*R*,3*S*)-glycidate racemates, respectively (**Figure. 2.22**, route *a*). However, the 2*S*- and 2*R*-*syn*-arylserine diastereomers cannot be accessed through a similar S_N2-type mechanism unless *Tc*PAM can rotate the substrate into a cisoid conformation that aligns C_α in a proper orientation for nucleophilic attack.

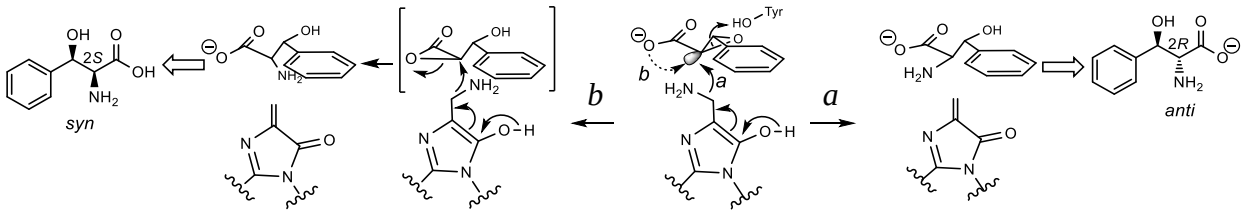

Figure. 2.22. *a*) Rendering of the mechanism showing attack of the NH_2-MIO on the σ* antibonding orbital (gray lobe) at C_α for the C–O σ bond of (2*S*,3*R*)-**14a** to produce (2*R*)-*anti*-phenylserine. *b*) A double inversion-of-configuration mechanism is envisioned to access the minor *syn*-stereoisomer that proceeds through a putative lactone intermediate.

Earlier mechanistic studies suggest that during its natural reaction, *Tc*PAM rotates the cinnamate intermediate about a central axis through a bicycle-pedal motion to invert the faces of the α- and β-carbons 180° from their original positions.[124,135] This rotation enables the NH_2 group of the MIO adduct to add to the opposite face of C_β from which it was removed from the phenylalanine substrate (see **Figure. 2.3**). The oxirane ring prevents rotations about the axis between C_α and C_β. Thus, a double inversion-of-configuration mechanism is envisioned to access the minor *syn*-stereoisomers (<10% relative abundance) that proceeds through a putative oxiranone intermediate (**Figure. 2.22**, route *b*).[137] Through the proposed oxiranone intermediate pathway, the (2*S*,3*R*)-**14a** that produces the more abundant (2*R*)-*anti*-phenylserine at 8.01 min

(**Figure. 2.19**C) likely also makes the 2*S*-*syn*-phenylserine isomer (**Figure. 2.22**) (see peak at 8.10 min). The (2*R*)-*syn*- phenylserine at 8.13 min (**Figure. 2.19**C) is likely derived from the (2*R*,3*S*)-**14a**. The other ring-substituted 3-arylglycidates behaved similarly (**Figure. 2.60**–**Figure. 2.61**).

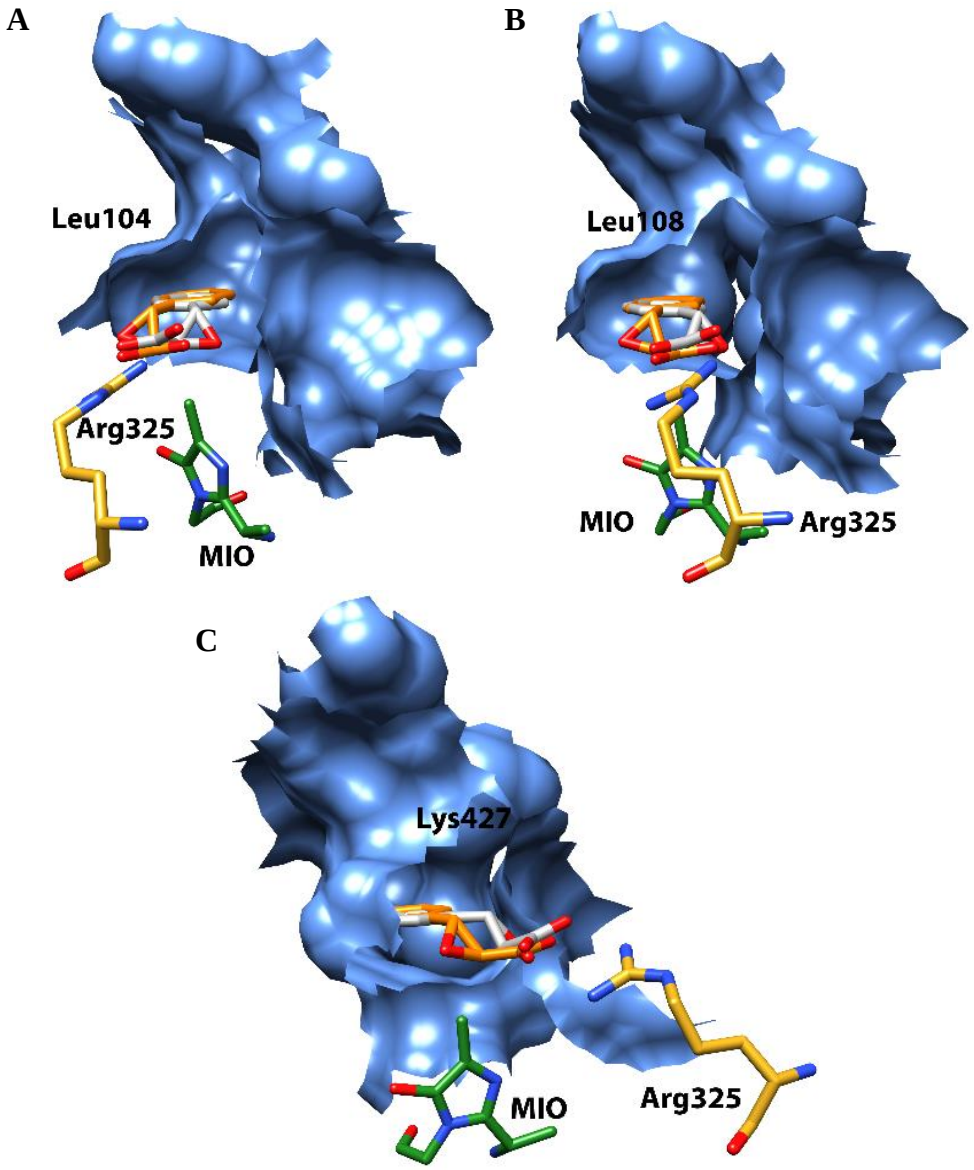

Figure. 2.23. Various viewing angles centering on the surfaces of A) Leu104, B) Leu108, and C) Lys427 deep in the aryl binding pocket of *Tc*PAM (PDB code 3NZ4) with poses of the docked (2*S*,3*R*)-**14a** (orange sticks) and (2*R*,3*S*)-**14a** (light-gray sticks).

2.3.12 Kinetics of Arylserine Biocatalysis.

The Michaelis parameters were measured by quantifying the underivatized biocatalyzed products by LC/MS-MRM analysis. The apparent K_M and k_{cat} of *Tc*PAM were calculated under steady-state conditions for the analogues of 3-arylglycidate with the amino donor (**12**) at 1 mM (**Table 2.7** and **Figure. 2.68** showing the conversion of four epoxide examples at 400 μM over 6 h). The catalytic efficiency (k_{cat}/K_M) of *Tc*PAM for 3'-CH_3-phenylglycidate (**14c**) was the best among all substrates tested; largely influenced by its relatively lower K_M compared to those for the 3'-halo (**14d**, **14e**, and **14f**), 3'-NO_2 (**14g**), 4'-NO_2 (**14h**), and 4'-CH_3 (**14i**) substrates. Also, the catalytic efficiencies of *Tc*PAM for **14c** and two other 3'-substituted phenylglycidates (3'-F (**14d**) and 3'-Cl (**14e**)) were superior to those of their 4'-substituted counterparts; k_{cat}/K_M values for the latter two were principally influenced by their higher k_{cat} compared to those of their 4'-substituted isomers (**14j** and **14k**).

We note that TcPAM catalyzes its natural α- to β-amino acid isomerization reaction at 3.0 min^{-1},[124] which is ∼10-fold faster than the average turnover rate (∼0.3 min−1) of TcPAM for the 3′-substituted arylglycidate substrates used in this study. However, the latter rate is similar to the average rate at which other MIO-dependent aminomutases catalyze their natural α- to β-amino acid isomerization reactions involved in specialized metabolism.[138] Thus, the turnover of the 3′-substituted arylglycidates by TcPAM is within the same order of magnitude as mutases that make β-amino acids in their natural hosts to confer an evolutionary advantage.

Because the calculated docking conformations of the arylglycidates agreed with those of other MIO-enzymes in complex with their natural phenylpropanoid substrates,[17,29,53,124] we, therefore, used the models to help interpret how the position of the substituents could potentially affect catalysis due to steric interactions. Substrate docking models show that for each ligand enantiomer,

one of the two 3'- ("*meta*"-) carbons of the aryl ring of the substrate can position its substituent in steric relief when pointed toward Lys427 (**Figure. 2.21**B) and Ile431 (**Figure. 2.21**C). This, in part, suggests that substrates **14c**, **14d**, and **14e** with relatively smaller 3'-substituents (CH_3, F, and Cl, respectively) are more able to adopt a catalytically competent conformation compared to their 4'-isomers. The latter place substituents on the 4'- ("*para*"-) carbon of each ligand in greater steric conflict with Leu104 (**Figure. 2.21**B and **Figure. 2.23**A), Leu108, and Leu227 (**Figure. 2.21**C**, Figure. 2.23**A and B), likely preventing epoxides **14i**, **14j**, and **14k** from being turned over as efficiently (**Table 2.7**) (**Figure. 2.69** and **Figure. 2.70**).

Table 2.7. Kinetics of *Tc*PAM for Turnover of Arylglycidates (**14a**–**14l)** to Arylserines (**15a**–**15l**) and Arylisoserines (**16a–16l**).

Entry	R	k_{cat}^{Ser} (min^{-1})	k_{cat}^{Iso} (min^{-1})	K_M (μM)	k_{cat}/K_M (M^{-1} s^{-1})	Entry	R	k_{cat}^{Ser} (min^{-1})	k_{cat}^{Iso} (min^{-1})	K_M (μM)	k_{cat}/K_M (M^{-1} s^{-1})
14a	H	0.39 (0.10)[a]	0.003 (<0.001)	340	19	**14g**	3'-NO_2	0.43 (0.07)	0.01 (0.001)	760	10
14b	3′-OCH_3	0.46 (0.14)	0.27 (0.15)	2000	6.5	**14h**	4'-NO_2	0.75 (0.11)	0.004 (<0.001)	610	21
14c	3′-CH_3	0.31 (0.01)	0.03 (0.001)	50	113	**14i**	4′-CH_3	0.17 (0.03)	0.11 (0.01)	450	10
14d	3'-F	0.62 (0.03)	0.009 (<0.001)	170	61	**14j**	4'-F	0.04 (<0.01)	0.005 (<0.001)	40	17
14e	3'-Cl	1.3 (0.1)	0.10 (0.01)	600	41	**14k**	4'-Cl	0.01 (<0.01)	0.002 (<0.001)	50	4.5
14f	3'-Br	0.02 (<0.01)	0.002 (<0.001)	140	2.5	**14l**	4'-Br	~0.04 (<0.01)	0.01 (<0.001)	50	15

[a]Standard deviation in parenthesis ($n = 3$). The "<" symbol indicates that the actual value, estimated to one significant figure, is shown. k_{cat}^{Ser} is the apparent k_{cat} of arylserine production, k_{cat}^{Iso} is the apparent k_{cat} of arylisoserine production, and k_{cat} is the turnover rate for the production of both arylserine and arylisoserine by *Tc*PAM. The K_M of *Tc*PAM for each substrate is calculated from the production of arylserine and arylisoserine combined.

Furthermore, the 3'-Cl-Phenylglycidate (**14e**) was turned over (k_{cat}) by *Tc*PAM faster than the other epoxides in this study and interestingly much more superior (>130-fold) than the 4'-Cl isomer (**14k**) (**Table 2.7**). The other 3'-substituted analogues turned over ~16-fold and ~2-fold faster than their 4'-substituted counterparts (**14j** and **14i**), which were the 3'-F- (**14d**) and 3'-CH_3- (**14c**)

phenylglycidates, respectively. The larger steric 3'-Br- (**14f**) and 4'-Br- (**14l**) substrates were turned over with poorer catalytic efficiency, due mainly to their equally poor k_{cat} values. The K_M values of *Tc*PAM for both Br-substituted substrates were similar yet lower (estimating tighter binding) than for other substrates such as **14d**, **14e**, **14g**, and **14h** that were turned over faster (**Table 2.7**). This suggests that a yet unknown phenomenon resulting in part from tighter binding and steric misalignment likely disrupted the turnover of the bulkier Br-substituted arylglycidates by *Tc*PAM (**Figure. 2.69**A and B, and **Figure. 2.70**A and B).

It was interesting to find that the 3-(3′-OCH_3-phenyl)glycidate (**14b**) with the largest estimated steric volume[129,139](26.4 Å3) was turned over similar to most 3′-substituted substrates with smaller substituents, such as H (4.5 Å3), F (7.7 Å3), or Cl (18.8 Å3) (see **14a**, **14c**, and **14d** as examples, **Table 2.7**). The significantly lower catalytic efficiency, yet similar turnover by TcPAM of **14b** as compared to those of **14a**, **14c**, and **14d** with smaller substituents, suggested that the larger-size OCH_3 group, through a curious pathway, affected the K_M but not the turnover, like the Br group.

The catalytic efficiency (k_{cat}/K_M) of *Tc*PAM for the 4'-NO_2-substituted arylglycidate (**14h**) was ~2-fold higher than for the 3'-NO_2-isomer (**14g**), which parallels the difference in their turnover (k_{cat}). This regiospecificity trend was similar to that described earlier for substrates 3'-Br- (**14f**) and 4'-Br- (**14l**), where the 4'-isomer was turned over slightly faster than the 3'-isomer.

2.3.13 Kinetics of Aryl*iso*serine Biocatalysis.

To make the arylisoserines, the NH_2-MIO adduct needs to align the phenylpropanoid of the phenylglycidate for occasional amino group attack at C_β instead of at C_α (See **Figure. 2.71** for a representative AutoDock modeled conformation of **14b**). We found by LC/ESI-MS/MS analysis that *Tc*PAM converted each substituted Phenylglycidate to an aryl*iso*serine (**Figure. 2.73**–**Figure. 2.75**). Among the substituted arylisoserines, the 3'-OCH_3-phenylisoserine isomer **16b** was made

most abundantly at a 37:63 ratio with its corresponding 3'-OCH_3-phenylserine **15b**, with the latter predominating (**Table 2.7**). The next most abundant arylisoserines made by *Tc*PAM were the 3'-Cl (**16e**) and 4'-CH_3 (**16i**) at ~10:90 and 40:60 ratios with their cognate arylserines **15e** and **15i**, respectively. The remaining Phenylglycidates were converted to lesser amounts ($\leq$0.03 min^{-1}) of their arylisoserines (**Table 2.7**).

The sterically demanding 3'-OCH_3 substituent likely "nudged" the substrate enough to place C_β close to and in alignment with the NH_2-MIO moiety to make the 3'-OCH_3-phenylisoserine (**16b**) more abundantly. However, the other epoxide substrates bearing 3'-or 4'-substituents with steric volumes [NO_2 (18.2 $Å^3$), Cl (14.3 $Å^3$), CH_3 (21.3 $Å^3$) and Br (24.5 $Å^3$)] equivalent to that of OCH_3 (26.4 $Å^3$) were turned over to their corresponding arylisoserines less efficiently. Thus, a combination of the different steric volumes, electronics, atom geometries, and the 3'- and 4'-positions of the substituents must place the carbon skeleton of epoxides into various conformations that unpredictably promote or preclude NH_2-MIO attack at C_β. Based on the putative docked conformation of **14b** (**Figure. 2.71**), the *anti*-stereochemistry between the hydroxyl and amino groups is expected for arylisoserines when the epoxide is opened by S_N2 amination at C_β.

The proposed *anti*-stereoisomerism of the arylisoserines biocatalyzed in this study is unlike the *syn*-stereochemistry of the phenylisoserine moiety found in the antineoplastic drug paclitaxel (see **Figure. 1.4**).[140] The paclitaxel pathway is presumed to proceed through a β-phenylalanyl taxane, which is hydroxylated to a penultimate phenylisoserinyl taxane intermediate,[141] but further evidence is needed to confirm this. Another report claims isolation of methyl phenylisoserinate by methanol extraction of *Taxus* plants as evidence of a putative, phenylisoserine preassembly pathway.[142] It is unclear, however, whether the phenylisoserinate ester was obtained by methanolysis of phenylisoserinyl taxanes, such as an advanced paclitaxel precursor, present in the

plant. Nonetheless, if *syn*-phenylisoserine indeed occurs as a metabolite in plants, its biosynthetic pathway in *Taxus* plants remains unknown. While the *trans*-3-arylglycidates were biocatalytically converted likely to *anti*-arylisoserines in this study, the results highlight 3-arylglycidates as potential naturally occurring precursors for direct amination to arylisoserines. We imagine that naturally occurring cinnamate, derived from phenylalanine by ammonia lyase activity in plants,[143] can be converted to 3-phenylglycidate by a plant α-ketoglutarate-dependent hydroxylase. This family of nonheme Fe(II) hydroxylases convert alkenes to epoxides,[144] and specifically cinnamate to 3-phenylglycidate in vitro.[145]

As noted earlier, *Tc*PAM catalyzes the isomerization of α-phenylalanine to β-phenylalanine in its natural reaction by rotating the arylacrylate intermediate inside the active site before being re-aminated at the C_β(**Figure. 2.3**).[124] This rotation pathway allowed by *Tc*PAM may play a role in torqueing the ring-opened *trans*-epoxide intermediates into a conformation needed for making *syn*-isoserine. In future studies, we look to dissect the stereoselectivity of the *Tc*PAM reaction for arylisoserine production.

2.4 Conclusion

The surrogate activity of TcPAM catalyzed the asymmetric and regioselective transfer of an NH_2 group from a sacrificial amine group donor (2*S*)-styryl-α-alanine to racemates of 3-arylglycidate analogues in one step. *Tc*PAM made underivatized *anti*-stereoisomers of arylserines predominantly while producing significantly less of the *syn*-stereoisomer, and these observations provided valuable insights into an extended mechanism of the natural α- to β-phenylalanine isomerization reaction. The electronic effects or steric volumes of the substituents on the ring of the arylglycidate substrates did not predictably change the regioselectivity of the nucleophilic

attack by NH_2. Docked poses of the arylglycidate racemate in the active site of *Tc*PAM suggested that the conserved Tyr80, a general acid present in all other MIO enzymes[146] and proximate to the (2*S*,3*R*)-glycidate, purportedly helped catalyze the more abundant (2*R*)-*anti*-arylserines. Docking analysis also identified Tyr322 as a putative general acid that likely facilitated protonation-initiated amination of the (2*R*,3*S*)-glycidate antipode to make the lesser abundant (2*S*)-*anti*-arylserines. In addition, (2*S*)-*syn*-β-hydroxy amino acid stereoisomers are commonly found in specialized glycopeptide and depsipeptides natural products. Application of an MIO-aminomutase described here to biocatalyze enantiodivergent arylserines with *anti*-stereoisomerism between the two chiral centers has industrial and pharmaceutical relevance, allowing the possibility to perform stereochemical structure/activity studies. For example, replacement of a naturally occurring *syn*-arylserine stereoisomer for rarer *anti*-arylserine stereoisomers in a bioactive drug candidate could increase drug bioavailability by slowing first-pass metabolism pathways or inhibiting bacterial resistance mechanisms of bioactive compounds built on this scaffold.[147,148] Future studies will assess the stereoselectivity and stereospecificity of *Tc*PAM with enantiopure glycidate substrates for making hydroxy amino acids. While the amino nucleophile of the loaded NH_2-MIO adduct of *Tc*PAM primarily added the NH_2 to C_α to open the epoxide-ring forming arylserines, the epoxides were also converted to their arylisoserines via NH_2 attack at C_β, likely yielding the *anti*-hydroxy amino acid isomers.

This work provides an alternative biocatalytic route to access phenylserine and phenylisoserine analogues starting from 3-phenylglycidates. This work extends the transaminase activity of MIO-aminomutases to a new class of acceptor molecules to produce hydroxy amino acids. These biocatalyzed and underivatized bifunctional arylisoserines can be used as direct entry points into the synthesis of value added compounds. For example, isoserines are bioactive structural motifs

of drugs such as the anticancer pharmaceutical paclitaxel and its analogues,[149-151] and a series of "KNI" HIV 1 protease inhibitors.[152] Foreseeably, the capacity of *Tc*PAM to produce arylisoserines from glycidates, in part, provides a starting point for us to design novel function into the enzyme.

APPENDIX

APPENDIX

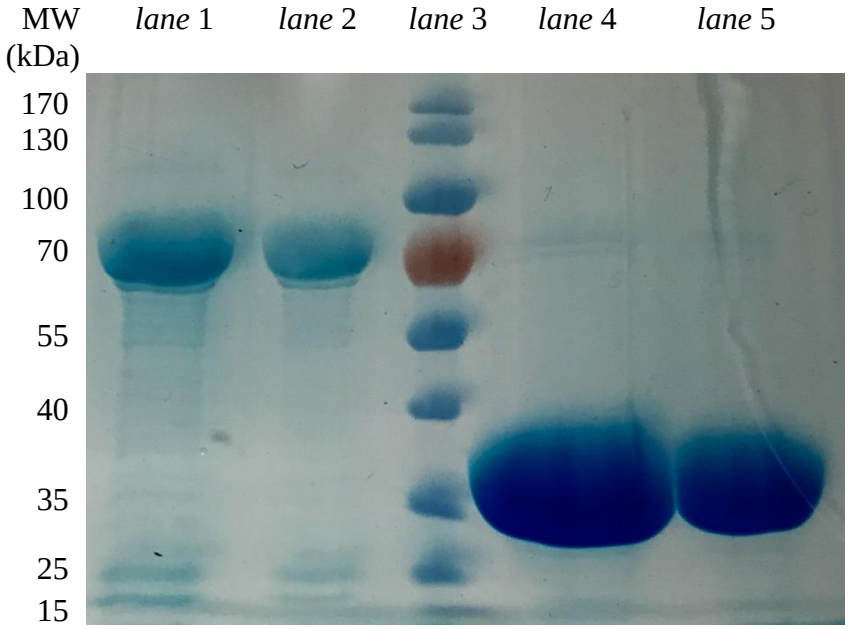

Figure. 2.24. SDS-PAGE gel of wild-type *Tc*PAM (82% pure) and (2*S*)-TA (99% pure) after Coomassie blue staining. Purity was estimated by a Kodak Gel Logic 100 Imaging System; *lane* 1: *Tc*PAM (10 µL of a 13.7 mg/mL solution); *lane* 2: *Tc*PAM (5 µL of a 13.7 mg/mL solution); *lane* 3: PageRuler © Prestained Ladder: MW (kDa) – 170, 130, 100, 70, 55, 40, 35, 25, 15; *lane* 4: (2*S*)-TA (10 µL of a 8.8 mg/mL solution); and *lane* 5: (2*S*)-TA (5 µL of a 8.8 mg/mL solution).

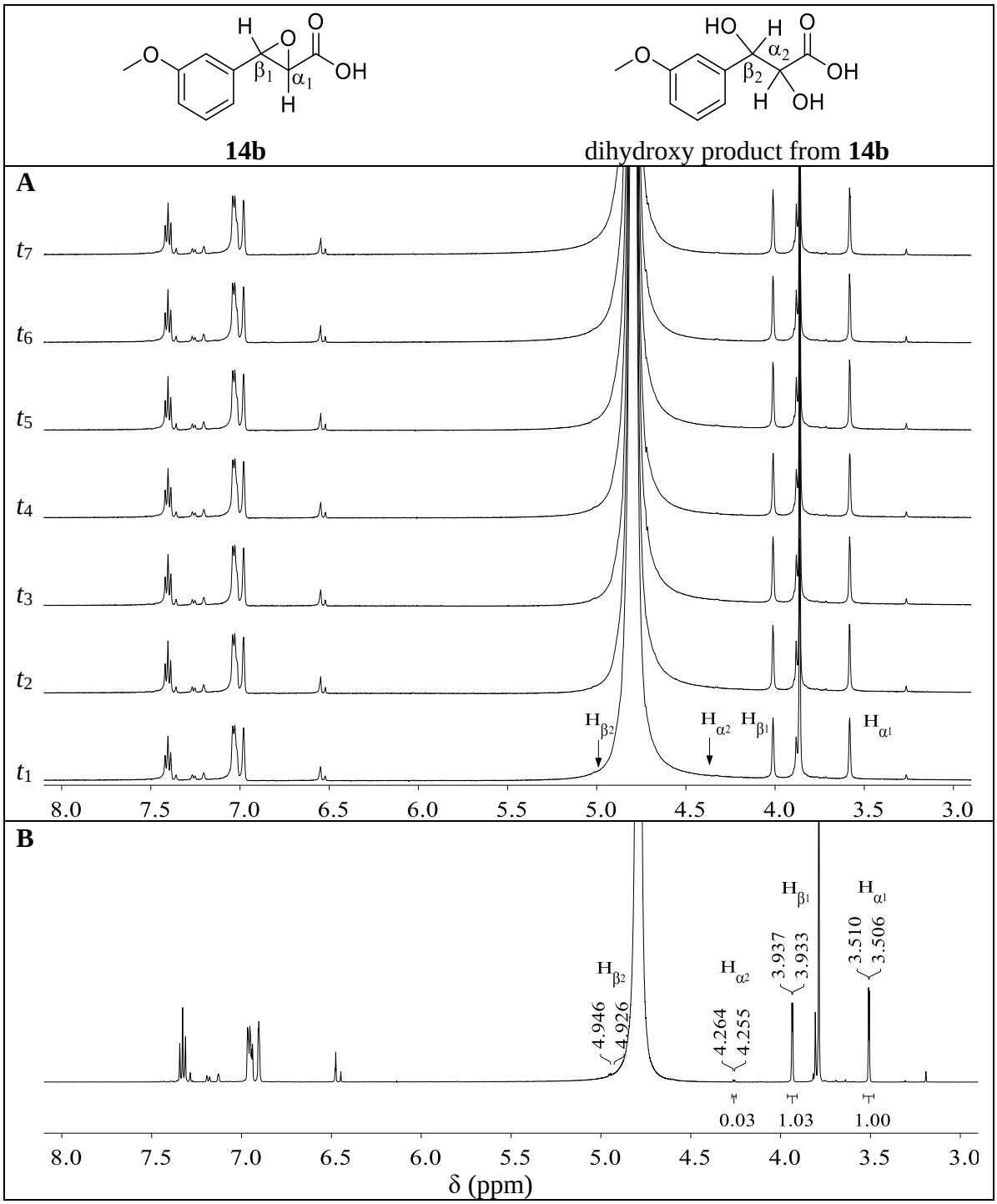

Figure. 2.25. ^{1}H NMR of 3-(3′-OCH_3-phenyl)glycidate (**14b**) in deuterated Assay Buffer. A) NMR spectra were recorded at 15 min intervals starting from t_1 to t_7. At t_1 = 0 min and at t_7 = 90 min, the ratio of **14b**:dihydroxy product = 100:0, and B) NMR spectrum after storing the sample in deuterated Assay Buffer at ~25 °C for 1 week, the ratio of **14b**:dihydroxy product = 100:3.

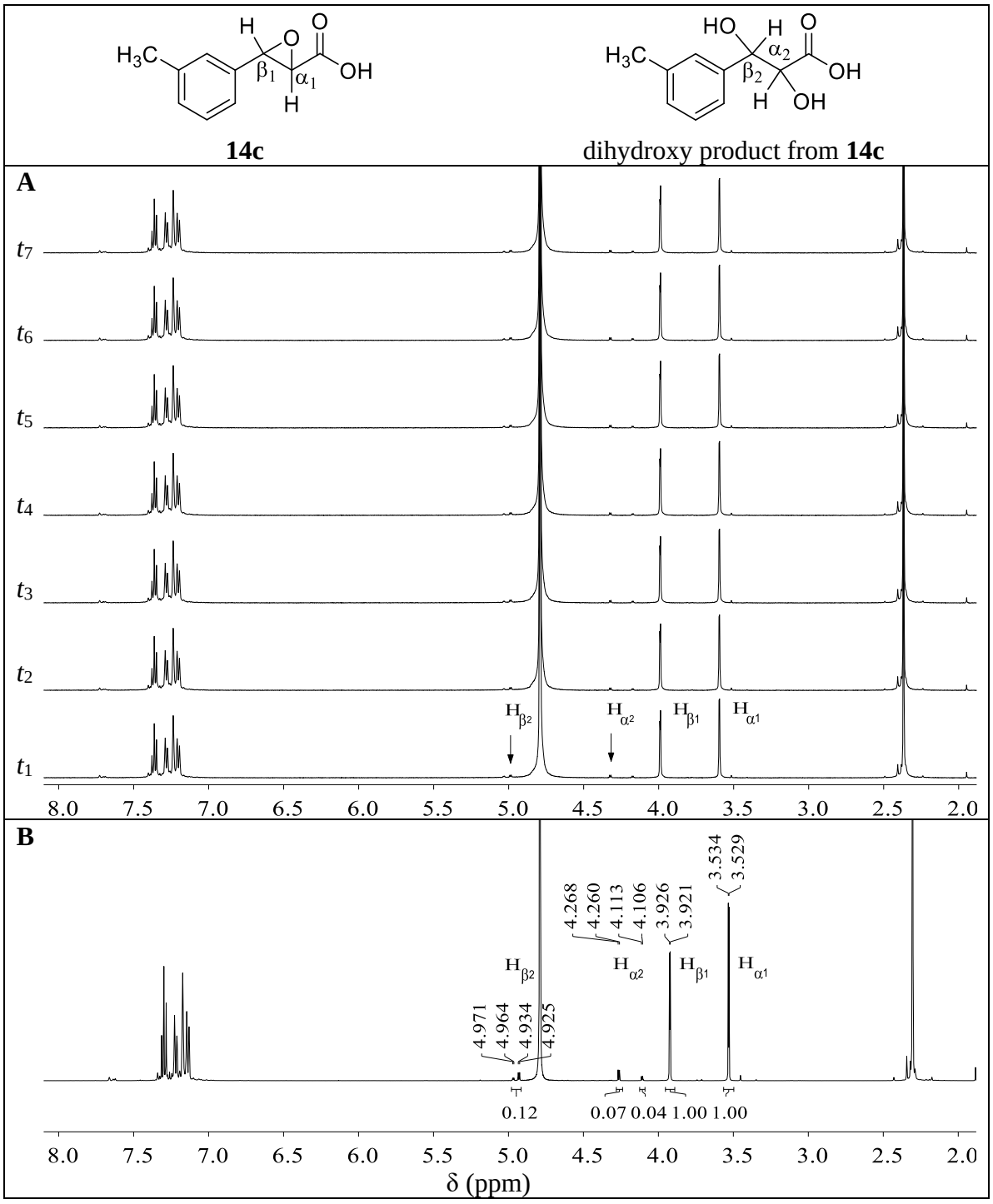

Figure. 2.26. ^{1}H NMR of 3-(3′-CH_3-phenyl)glycidate (**14c**) in deuterated Assay Buffer. A) NMR spectra were recorded at 15 min intervals starting from t_1 to t_7. At t_1 = 0 min and at t_7 = 90 min, the ratio of **14c**:dihydroxy product = 100:7, and B) NMR spectrum after storing the sample in deuterated Assay Buffer at ~25 °C for 1 week, the ratio of **14c**:dihydroxy product = 100:12.

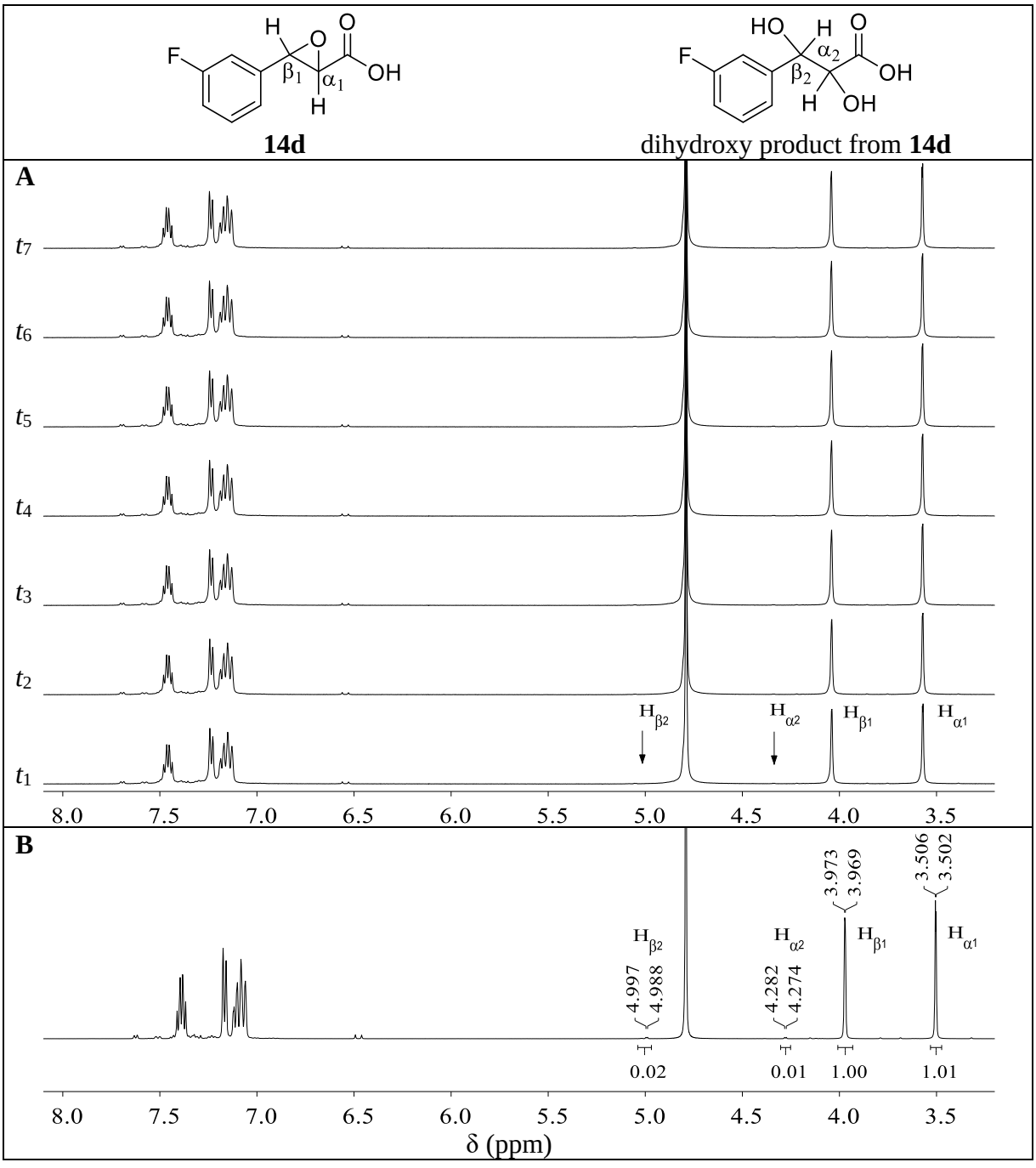

Figure. 2.27. ^{1}H NMR of 3-(3′-F-phenyl)glycidate (**14d**) in deuterated Assay Buffer. A) NMR spectra were recorded at 15 min intervals starting from t_1 to t_7. At t_1 = 0 min and at t_7 = 90 min, the ratio of **14d**:dihydroxy product = 100:0, and B) NMR spectrum after storing the sample in deuterated Assay Buffer at ~25 °C for 1 week, the ratio of **14d**:dihydroxy product = 100:2.

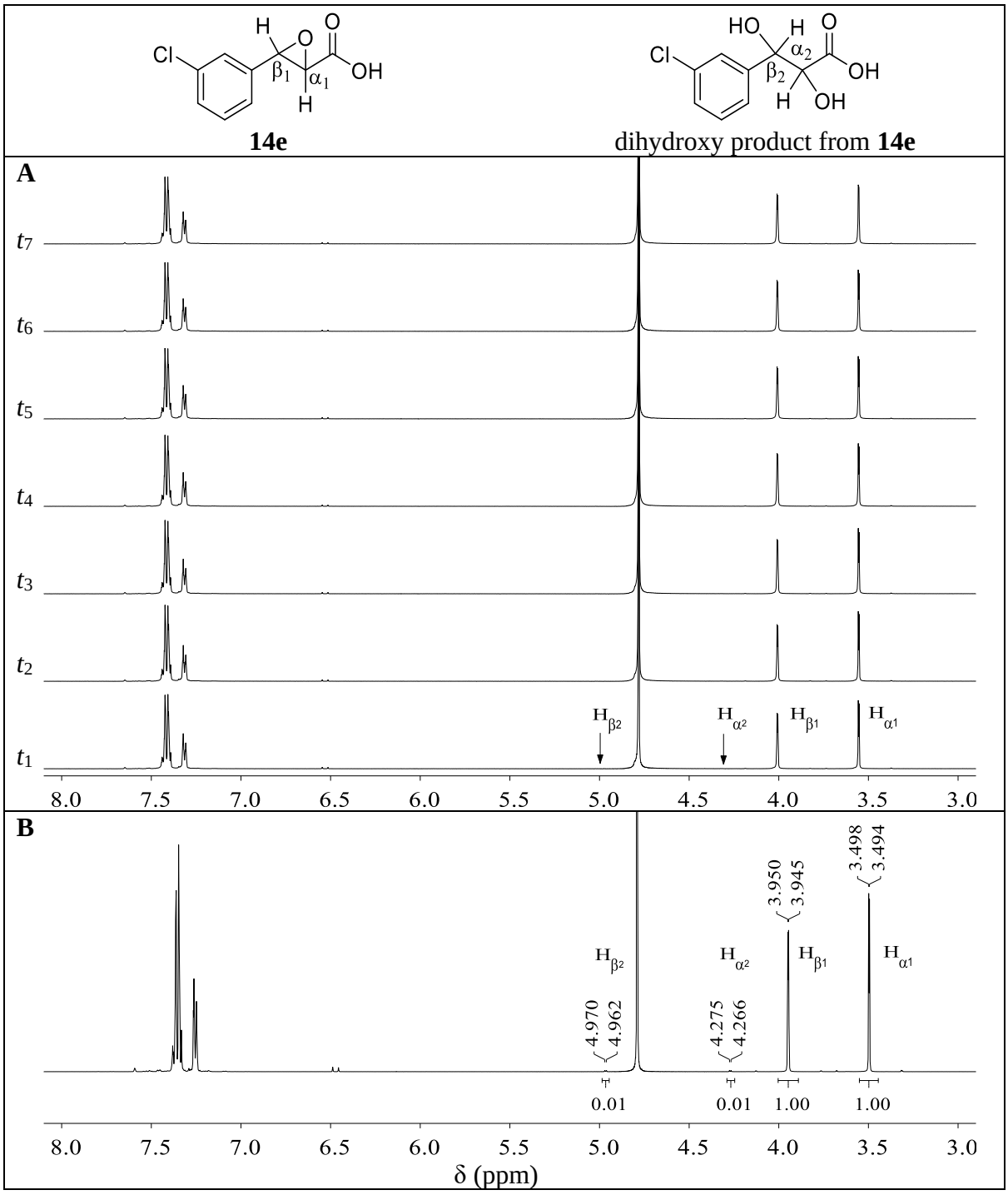

Figure. 2.28. ^{1}H NMR of 3-(3′-Cl-phenyl)glycidate (**14e**) in deuterated Assay Buffer. A) NMR spectra were recorded at 15 min intervals starting from t_1 to t_7. At t_1 = 0 min and at t_7 = 90 min, the ratio of **14e**:dihydroxy product = 100:0, and B) NMR spectrum after storing the sample in deuterated Assay Buffer at ~25 °C for 1 week, the ratio of **14e**:dihydroxy product = 100:1.

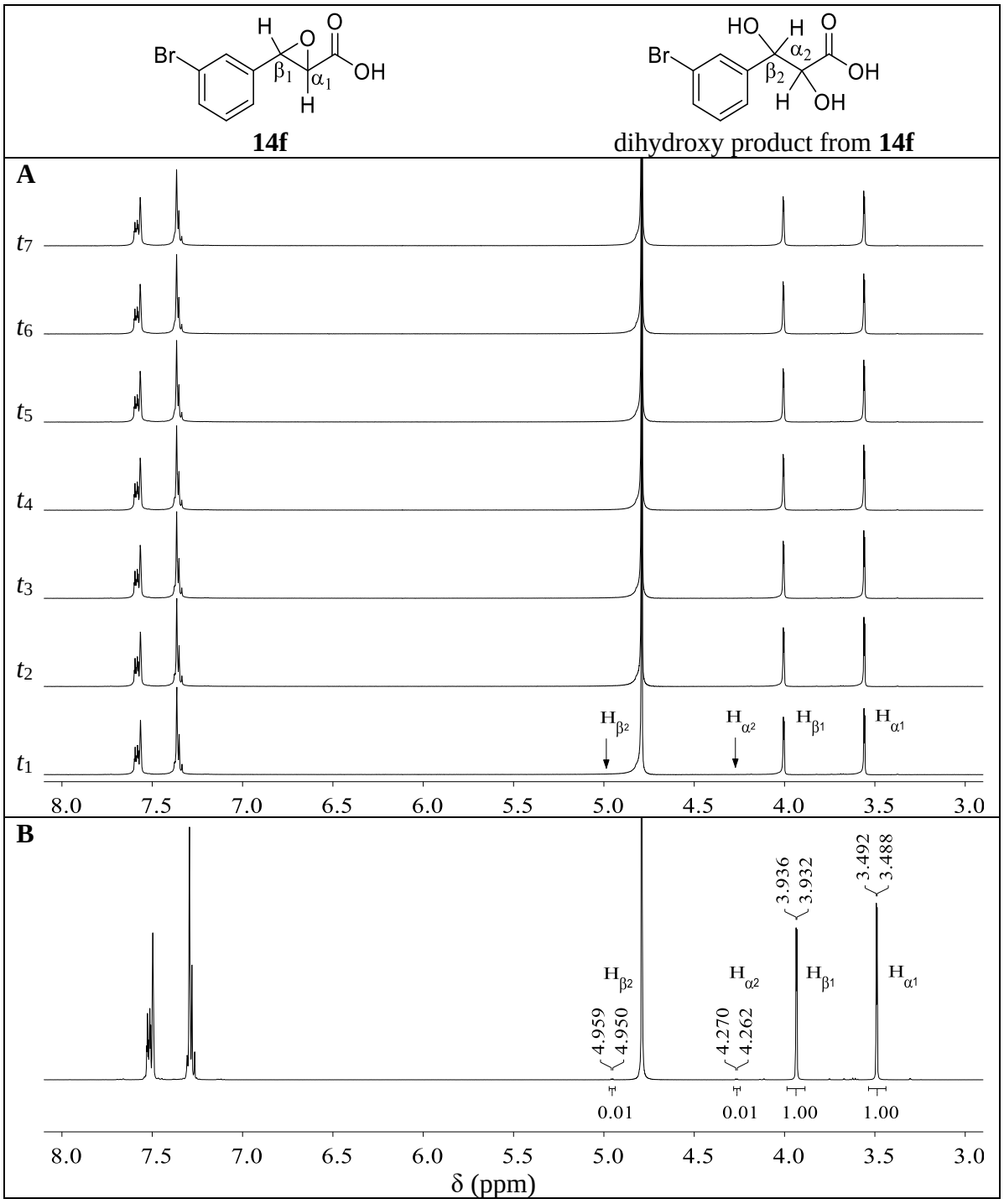

Figure. 2.29. ^{1}H NMR of 3-(3′-Br-phenyl)glycidate (**14f**) in deuterated Assay Buffer. A) NMR spectra were recorded at 15 min intervals starting from t_1 to t_7. At t_1 = 0 min and at t_7 = 90 min, the ratio of **14f**:dihydroxy product = 100:0, and B) NMR spectrum after storing the sample in deuterated Assay Buffer at ~25 °C for 1 week, the ratio of **14f**:dihydroxy product = 100:1.

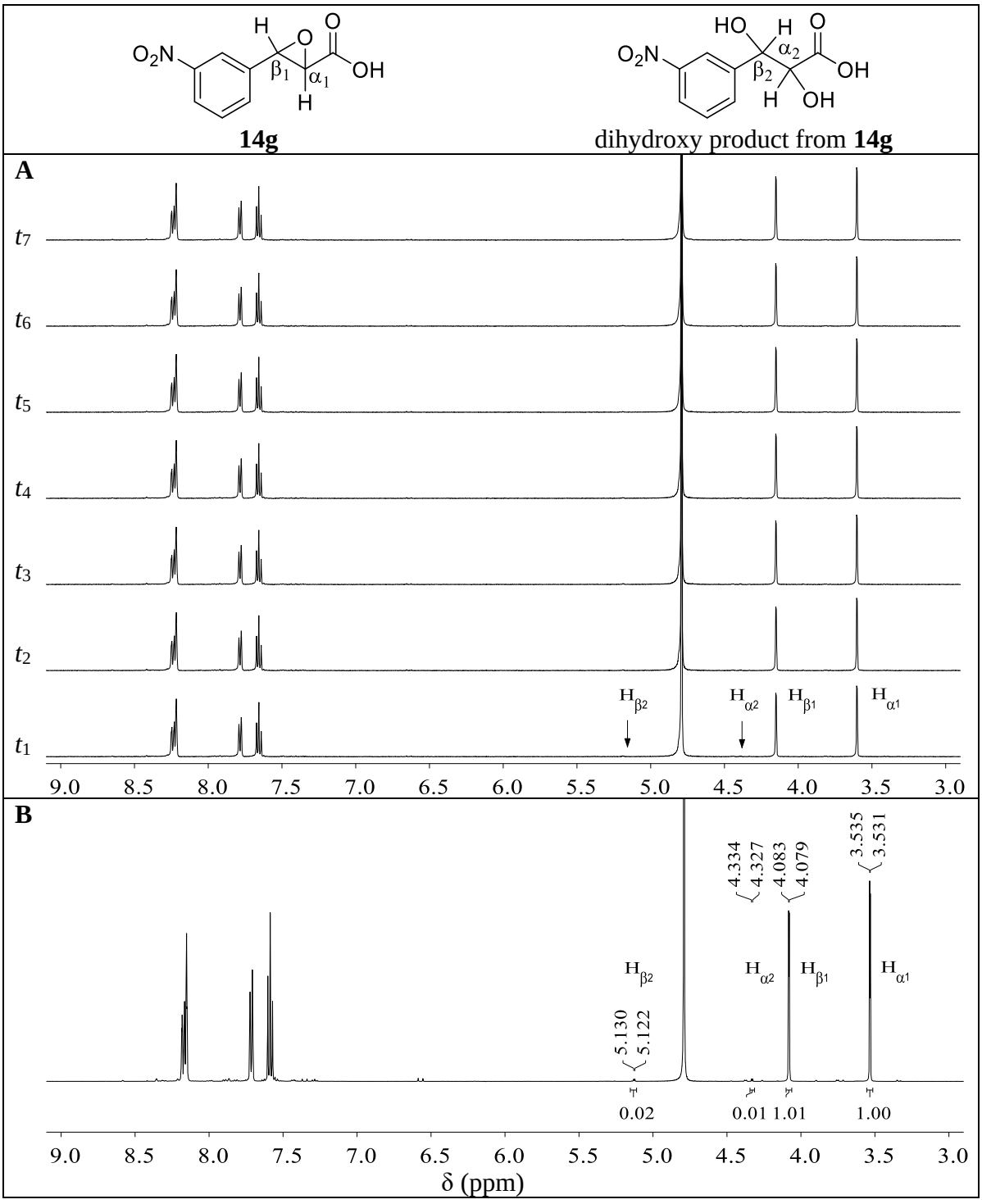

Figure. 2.30. ^{1}H NMR of 3-(3′-NO_2-phenyl)glycidate (**14g**) in deuterated Assay Buffer. A) NMR spectra were recorded at 15 min intervals starting from t_1 to t_7. At t_1 = 0 min and at t_7 = 90 min, the ratio of **14g**:dihydroxy = 100:0, and B) ^{1}H NMR spectrum after storing the sample in deuterated Assay Buffer at ~25 °C for 1 week, the ratio of the ratio of **14g**:dihydroxy product = 100:2.

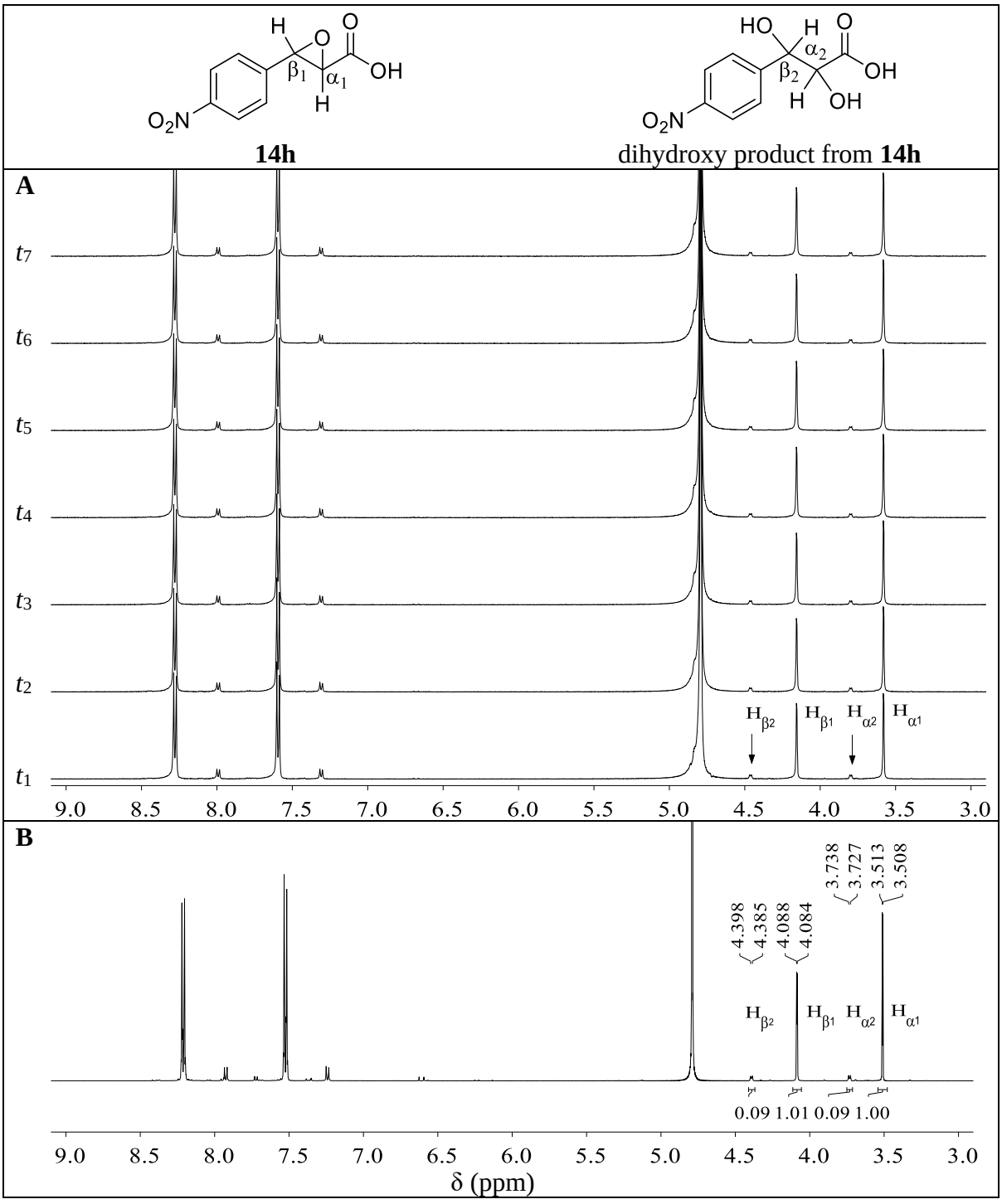

Figure. 2.31. ^{1}H NMR of 3-(4′-NO_2-phenyl)glycidate (**14h**) in deuterated Assay Buffer. A) NMR spectra were recorded at 15 min intervals starting from t_1 to t_7. At t_1 = 0 min and t_7 = 90 min, the ratio of **14h**:dihydroxy product = 100:9, and B) NMR spectrum after storing the sample in deuterated Assay Buffer at ~25 °C for 1 week, the ratio of **14h**:dihydroxy product = 100:9.

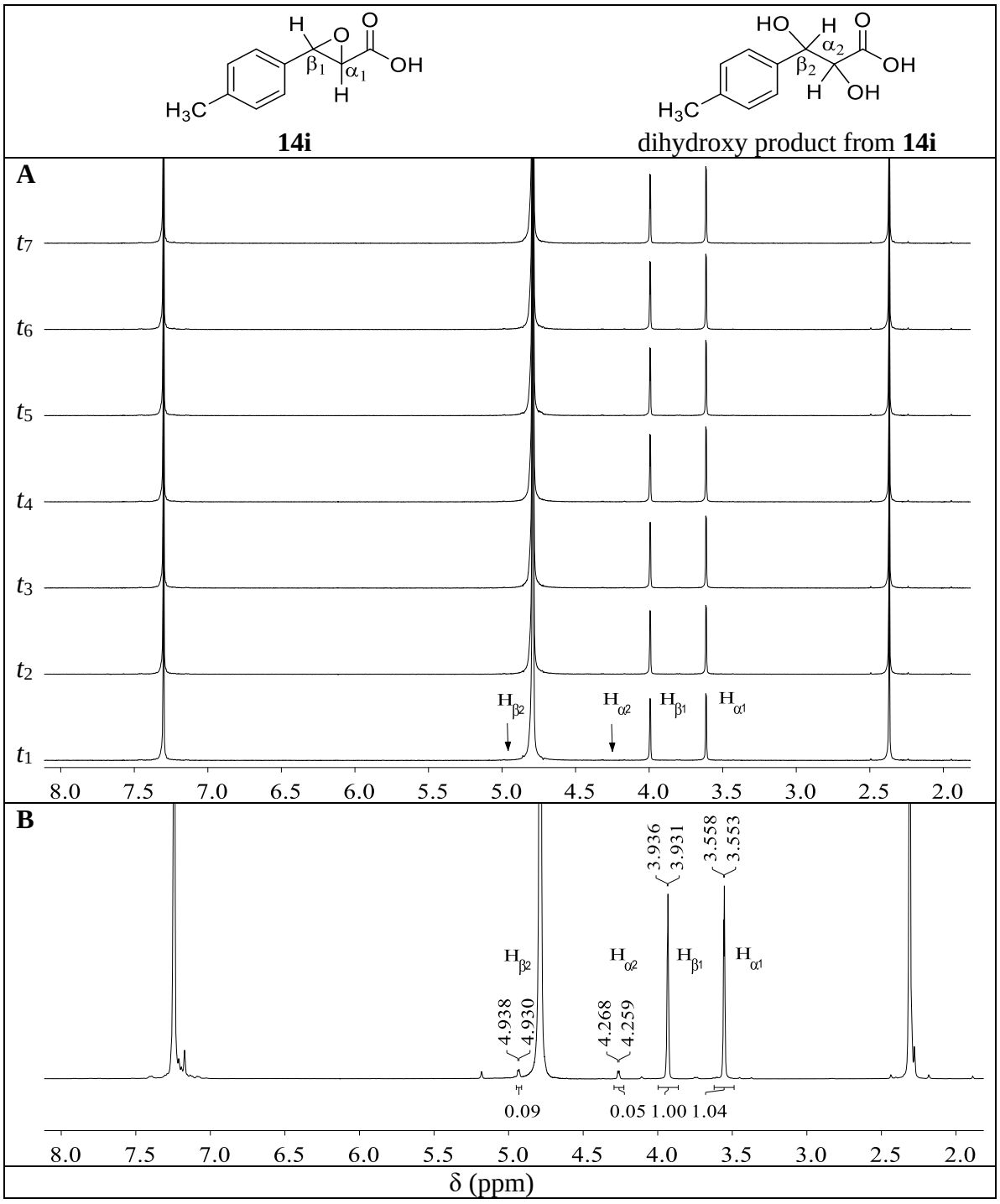

Figure. 2.32. ^{1}H NMR of 3-(4′-CH_3-phenyl)glycidate (**14i**) in deuterated Assay Buffer. A) NMR spectra were recorded at 15 min intervals starting from t_1 to t_7. At t_1 = 0 min and at t_7 = 90 min, the ratio of **14i**:dihydroxy product = 100:1, and B) NMR spectrum after storing the sample in deuterated Assay Buffer at ~25 °C for 1 week, the ratio of **14i**:dihydroxy product = 100:5.

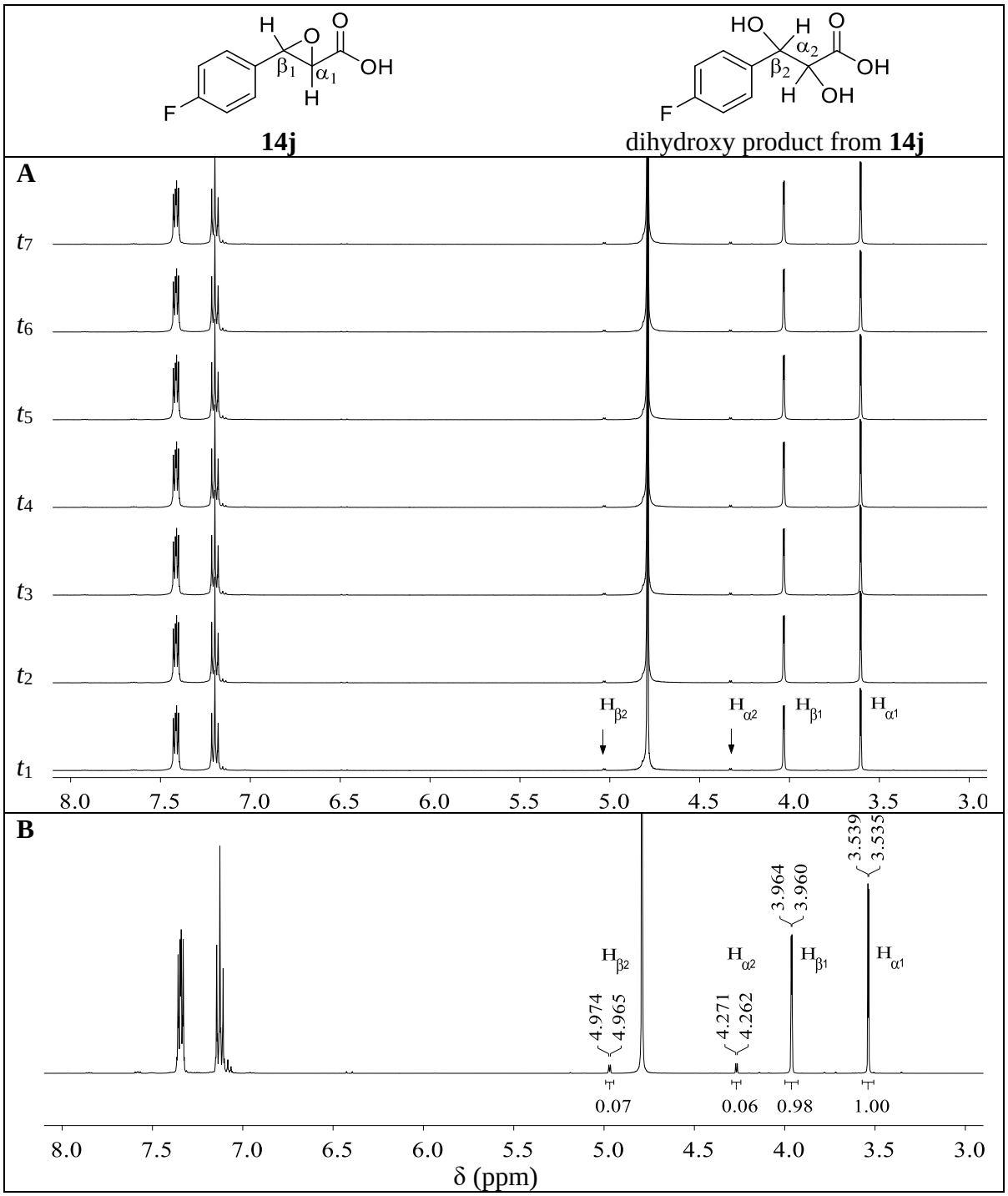

Figure. 2.33. ^{1}H NMR of 3-(4′-F-phenyl)glycidate (**14j**) in deuterated Assay Buffer. A) NMR spectra were recorded at 15 min intervals starting from t_1 to t_7. At t_1 = 0 min and t_7 = 90 min, the ratio of **14j**:dihydroxy product = 100:4, and B) NMR spectrum after storing the sample in deuterated Assay Buffer at ~25 °C for 1 week, the ratio of **14j**:dihydroxy product = 100:7.

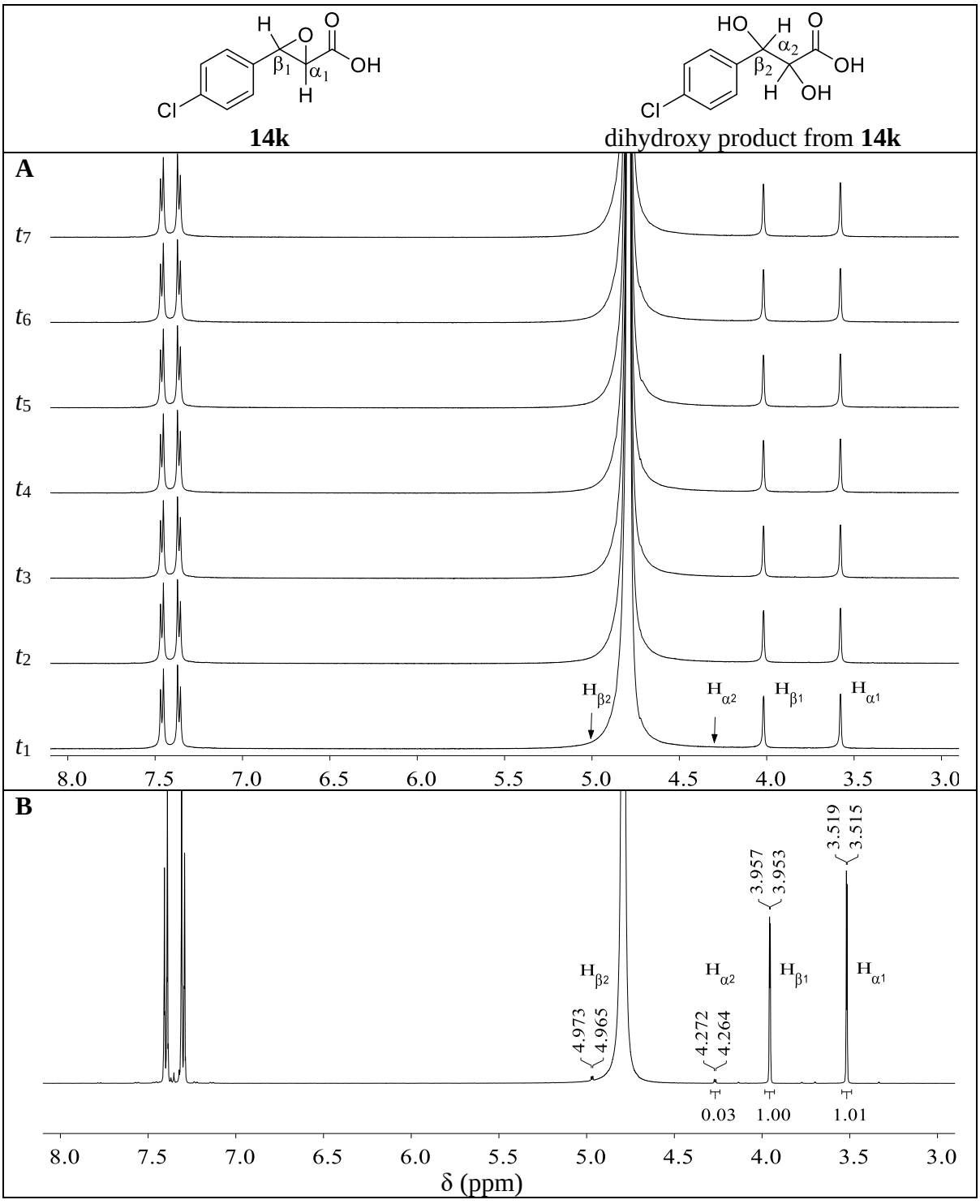

Figure. 2.34. ^{1}H NMR of 3-(4′-Cl-phenyl)glycidate (**14k**) in deuterated Assay Buffer. A) NMR spectra were recorded at 15 min intervals starting from t_1 to t_7. At t_1 = 0 min and t_7 = 90 min, the ratio of **14k**:dihydroxy product = 100:0, and B) NMR spectrum after storing the sample in deuterated Assay Buffer at ~25 °C for 1 week, the ratio of **14k**:dihydroxy product = 100:3.

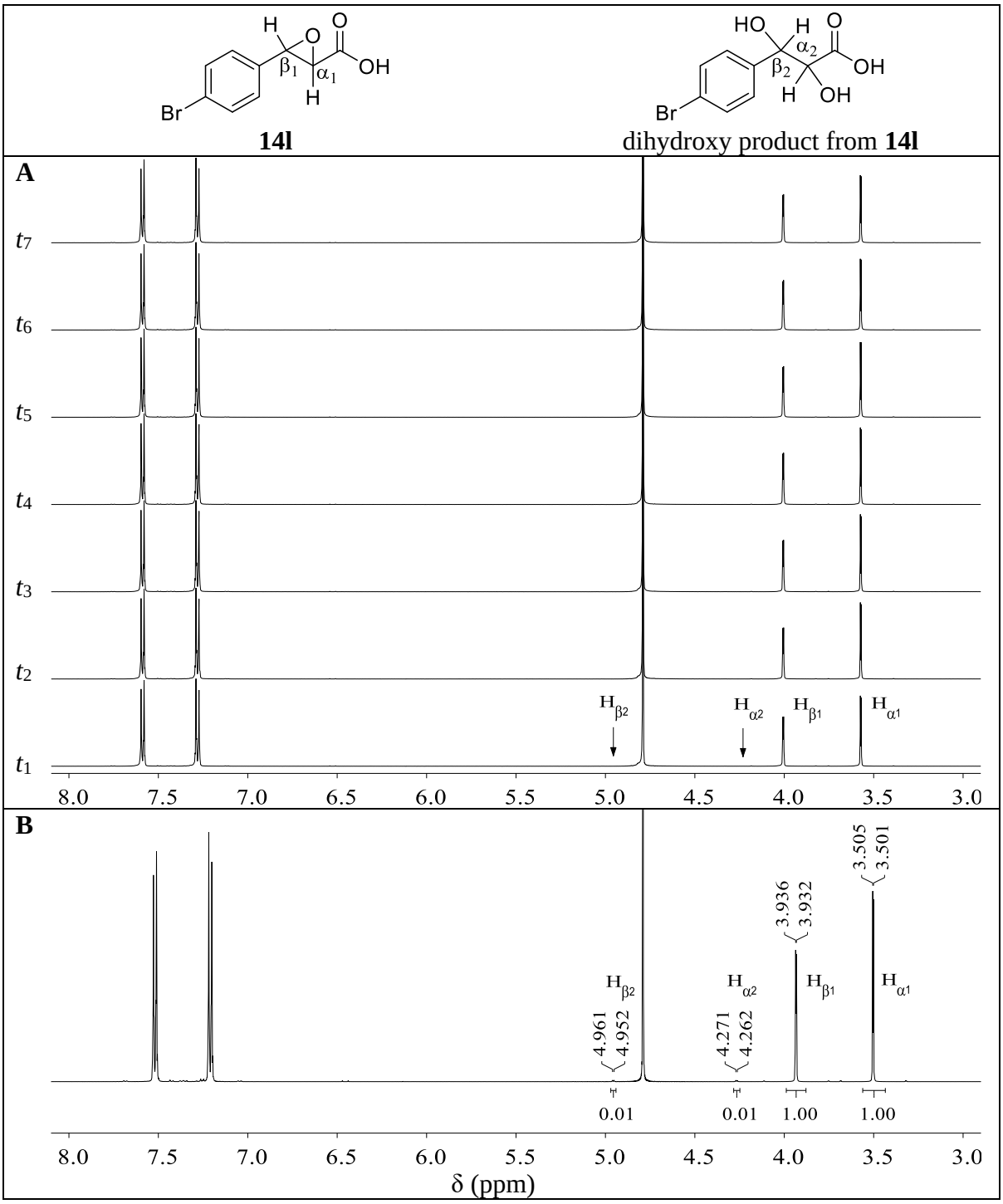

Figure. 2.35. ^{1}H NMR of 3-(4′-Br-phenyl)glycidate (**14l**) in deuterated Assay Buffer. A) NMR spectra were recorded at 15 min intervals starting from t_1 to t_7. At t_1 = 0 min and t_7 = 90 min, the ratio of **14l**:dihydroxy product = 100:0, and B) NMR spectrum after storing the sample in deuterated Assay Buffer at ~25 °C for 1 week, the ratio of **14l**:dihydroxy product = 100:1.

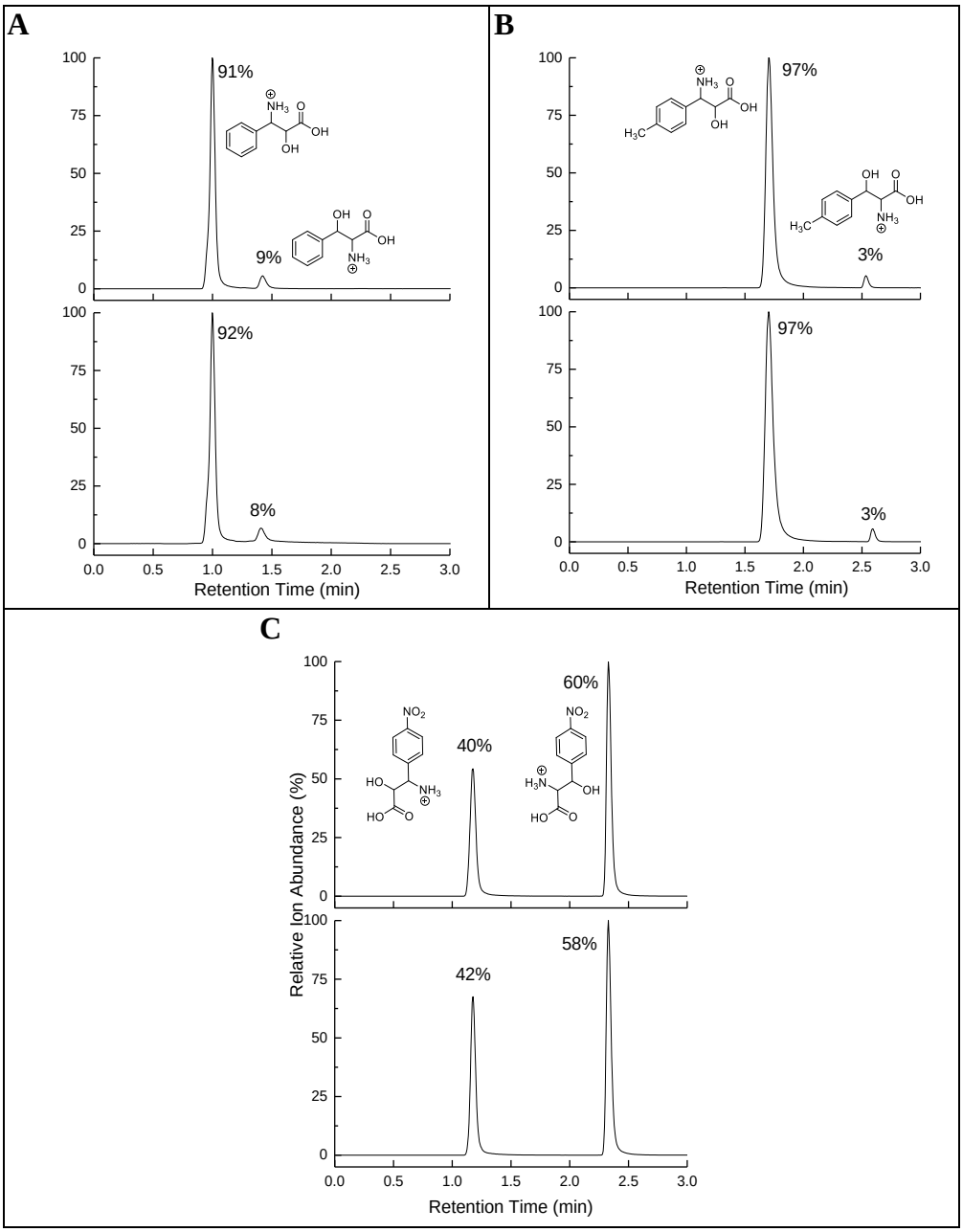

Figure. 2.36. A) Relative abundances of arylisoserine (**16a)** and arylserine (**15a**) products made from C_β- and C_α-amination, respectively, of 3-phenylglycidate (**14a**) (1 mM) when incubated with 2M NH_4OH and *Tc*PAM (100 µg/mL) (*top trace*) and without *Tc*PAM (*bottom trace*). B) Relative abundances of arylisoserine (**16i)** and arylserine (**15i**) products made from C_β- and C_α-amination, respectively, of 3-(4'-CH_3-phenyl)glycidate (**14i**) (1 mM) when incubated with 2M NH_4OH and *Tc*PAM (100 µg/mL) (*top trace*) and without *Tc*PAM (*bottom trace*). C) Relative abundances of arylisoserine (**16h)** and arylserine (**15h**) products made from C_β- and C_α-amination, respectively, of 3-(4'-NO_2-phenyl)glycidate (**14h**) (1 mM) when incubated with 2M NH_4OH and *Tc*PAM (100 µg/mL) (*top trace*) and without *Tc*PAM (*bottom trace*).

GC/EI-MS Analysis of Phenylserine Analogues Derivatized as *O*-Trimethylsilyl *N*-[(2S)-2-Methylbutyryl] Methyl Esters

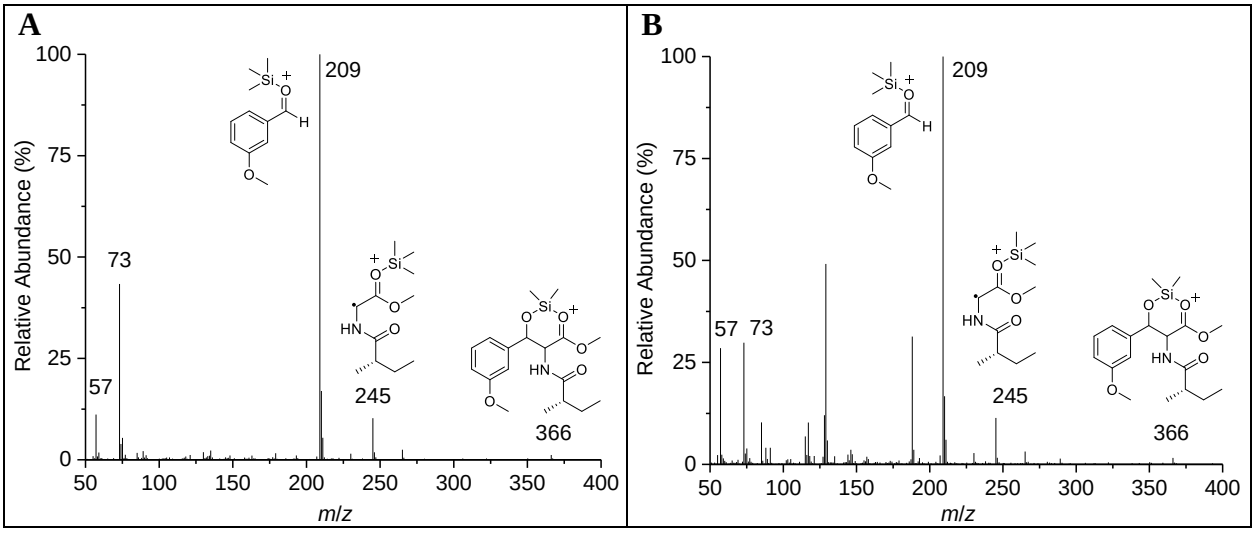

Figure. 2.37. GC/EI-MS spectra of A) authentic (2*S*/2*R*)-*anti*-3′-OCH_3-phenylserine (**15b**) and B) 3′-OCH_3-phenylserine biocatalyzed from 3-(3′-OCH_3-phenyl)glycidate (**14b**) by *Tc*PAM catalysis. Each hydroxyamino acid was derivatized as their *O*-trimethylsilyl *N*-[(2*S*)-2-methylbutyryl] methyl ester. The molecular ion ($M^{\bullet+}$, *m*/*z* 381) was not observed for either analyte.

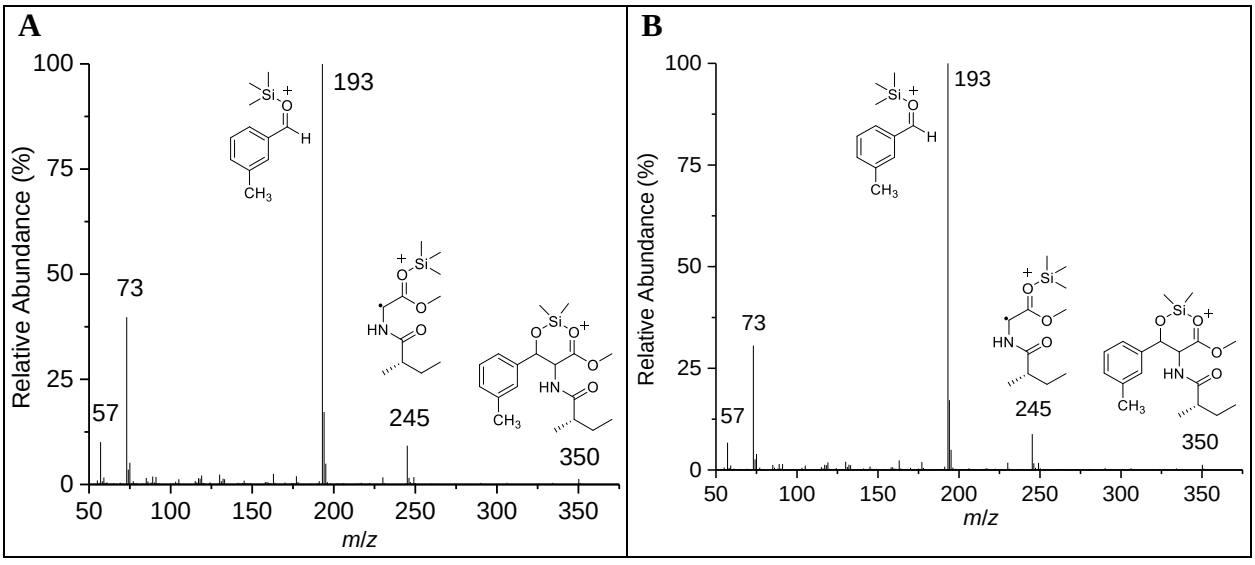

Figure. 2.38. GC/EI-MS spectra of A) authentic (2*S*/2*R*)-*anti*-3′-CH_3-phenylserine (**15c**) and B) 3′-CH_3-phenylserine biocatalyzed from 3-(3′-CH_3-phenyl)glycidate (**14c**) by *Tc*PAM catalysis. Each hydroxyamino acid was derivatized as their *O*-trimethylsilyl *N*-[(2*S*)-2-methylbutyryl] methyl ester. The molecular ion ($M^{\bullet+}$, *m*/*z* 365) was not observed for either analyte.

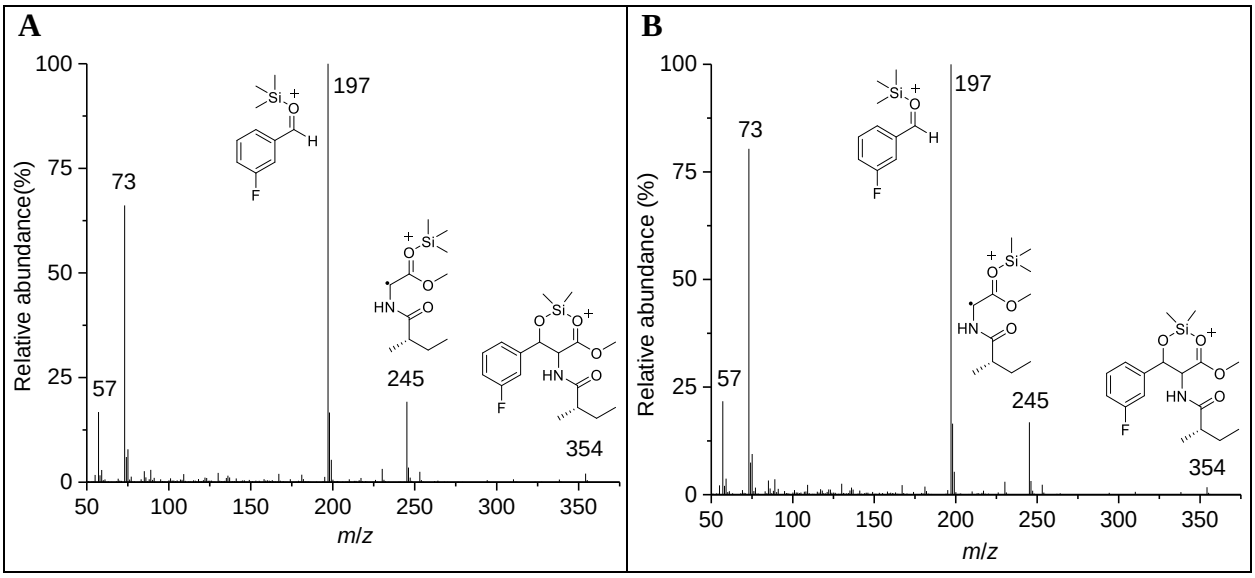

Figure. 2.39. GC/EI-MS spectra of A) authentic (2*S*/2*R*)-*anti*-3′-F-phenylserine (**15d**) and B) 3′-F-phenylserine biocatalyzed from 3-(3′-F-phenyl)glycidate (**14d**) by *Tc*PAM catalysis. Each hydroxyamino acid was derivatized as their *O*-trimethylsilyl *N*-[(2*S*)-2-methylbutyryl] methyl ester. The molecular ion ($M^{\bullet+}$, *m*/*z* 369) was not observed for either analyte.

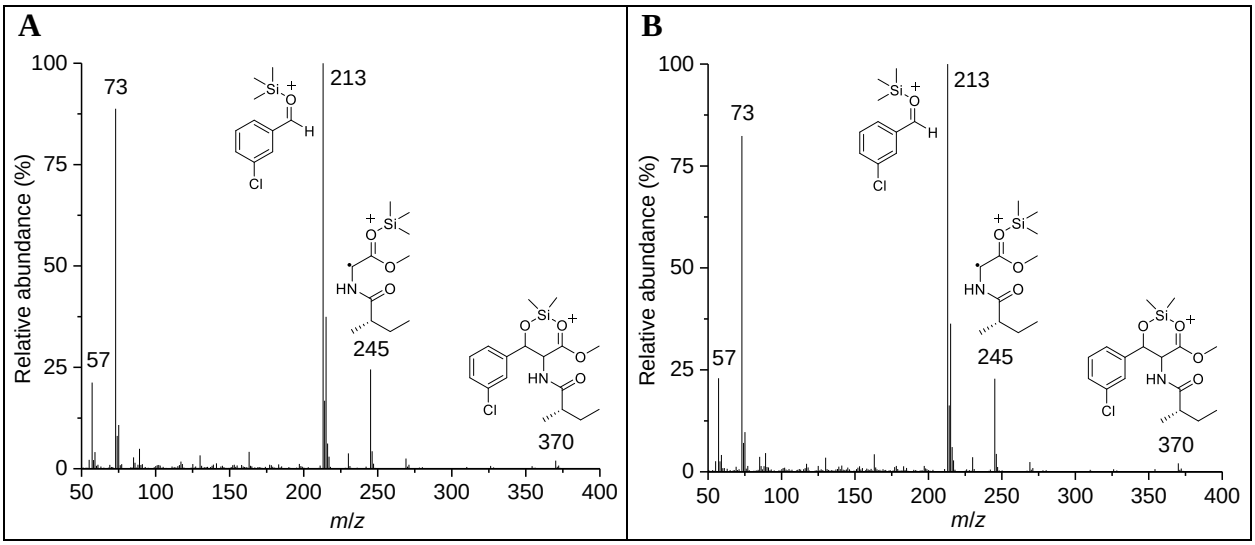

Figure. 2.40. GC/EI-MS spectra of A) authentic (2*S*/2*R*)-*anti*-3′-Cl-phenylserine (**15e**) and B) 3′-Cl-phenylserine biocatalyzed from 3-(3′-Cl-phenyl)glycidate (**14e**) by *Tc*PAM catalysis. Each hydroxyamino acid was derivatized as their *O*-trimethylsilyl *N*-[(2*S*)-2-methylbutyryl] methyl ester. The molecular ion ($M^{\bullet+}$, *m*/*z* 385) was not observed for either analyte.

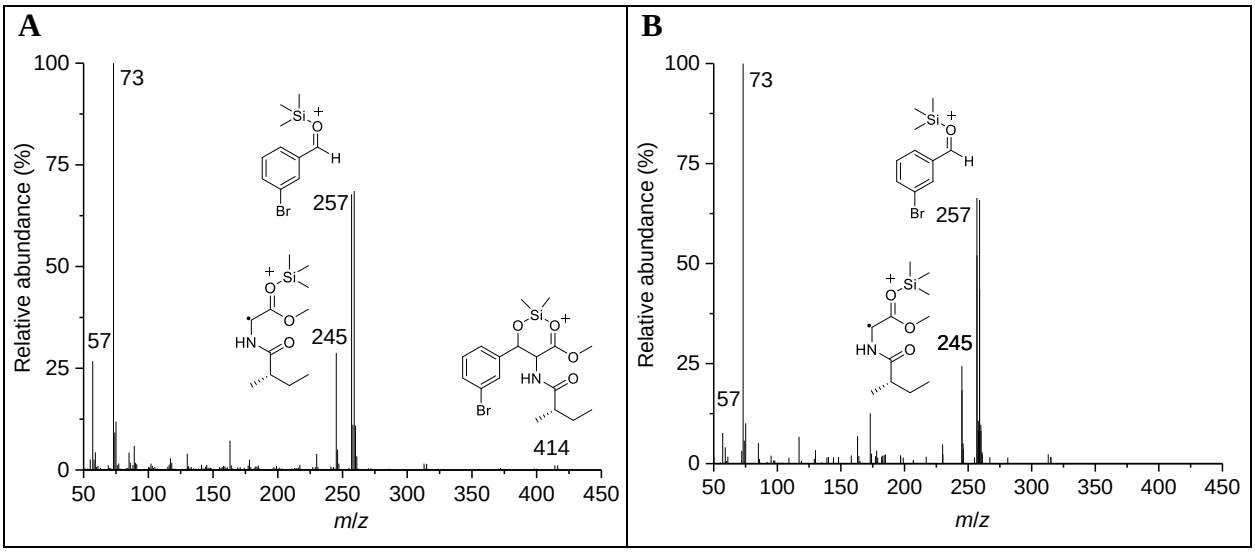

Figure. 2.41. GC/EI-MS spectra of A) authentic (2*S*/2*R*)-*anti*-3′-Br-phenylserine (**15f**) and B) 3′-Br-phenylserine biocatalyzed from 3-(3′-Br-phenyl)glycidate (**14f**) by *Tc*PAM catalysis. Each hydroxyamino acid was derivatized as their *O*-trimethylsilyl *N*-[(2*S*)-2-methylbutyryl] methyl ester. The molecular ion ($M^{\bullet+}$, *m*/*z* 429) was not observed for either analyte.

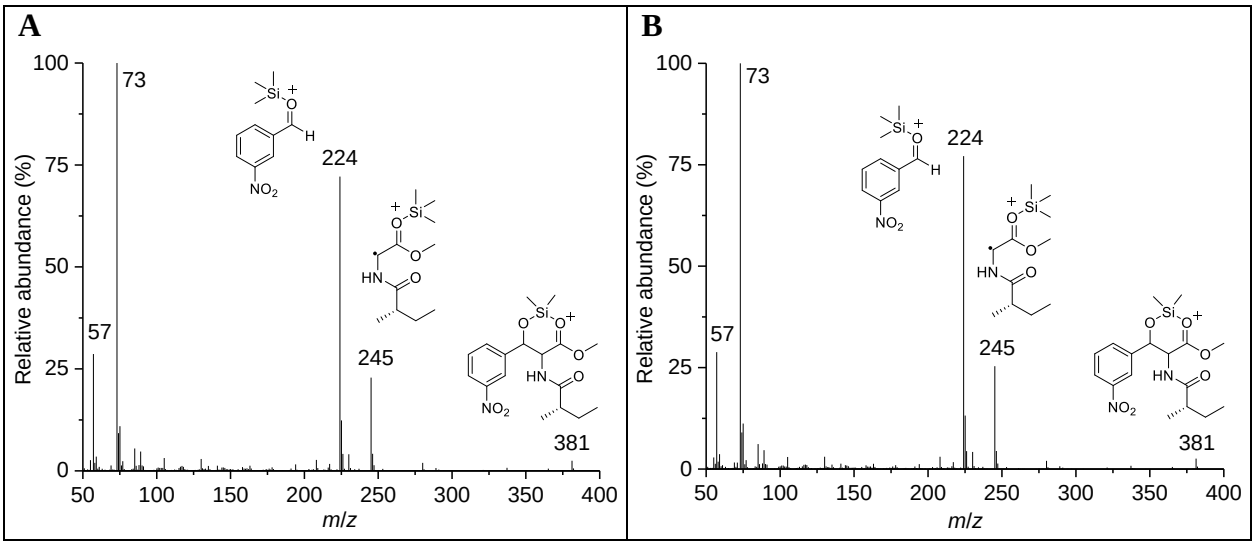

Figure. 2.42. GC/EI-MS spectra of A) authentic (2*S*/2*R*)-*anti*-3′-NO_2-phenylserine (**15g**) and B) 3′-NO_2-phenylserine biocatalyzed from 3-(3′-NO_2-phenyl)glycidate (**14g**) by *Tc*PAM catalysis. Each hydroxyamino acid was derivatized as their *O*-trimethylsilyl *N*-[(2*S*)-2-methylbutyryl] methyl ester. The molecular ion ($M^{\bullet+}$, *m*/*z* 396) was not observed for either analyte.

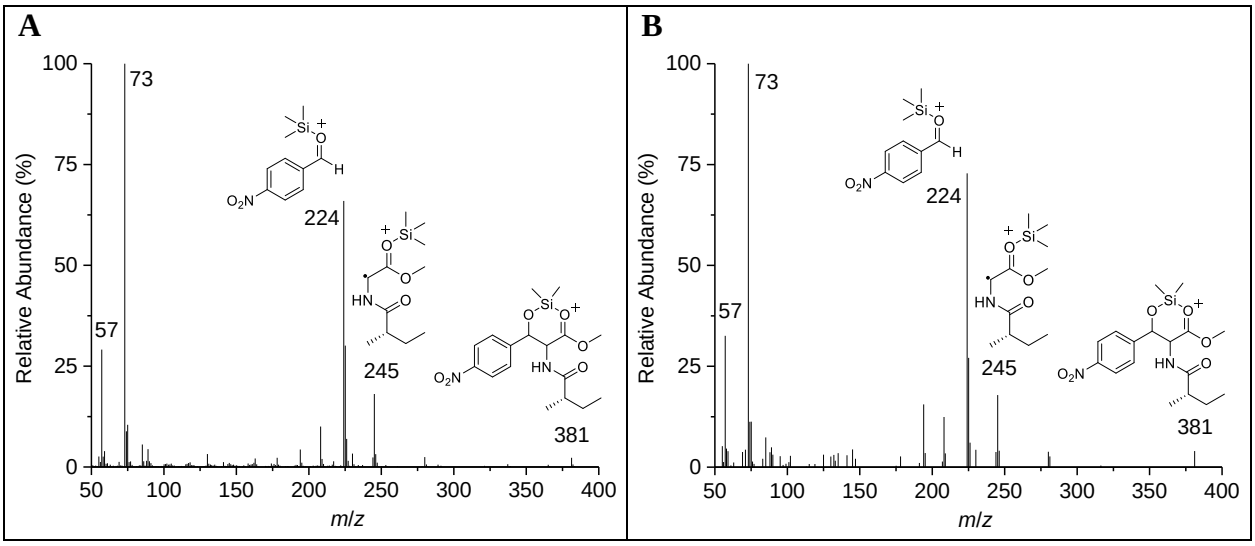

Figure. 2.43. GC/EI-MS spectra of A) authentic (2*S*/2*R*)-*anti*-4′-NO_2-phenylserine (**15h**) and B) 4′-NO_2-phenylserine biocatalyzed from 3-(4′-NO_2-phenyl)glycidate (**14h**) by *Tc*PAM catalysis. Each hydroxyamino acid was derivatized as their *O*-trimethylsilyl *N*-[(2*S*)-2-methylbutyryl] methyl ester. The molecular ion ($M^{\bullet+}$, *m*/*z* 396) was not observed for either analyte.

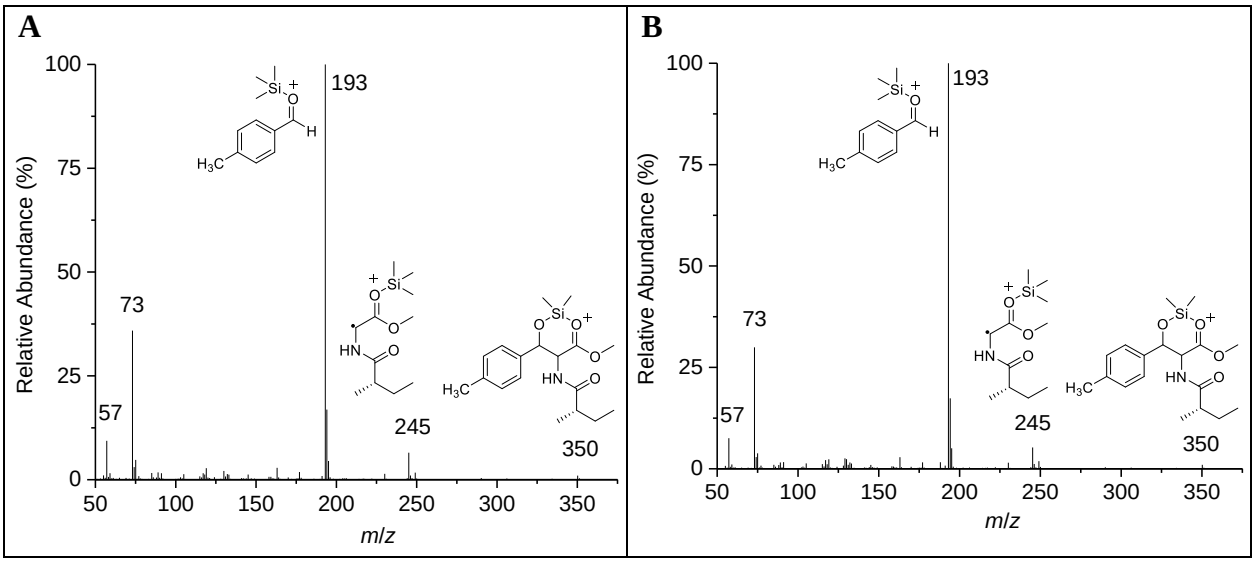

Figure. 2.44. GC/EI-MS spectra of A) authentic (2*S*/2*R*)-*anti*-4′-CH_3-phenylserine (**15i**) and B) 4′-CH_3-phenylserine biocatalyzed from 3-(4′-CH_3-phenyl)glycidate (**14i**) by *Tc*PAM catalysis. Each hydroxyamino acid was derivatized as their *O*-trimethylsilyl *N*-[(2*S*)-2-methylbutyryl] methyl ester. The molecular ion ($M^{\bullet+}$, *m*/*z* 365) was not observed for either analyte.

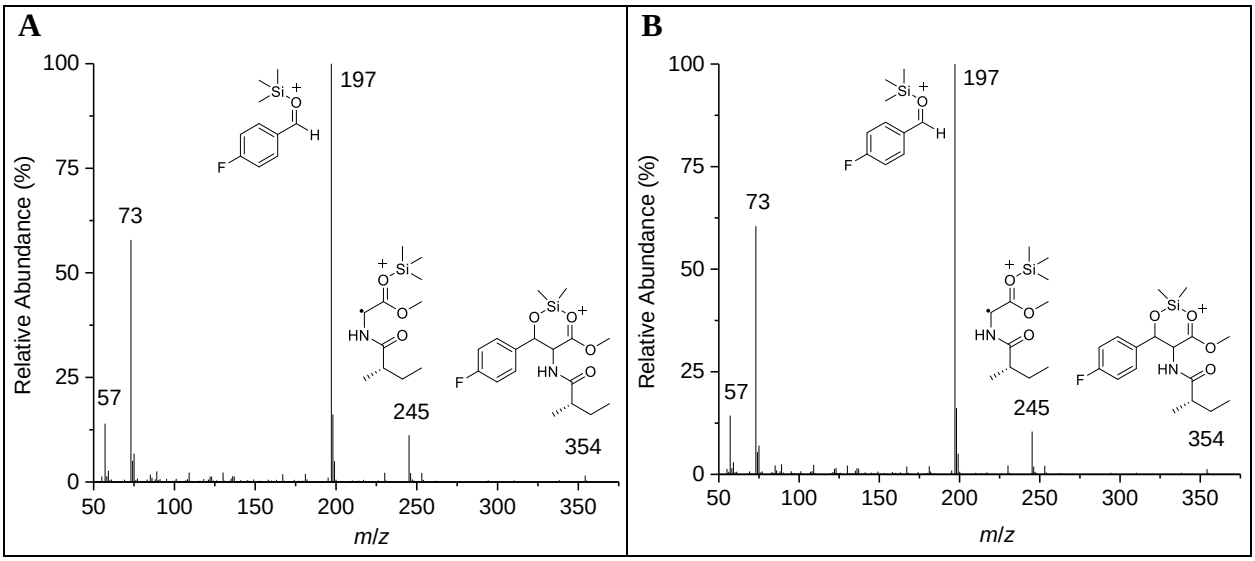

Figure. 2.45. GC/EI-MS spectra of A) authentic (2*S*/2*R*)-*anti*-4′-F-phenylserine (**15j**) and B) 4′-F-phenylserine biocatalyzed from 3-(4′-F-phenyl)glycidate (**14j**) by *Tc*PAM catalysis. Each hydroxyamino acid was derivatized as their *O*-trimethylsilyl *N*-[(2*S*)-2-methylbutyryl] methyl ester. The molecular ion ($M^{\bullet+}$, *m*/*z* 369) was not observed for either analyte.

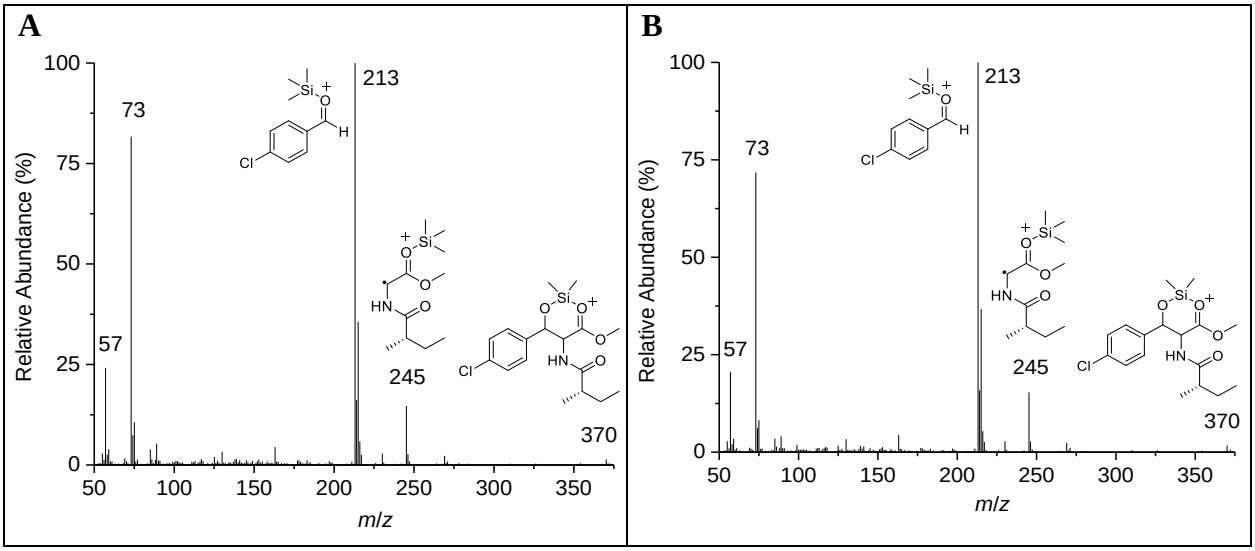

Figure. 2.46. GC/EI-MS spectra of A) authentic (2*S*/2*R*)-*anti*-4′-Cl-phenylserine (**15k**) and B) 4′-Cl-phenylserine biocatalyzed from 3-(4′-Cl-phenyl)glycidate (**14k**) by *Tc*PAM catalysis. Each hydroxyamino acid was derivatized as their *O*-trimethylsilyl *N*-[(2*S*)-2-methylbutyryl] methyl ester. The molecular ion ($M^{\bullet+}$, *m*/*z* 385) was not observed for either analyte.

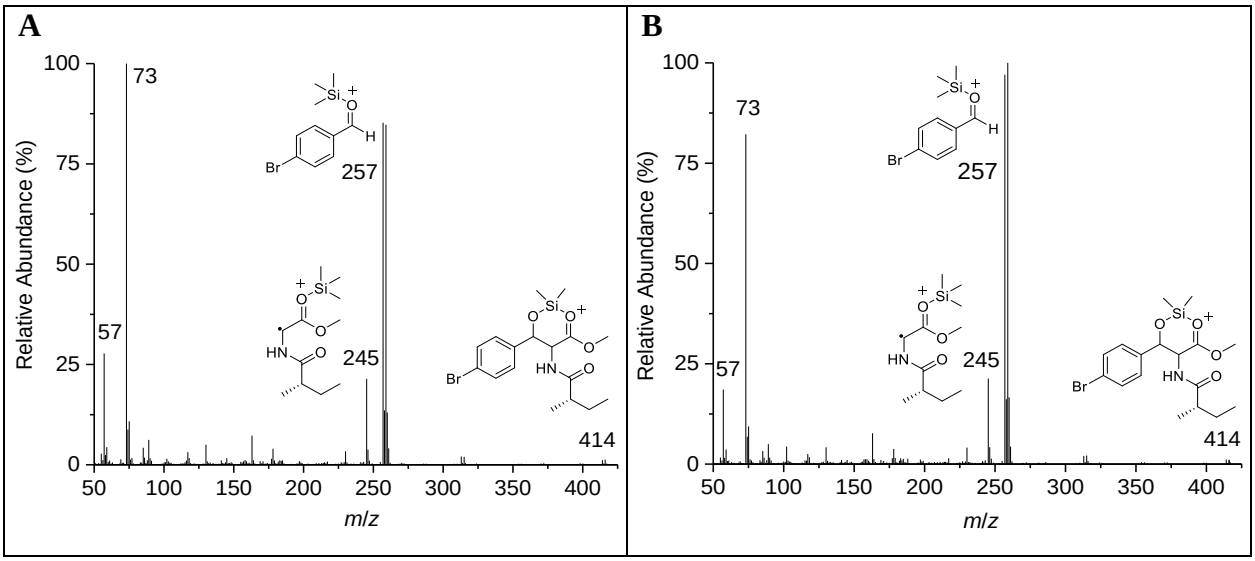

Figure. 2.47. GC/EI-MS spectra of A) authentic (2*S*/2*R*)-*anti*-4′-Br-phenylserine (**15l**) and B) 4′-Br-phenylserine biocatalyzed from 3-(4′-Br-phenyl)glycidate (**14l**) by *Tc*PAM catalysis. Each hydroxyamino acid was derivatized as their *O*-trimethylsilyl *N*-[(2*S*)-2-methylbutyryl] methyl ester. The molecular ion ($M^{\bullet+}$, *m*/*z* 429) was not observed for either analyte.

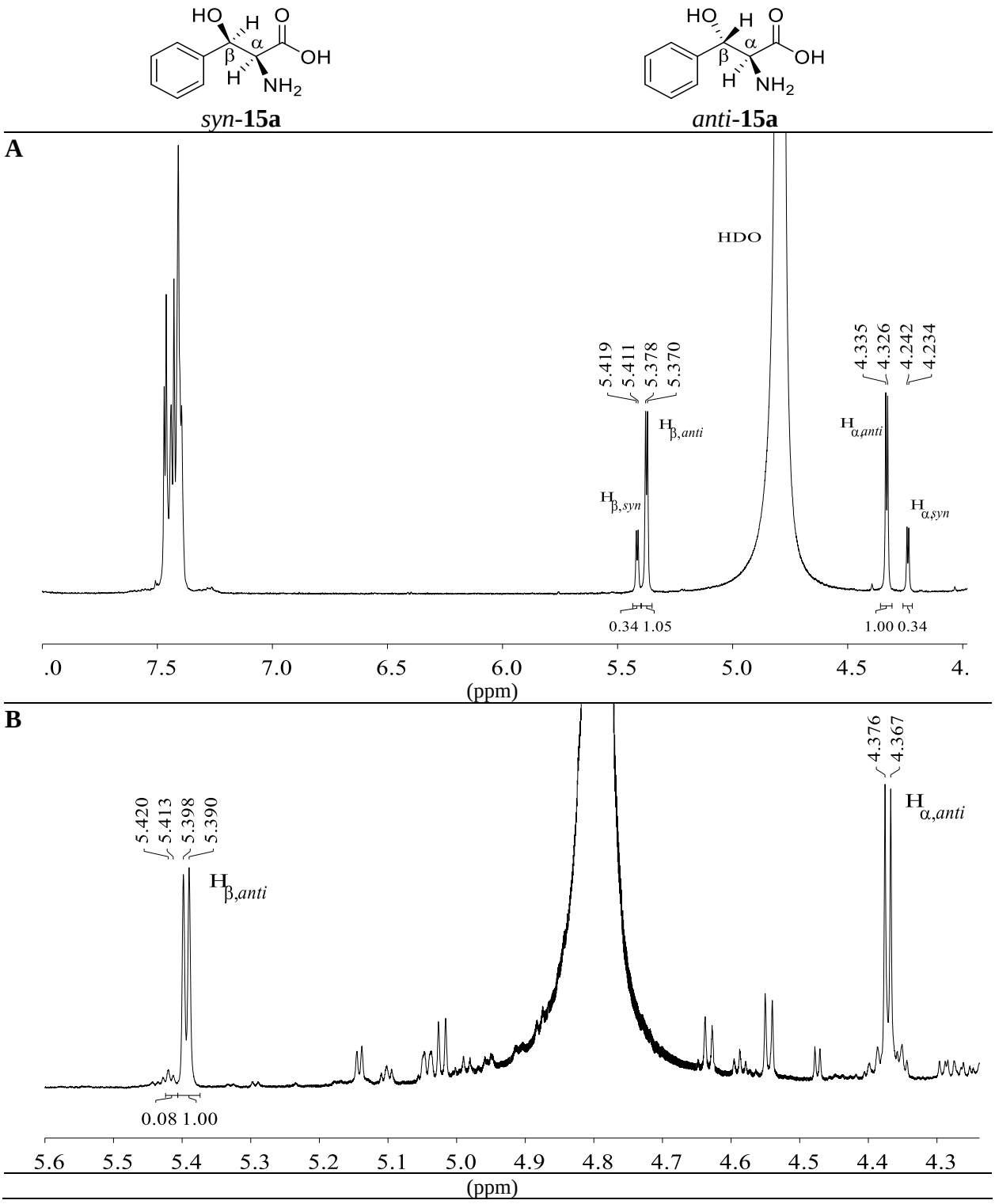

Figure. 2.48. Partial ^{1}H NMR (500 MHz, D_2O at pH 1.5) spectra of A) chemically synthesized phenylserine (**15a**) and B) biosynthetic phenylserine produced from phenylglycidate (**14a**) by *Tc*PAM.

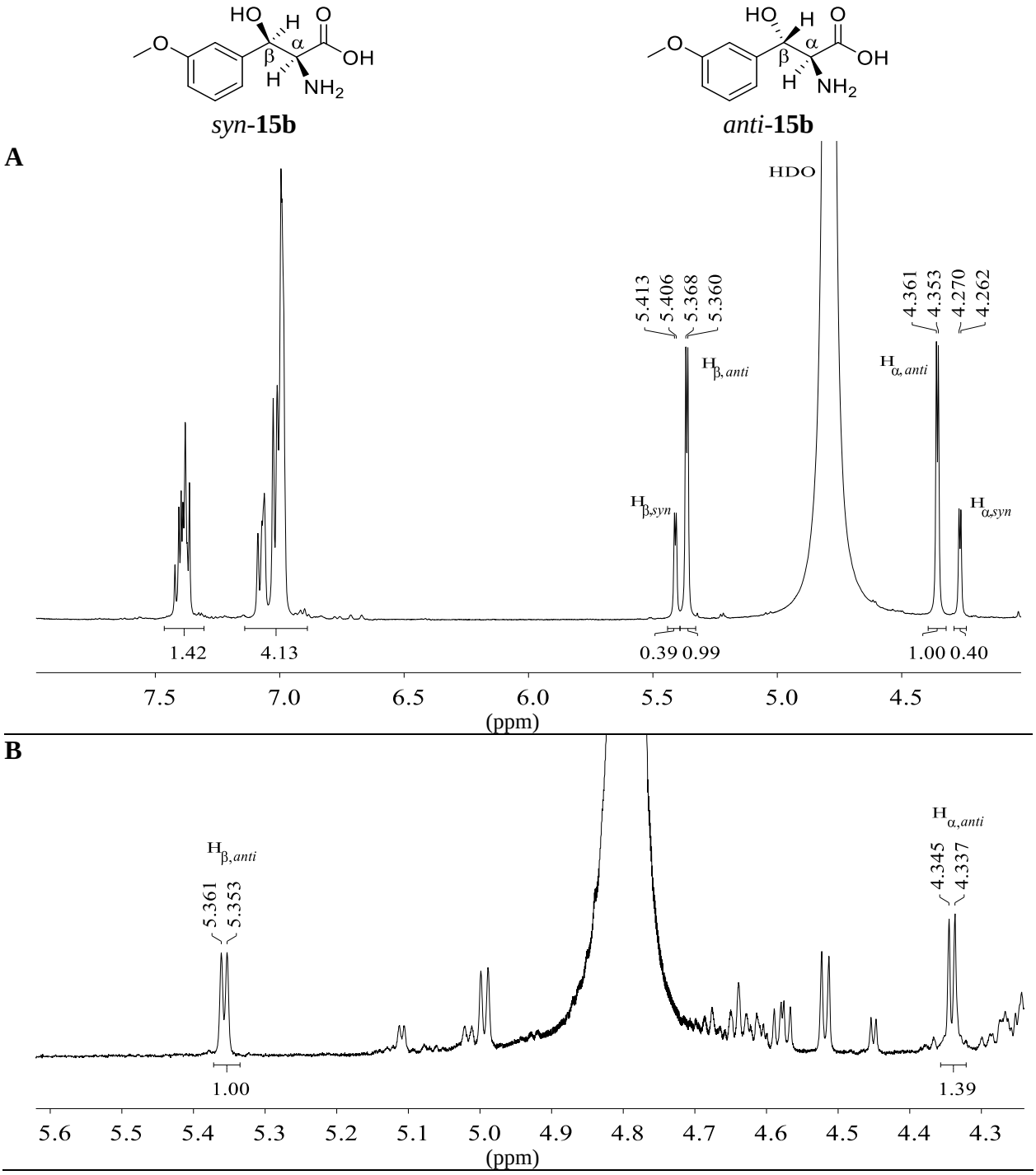

Figure. 2.49. Partial ^{1}H NMR (500 MHz, D_2O at pH 1.5) spectra of A) chemically synthesized 3′-OCH_3-phenylserine (**15b**) and B) biosynthetic 3′-OCH_3-phenylserine produced from 3-(3′-OCH_3-phenyl)glycidate (**14b**) by *Tc*PAM.

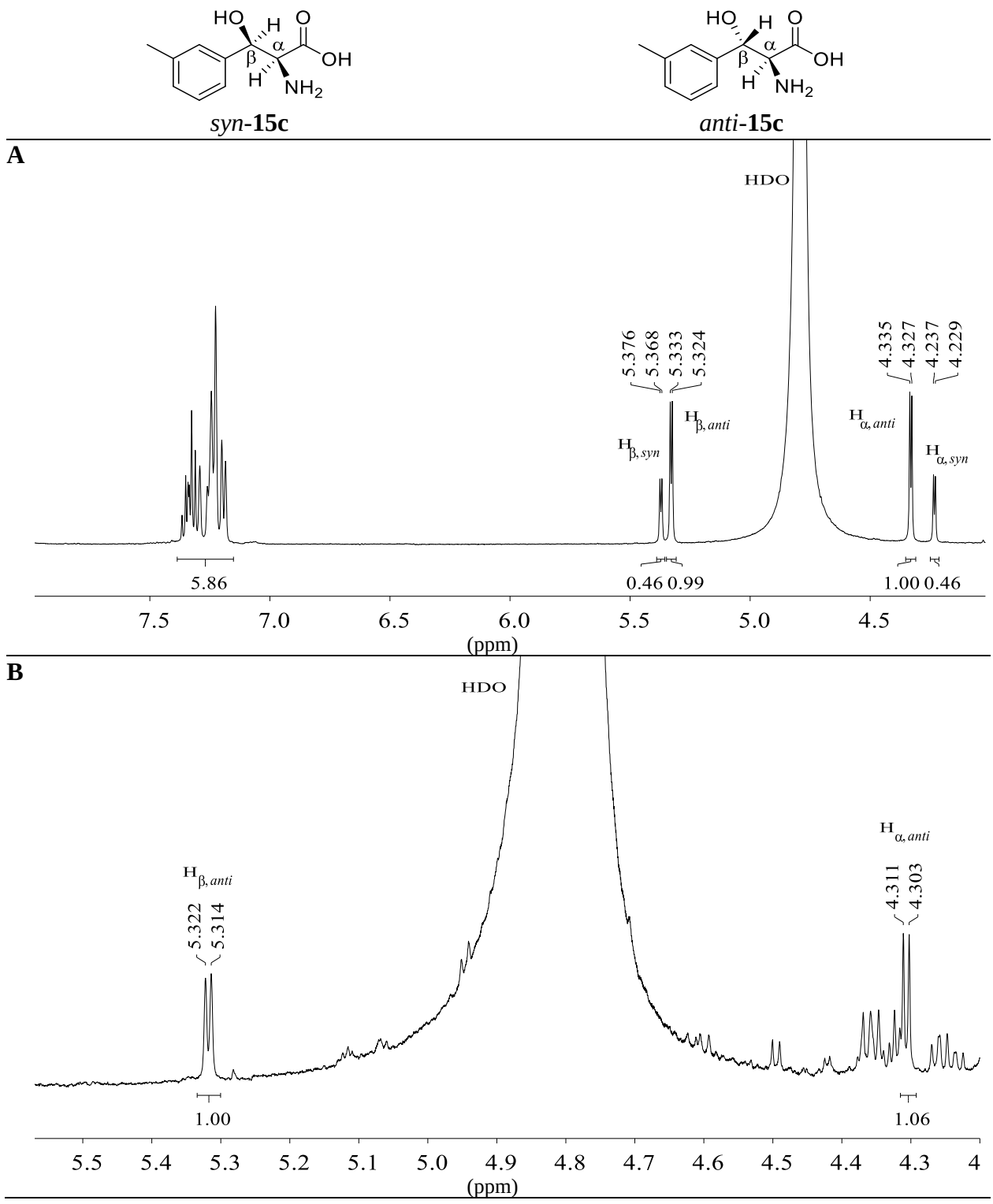

Figure. 2.50. Partial ^{1}H NMR (500 MHz, D_2O at pH 1.5) spectra of A) chemically synthesized 3′-CH_3-phenylserine (**15c**) and B) biosynthetic 3′-CH_3-phenylserine produced from 3-(3′-CH_3-phenyl)glycidate (**14c**) by *Tc*PAM.

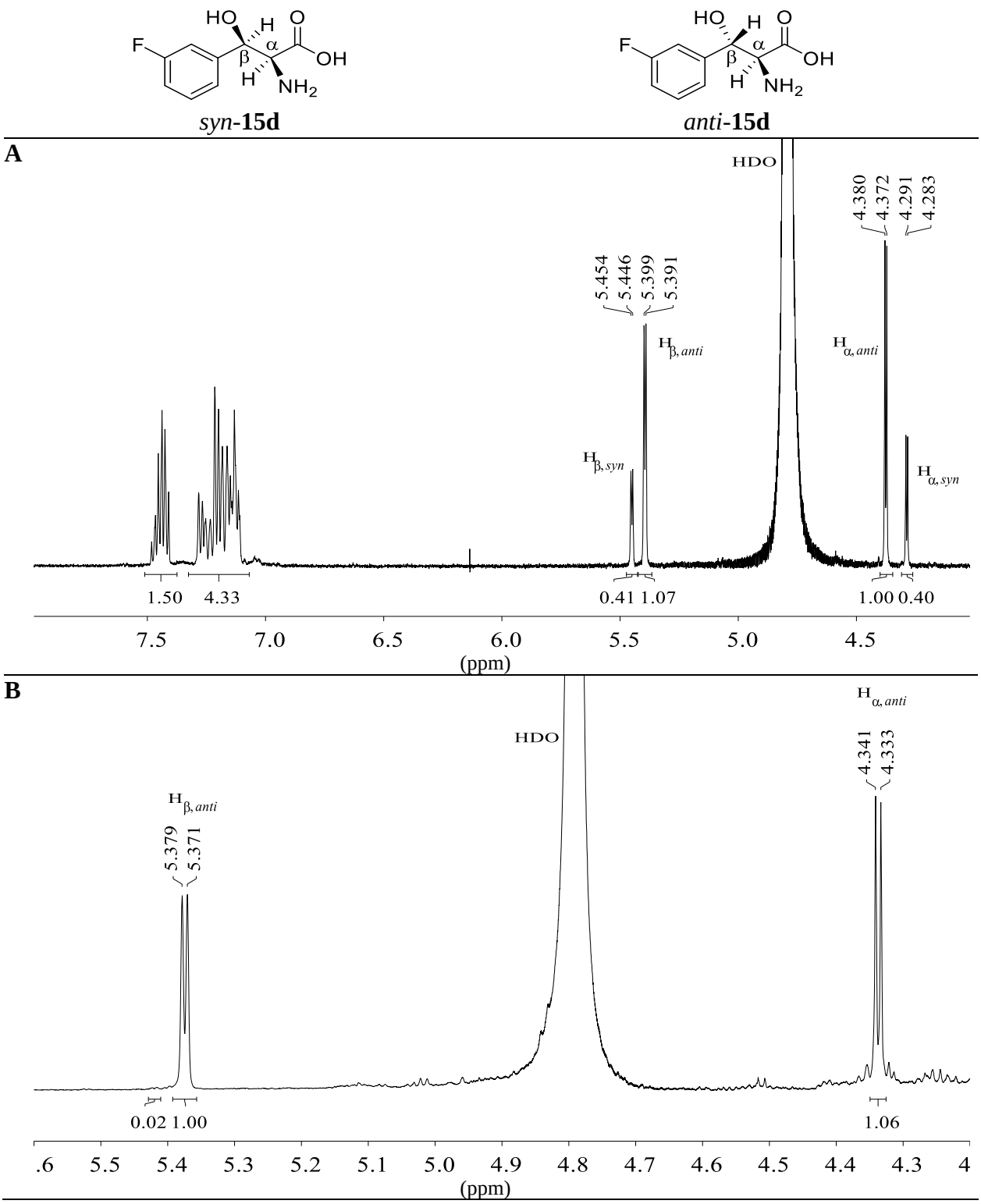

Figure. 2.51. Partial ^{1}H NMR (500 MHz, D_2O at pH 1.5) spectra of A) chemically synthesized 3′-F-phenylserine (**15d**) and B) biosynthetic 3′-F-phenylserine produced from 3-(3′-F-phenyl)glycidate (**14d**) with *Tc*PAM.

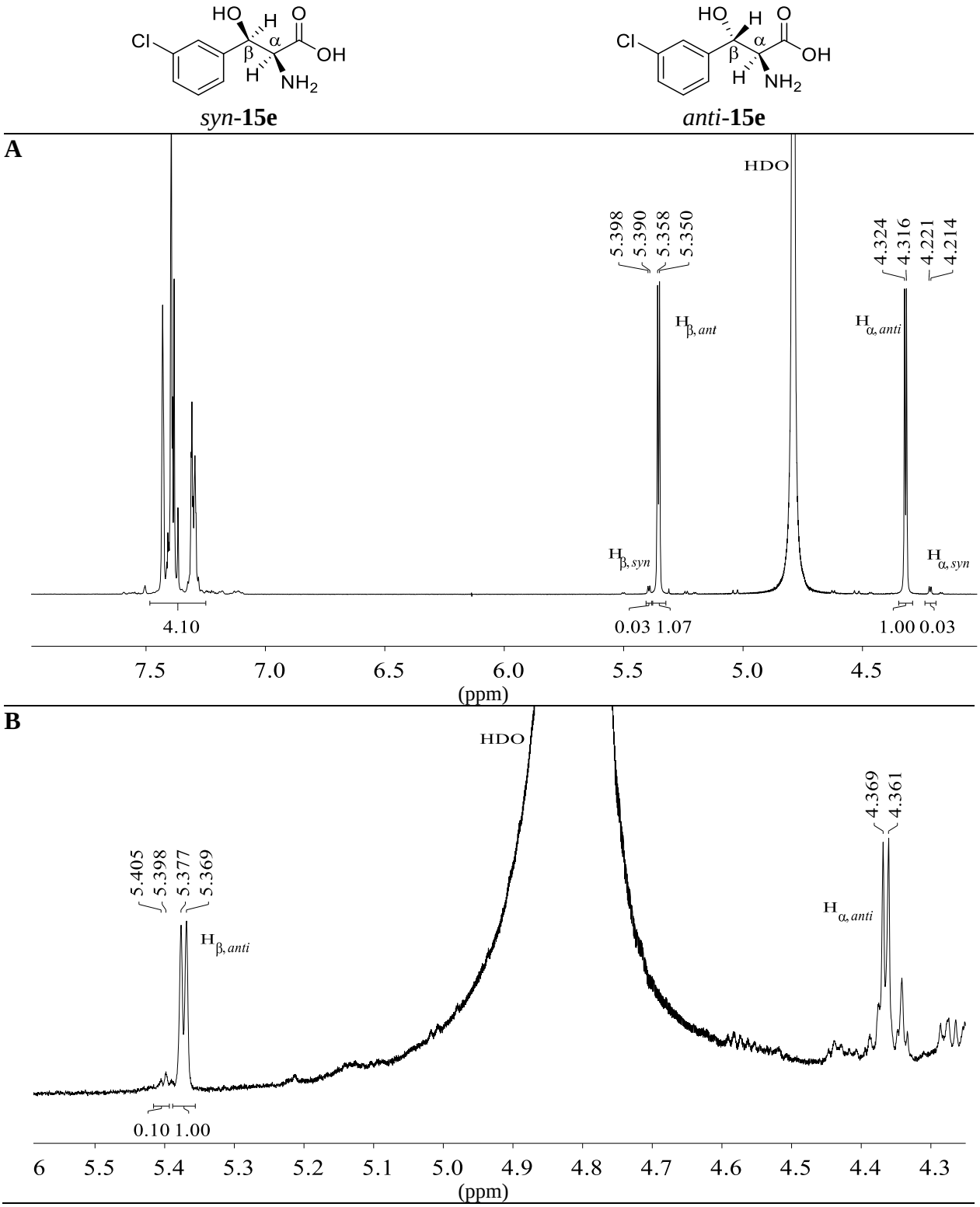

Figure. 2.52. Partial ^{1}H NMR (500 MHz, D_2O at pH 1.5) spectra of A) chemically synthesized 3′-Cl-phenylserine (**15e**) and B) biosynthetic 3′-Cl-phenylserine produced from 3-(3′-Cl-phenyl)glycidate (**14e**) by *Tc*PAM.

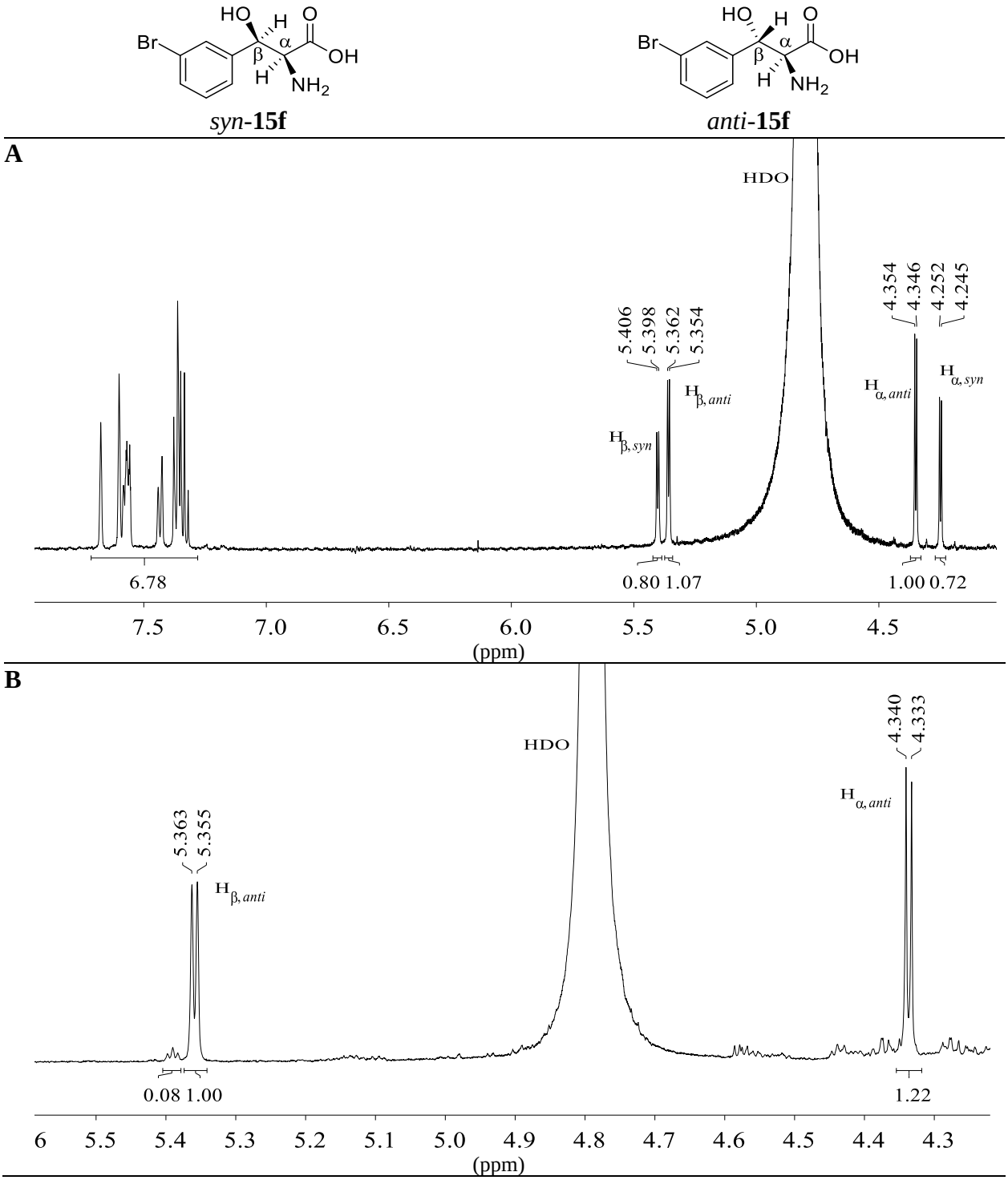

Figure. 2.53. Partial ^{1}H NMR (500 MHz, D_2O at pH 1.5) spectra of A) chemically synthesized 3′-Br-phenylserine (**15f**) and B) biosynthetic 3′-Br-phenylserine produced from 3-(3′-Br-phenyl)glycidate (**14f**) by *Tc*PAM.

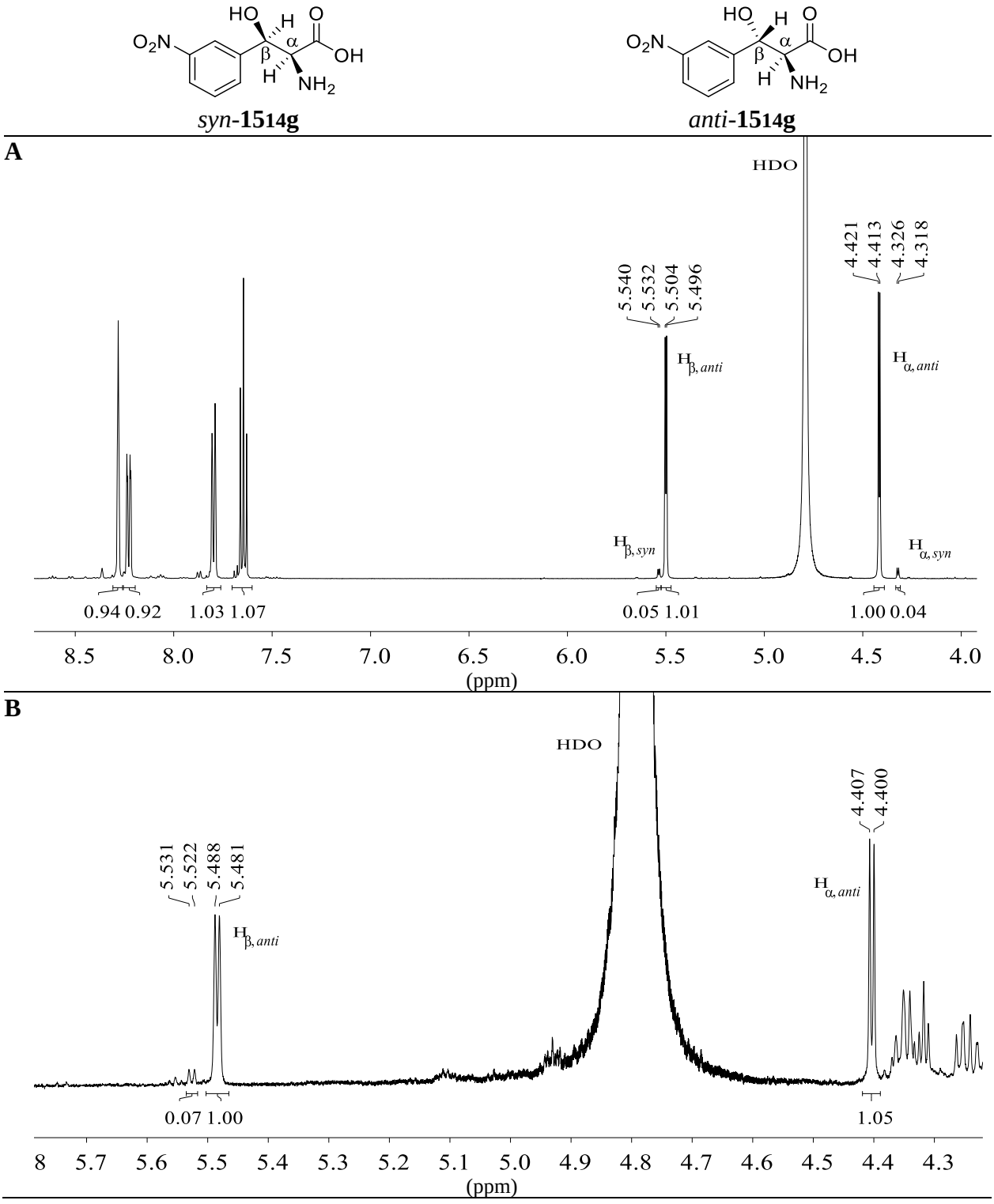

Figure. 2.54. Partial ^{1}H NMR (500 MHz, D_2O at pH 1.5) spectra of A) chemically synthesized 3′-NO_2-phenylserine (**15g**) and B) biosynthetic 3′-NO_2-phenylserine produced from 3-(3′-NO_2-phenyl)glycidate (**14g**) by *Tc*PAM.

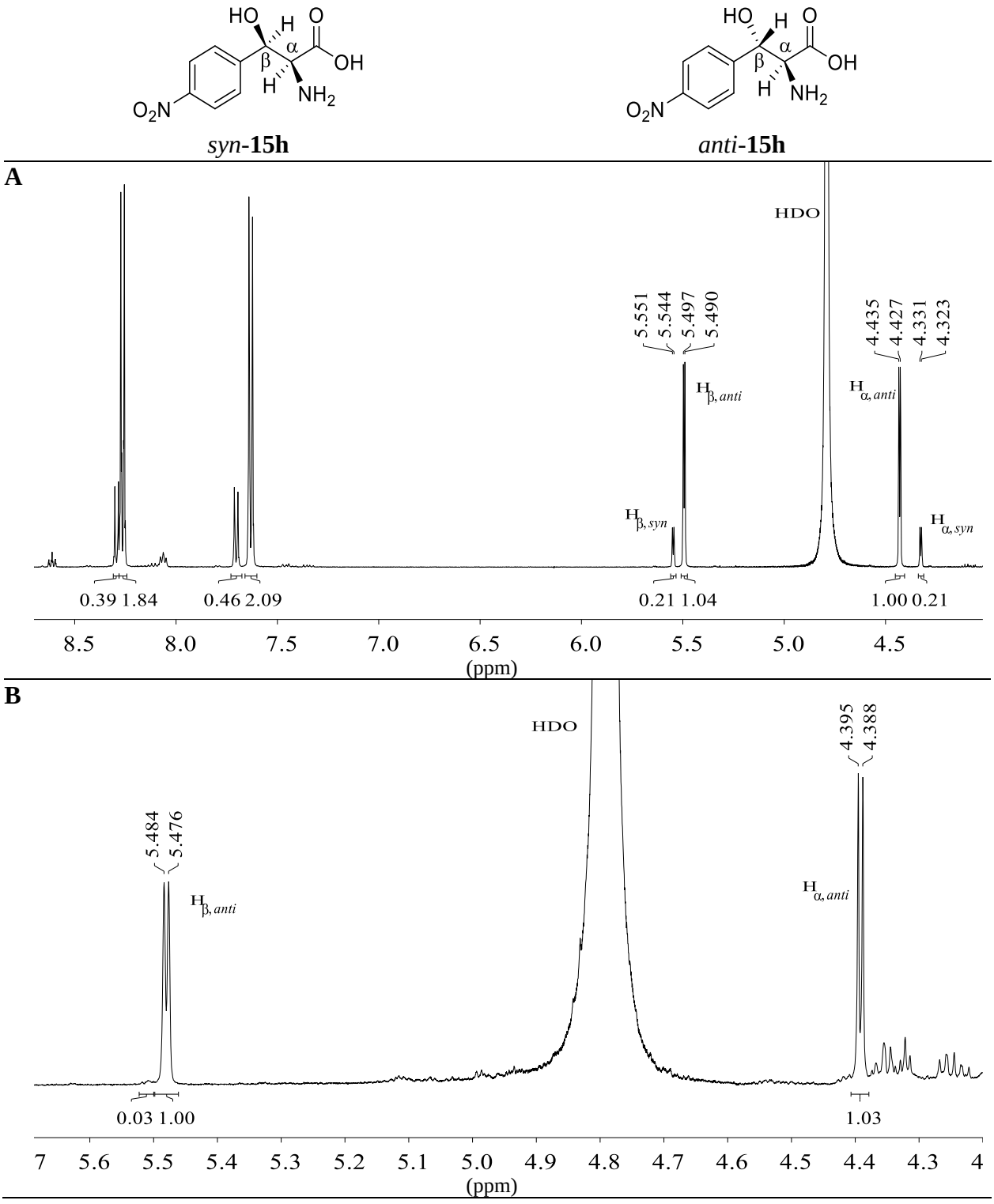

Figure. 2.55. Partial ^{1}H NMR (500 MHz, D_2O at pH 1.5) spectra of A) chemically synthesized 4′-NO_2-phenylserine (**15h**) and B) biosynthetic 4′-NO_2-phenylserine produced from 3-(4′-NO_2-phenyl)glycidate (**14h**) by *Tc*PAM.

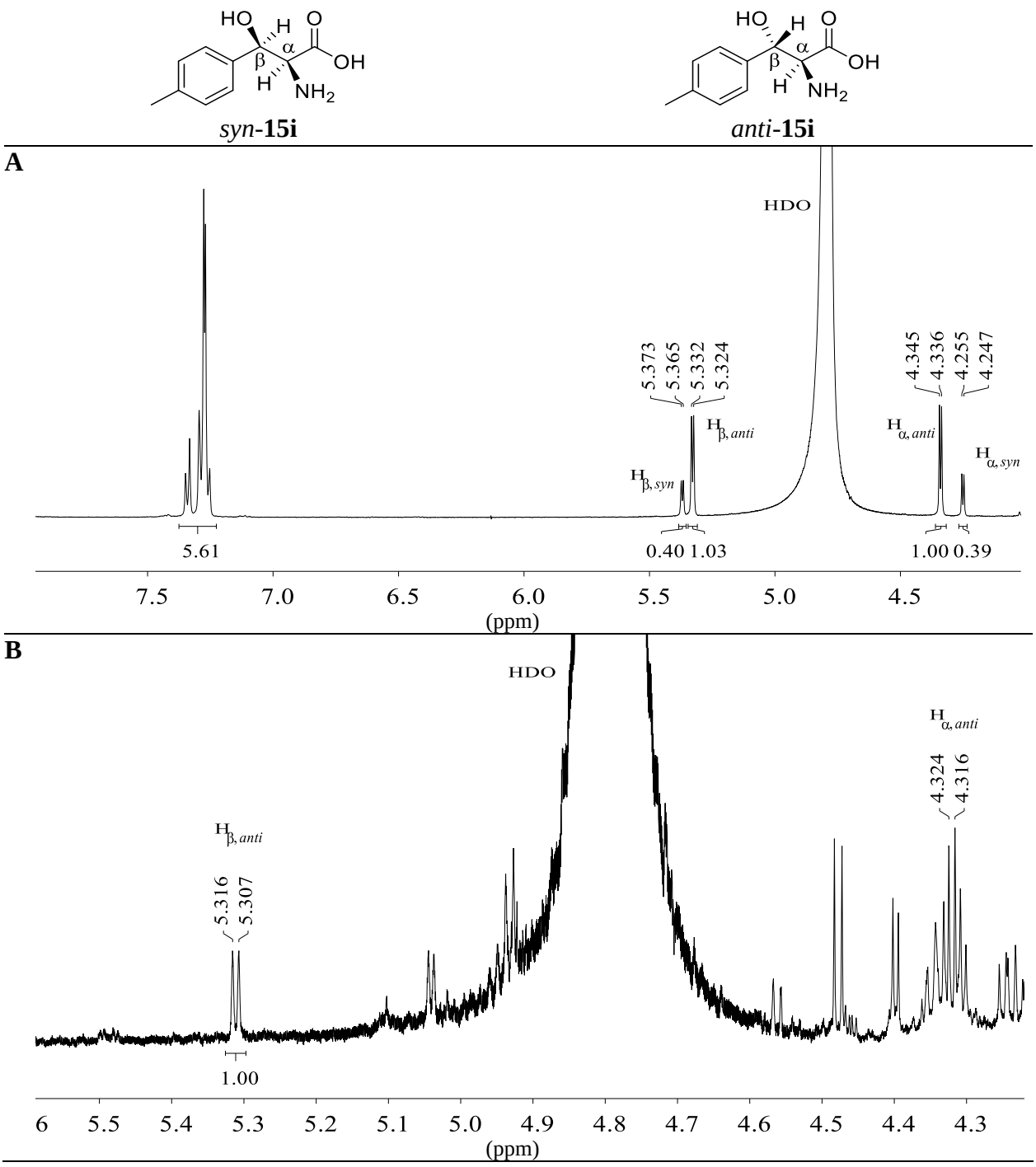

Figure. 2.56. Partial ^{1}H NMR (500 MHz, D_2O at pH 1.5) spectra of A) chemically synthesized 4′-CH_3-phenylserine (**15i**) and B) biosynthetic 4′-CH_3-phenylserine produced from 3-(4′-CH_3-phenyl)glycidate (**14i**) by *Tc*PAM.

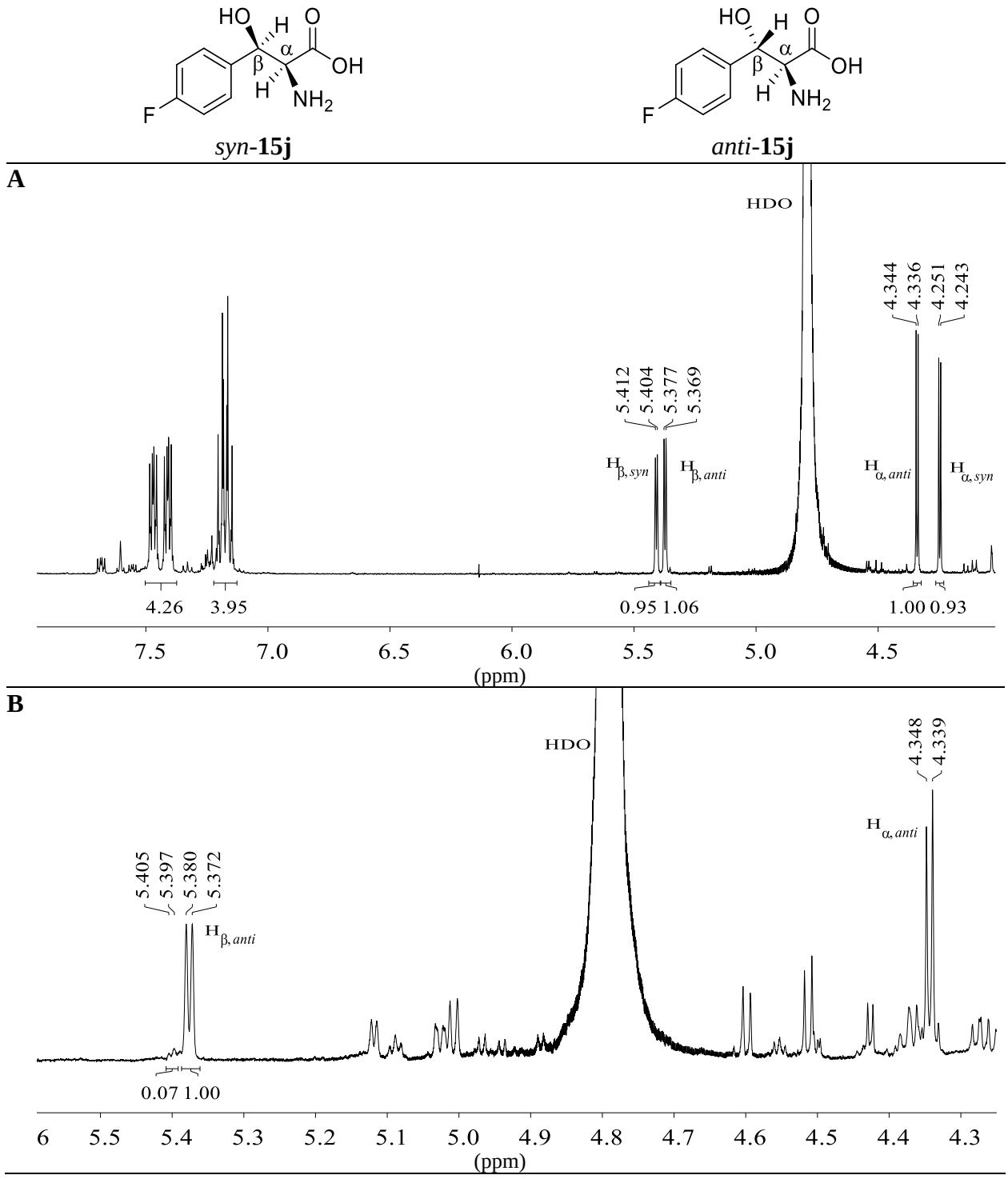

Figure. 2.57. Partial ^{1}H NMR (500 MHz, D_2O at pH 1.5) spectra of A) chemically synthesized 4′-F-phenylserine (**15j**) and B) biosynthetic 4′-F-phenylserine produced from 3-(4′-F-phenyl)glycidate (**14j**) by *Tc*PAM

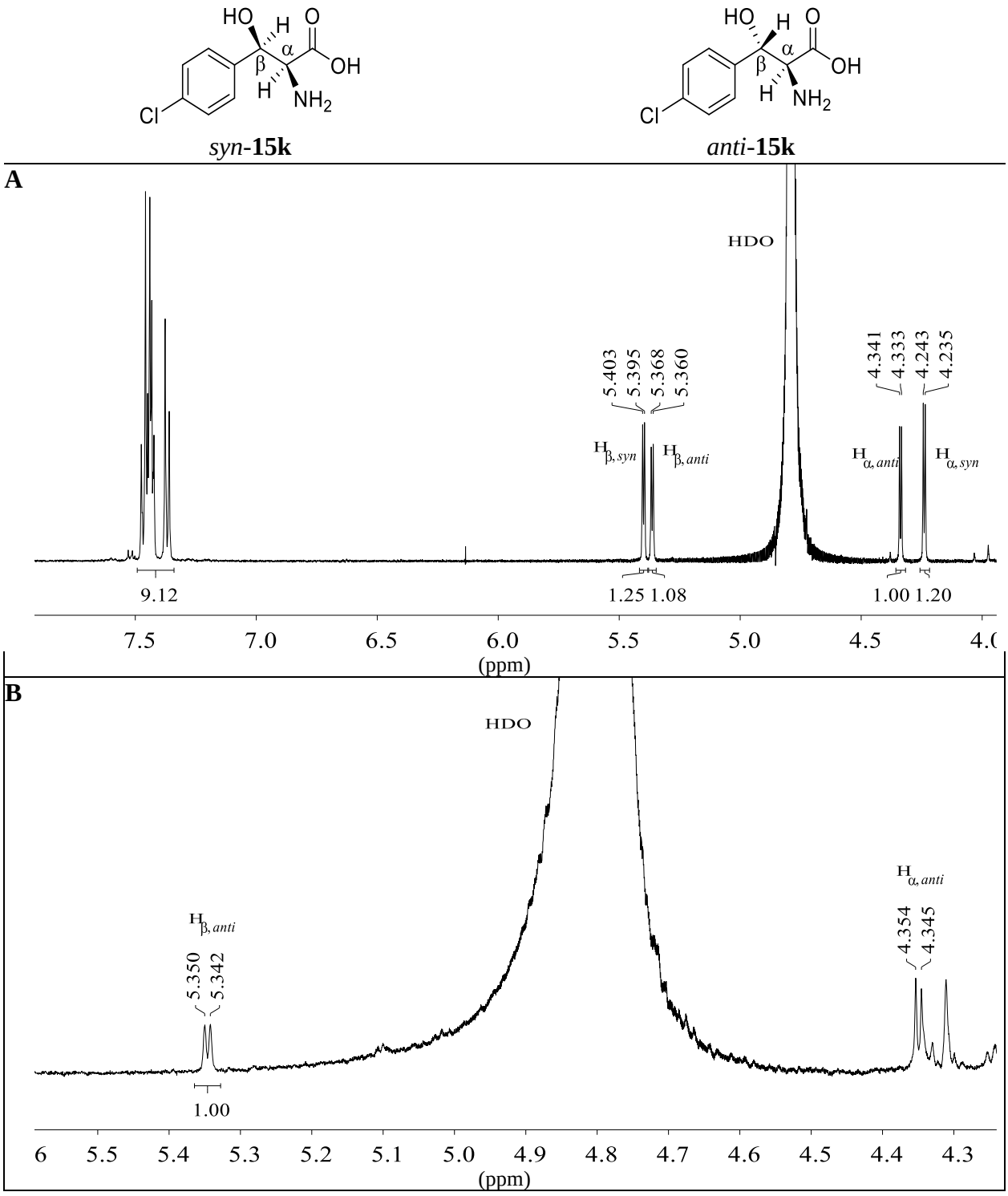

Figure. 2.58. Partial ^{1}H NMR (500 MHz, D_2O at pH 1.5) spectra of A) chemically synthesized 4′-Cl-phenylserine (**15k**) and B) biosynthetic 4′-Cl-phenylserine produced from 3-(4′-Cl-phenyl)glycidate (**14k**) by *Tc*PAM.

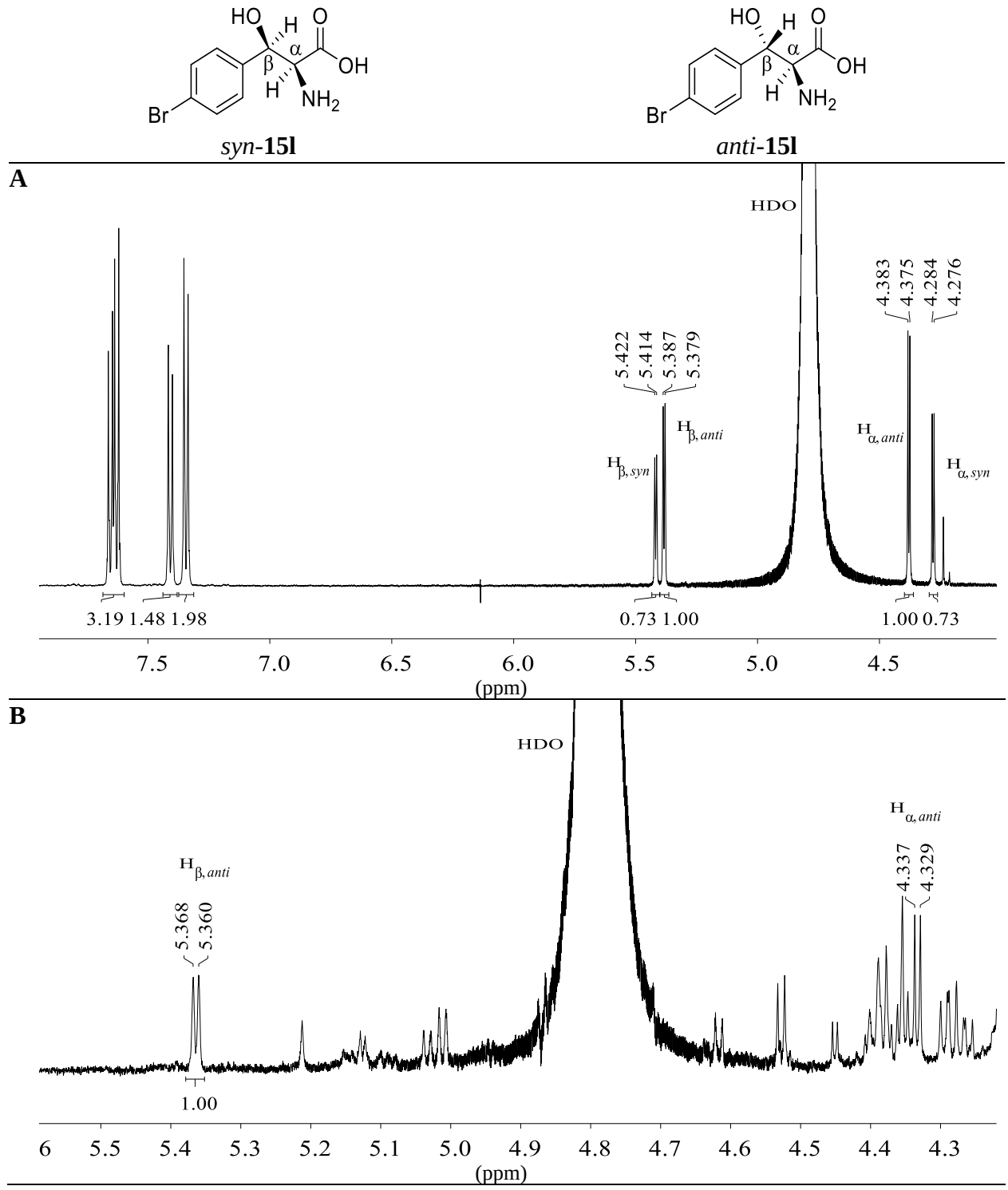

Figure. 2.59. Partial ^{1}H NMR (500 MHz, D_2O at pH 1.5) spectra of A) chemically synthesized 4′-Br-phenylserine (**15l**) and B) biosynthetic 4′-Br-phenylserine produced from 3-(4′-Br-phenyl)glycidate (**14l**) by *Tc*PAM.

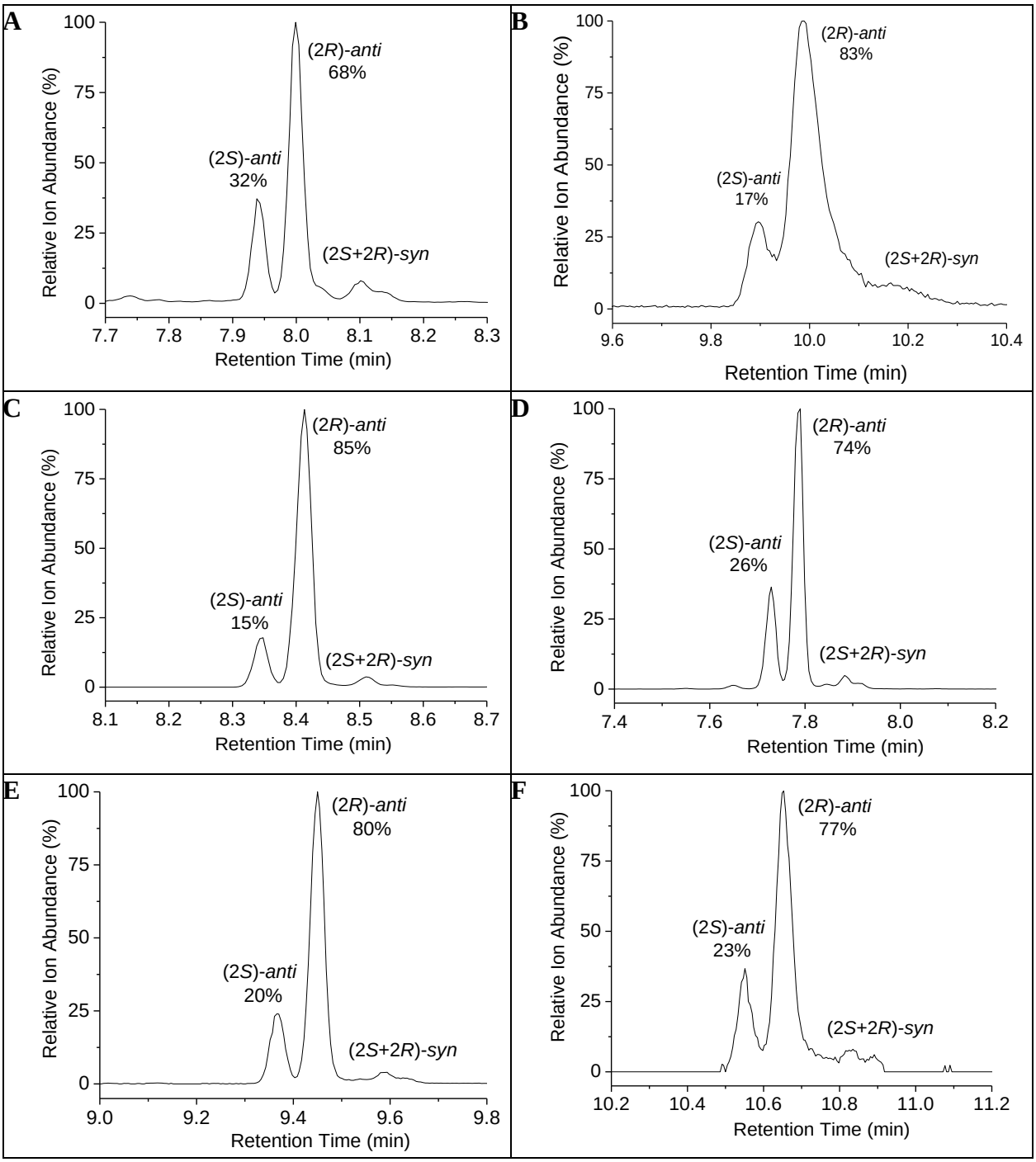

Figure. 2.60. GC/EI-MS extracted-ion chromatograms of biosynthetic arylserines derivatized as their *O*-trimethylsilyl *N*-[(2*S*)-2-methylbutyryl] methyl esters A) phenylserine (**15a**) (extracted ion *m*/*z* 179), B) 3′-OCH_3-phenylserine (**15b**) (extracted ion *m*/*z* 209), C) 3′-methylphenylserine (**15c**) (extracted ion *m*/*z* 193), D) 3′-F-phenylserine (**15d**) (extracted ion *m*/*z* 197), E) 3′-Cl-phenylserine (**15e**) (extracted ion *m*/*z* 213), and F) 3′-Br-phenylserine (**15f**) (extracted ion *m*/*z* 257).

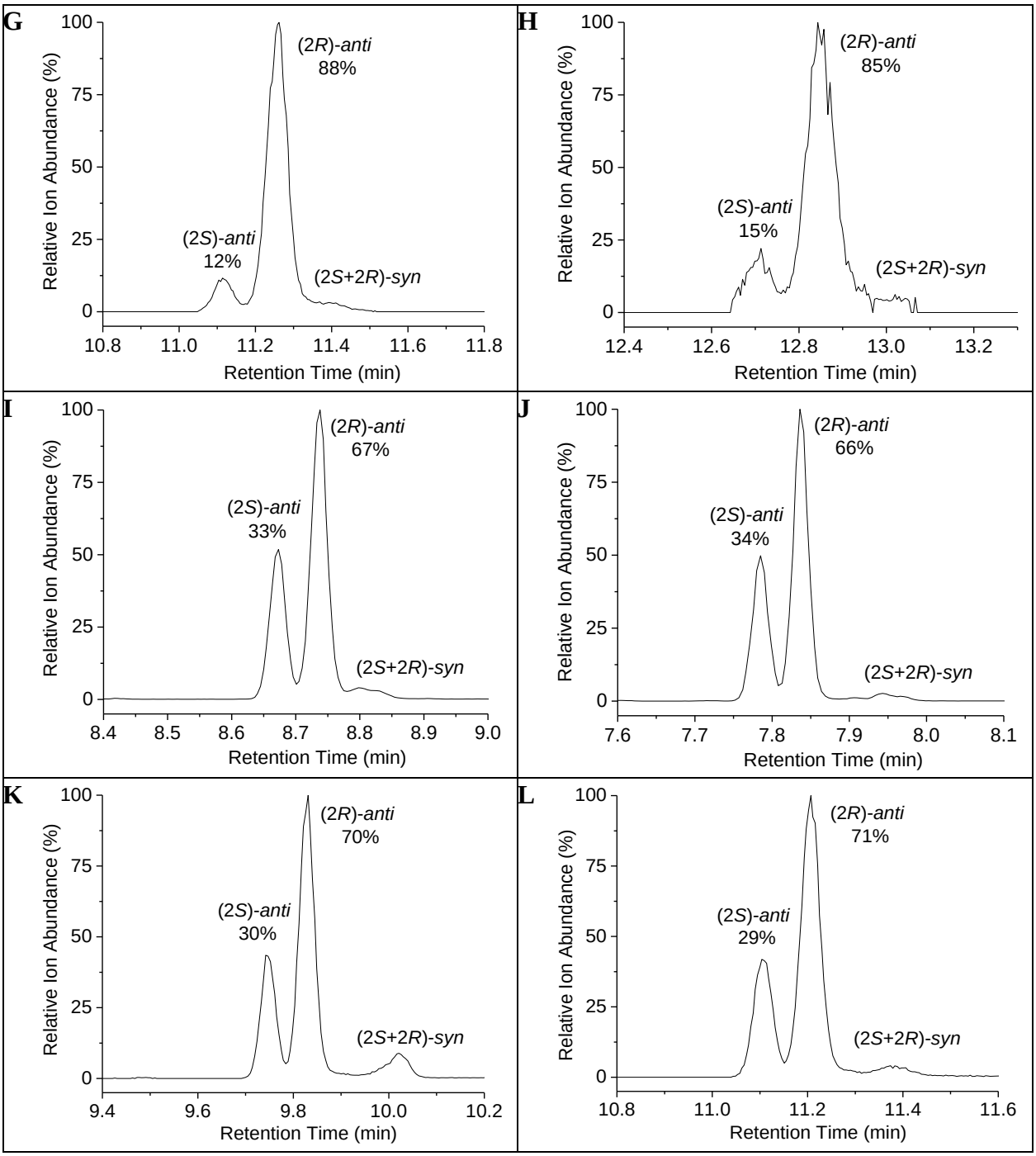

Figure. 2.61. GC/EI-MS extracted-ion chromatograms of biosynthetic arylserines derivatized as their *O*-trimethylsilyl *N*-[(2*S*)-2-methylbutyryl] methyl esters G) 3′-NO_2-phenylserine (**15g**) (extracted ion *m*/*z* 224), H) 4′-NO_2-phenylserine (**15h**) (extracted ion *m*/*z* 224), I) 4′-CH_3-phenylserine (**15i**) (extracted ion *m*/*z* 193), J) 4′-F-phenylserine (**15j**) (extracted ion *m*/*z* 197), K) 4′-Cl-phenylserine (**15k**) (extracted ion *m*/*z* 213), and L) 4′-Br-phenylserine (**15l**) (extracted ion *m*/*z* 257)

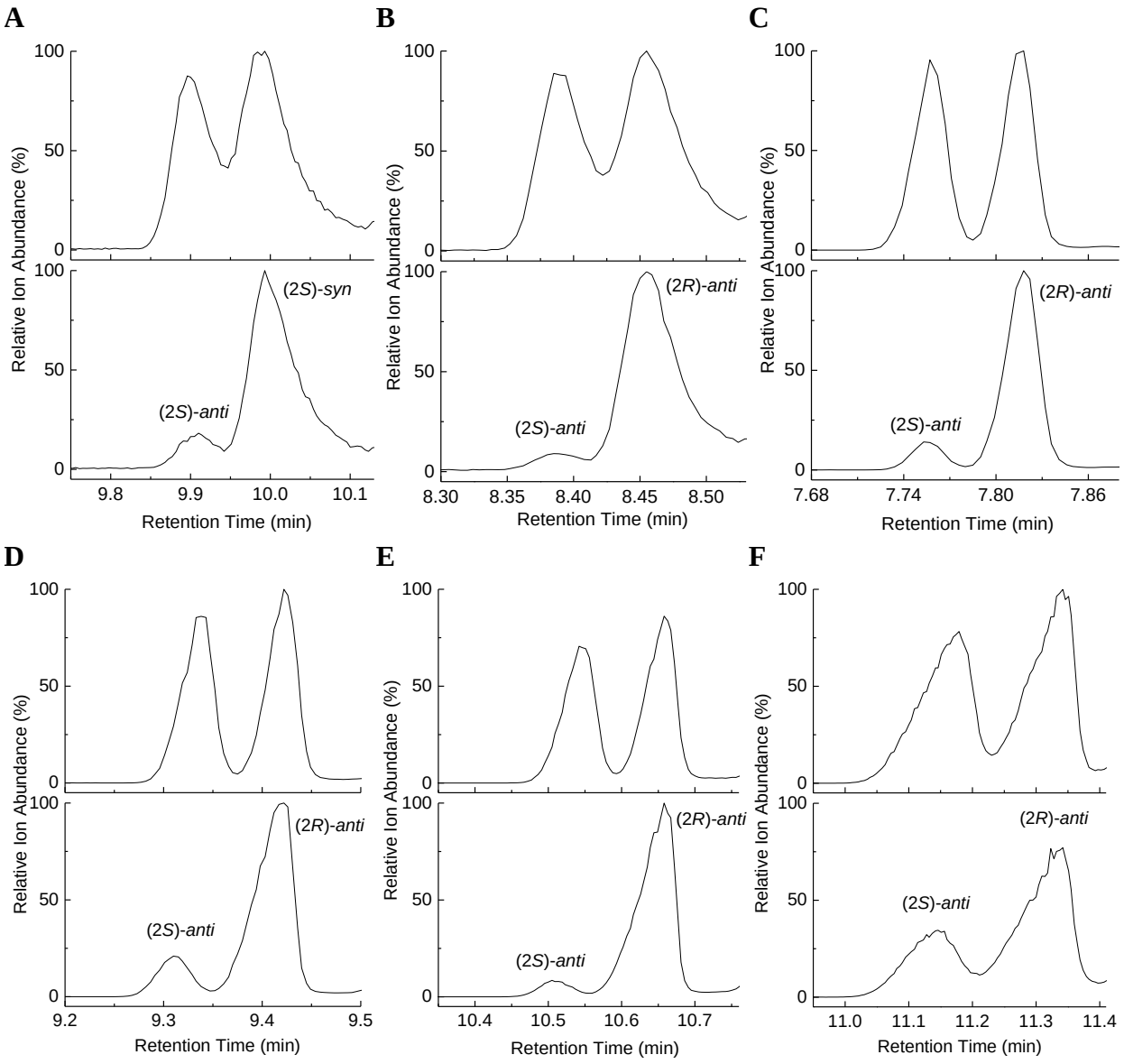

Figure. 2.62. GC/EI-MS extracted-ion chromatograms of synthetic arylserines derivatized as their *O*-trimethylsilyl *N*-[(2*S*)-2-methylbutyryl] methyl ester before (*top trace*) and after 10-min treatment with (2*S*)-TA (*bottom trace*): A) 3′-OCH_3-phenylserine (**15b**) (extracted ion *m*/*z* 209), B) 3′-CH_3-phenylserine (**15c**) (extracted ion *m*/*z* 193), C) 3′-F-phenylserine (**15d**) (extracted ion *m*/*z* 197), D) 3′-Cl-phenylserine (**15e**) (extracted ion *m*/*z* 213), E) 3′-Br-phenylserine (**15f**) (extracted ion *m*/*z* 257), and F) 3′-NO_2-phenylserine (**15g**) (extracted ion *m*/*z* 224).

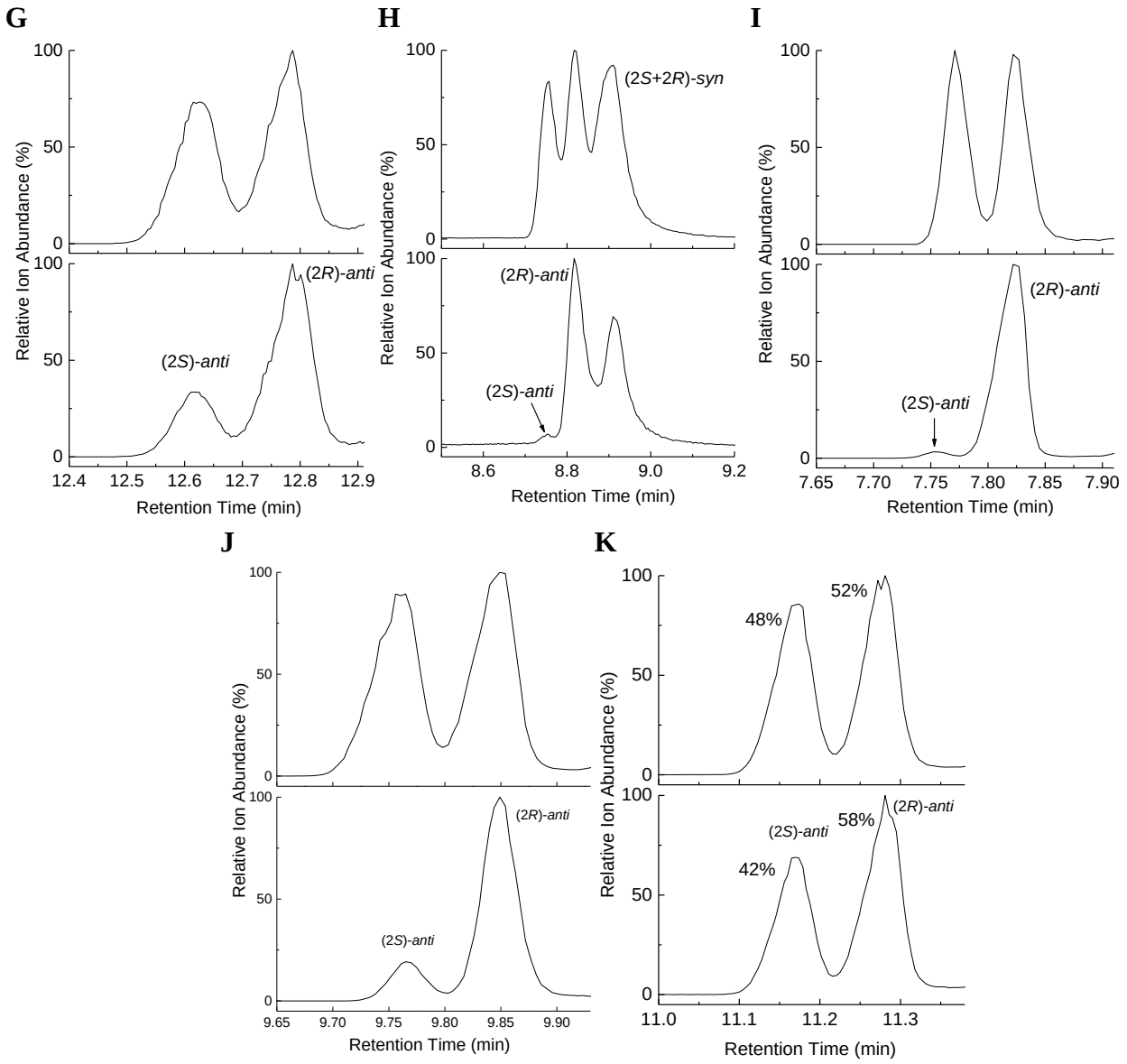

Figure. 2.63. GC/EI-MS extracted-ion chromatograms of synthetic arylserines derivatized as their *O*-trimethylsilyl *N*-[(2*S*)-2-methylbutyryl] methyl ester before (*top trace*) and after 10-min treatment with (2*S*)-TA (*bottom trace*): G) 4′-NO_2-phenylserine (**15h**) (extracted ion *m*/*z* 224); H) 4′-CH_3-phenylserine (**15i**) (extracted ion *m*/*z* 193), I) 4′-F-phenylserine (**15j**) (extracted ion *m*/*z* 197), J) 4′-Cl-phenylserine (**15k**) (extracted ion *m*/*z* 213) and K) 4′-Br-phenylserine (**15l**) (extracted ion *m*/*z* 257).

Michaelis-Menten Plots of *Tc*PAM Biocatalytic Conversion of Arylserine Analogues.

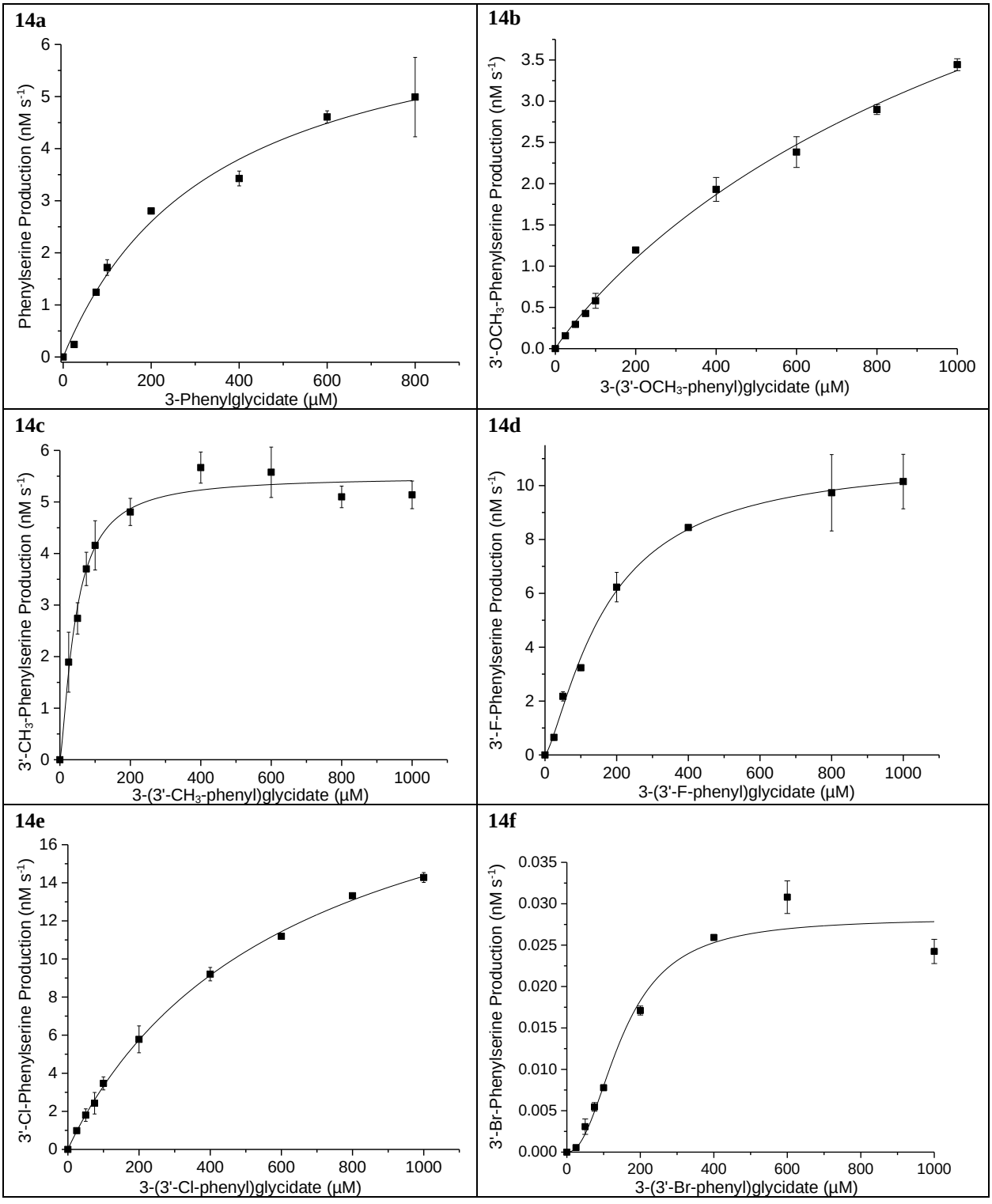

Figure. 2.64. Michaelis-Menten kinetics for the turnover of arylglycidate analogues (**14a**–**14f**) to their corresponding arylserines (**15a**–**15f**).

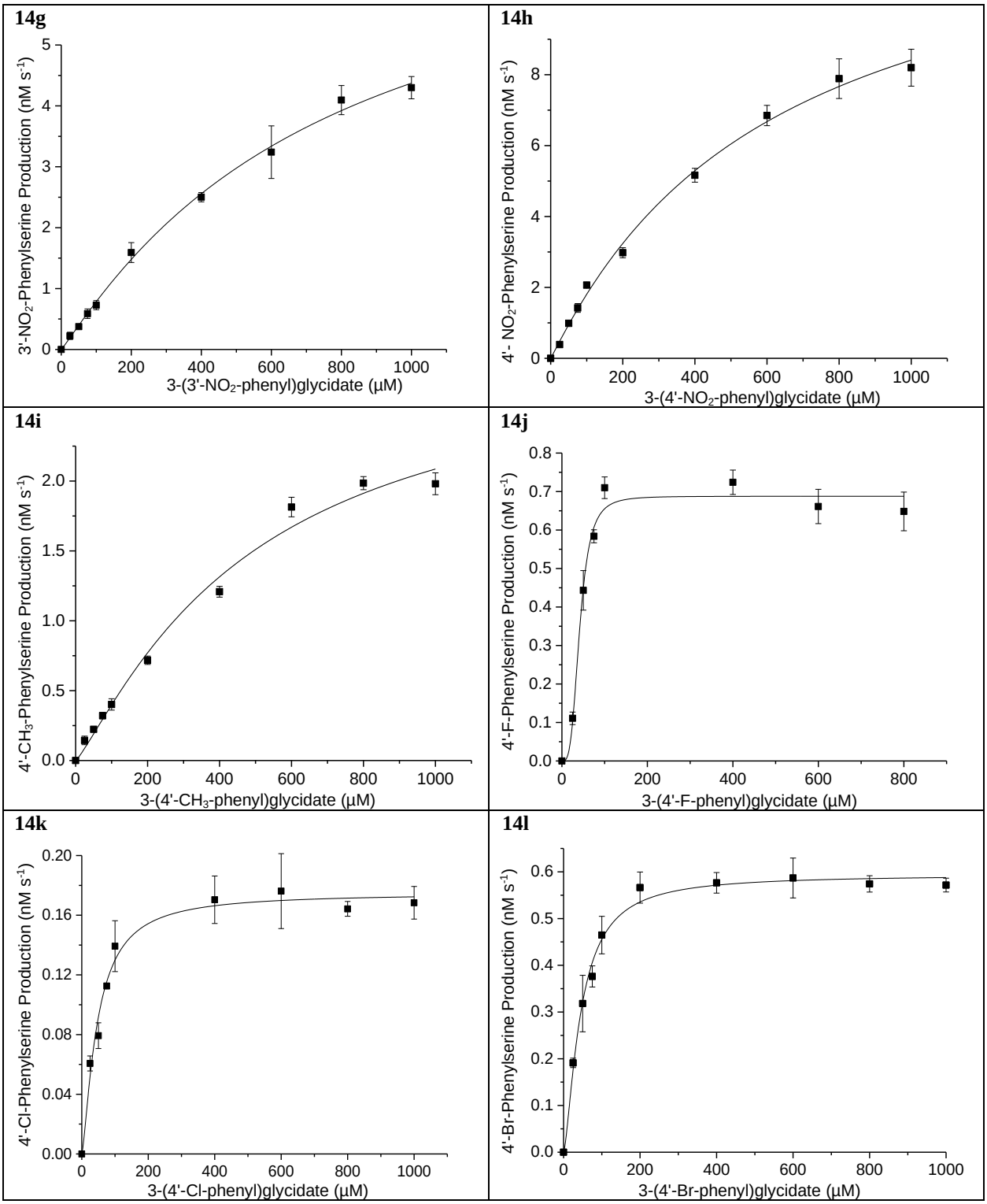

Figure. 2.65. Michaelis-Menten kinetics for the turnover of arylglycidate analogues (**14g**–**14l**) to their corresponding arylserines (**15g**–**15l**).

Michaelis-Menten Plots of *Tc*PAM Biocatalytic Conversion of Aryl*iso*serine Analogues.

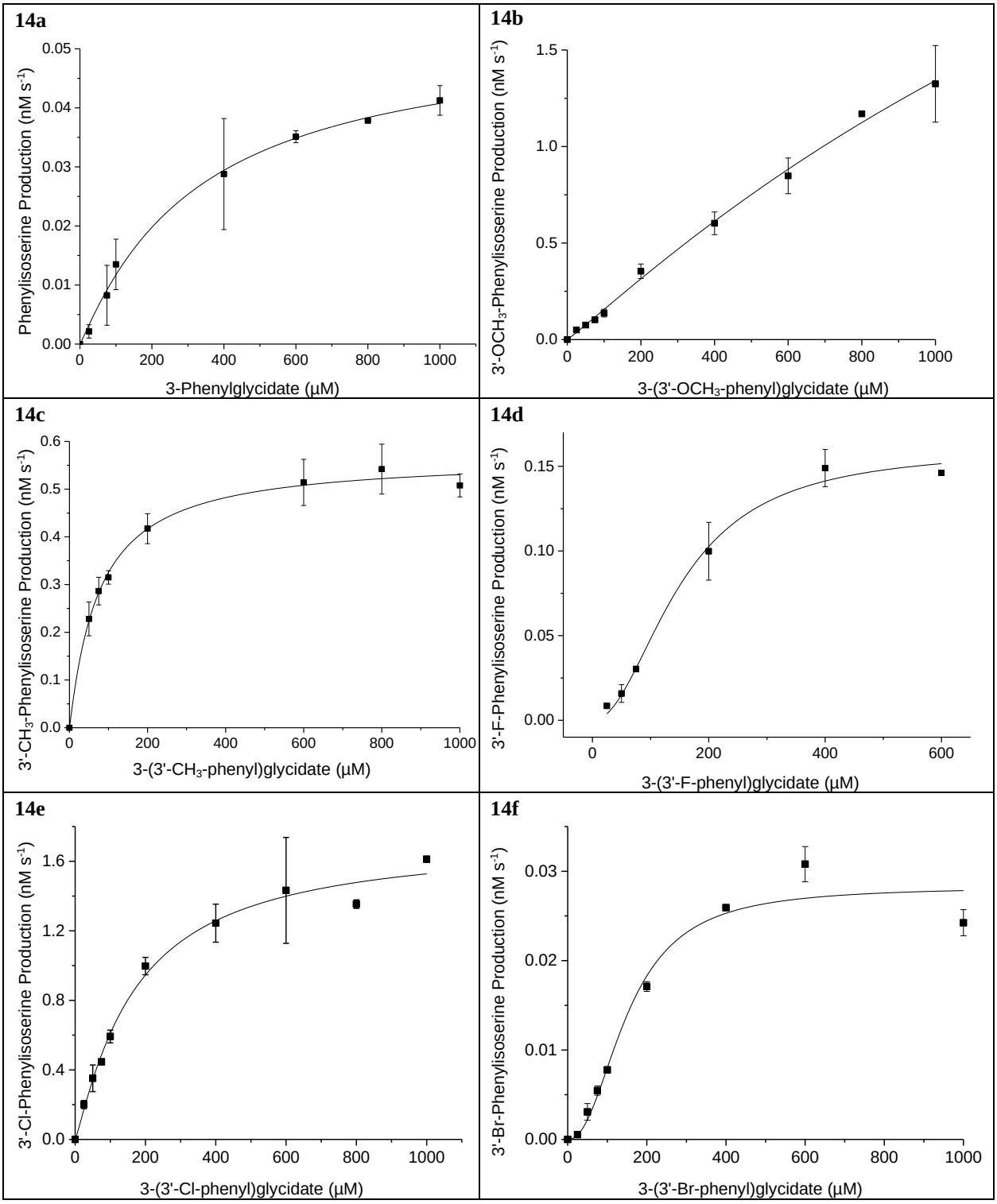

Figure. 2.66. Michaelis-Menten kinetics for the turnover of arylglycidate analogues (**14a**–**14f**) to their corresponding aryl*iso*serines (**16a**–**16f**).

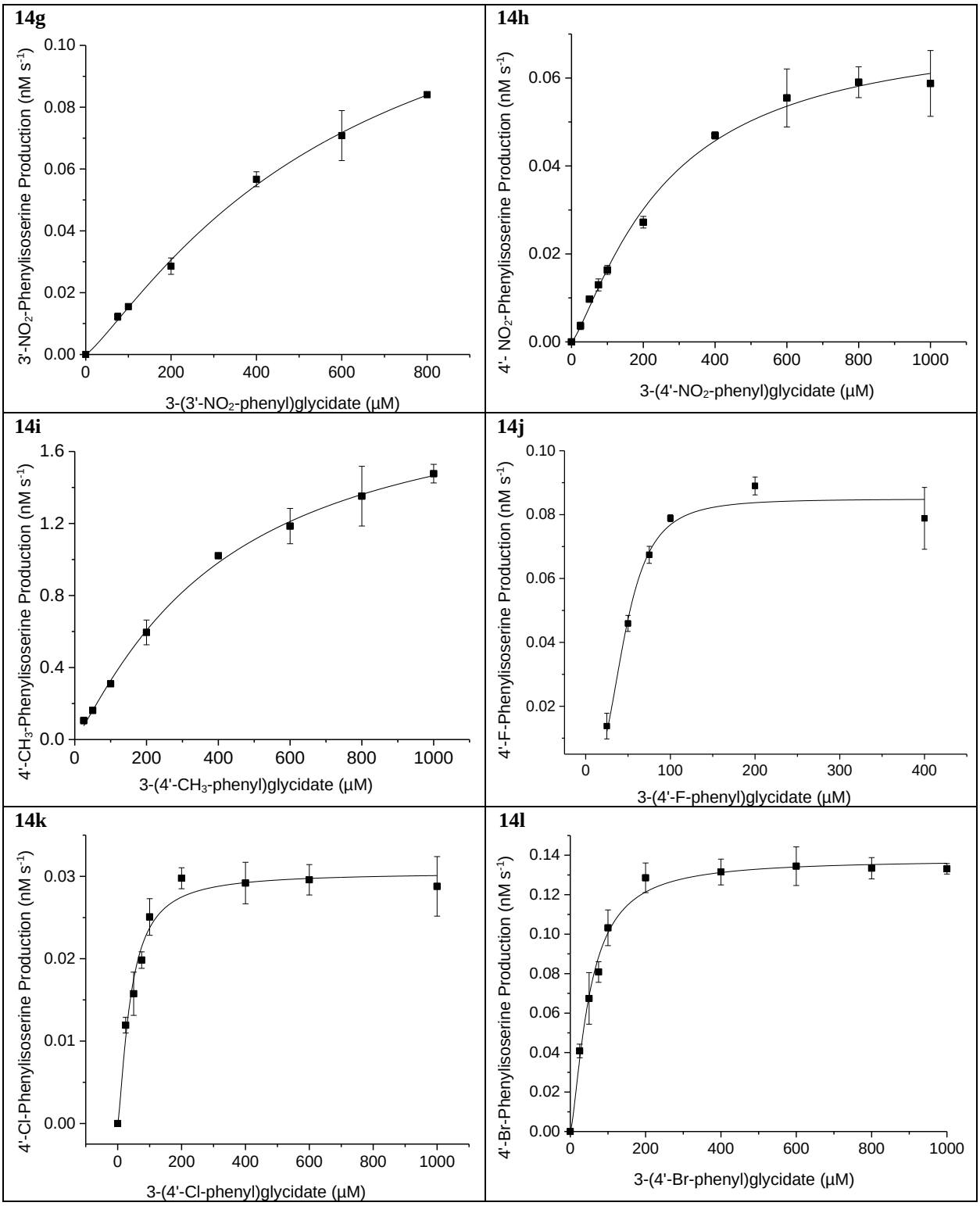

Figure. 2.67. Michaelis-Menten kinetics for the turnover of arylglycidate analogues (**14g**–**14l**) to their corresponding arylisoserines (**16g**–**16l**).

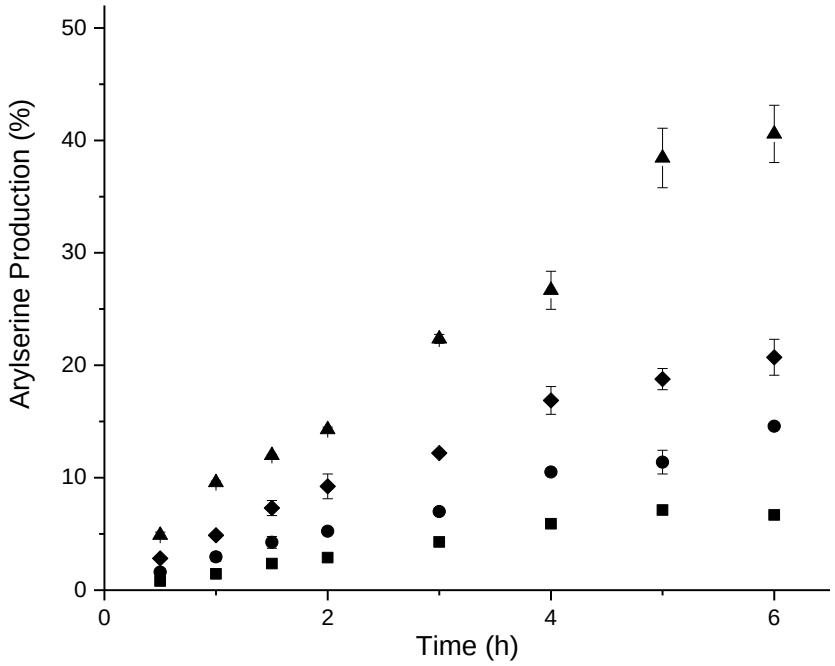

Figure. 2.68. The six-hour time course for the conversion of four representative 3-arylglycidate racemates [3-phenylglycidate (**14a**) (●), 3′-F- (**14d**) (♦), 3′-Cl- (**14e**) (▲), and 4′-Cl- (**14k**) (■) phenylglycidate (each at 400 µM)] to their corresponding arylserines in assays containing *Tc*PAM (100 µg/mL), and (2*S*)-styryl-α-alanine (1 mM) in 50 mM NaH_2PO_4/Na_2HPO_4 (pH 8.0), n = 3. Arylserine production is shown as a percentage relative to the initial epoxide substrate concentration. These example epoxides were turned over by *Tc*PAM from fastest (3'-Cl) to slowest (4'-Cl).

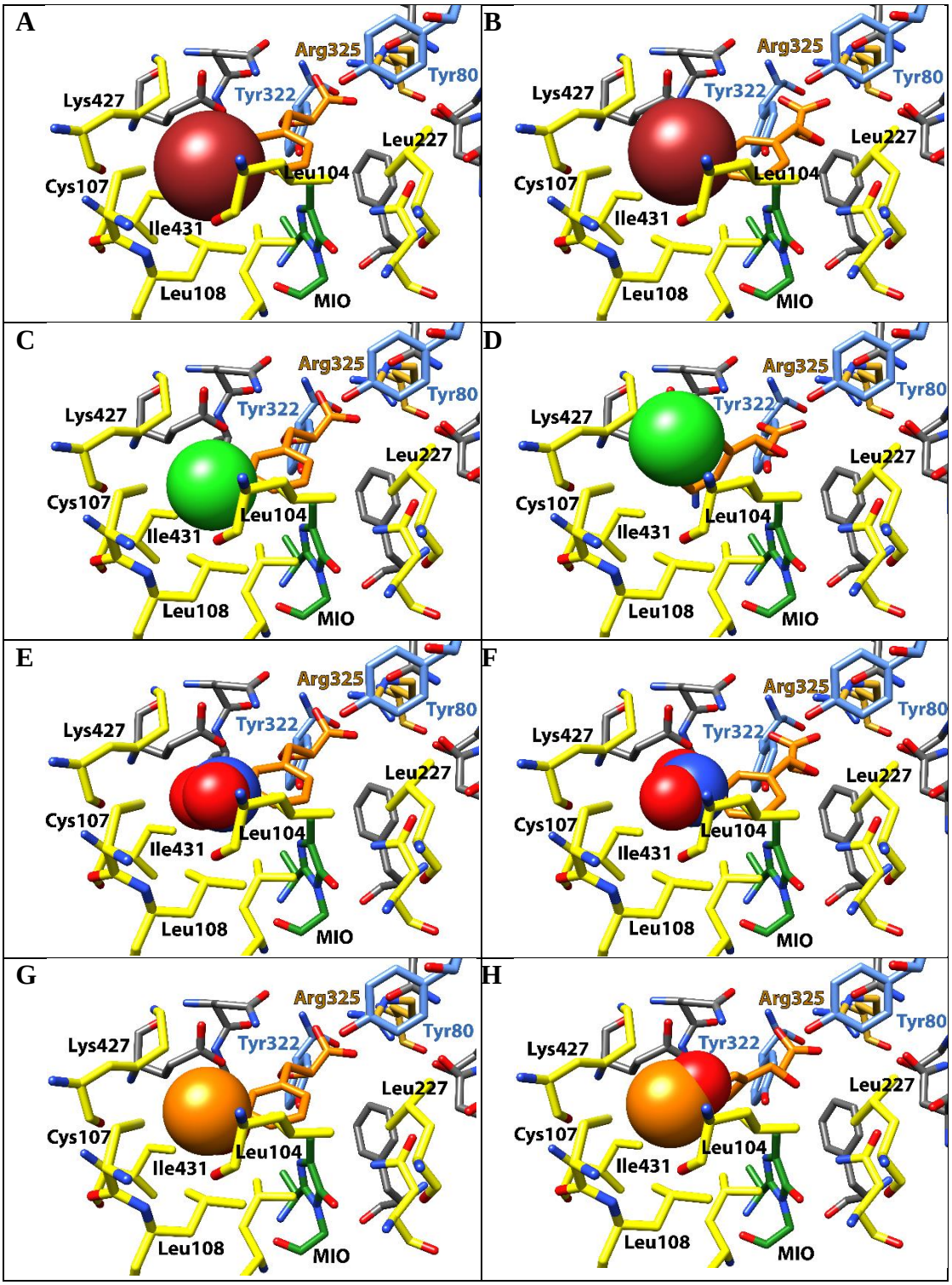

Figure. 2.69. Lowest energy binding poses are shown of A) (2*R*,3*S*)-**14f**; B) (2*S*,3*R*)-**14f**; C) (2*R*,3*S*)-**14e**; D) (2*S*,3*R*)-**14e**; E) (2*R*,3*S*)-**14g**; F) (2*S*,3*R*)-**14g**; G) (2*R*,3*S*)-**14b**; and H) (2*S*,3*R*)-**14b**.

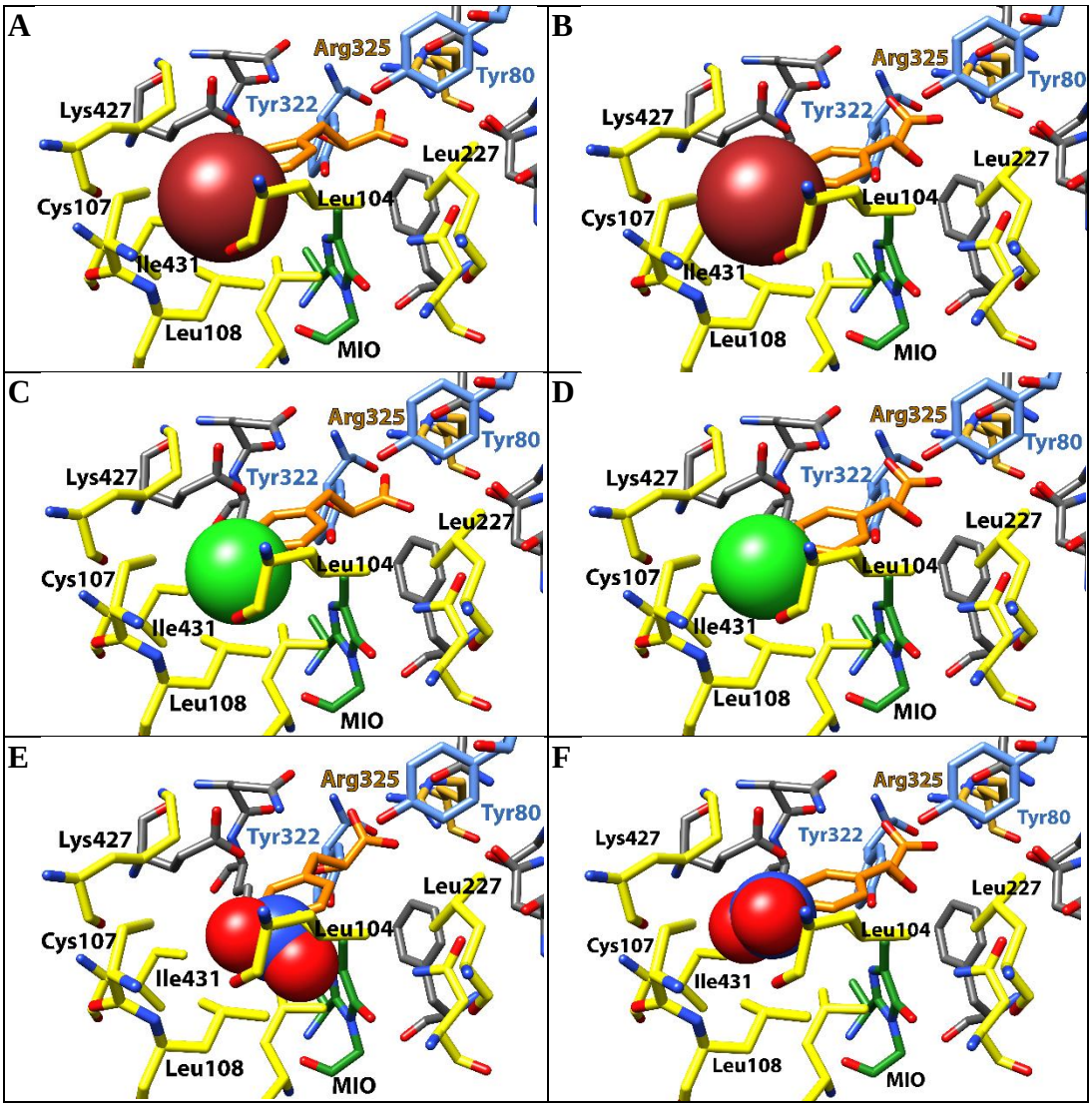

Figure. 2.70. Lowest energy binding poses are shown of A) (2*R*,3*S*)-**14l**; B) (2*S*,3*R*)-**14l**; C) (2*R*,3*S*)-**14k**; D) (2*S*,3*R*)-**14k**; E) (2*R*,3*S*)-**14h**; and F) (2*S*,3*R*)-**14h**.

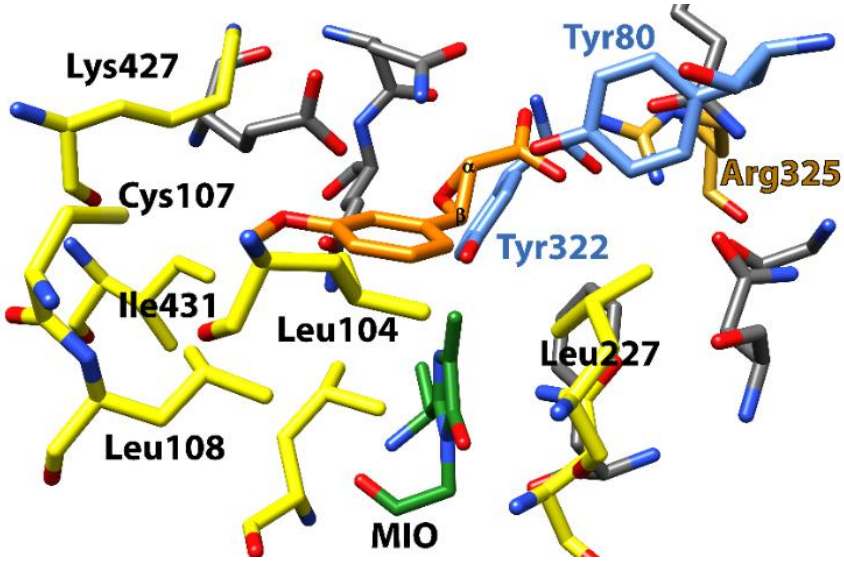

Figure. 2.71. Putative binding pose of (2*S*,3*R*)-3-(3'-OCH_3-phenyl)glycidate (**14b**) in a conformation aligned for NH_2-MIO attack at C_β (labeled 'β') to make the arylisoserine (**16b**). C_α is labeled with 'α' for reference.

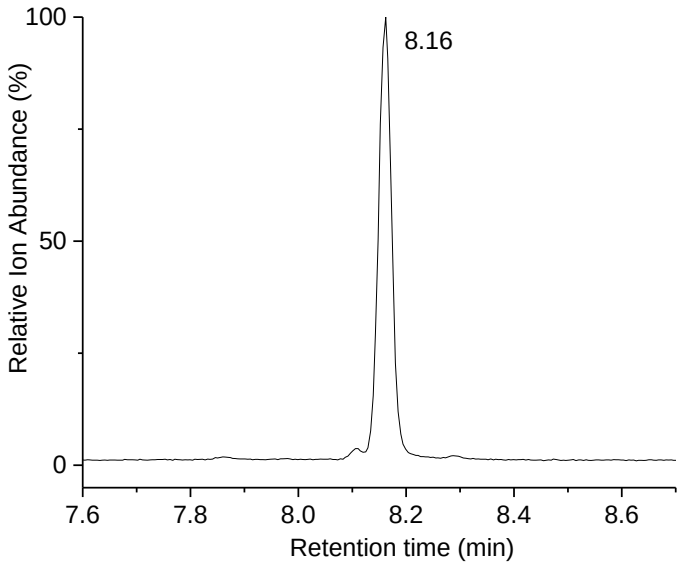

Figure. 2.72. GC/EI-MS extracted ion (*m*/*z* 106) chromatogram of authentic (2*R*,3*S*)-*syn*-phenylisoserine (**16a**) derivatized as its *O*-trimethylsilyl *N*-[(2*S*)-2-methylbutyryl] methyl ester (**18a**).

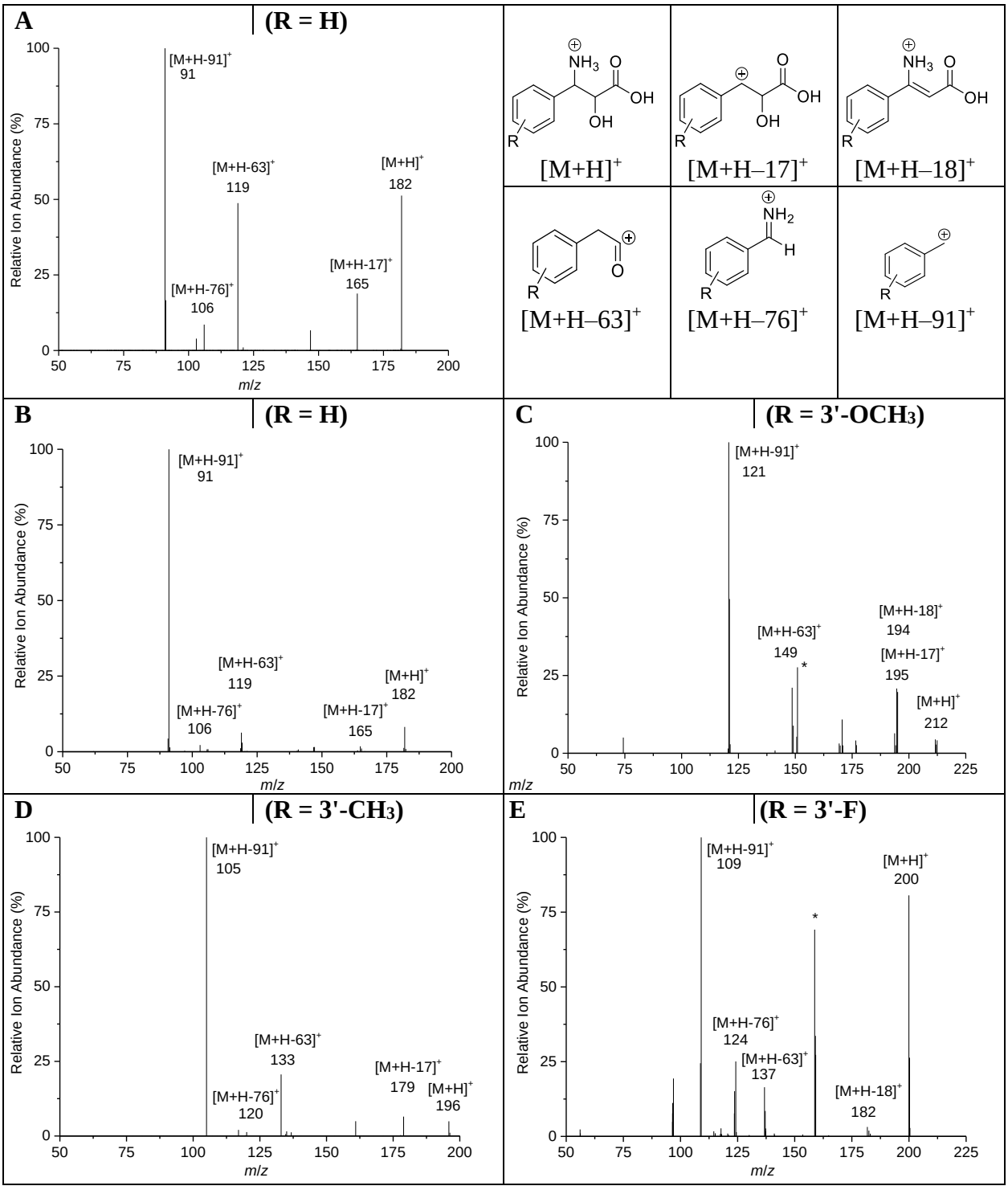

Figure. 2.73. LC-ESI-MS/MS spectra of A) authentic (2*R*,3*S*)-*syn*-phenylisoserine (**16a**) (structures of diagnostic fragment ions are shown and used to characterize the fragment ions of the biocatalyzed arylisoserine analogues (below). B) phenylisoserine (**16a**); C) 3'-OCH_3-phenylisoserine (**16b**); D) 3'-CH_3-phenylisoserine (**16c**); and E) 3'-F-phenylisoserine (**16d**) biocatalyzed by *Tc*PAM from the corresponding 3-arylglycidates.

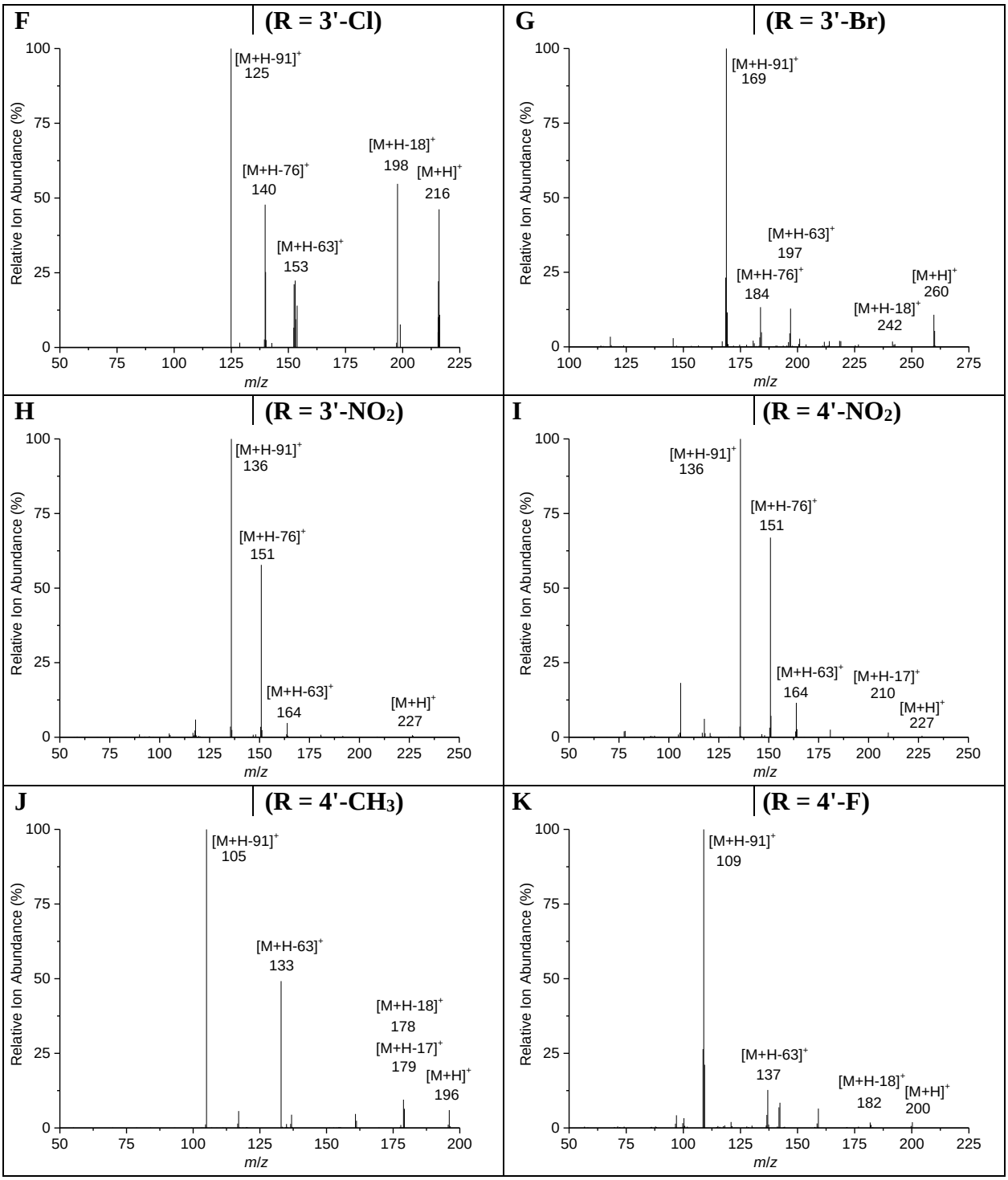

Figure. 2.74. LC-ESI-MS/MS spectra of F) 3'-Cl-phenylisoserine (**16e**); G) 3'-Br-phenylisoserine (**16f**); H) 3'-NO_2-phenylisoserine (**16g**); I) 4'-NO_2-phenylisoserine (**16h**); J) 4'-CH_3-phenylisoserine (**16i**); and K) 4'-F-phenylisoserine (**16j**) biocatalyzed by *Tc*PAM from the corresponding 3-arylglycidates.

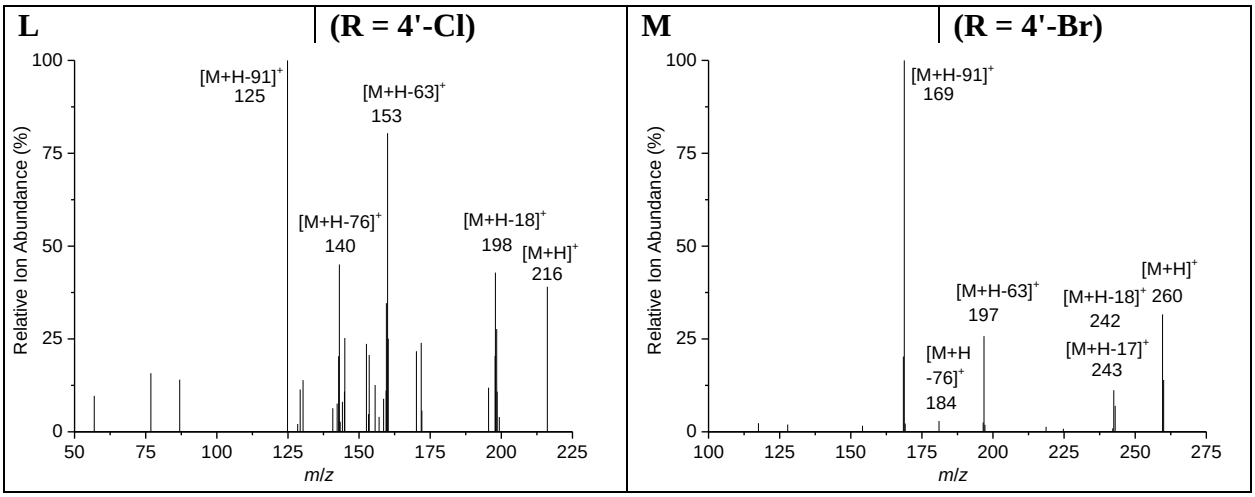

Figure. 2.75. LC-ESI-MS/MS spectra of L) 4'-Cl-phenylisoserine (**16k**) and M) 4'-Br-phenylisoserine (**16l**) biocatalyzed by *Tc*PAM from their corresponding 3-arylglycidates.

REFERENCES

REFERENCES

1. NC-IUBMB, and Webb, E. (1992) Classification and Nomenclature of Enzymes In *Enzyme Nomenclature*, pp 5-22, Academic Press, San Diego.

2. Cai, C. Z., Han, L. Y., Ji, Z. L., and Chen, Y. Z. (2004) Enzyme Family Classification by Support Vector Machines, *Proteins 55*, 66-76.

3. Wu, B., Szymański, W., Heberling, M. M., Feringa, B. L., and Janssen, D. B. (2011) Aminomutases: Mechanistic Diversity, Biotechnological Applications and Future Perspectives, *Trends Biotechnol. 29*, 352-362.

4. Turner, N. J., and Truppo, M. D. (2013) Biocatalysis Enters a New Era, *Curr. Opin. Chem. Biol. 17*, 212-214.

5. Lepore, B. W., Ruzicka, F. J., Frey, P. A., and Ringe, D. (2005) The X-Ray Crystal Structure of Lysine-2,3-Aminomutase From *Clostridium subterminale*, *Proc. Natl. Acad. Sci. USA 102*, 13819.

6. Baraniak, J., Moss, M. L., and Frey, P. A. (1989) Lysine 2,3-Aminomutase. Support for a Mechanism of Hydrogen Transfer Involving S-Adenosylmethionine, *J. Biol. Chem. 264*, 1357-1360.

7. Berkovitch, F., Behshad, E., Tang, K.-H., Enns, E. A., Frey, P. A., and Drennan, C. L. (2004) A Locking Mechanism Preventing Radical Damage in the Absence of Substrate, As Revealed by the X-Ray Structure of Lysine 5,6-Aminomutase, *Proc. Natl. Acad. Sci. USA 101*, 15870-15875.

8. Stadtman, T. C., and Renz, P. (1968) Anaerobic Degradation of Lysine: V. Some Properties of the Cobamide Coenzyme-Dependent β-Lysine Mutase of *Clostridium sticklandii*, *Arch. Biochem. Biophys. 125*, 226-239.

9. Sandala, G. M., Smith, D. M., and Radom, L. (2006) In Search of Radical Intermediates in the Reactions Catalyzed by Lysine 2,3-Aminomutase and Lysine 5,6-Aminomutase, *J. Am. Chem. Soc. 128*, 16004-16005.

10. Chang, C. H., and Frey, P. A. (2000) Cloning, Sequencing, Heterologous Expression, Purification, and Characterization of Adenosylcobalamin-Dependentd-Lysine 5,6-Aminomutase from *Clostridium sticklandii*, *J. Biol. Chem. 275*, 106-114.

11. Morley, C. G. D., and Stadtman, T. C. (1970) Fermentation of D-α-Lysine. Purification and Properties of an Adenosine Triphosphate Regulated B12-Coenzyme-Dependent D-α-Lysine Mutase Complex from *Clostridium sticklandii*, *Biochemistry 9*, 4890-4900.

12. Wolthers, K. R., Rigby, S. E. J., and Scrutton, N. S. (2008) Mechanism of Radical-Based Catalysis in the Reaction Catalyzed by Adenosylcobalamin-Dependent Ornithine 4,5-Aminomutase, *J. Biol. Chem. 283*, 34615-34625.

13. Tseng, C.-H., Yang, C.-H., Lin, H.-J., Wu, C., and Chen, H.-P. (2007) The S Subunit of D-Ornithine Aminomutase From *Clostridium sticklandii* Is Responsible for the Allosteric Regulation in D-α-Lysine Aminomutase, *FEMS Microbiol. Lett. 274*, 148-153.

14. Wanninayake, U., and Walker, K. D. (2013) A Bacterial Tyrosine Aminomutase Proceeds Through Retention or Inversion of Stereochemistry to Catalyze Its Isomerization Reaction, *J. Am. Chem. Soc. 135*, 11193-11204.

15. Christianson, C. V., Montavon, T. J., Van Lanen, S. G., Shen, B., and Bruner, S. D. (2007) The Structure of L-Tyrosine 2,3-Aminomutase from the C-1027 Enediyne Antitumor Antibiotic Biosynthetic Pathway, *Biochemistry 46*, 7205-7214.

16. Yan, J., Aboshi, T., Teraishi, M., Strickler, S. R., Spindel, J. E., Tung, C.-W., Takata, R., Matsumoto, F., Maesaka, Y., McCouch, S. R., Okumoto, Y., Mori, N., and Jander, G. (2015) The Tyrosine Aminomutase TAM1 Is Required for β-Tyrosine Biosynthesis in Rice, *The Plant Cell 27*, 1265-1278.

17. Montavon, T. J., Christianson, C. V., Festin, G. M., Shen, B., and Bruner, S. D. (2008) Design and Characterization of Mechanism-Based Inhibitors for the Tyrosine Aminomutase *Sg*TAM, *Bioorg. Med. Chem. Lett. 18*, 3099-3102.

18. Rachid, S., Krug, D., Weissman, K. J., and Müller, R. (2007) Biosynthesis of (*R*)-β-Tyrosine and Its Incorporation into the Highly Cytotoxic Chondramides Produced by *Chondromyces crocatus*, *J. Biol. Chem. 282*, 21810-21817.

19. Krug, D., and Müller, R. (2009) Discovery of Additional Members of the Tyrosine Aminomutase Enzyme Family and the Mutational Analysis of CmdF, *ChemBioChem 10*, 741-750.

20. Walter, T., King, Z., and Walker, K. D. (2016) A Tyrosine Aminomutase from Rice (*Oryza sativa*) Isomerizes (*S*)-α- to (*R*)-β-Tyrosine with Unique High Enantioselectivity and Retention of Configuration, *Biochemistry 55*, 1-4.

21. Poston, J. M. (1976) Leucine 2,3-Aminomutase, an Enzyme of Leucine Catabolism, *J. Biol. Chem. 251*, 1859-1863.

22. Poston, J. M. (1977) Leucine 2,3-Aminomutase: A Cobalamin-Dependent Enzyme Present in Bean Seedlings, *Science 195*, 301.

23. Tyacke, R. J., Contestabile, R., Grimm, B., Harwood, J. L., and John, R. A. (1995) Reactions of Glutamate Semialdehyde Aminotransferase (Glutamate-1-Semialdehyde 2,1 Aminomutase) With Vinyl and Acetylenic Substrate Analogues Analysed by Rapid Scanning Spectrophotometry, *Biochem. J 309 (Pt 1)*, 307-313.

24. Song, Y., Pu, H., Jiang, T., Zhang, L., and Ouyang, M. (2016) Crystal Structure of Glutamate-1-Semialdehyde-2,1-Aminomutase from *Arabidopsis thaliana*, *Acta Crystallogr F Struct Biol Commun 72*, 448-456.

25. Ruzicka, F. J., and Frey, P. A. (2007) Glutamate 2,3-Aminomutase: A New Member of the Radical SAM Superfamily of Enzymes, *Biochim. Biophys. Acta 1774*, 286-296.

26. Walker, K. D., and Floss, H. G. (1998) Detection of a Phenylalanine Aminomutase in Cell-Free Extracts of *Taxus brevifolia* and Preliminary Characterization of Its Reaction, *J. Am. Chem. Soc. 120*, 5333-5334.

27. Walker, K. D., Klettke, K., Akiyama, T., and Croteau, R. (2004) Cloning, Heterologous Expression, and Characterization of a Phenylalanine Aminomutase Involved in Taxol Biosynthesis, *J. Biol. Chem. 279*, 53947-53954.

28. Magarvey, N. A., Fortin, P. D., Thomas, P. M., Kelleher, N. L., and Walsh, C. T. (2008) Gatekeeping *versus* Promiscuity in the Early Stages of the Andrimid Biosynthetic Assembly Line, *ACS Chem. Biol. 3*, 542-554.

29. Strom, S., Wanninayake, U., Ratnayake, N. D., Walker, K. D., and Geiger, J. H. (2012) Insights into the Mechanistic Pathway of the *Pantoea agglomerans* Phenylalanine Aminomutase, *Angew. Chem. Int. Ed. 51*, 2898-2902.

30. Huang, S.-X., Lohman, J. R., Huang, T., and Shen, B. (2013) A New Member of the 4-Methylideneimidazole-5-One-Containing Aminomutase Family From the Enediyne Kedarcidin Biosynthetic Pathway, *Proc. Natl. Acad. Sci. U S A 110*, 8069-8074.

31. Christenson, S. D., Liu, W., Toney, M. D., and Shen, B. (2003) A Novel 4-Methylideneimidazole-5-one-Containing Tyrosine Aminomutase in Enediyne Antitumor Antibiotic C-1027 Biosynthesis, *J. Am. Chem. Soc. 125*, 6062-6063.

32. Wu, P. C., Kroening, T. A., White, P. J., and Kendrick, K. E. (1992) Purification of Histidase from *Streptomyces griseus* and Nucleotide Sequence of the hutH Structural Gene, *J. Bacteriol. 174*, 1647.

33. Xiang, L., and Moore, B. S. (2002) Inactivation, Complementation, and Heterologous Expression of encP, a Novel Bacterial Phenylalanine Ammonia-Lyase Gene, *J. Biol. Chem. 277*, 32505-32509.

34. Schwede, T. F., Rétey, J., and Schulz, G. E. (1999) Crystal Structure of Histidine Ammonia-Lyase Revealing a Novel Polypeptide Modification as the Catalytic Electrophile, *Biochemistry 38*, 5355-5361.

35. Silverman, R. B. (2002) Eliminations and Additions In *Organic Chemistry of Enzyme-Catalyzed Reactions* 2 ed., pp 424-428, Academic Press, San Diego.

36. Wickner, R. B. (1969) Dehydroalanine in Histidine Ammonia Lyase, *J. Biol. Chem. 244*, 6550-6552.

37. Hanson, K. R., and Havir, E. A. (1970) L-Phenylalanine Ammonia-Lyase: IV. Evidence That the Prosthetic Group Contains a Dehydroalanyl Residue and Mechanism of Action, *Arch. Biochem. Biophys. 141*, 1-17.

38. Jennewein, S., Wildung, M. R., Chau, M., Walker, K., and Croteau, R. (2004) Random Sequencing of an Induced *Taxus* Cell cDNA Library for Identification of Clones Involved in Taxol Biosynthesis, *Proc. Natl. Acad. Sci. U S A 101*, 9149.

39. Steele, C. L., Chen, Y., Dougherty, B. A., Hofstead, S., Lam, K. S., Li, W., and Xing, Z. (2003) U. S. Patent, AN 2003:633941.

40. Ratnayake, N. D., Wanninayake, U., Geiger, J. H., and Walker, K. D. (2011) Stereochemistry and Mechanism of a Microbial Phenylalanine Aminomutase, *J. Am. Chem. Soc. 133*, 8531-8533.

41. Van Lanen, S. G., Oh, T.-j., Liu, W., Wendt-Pienkowski, E., and Shen, B. (2007) Characterization of the Maduropeptin Biosynthetic Gene Cluster from *Actinomadura madurae* ATCC 39144 Supporting a Unifying Paradigm for Enediyne Biosynthesis, *J. Am. Chem. Soc. 129*, 13082-13094.

42. Mutatu, W., Klettke, K. L., Foster, C., and Walker, K. D. (2007) Unusual Mechanism for an Aminomutase Rearrangement: Retention of Configuration at the Migration Termini, *Biochemistry 46*, 9785-9794.

43. Christenson, S. D., Wu, W., Spies, M. A., Shen, B., and Toney, M. D. (2003) Kinetic Analysis of the 4-Methylideneimidazole-5-one-Containing Tyrosine Aminomutase in Enediyne Antitumor Antibiotic C-1027 Biosynthesis, *Biochemistry 42*, 12708-12718.

44. Turner, N. J. (2011) Ammonia Lyases and Aminomutases As Biocatalysts for the Synthesis of α-Amino and β-Amino Acids, *Curr. Opin. Chem. Biol. 15*, 234-240.

45. Cox, B. M., Bilsborrow, J. B., and Walker, K. D. (2009) Enhanced Conversion of Racemic α-Arylalanines to (*R*)-β-Arylalanines by Coupled Racemase/Aminomutase Catalysis, *J. Org. Chem. 74*, 6953-6959.

46. Verkuijl, B. J. V., Szymanski, W., Wu, B., Minnaard, A. J., Janssen, D. B., de Vries, J. G., and Feringa, B. L. (2010) Enantiomerically Pure β-Phenylalanine Analogues From α-β-Phenylalanine Mixtures in a Single Reactive Extraction Step, *Chem. Commun. 46*, 901-903.

47. Wu, B., Szymański, W., de Wildeman, S., Poelarends, G. J., Feringa, B. L., and Janssen, D. B. (2010) Efficient Tandem Biocatalytic Process for the Kinetic Resolution of Aromatic β-Amino Acids, *Adv. Synth. Catal. 352*, 1409-1412.

48. Shee, P. K., Ratnayake, N. D., Walter, T., Goethe, O., Onyeozili, E. N., and Walker, K. D. (2019) Exploring the Scope of an α/β-Aminomutase for the Amination of Cinnamate Epoxides to Arylserines and Arylisoserines, *ACS Catal. 9*, 7418-7430.

49. Szymanski, W., Wu, B., Weiner, B., de Wildeman, S., Feringa, B. L., and Janssen, D. B. (2009) Phenylalanine Aminomutase-Catalyzed Addition of Ammonia to Substituted Cinnamic Acids: A Route to Enantiopure α- and β-Amino Acids, *J. Org. Chem. 74*, 9152-9157.

50. Wanninayake, U., Deporre, Y., Ondari, M., and Walker, K. D. (2011) (*S*)-Styryl-α-Alanine Used to Probe the Intermolecular Mechanism of an Intramolecular MIO-Aminomutase, *Biochemistry 50,* 10082-10090.

51. Wanninayake, U., and Walker, K. D. (2012) Assessing the Deamination Rate of a Covalent Aminomutase Adduct by Burst Phase Analysis, *Biochemistry 51*, 5226-5228.

52. Wu, B., Szymanski, W., Wietzes, P., de Wildeman, S., Poelarends, G. J., Feringa, B. L., and Janssen, D. B. (2009) Enzymatic Synthesis of Enantiopure α- and β-Amino Acids by Phenylalanine Aminomutase-Catalysed Amination of Cinnamic Acid Derivatives, *ChemBioChem 10,* 338-344.

53. Wu, B., Szymański, W., Wybenga, G. G., Heberling, M. M., Bartsch, S., de Wildeman, S., Poelarends, G. J., Feringa, B. L., Dijkstra, B. W., and Janssen, D. B. (2012) Mechanism-Inspired Engineering of Phenylalanine Aminomutase for Enhanced β-Regioselective Asymmetric Amination of Cinnamates, *Angew. Chem. Int. Ed. 51,* 482-486.

54. Li, R., Wijma, H. J., Song, L., Cui, Y., Otzen, M., Tian, Y. e., Du, J., Li, T., Niu, D., Chen, Y., Feng, J., Han, J., Chen, H., Tao, Y., Janssen, D. B., and Wu, B. (2018) Computational Redesign of Enzymes for Regio- and Enantioselective Hydroamination, *Nat. Chem. Biol. 14*, 664-670.

55. Blaskovich, M. A. T. (2016) Unusual Amino Acids in Medicinal Chemistry, *J. Med. Chem. 59*, 10807-10836.

56. Boville, C. E., Scheele, R. A., Koch, P., Brinkmann-Chen, S., Buller, A. R., and Arnold, F. H. (2018) Engineered Biosynthesis of β-Alkyl Tryptophan Analogues, *Angew. Chem. Int. Ed. 57*, 14764-14768.

57. Robinson, B. S., Riccardi, K. A., Gong, Y. F., Guo, Q., Stock, D. A., Blair, W. S., Terry, B. J., Deminie, C. A., Djang, F., Colonno, R. J., and Lin, P. F. (2000) BMS-232632, a Highly Potent Human Immunodeficiency Virus Protease Inhibitor That Can Be Used in Combination With Other Available Antiretroviral Agents, *Antimicrob. Agents Chemother. 44*, 2093-2099.

58. Qian, W.-J., Park, J.-E., Lee, K. S., and Burke, T. R. (2012) Non-Proteinogenic Amino Acids in the pThr-2 Position of a Pentamer Peptide That Confer High Binding Affinity for the Polo Box Domain (PBD) of Polo-Like Kinase 1 (Plk1), *Bioorg. Med. Chem. Lett. 22*, 7306-7308.

59. Zhou, H., Xie, X., and Tang, Y. (2008) Engineering Natural Products using Combinatorial Biosynthesis and Biocatalysis, *Curr. Opin. Biotechnol. 19*, 590-596.

60. Yuan, L.-F., Li, G.-D., Ren, X.-J., Nian, H., Li, X.-R., and Zhang, X.-M. (2015) Rapamycin Ameliorates Experimental Autoimmune Uveoretinitis by Inhibiting Th1/Th2/Th17 Cells and Upregulating CD4+CD25+ Foxp3 Regulatory T Cells, *Int J Ophthalmol 8*, 659-664.

61. Luca, G., Rossella De, M., and Lucia, C. (2010) Chemical Modifications Designed to Improve Peptide Stability: Incorporation of Non-Natural Amino Acids, Pseudo-Peptide Bonds, and Cyclization, *Curr. Pharm. Des. 16*, 3185-3203.

62. Shen, Z., Lv, C., and Zeng, S. (2016) Significance and Challenges of Stereoselectivity Assessing methods in Drug Metabolism, *Journal of Pharmaceutical Analysis 6*, 1-10.

63. Cao, M., Feng, Y., Zhang, Y., Kang, W., Lian, K., and Ai, L. (2018) Studies on the Metabolism and Degradation of Vancomycin in Simulated *in vitro* and Aquatic Environment by UHPLC-Triple-TOF-MS/MS, *Sci. Rep. 8*, 15471-15471.

64. Evans, D. A., Wood, M. R., Trotter, B. W., Richardson, T. I., Barrow, J. C., and Katz, J. L. (1998) Total Syntheses of Vancomycin and Eremomycin Aglycons, *Angew. Chem. Int. Ed. 37*, 2700-2704.

65. Rao, A. V. R., Gurjar, M. K., Reddy, K. L., and Rao, A. S. (1995) Studies Directed Toward the Synthesis of Vancomycin and Related Cyclic Peptides, *Chem. Rev. 95*, 2135-2167.

66. Hughes, C. S., Longo, E., Phillips-Jones, M. K., and Hussain, R. (2017) Characterisation of the Selective Binding of Antibiotics Vancomycin and Teicoplanin by the VanS Receptor Regulating Type a Vancomycin Resistance in the Enterococci, *Biochim. Biophys. Acta Gen. Subj. 1861*, 1951-1959.

67. Fraunfelder, F. W., and Fraunfelder, F. T. (2013) Restricting Topical Ocular Chloramphenicol Eye Drop Use in the United States. Did We Overreact?, *Am. J. Ophthalmol. 156*, 420-422.

68. Goldstein, D. S. (2006) L-Dihydroxyphenylserine (L-DOPS): A Norepinephrine Prodrug, *Cardiovasc. Drug Rev. 24*, 189-203.

69. Maruyama, W., Naoi, M., and Narabayashi, H. (1996) The Metabolism of L-DOPA and L-*threo*-3,4-Dihydroxyphenylserine and Their Effects on Monoamines in the Human Brain: Analysis of the Intraventricular Fluid From Parkinsonian Patients, *J. Neurol. Sci. 139*, 141-148.

70. Milanowski, D. J., Gustafson, K. R., Rashid, M. A., Pannell, L. K., McMahon, J. B., and Boyd, M. R. (2004) Gymnangiamide, a Cytotoxic Pentapeptide from the Marine Hydroid *Gymnangium regae*, *J. Org. Chem. 69*, 3036-3042.

71. Zhang, Y., Farrants, H., and Li, X. (2014) Adding a Functional Handle to Nature's Building Blocks: The Asymmetric Synthesis of β-Hydroxy-α-Amino Acids, *Chem. Asian J. 9*, 1752-1764.

72. Davies, S. G., Fletcher, A. M., Frost, A. B., Roberts, P. M., and Thomson, J. E. (2014) Trading N and O. Part 2: Exploiting Aziridinium Intermediates for the Synthesis of β-Hydroxy-α-Amino Acids, *Tetrahedron 70*, 5849-5862.

73. Crich, D., and Banerjee, A. (2006) Expedient Synthesis of *syn*-β-Hydroxy-α-Amino Acid Derivatives: Phenylalanine, Tyrosine, Histidine and Tryptophan, *J. Org. Chem. 71*, 7106-7109.

74. Straukas, J., Dirvianskytė, N., Astrauskas, V., and Butkus, E. (2002) Synthesis of N-Arylsulfonyl DL-Phenylserine Derivatives Exhibiting Anti-Inflammatory Activity in Experimental Studies, *Il Farmaco 57*, 803-808.

75. Zhang, Y., Xu, C., Lam, H. Y., Lee, C. L., and Li, X. (2013) Protein Chemical Synthesis by Serine and Threonine Ligation, *Proc. Natl. Acad. Sci. U S A 110*, 6657.

76. Leblond, B., Beausoleil, E., Taverne, T., and Donello John, E. (2006) 3-Heterocyclyl-3-Hydroxy-2-Amino-Propionic Acid Amides and Related Compounds Having Analgesic and/or Immunostimulant Activity, ALLERGAN, INC, EP20060719438.

77. Donello John, E., Schweighoffer Fabien, J., and Leblond, B. (2007) Methods for Treating Chronic Pain Using 3-Aryl-3-Hydroxy-2-Amino-Propionic Acid Amides, 3-Heteroaryl-3-Hydroxy-2-Amino-Propionic Acid Amides and Related Compounds, ALLERGAN, INC, WO2007US73806.

78. Ambrus, G. F., Kurjan, K. C., Zanon, J., Libralon, G., and Faveri, C. D. (2015) (−)-(2R,3S)-2-Amino-3-Hydroxy-3-Pyridin-4-yl-1-Pyrrolidin-1-yl-Propan-1-one (L)-(+) Tartrate Salt, Its Method of Production and Use,

79. Schmidt, M. A., Reiff, E. A., Qian, X., Hang, C., Truc, V. C., Natalie, K. J., Wang, C., Albrecht, J., Lee, A. G., Lo, E. T., Guo, Z., Goswami, A., Goldberg, S., Pesti, J., and Rossano, L. T. (2015) Development of a Two-Step, Enantioselective Synthesis of an Amino Alcohol Drug Candidate, *Org. Process Res. Dev. 19*, 1317-1322.

80. Umezawa, H., Aoyagi, T., Suda, H., Hamada, M., and Takeuchi, T. (1976) Bestatin, an Inhibitor of Aminopeptidase B, Produced by Actinomycetes, *J. Antibiot. (Tokyo) 29*, 97-99.

81. Hettinger, T. P., and Craig, L. C. (1970) Edeine. IV. Structures of the Antibiotic Peptides Edeines A1 and B1, *Biochemistry 9*, 1224-1232.

82. Heaney-Kieras, J., and Kurylo-Borowska, Z. (1980) Tatumine, a Peptide from *Bacillus brevis* Vm4-572-403, *J. Antibiot. (Tokyo) 33*, 359-363.

83. Okino, T., Matsuda, H., Murakami, M., and Yamaguchi, K. (1993) Microginin, an Angiotensin-Converting Enzyme Inhibitor from the Blue-Green Alga *Microcystis aeruginosa*, *Tetrahedron Lett. 34*, 501-504.

84. Warmerdam, E. G. J. C., van Rijn, R. D., Brussee, J., Kruse, C. G., and Gen, A. v. d. (1996) Synthesis of α-Hydroxy-β-amino acids from Chiral Cyanohydrins, *Tetrahedron Asymmetry 7*, 1723-1732.

85. Nozaki, K., Sato, N., and Takaya, H. (1993) Enantioselective Synthesis of L- and D-Isoserine via Asymmetric Hydrogenation of Methyl N-phthaloyl-3-amino-2-oxopropanoate, *Tetrahedron Asymmetry 4*, 2179-2182.

86. Wolf, J.-P., and Pfander, H. (1987) Synthese von 'D-Isothreonin' und 'L-Alloisothreonin' aus L-Alanin, *Helv. Chim. Acta 70*, 116-120.

87. Bannage, M. E., Burke, A. J., Davies, S. G., and Goodwin, C. J. (1994) Asymmetric Synthesis of (2*S*,3*R*)-3-Amino-2-hydroxydecanoic acid: The Unknown Amino Acid Component of Microginin, *Tetrahedron Asymmetry 5*, 203-206.

88. Herranz, R., Castro-Pichel, J., Vinuesa, S., and Garcia-Lopez, M. T. (1990) An Improved One-pot Method for the Stereoselective Synthesis of the (2*S*,3*R*)-3-Amino-2-hydroxy acids: Key Intermediates for Bestatin and Amastatin, *J. Org. Chem. 55*, 2232-2234.

89. Davis, F. A., Reddy, R. T., and Reddy, R. E. (1992) Asymmetric Synthesis of Sulfinimines: Applications to the Synthesis of Nonracemic β-Amino acids and α-Hydroxyl-β-amino acids, *J. Org. Chem. 57*, 6387-6389.

90. Hasegawa, K., Shimada, M., Takeuchi, S., Fujiwara, H., Imai, Y., Iwasa, N., Wada, S., Eguchi, H., Oishi, T., Sugiyama, T., Suzuki, M., Nishiyama, M., and Fujiwara, K. (2020) A Phase 2 Study of Intraperitoneal Carboplatin Plus Intravenous Dose-Dense Paclitaxel in Front-Line Treatment of Suboptimal Residual Ovarian Cancer, *Br. J. Cancer 122*, 766-770.

91. Ozols, R. F., Bundy, B. N., Greer, B. E., Fowler, J. M., Clarke-Pearson, D., Burger, R. A., Mannel, R. S., DeGeest, K., Hartenbach, E. M., and Baergen, R. (2003) Phase III Trial of Carboplatin and Paclitaxel Compared With Cisplatin and Paclitaxel in Patients With Optimally Resected Stage III Ovarian Cancer: A Gynecologic Oncology Group Study, *J. Clin. Oncol. 21*, 3194-3200.

92. Komiyama, S., Kato, K., Inokuchi, Y., Takano, H., Matsumoto, T., Hongo, A., Asai-Sato, M., Arakawa, A., Kamiura, S., Tabata, T., Takeshima, N., and Sugiyama, T. (2019) Bevacizumab Combined With Platinum–Taxane Chemotherapy As First-Line Treatment for Advanced Ovarian Cancer: A Prospective Observational Study of Safety and Efficacy in Japanese Patients (JGOG3022 Trial), *Int. J. Clin. Oncol. 24*, 103-114.

93. Raab, M., Sanhaji, M., Zhou, S., Rödel, F., El-Balat, A., Becker, S., and Strebhardt, K. (2019) Blocking Mitotic Exit of Ovarian Cancer Cells by Pharmaceutical Inhibition of the Anaphase-Promoting Complex Reduces Chromosomal Instability, *Neoplasia 21*, 363-375.

94. Slamon, D. J., Leyland-Jones, B., Shak, S., Fuchs, H., Paton, V., Bajamonde, A., Fleming, T., Eiermann, W., Wolter, J., Pegram, M., Baselga, J., and Norton, L. (2001) Use of

Chemotherapy Plus a Monoclonal Antibody Against HER2 for Metastatic Breast Cancer That Overexpresses HER2, *New Engl. J. Med. 344*, 783-792.

95. Miller, K., Wang, M., Gralow, J., Dickler, M., Cobleigh, M., Perez, E. A., Shenkier, T., Cella, D., and Davidson, N. E. (2007) Paclitaxel Plus Bevacizumab versus Paclitaxel Alone for Metastatic Breast Cancer, *New Engl. J. Med. 357*, 2666-2676.

96. Zhang, L., Wu, C., Mu, S., Xue, W., and Ma, D. (2019) A Chemotherapeutic Self-Sensibilized Drug Carrier Delivering Paclitaxel for the Enhanced Chemotherapy to Human Breast MDA-MB-231 Cells, *Colloids Surf. B. Biointerfaces 181*, 902-909.

97. Takada, K., Kashiwagi, S., Goto, W., Asano, Y., Morisaki, T., Fujita, H., Takashima, T., Ohsawa, M., Hirakawa, K., and Ohira, M. (2018) Analysis of HER Family (HER1-4) Expression as a Biomarker in Combination Therapy with Pertuzumab, Trastuzumab and Docetaxel for Advanced HER2-positive Breast Cancer, *Anticancer Res. 38*, 2285-2294.

98. Montero, A., Fossella, F., Hortobagyi, G., and Valero, V. (2005) Docetaxel for Treatment of Solid Tumours: A Systematic Review of Clinical Data, *Lancet Oncol. 6*, 229-239.

99. Kwon, E. D., Drake, C. G., Scher, H. I., Fizazi, K., Bossi, A., van den Eertwegh, A. J. M., Krainer, M., Houede, N., Santos, R., Mahammedi, H., Ng, S., Maio, M., Franke, F. A., Sundar, S., Agarwal, N., Bergman, A. M., Ciuleanu, T. E., Korbenfeld, E., Sengeløv, L., Hansen, S., Logothetis, C., Beer, T. M., McHenry, M. B., Gagnier, P., Liu, D., and Gerritsen, W. R. (2014) Ipilimumab Versus Placebo After Radiotherapy in Patients With Metastatic Castration-Resistant Prostate Cancer That Had Progressed After Docetaxel Chemotherapy (CA184-043): A Multicentre, Randomised, Double-Blind, Phase 3 Trial, *The Lancet Oncology 15*, 700-712.

100. Yared J, and K., T. (2012) Update on Taxane Development: New Analogs and New Formulations, *Drug Des. Devel. Ther. 6*, 371-384.

101. de Bono, J. S., Oudard, S., Ozguroglu, M., Hansen, S., Machiels, J.-P., Kocak, I., Gravis, G., Bodrogi, I., Mackenzie, M. J., Shen, L., Roessner, M., Gupta, S., and Sartor, A. O. (2010) Prednisone Plus Cabazitaxel or Mitoxantrone for Metastatic Castration-Resistant Prostate Cancer Progressing After Docetaxel Treatment: A Randomised Open-Label Trial, *The Lancet 376*, 1147-1154.

102. Lin, J., Den, R. B., Greenspan, J., Showalter, T. N., Hoffman-Censits, J. H., Lallas, C. D., Trabulsi, E. J., Gomella, L. G., Hurwitz, M. D., Leiby, B., Dicker, A. P., and Kelly, W. K. (2020) Phase I Trial of Weekly Cabazitaxel with Concurrent Intensity Modulated Radiation and Androgen Deprivation Therapy for the Treatment of High-Risk Prostate Cancer, *International Journal of Radiation Oncology*Biology*Physics 106*, 939-947.

103. Karantanos, T., Corn, P. G., and Thompson, T. C. (2013) Prostate Cancer Progression After Androgen Deprivation Therapy: Mechanisms of Castrate Resistance and Novel Therapeutic Approaches, *Oncogene 32*, 5501-5511.

104. Miranda, I. L., Lopes, Í. K. B., Diaz, M. A. N., and Diaz, G. (2016) Synthesis Approaches to (−)-Cytoxazone, a Novel Cytokine Modulator, and Related Structures, *Molecules 21*, 1176.

105. Kakeya, H., Morishita, M., Koshino, H., Morita, T.-i., Kobayashi, K., and Osada, H. (1999) Cytoxazone: A Novel Cytokine Modulator Containing a 2-Oxazolidinone Ring Produced by *Streptomyces sp.*, *The Journal of Organic Chemistry 64*, 1052-1053.

106. Krawczyk, E., Kniotek, M., Nowaczyk, M., Dzieciatkowski, T., Przybylski, M., Majewska, A., and Luczak, M. (2006) N-Acetylphenylisoserinates of Lactarius Sesquiterpenoid Alcohols - Cytotoxic, Antiviral, Antiproliferative and Immunotropic Activities *in vitro*, *Planta Med. 72*, 615-620.

107. Kopczacki, P., Gumułka, M., Masnyk, M., Grabarczyk, H., Nowak, G., and Daniewski, W. M. (2001) Synthesis and Antifeedant Properties of N-Benzoylphenylisoserinates of *Lactarius* Sesquiterpenoid Alcohols, *Phytochemistry 58*, 775-787.

108. Fan, S., Liu, S., Zhang, H., Liu, Y., Yang, Y., and Jin, L. (2014) Biocatalytic Synthesis of Enantiopure β-Methoxy-β-Arylalanine Derivatives, *Eur. J. Org. Chem. 2014*, 5591-5597.

109. Duckers, N., Baer, K., Simon, S., Groger, H., and Hummel, W. (2010) Threonine Aldolases-Screening, Properties and Applications in the Synthesis of Non-Proteinogenic β-Hydroxy-α-Amino Acids, *Appl. Microbiol. Biotechnol. 88*, 409-424.

110. Hernandez-Juan, F. A., Richardson, R. D., and Dixon, D. J. (2006) A Stereoselective Oxy-Michael Route to Protected β-Aryl-β-Hydroxy-α-Amino Acids, *Synlett 2006*, 2673-2675.

111. Guanti, G., Banfi, L., and Narisano, E. (1988) Enantiospecific and Diastereoselective Synthesis of *anti*-α-Hydrazino- and α-Amino-β-Hydroxyacids Through "Electrophilic Amination" of β-Hydroxyesters, *Tetrahedron 44*, 5553-5562.

112. Li, G., Chang, H.-T., and Sharpless, K. B. (1996) Catalytic Asymmetric Aminohydroxylation (AA) of Olefins, *Angew. Chem. Int. Ed. Engl. 35*, 451-454.

113. Schollkopf, U. (1983) Asymmetric Syntheses of Amino Acids via Metalated Bis-Lactim Ethers of 2,5-Diketopiperazines, In *Pure Appl. Chem.*, p 1799.

114. Challener, C. A. (2016) Going Green with Biocatalysis, *Pharm. Technol. 40*, 24-25.

115. Challener, C. A. (2014) Synthetic Biology: The Next Frontier in Chiral Chemistry for API Synthesis, *Pharm. Technol. 38*.

116. Blamey, J. M., Fischer, F., Meyer, H.-P., Sarmiento, F., and Zinn, M. (2017) Chapter 14 - Enzymatic Biocatalysis in Chemical Transformations: A Promising and Emerging Field in Green Chemistry Practice In *Biotechnology of Microbial Enzymes* (Brahmachari, G., Ed.), pp 347-403, Academic Press.

117. Williams, G., and Hall, M., (Eds.) (2018) *Modern Biocatalysis: Advances Towards Synthetic Biological Systems*, The Royal Society of Chemistry, London, United Kingdom.

118. Zawodny, W., Montgomery, S. L., Marshall, J. R., Finnigan, J. D., Turner, N. J., and Clayden, J. (2018) Chemoenzymatic Synthesis of Substituted Azepanes by Sequential Biocatalytic Reduction and Organolithium-Mediated Rearrangement, *J. Am. Chem. Soc. 140*, 17872-17877.

119. Wen, W., Chen, L., Luo, M.-J., Zhang, Y., Chen, Y.-C., Ouyang, Q., and Guo, Q.-X. (2018) Chiral Aldehyde Catalysis for the Catalytic Asymmetric Activation of Glycine Esters, *J. Am. Chem. Soc. 140*, 9774-9780.

120. The Cahn-Ingold-Prelog (CIP) (*R*,*S*) convention is use here instead of the older D/L conventions to assign the absolute configuration at the α-carbon of the β-hydroxy α-amino acids. CIP rules are used also to describe the product selectivity of a TA based on the stereochemistry of the α-carbon. The syn/anti are used instead of *threo*/*erythro*-diastereomeric descriptors, respectively, to designate the relative stereochemistry at the α- and β-carbons in the zigzag configuration.

121. Baer, K., Dückers, N., Rosenbaum, T., Leggewie, C., Simon, S., Kraußer, M., Oßwald, S., Hummel, W., and Gröger, H. (2011) A Study Towards Efficient L-Threonine Aldolase-Catalyzed Enantio- and Diastereoselective Aldol Reactions of Glycine With Substituted Benzaldehydes: Biocatalyst Production and Process Development, *Tetrahedron Asymmetry 22*, 925-928.

122. Liu, J. Q., Odani, M., Yasuoka, T., Dairi, T., Itoh, N., Kataoka, M., Shimizu, S., and Yamada, H. (2000) Gene Cloning and Overproduction of Low-Specificity D-Threonine Aldolase From *Alcaligenes xylosoxidans* and Its Application for Production of a Key Intermediate for Parkinsonism Drug, *Appl. Microbiol. Biotechnol. 54*, 44-51.

123. Steele, C. L., Chen, Y., Dougherty, B. A., Li, W., Hofstead, S., Lam, K. S., Xing, Z., and Chiang, S.-J. (2005) Purification, Cloning, and Functional Expression of Phenylalanine Aminomutase: The First Committed Step in Taxol Side-Chain Biosynthesis, *Arch. Biochem. Biophys. 438*, 1-10.

124. Feng, L., Wanninayake, U., Strom, S., Geiger, J., and Walker, K. D. (2011) Mechanistic, Mutational, and Structural Evaluation of a *Taxus* Phenylalanine Aminomutase, *Biochemistry 50*, 2919-2930.

125. Corey, P. F., and Ward, F. E. (1986) Buffered Potassium Peroxymonosulfate-Acetone Epoxidation of α,β-Unsaturated Acids, *J. Org. Chem. 51*, 1925-1926.

126. Smolarsky, M., and Koshland, D. E. (1980) Inactivation of the Opiate Receptor in Bovine Caudate Nucleus by Azide Enkephalin Analogs, *J. Biol. Chem. 255*, 7244-7249.

127. Trott, O., and Olson, A. J. (2010) AutoDock Vina: Improving the Speed and Accuracy of Docking with a New Scoring Function, Efficient Optimization, and Multithreading, *J. Comput. Chem. 31*, 455-461.

128. Morris, G. M., Huey, R., Lindstrom, W., Sanner, M. F., Belew, R. K., Goodsell, D. S., and Olson, A. J. (2009) AutoDock4 and AutoDockTools4: Automated Docking with Selective Receptor Flexibility, *J. Comput. Chem. 30*, 2785-2791.

129. Connolly, M. L. (1993) The Molecular Surface Package, *J. Mol. Graphics 11*, 139-141.

130. Srivastava, R. P., and McChesney, J. D. (1995) A Practical and Inexpensive Synthesis of the Taxol C-13 Side Chain; N-Benzoyl-(2R,3S)-3-Phenylisoserine, *Nat. Prod. Lett. 6*, 147-152.

131. Hammett, L. P. (1937) The Effect of Structure upon the Reactions of Organic Compounds. Benzene Derivatives, *J. Am. Chem. Soc. 59*, 96-103.

132. Feske, B. D., Kaluzna, I. A., and Stewart, J. D. (2005) Enantiodivergent, Biocatalytic Routes to Both Taxol Side Chain Antipodes, *J. Org. Chem. 70*, 9654-9657.

133. Futagawa, S., Inui, T., and Shiba, T. (1973) Nuclear Magnetic Resonance Study of the Stereoisomeric 2-Oxazolidone and 2-Phenyl-2-oxazoline Derivatives of α-Amino-β-Hydroxy Acids, *Bull. Chem. Soc. Jpn. 46*, 3308-3310.

134. Liu, J.-Q., Dairi, T., Itoh, N., Kataoka, M., Shimizu, S., and Yamada, H. (1998) Gene Cloning, Biochemical Characterization and Physiological Role of a Thermostable Low-Specificity L-Threonine Aldolase from *Escherichia coli*, *Eur. J. Biochem. 255*, 220-226.

135. Wybenga, G. G., Szymanski, W., Wu, B., Feringa, B. L., Janssen, D. B., and Dijkstra, B. W. (2014) Structural Investigations into the Stereochemistry and Activity of a Phenylalanine-2,3-aminomutase from *Taxus chinensis*, *Biochemistry 53*, 3187-3198.

136. Pettersen, E. F., Goddard, T. D., Huang, C. C., Couch, G. S., Greenblatt, D. M., Meng, E. C., and Ferrin, T. E. (2004) UCSF Chimera—A Visualization System for Exploratory Research and Analysis, *J. Comput. Chem. 25*, 1605-1612.

137. Hariharan, V. A., Denton, T. T., Paraszcszak, S., McEvoy, K., Jeitner, T. M., Krasnikov, B. F., and Cooper, A. J. L. (2017) The Enzymology of 2-Hydroxyglutarate, 2-Hydroxyglutaramate and 2-Hydroxysuccinamate and Their Relationship to Oncometabolites, *Biology 6*, 24.

138. Lohman, J. R., and Shen, B. (2012) 4-Methylideneimidazole-5-One-Containing Aminomutases in Enediyne Biosynthesis In *Methods Enzymol.* (Hopwood, D. A., Ed.), Vol. 516, pp 299-319, Academic Press.

139. Thornburg, C. K., Wortas-Strom, S., Nosrati, M., Geiger, J. H., and Walker, K. D. (2015) Kinetically and Crystallographically Guided Mutations of a Benzoate CoA Ligase (BadA) Elucidate Mechanism and Expand Substrate Permissivity, *Biochemistry 54*, 6230-6242.

140. Galla, Z., Beke, F., Forró, E., and Fülöp, F. (2016) Enantioselective Hydrolysis of 3,4-Disubstituted β-lactams. An Efficient Enzymatic Method for the Preparation of a Key Taxol Side-Chain Intermediate, *J. Mol. Catal. B: Enzym. 123*, 107-112.

141. Long, R. M., and Croteau, R. (2005) Preliminary Assessment of the C13-Side Chain 2′-Hydroxylase Involved in Taxol Biosynthesis, *Biochem. Biophys. Res. Commun. 338*, 410-417.

142. Tachibana, S., Watanabe, E., Ueno, J., Tokubuchi, K., and Itoh, K. (2005) Isolation of Phenylisoserine Methyl Ester from the Leaves of *Taxus cuspidata* var. *nana*, *J. Wood Sci. 51*, 176-180.

143. Camm, E. L., and Towers, G. H. N. (1973) Phenylalanine Ammonia Lyase, *Phytochemistry 12*, 961-973.

144. Farrow, S. C., and Facchini, P. J. (2014) Functional Diversity of 2-Oxoglutarate/Fe(II)-Dependent Dioxygenases in Plant Metabolism, *Frontiers in Plant Science 5*.

145. Griffin, S. L., Godbey, J. A., Oman, T. J., Embrey, S. K., Karnoup, A., Kuppannan, K., Barnett, B. W., Lin, G., Harpham, N. V. J., Juba, A. N., Schafer, B. W., and Cicchillo, R. M. (2013) Characterization of Aryloxyalkanoate Dioxygenase-12, a Nonheme Fe(II)/α-Ketoglutarate-Dependent Dioxygenase, Expressed in Transgenic Soybean and *Pseudomonas fluorescens*, *J. Agric. Food. Chem. 61*, 6589-6596.

146. Attanayake, G., Walter, T., and Walker, K. D. (2018) Understanding Which Residues of the Active Site and Loop Structure of a Tyrosine Aminomutase Define Its Mutase and Lyase Activities, *Biochemistry 57*, 3503-3514.

147. Wang, X., Zheng, M., Liu, J., Huang, Z., Bai, Y., Ren, Z., Wang, Z., Tian, Y., Qiao, Z., Liu, W., and Feng, F. (2017) Differences of First-Pass Effect in the Liver and Intestine Contribute to the Stereoselective Pharmacokinetics of Rhynchophylline and Isorhynchophylline Epimers in Rats, *J. Ethnopharmacol. 209*, 175-183.

148. Bhateria, M., Rachumallu, R., Yerrabelli, S., Saxena, A. K., and Bhatta, R. S. (2017) Insight Into Stereoselective Disposition of Enantiomers of a Potent Antithrombotic Agent, S002-333 Following Administration of the Racemic Compound to Mice, *Eur. J. Pharm. Sci. 101*, 107-114.

149. Yang, C.-P. H., Wang, C., Ojima, I., and Horwitz, S. B. (2018) Taxol Analogues Exhibit Differential Effects on Photoaffinity Labeling of β-Tubulin and the Multidrug Resistance Associated P-Glycoprotein, *J. Nat. Prod. 81*, 600-606.

150. Baloglu, E., Hoch, J. M., Chatterjee, S. K., Ravindra, R., Bane, S., and Kingston, D. G. I. (2003) Synthesis and Biological Evaluation of C-3′NH/C-10 and C-2/C-10 Modified Paclitaxel Analogues, *Biorg. Med. Chem. 11*, 1557-1568.

151. Baloglu, E., and Kingston, D. G. I. (1999) The Taxane Diterpenoids, *J. Nat. Prod. 62*, 1448-1472.

152. Hamada, Y., and Kiso, Y. (2016) New Directions for Protease Inhibitors Directed Drug Discovery, *Peptide Science 106*, 563-579.

Chapter 3: Insight into the Mechanism of Regio- and Stereoselective Amination of Enantiopure 3-Phenylglycidate Isomers to Phenylserine by *Tc*PAM.

3.1 Introduction

The 5-methylidene-3,5-dihydro-4*H*-imidazol-4-one (MIO) family (EC 4.3.1.0 and 5.4.3.0) contains aminomutases (AMs) and ammonia lyases (ALs). MIO-AMs catalyze the reversible cross exchange of an amine group and a hydrogen atom present on vicinal carbon of an amino acid, thus, allowing the interconversion between α-amino acids and their corresponding β-amino acid isomers,[1-7] while the ALs catalyze the reversible conversion between an α/β-amino acid and its dehydroaminated analogue, the acrylates (**Figure. 3.1**A).[8-14] Several MIO-AMs have been engineered to convert aromatic α-amino acids to aromatic β-amino acids with higher enantioselectivity.[15-17] AMs were also engineered by random mutagenesis within the active site (**Figure. 3.1**B)[18-20] or repurposed using a non-natural amine donor substrate (**Figure. 3.1**C)[21] to undergo amination of various ring-substituted arylacrylates to produce corresponding aromatic α- and β-amino acids. The application of AMs has also been extended to β-heteroaryl-α-amino acids to produce the corresponding β-amino acids.[22] Similarly, ALs have been repurposed to achieve a broader substrate scope to convert acrylates, with electron-donating or -withdrawing substituents on the aryl ring, to aromatic α/β-amino acids through regioselective amination. Enantioselective α-amination of arylacrylates was achieved through active site mutagenesis of ALs from *Petroselinum crispum* (*Pc*PAL) and *Anabaena variabilis* (*Av*PAL), whereas mutated AL from *Streptomyces maritimus* (EncP) and AM from *Taxus chinensis* (*Tch*PAM) resulted in enantioselective β-amination of arylacrylates (**Figure. 3.1**B).[11,14,23,24] An engineered methylaspartate ammonia lyase (MAL) from *Clostridium tetanomorphum* exhibited significant expansion of the substrate scope for both the amine donor and substituted mesaconate. Several

combinations of aliphatic and primary aromatic amines were coupled regio- and stereo-selectively to many different mesaconate analogues to make (2*S*)-*syn*-aspartate analogues (**Figure. 3.1D**).[25,26] Besides employing MIO-enzymes to make amino acids, other efforts looked to explore mutants that converted acyclic α-amino acids to their acrylates. In another study, propargylglycine, an acyclic amino acid, was converted to (*E*)-pent-2-ene-4-ynoate by an MIO-AL from *Petroselinum crispum.*[27] Active site mutagenesis on a PAM from *Taxus chinensis* resulted in a 44-fold increase of the PAL activity in the enantioselective deamination of (*R*)-β-phenylalanine to cinnamic acid.[28]

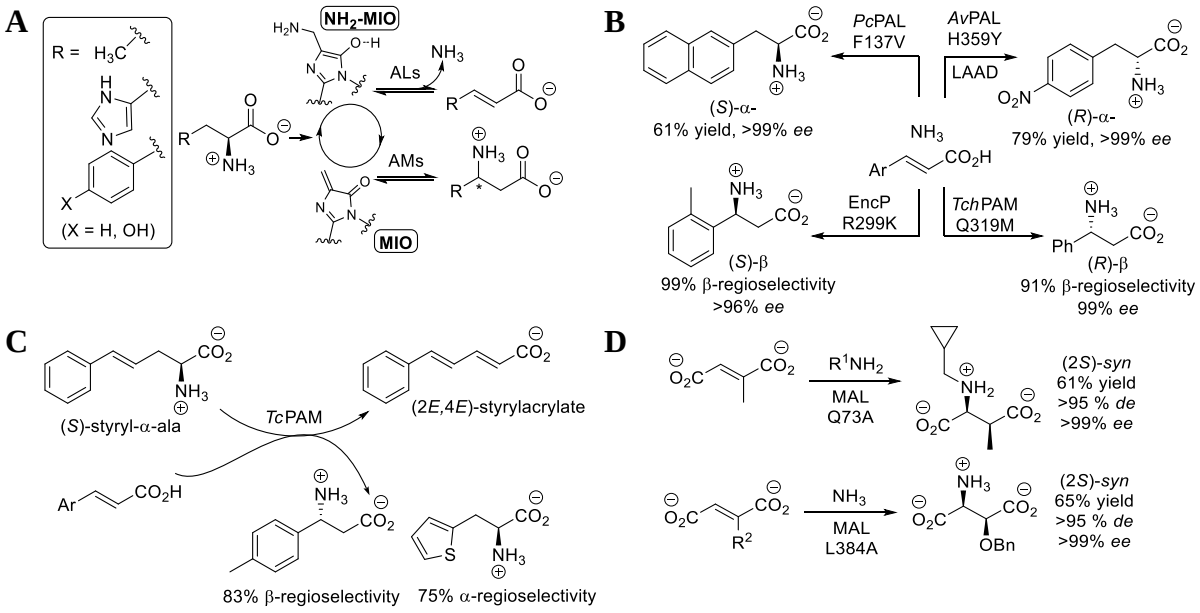

Figure. 3.1. A) Reactions catalyzed by MIO-dependent ammonia lyases (ALs) and aminomutases (AMs), making either the acrylate or β-amino acid from the corresponding α-amino acid. The MIO and aminated-MIO (NH_2-MIO) are shown. The asterisk (*) identifies an (*R*/*S*)-chiral center; B) Production of either enantiomer of α- and β-arylalanine using engineered PAL/PAM catalysis; C) PAM-mediated amine transfer from (*S*)-styryl-α-alanine to acrylate acceptors. D) Addition of ammonia and primary amines to mesaconate analogues using engineered methylaspartate ammonia lyase (MAL) to produce (2*S*)-*syn*-aspartate analogues.

While much of the mechanistic analysis involving MIO-enzymes has centered either on deaminating amino acids to their acrylates or aminating acrylates to α- or β-amino acids, our earlier work explored a new application of MIO-enzyme chemistry where we expanded the transaminase activity of MIO-aminomutases to a new class of substrates, the epoxides, producing amino

alcohols. We repurposed an MIO-dependent phenylalanine aminomutase from *Taxus canadensis* (*Tc*PAM) to convert *trans*-3-arylglycidates (i.e., *trans*-arylacrylate epoxides) to *anti*-arylserines.[29] *Tc*PAM normally isomerizes (2*S*)-α-phenylalanine to (3*R*)-β-phenylalanine.[30,31] and was shown to have broad substrate specificity for non-natural α-arylalanines including the chain extended (2*S*)-styryl-α-alanine.[21] In a kinetic study on *Tc*PAM, the residence time of the NH_2-MIO adduct was measured, after (2*S*)-styryl-α-alanine donated its amino group to the enzyme, and the (2*E*,4*E*)-styrylacrylate product was released.[32] The burst phase study revealed that the aminated *Tc*PAM (NH_2-MIO) lifetime was long enough to transfer the amino group intermolecularly from (2*S*)-styryl-α-alanine to various arylacrylates making enantiopure α- and β-arylamino acids.[21]

Encouraged by the intrinsic intermolecular transaminase activities exhibited by MIO-PAMs,[30,33] we used *Tc*PAM and (2*S*)-styryl-α-alanine to convert *trans*-3-arylglycidate racemates to arylserines and arylisoserines. In our previous substrate specificity study (described in **Chapter 2** of this thesis), we showed that *Tc*PAM has broad substrate specificity and stereoselectivity toward forming (2*R*)-*anti*-arylserines over their (2*S*)-*anti*-isomers, ranging from 66:34 for 4′-F-phenylserine to 88:12 for 3′-NO_2-phenylserine.[29] We also used crystal structures of *Tc*PAM in our earlier study to visualize the *Tc*PAM active site and infer the stereocontrol observed for the conversion of *trans*-3-arylglycidates to their corresponding *anti*-arylserines.[18,34] From these data, we hypothesized that two active site tyrosine residues acted separately as general acids to facilitate stereoselective ring-opening of the glycidate racemates. In this study, we looked to verify that the isomeric ratio of the (2*R*)-*anti* and (2*S*)-*anti*-phenylserine products catalyzed by *Tc*PAM resulted from stereoselectivity for each isomer in the racemic mixture and not from bond rotation within one of the glycidate substrate isomers during catalysis. We also established the correlation between the glycidate enantiomer and the small amount of *syn*-phenylserine formed, which

provided valuable insight into the mechanism of amine group transfer from NH_2-MIO to the glycidate backbone during catalysis.

To test this hypothesis, here, we synthesized enantiopure 3-phenylglycidates from cinnamyl alcohol using the asymmetric Sharpless epoxidation reaction,[35] followed by $RuCl_3$-catalyzed oxidation of the primary alcohol to the carboxylate.[36] *Tc*PAM was incubated with each 3-phenylglycidate enantiomer, and the absolute configurations of the biocatalyzed *anti*-phenylserine (major) and phenyl*iso*serine (minor) were evaluated to gain further insights on the substrate specificity and selectivity of *Tc*PAM for aminating 3-phenylglycidates.[29] The apparent Michaelis-Menten kinetic parameters of *Tc*PAM in a competitive inhibition ping-pong mechanism for each 3-phenylglycidate enantiomer were measured. Here we summarize the details of these studies.

3.2 Experimental

3.2.1 Chemicals and Reagents

trans-Cinnamyl alcohol, (+)-diethyl tartrate (DET), (–)-DET, sodium *meta*periodate, *tert*-butyl hydroperoxide solution (5.0 – 6.0 M) in nonane, chlorotrimethylsilane, and (2*S*)-(+)-methylbutyric anhydride were purchased from Millipore-Sigma (Burlington, MA). Titanium(IV) isopropoxide and ruthenium (III) chloride hydrate were purchased from Oakwood Chemical (Estill, SC). (2*S*)-Styryl-α-alanine and (2*R*,3*R*)-*anti*-phenylisoserine were purchased from Chem Impex (Wood Dale, IL). (2*S*)-*syn*-Phenylserine and (2*R*,3*S*)-phenylisoserine hydrochloride was purchased from Bachem (Torrance, CA). All chemicals were used without further purification unless noted.

3.2.2 Synthesis of (2*R*,3*R*)-3-Phenylglycidol (21a)[35]

A mixture of $Ti(O\textit{i}\text{-}Pr)_4$ (288 mg, 1.01 mmol), (–)-DET (241 mg, 1.2 mmol), and activated, powdered 4 Å MS (500 mg) were stirred in anhydrous dichloromethane (CH_2Cl_2) (20 mL) at –30 °C for 30 min. The reaction mixture was incubated over 30 min intervals before adding the next

reagent so the chiral Ti-DET complex could form and coordinate with each subsequent reactant at low temperature. Afterward, cinnamyl alcohol (**20**) (1.05 g, 7.8 mmol) dissolved in anhydrous CH_2Cl_2 (2 mL) was then added, and the resulting mixture was stirred at -30 °C for 30 min. The mixture was treated with 5.5 M *t*-BuOOH in nonane (3.6 mL, 19.5 mmol), stirred for 16 h at -30 °C, warmed to 0 °C over 1 h, and poured into a freshly prepared solution of $FeSO_4$ (1.2 g) and tartaric acid (350 mg) in deionized H_2O (2 mL) precooled to 0 °C. The two-phase solution was stirred for 30 min, and the aqueous phase was separated and extracted with diethyl ether (Et_2O) (2 × 10 mL). The combined organic layers were dried over anhydrous Na_2SO_4, filtered, and concentrated under vacuum to give a pale-yellow oil. The product was dissolved in Et_2O (50 mL), cooled to 0 °C, and treated with a 30% (w/v) solution of NaOH in saturated brine (1 mL) precooled to 0 °C. The two-phase mixture was stirred for 1 h at rt, and the aqueous layer was separated and treated with Et_2O (2 × 10 mL). The combined organic extracts were dried (Na_2SO_4) and concentrated under vacuum. The resulting crude product was purified by flash column chromatography (silica gel, EtOAc/hexanes, 1:4) to yield (2*R*,3*R*)-3-phenylglycidol (**21a**) as a clear liquid. Isolated yield: 440 mg (38%); 92% *ee* (based on HPLC separation). $[\alpha]_D^{22}$ +49° (*c* 1.00, $CHCl_3$), reported $[\alpha]_D^{20}$ +45.9° (*c* 1.00, $CHCl_3$).[37] R_f = 0.5 of silica gel TLC (EtOAc/hexanes, 40:60). ^{1}H NMR (500 MHz, $CDCl_3$) δ 7.39 – 7.27 (m, 5H), 4.06 (ddd, *J* = 12.7, 5.2, 2.4 Hz, 1H), 3.94 (d, *J* = 2.2 Hz, 1H), 3.81 (ddd, *J* = 12.7, 7.9, 3.8 Hz, 1H), 3.23 (dt, *J* = 3.7, 2.3 Hz, 1H), 1.79 (dd, *J* = 7.8, 5.2 Hz, 1H). ^{13}C NMR (126 MHz, $CDCl_3$): δ 136.8, 128.7, 128.5, 125.9, 62.5, 61.3, 55.7.

3.2.3 Synthesis of (2*S*,3*S*)-3-Phenylglycidol (21b).

The following synthesis is based on a reported procedure,[35] and is analogous to that used to convert cinnamyl alcohol **20** to **21a**, except (+)-DET was used instead of (–)-DET. The final

glycidol product (**21b**) was purified by flash column chromatography (silica gel, EtOAc/hexanes, 1:4) to yield (2*S*,3*S*)-3-phenylglycidol (**21b**) as a clear liquid. Isolated yield: 379 mg (33%); 90% *ee* based on measured specific optical rotation: $[\alpha]_D^{22}$ –48° (*c* 1.00, $CHCl_3$), reported $[\alpha]_D^{20}$ –50.1° (*c* 1.00, $CHCl_3$).[37] R_f = 0.5 on silica gel TLC (EtOAc/hexanes, 40:60). ^{1}H NMR (500 MHz, $CDCl_3$): δ 7.43 – 7.23 (m, 5H), 4.04 (dd, *J* = 12.8, 2.4 Hz, 1H), 3.94 (d, *J* = 2.2 Hz, 1H), 3.78 (dd, *J* = 12.8, 4.2 Hz, 1H), 3.31 – 3.16 (m, 2H). ^{13}C NMR (126 MHz, $CDCl_3$) δ 136.6, 128.5, 128.3, 125.7, 62.7, 61.4, 55.7.

3.2.4 General Procedure to Characterize the Enantiomeric Excess of Glycidols (21a and 21b).

To measure the enantiomeric excess (*ee*) of the 3-phenylglycidols, synthesized and purified 3-phenylglycidol (2 mg) (**21a** or **21b**) was dissolved in Et_2O (2 mL), and an aliquot (10 µL) of this solution was analyzed in HPLC (Agilent 1260) equipped with a chiral column (Chiralcel OD-H, 5µm, 4.6 mm x 150 mm) with *i*-PrOH/Hex (90:10) as the solvent at a flow rate of 1 mL/min.

3.2.5 Synthesis of Potassium (2*S*,3*R*)-3-Phenylglycidate (14aa) from 21a.

The following synthesis is based on a reported method.[36] $RuCl_3$•H_2O (6 mg, 29 µM) was added to a biphasic mixture of solvents (CCl_4 (2 mL), acetonitrile (2 mL), and water (3 mL)) containing **21a** (0.2 g, 1.32 mmol), sodium *meta*periodate 0.85 g, 3.96 mmol), and sodium bicarbonate (0.55 g, 6.6 mmol). The mixture was stirred for 72 h, then additional $RuCl_3$•H_2O (6 mg, 29 µM) and sodium *meta*periodate (0.32 g, 1.5 mmol) were added, and the reaction was stirred for 24 h. CH_2Cl_2 (8 mL) and then water (2 mL) were added to the sodium carboxylate solution. The product mixture was cooled to 0 °C, and the water layer was adjusted to pH 4.0 (6 M HCl). The aqueous layer was then extracted with Et_2O (2 × 15 mL). The combined organic layers were dried (Na_2SO_4), and the solvent was removed under vacuum to yield the carboxylic acid as a yellow oil. The carboxylic

acid was dissolved in acetone (5 mL) and water (0.5 mL) and (100 mg, 1 mmol) and treated with $KHCO_3$ to convert to its potassium salt (**14aa**) to avoid potential α-decarboxylation. The final epoxides contained unreacted salts. Dioxane (10 μmol) was the internal standard used to quantify the 3-phenylglycidate stock solutions in Assay Buffer (50 mM NaH_2PO_4/Na_2HPO_4 buffer (pH 8.0)). Isolated yield: 171 mg (63%). ^{1}H NMR (500 MHz, D_2O) δ 7.42 – 7.35 (m, 5H), 3.97 (d, *J* = 2.5 Hz, 1H), 3.56 (d, *J* = 2.0 Hz, 1H). ^{13}C NMR (126 MHz, D_2O) δ 175.4, 135.5, 128.9, 128.7, 126.0, 58.8, 57.4. HRMS (ESI-TOF) *m*/*z*: $[M - K]^-$ for $C_9H_7O_3$: found 163.0403; calcd 163.0395.

3.2.6 Synthesis of Potassium (2*R*,3*S*)-3-Phenylglycidate (14ab) from 21b.

The potassium salt of (2*R*,3*S*)-3-phenylglycidate (**14ab**) was prepared following the same procedure to convert **21a** to **14aa**.[36] Isolated yield: 185 mg (68%). ^{1}H NMR (500 MHz, D_2O) δ 7.42 – 7.35 (m, 5H), 3.97 (d, *J* = 2.5 Hz, 1H), 3.56 (d, *J* = 2.0 Hz, 1H). ^{13}C NMR (126 MHz, D_2O) δ 175.4, 135.5, 128.9, 128.7, 126.0, 58.8, 57.4. HRMS (ESI-TOF) *m*/*z*: $[M – K]^-$ for $C_9H_7O_3$: found 163.0402; calcd 163.0395.

3.2.7 Enantiopurity of the Synthesized 3-Phenylglycidates.

The glycidates were suspended in H_2O (1 mL) at 0 °C and titrated with 6 N HCl to pH 3. The resulting 3-phenylglycidic acids were extracted into EtOAc (1 × 2 mL), and the organic fractions were combined, separated, and treated with diazomethane (0.9 equiv) dissolved in Et_2O to measure the enantiomeric excess (*ee*) of each synthetic potassium 3-phenylglycidate (0.05 mmol) enantiomer.

A stock of racemic potassium 3-phenylglycidate, synthesized previously,[29] was also converted to the corresponding methyl ester by reacting with diazomethane. An aliquot (1 μL) of the racemic and enantio-enriched methyl 3-phenylglycidates was analyzed by gas chromatography/electron-impact mass spectrometry (GC/EI-MS) using an Agilent 6890N gas chromatograph equipped with

a capillary chiral GC column (25 m × 0.25 mm × 0.39 mm; CP Chirasil-Dex CB, thickness 0.25 μm; Agilent Technologies, Santa Clara, CA) with He as the carrier gas (flow rate, 1 mL/min). The injector port (at 250 °C) was set to splitless injection mode. A 1-uL aliquot of each sample was injected using an Agilent 7683 auto-sampler (Agilent, Atlanta, GA). Initial column temperature started at 70 °C, then increased at 40 °C/min to 95 °C with a 7 min hold, ramped at 10 °C/min to 150 °C, then increased by 30 °C/min to 175 °C, and returned to 70 °C over 3 min. The gas chromatograph was coupled to a mass-selective detector (Agilent, 5973 inert) operated in electron impact mode (70 eV ionization voltage). All spectra were recorded in the mass range of 50 – 375 *m*/*z* to analyze the methyl phenylglycidates.

3.2.8 Production of Phenylserine by *Tc*PAM Biocatalysis.

A solution of (2*S*)-styryl-α-alanine (1 mM) in Assay Buffer was preincubated with *Tc*PAM (100 μg/mL) for 2 min, and then a potassium 3-phenylglycidate enantiomer (**14aa** or **14ab**) (1 mM) was added. The assay was incubated at 31 °C and gently mixed on a rocking shaker (100 rpm) for 2.5 h. The reaction was quenched with 10% formic acid (pH 3.0).

3.2.9 General Method for Chiral Auxiliary Derivatization of Phenylserines and Phenylisoserines.

A mixture of all four stereoisomers of phenylserine (0.2 mmol), synthesized previously,[29] was dissolved in Assay Buffer. To this solution were added pyridine (50 μL, 0.62 mmol) and (*2S*)-2-methylbutyric anhydride (50 μL, 0.25 mmol), and the reaction mixture was stirred for 15 min at ~25 °C. The pH was adjusted to 3.0 (6 M HCl), and the *N*-protected phenylserine was extracted with EtOAc (1 × 2 mL). The organic layer was evaporated under a stream of nitrogen gas, and the resultant residue was dissolved in 3:1 EtOAc/MeOH (v/v) (1 mL). Diazomethane dissolved in Et_2O was added dropwise until the yellow color persisted to obtain the methyl esters, and the

solvent was removed under a stream of nitrogen gas. The resulting methyl ester was dissolved in CH_2Cl_2 (1 mL), to which pyridine (70 µL, 0.86 mmol) and chlorotrimethylsilane (100 µL, 0.79 mmol) were added. The solution was stirred for 15 min at ~25 °C, and the reaction was quenched with water (1 mL), and the organic layer was separated and analyzed by GC/EI-MS.

To access authentic standards of *anti*-phenylisoserine enantiomers, enantiopure potassium 3-phenylglycidates, **14aa** and **14ab**, and a stock of racemic potassium 3-phenylglycidates, characterized and synthesized previously,[29] were treated separately with NH_4OH (2 M) in Assay buffer (1 mL) for 1 h. The hydroxy amino acids derived from the synthetic amination of the glycidates and authentic (2*R*,3*S*)-*syn*-phenylisoserine were then derivatized to their (*2S*)-2-methylbutyramide chiral auxiliaries, followed by methyl esterification and *O*-silyl etherification, as done with the phenylserines. Each derivatized phenylisoserine sample was analyzed by GC/EI-MS on an Agilent 6890N gas chromatograph equipped with a capillary GC column (30 m × 0.25 mm × 0.25 uM + 5 m EZ-Guard; VF-5MS; Agilent Technologies, Santa Clara, CA) with He as the carrier gas (flow rate, 1 mL/min). The injector port (at 250 °C) was set to splitless injection mode. A 1-uL aliquot of each sample was injected using an Agilent 7683 auto-sampler (Agilent, Atlanta, GA). Initial column temperature started at 50 °C, then increased at 50 °C/min to 150 °C, followed by 20 °C/min to 200 °C, then ramped at 10 °C/min to 225 °C with a 5-min hold, and finally increased by 25 °C/min to 250 °C. The gas chromatograph was coupled to a mass-selective detector (Agilent, 5973 inert) operated in electron impact mode (70 eV ionization voltage). All spectra were recorded in the mass range of 50 – 375 *m*/*z* to analyze the hydroxy amino acids derivatized as their *O*-trimethylsilyl *N*-[(2*S*)-2-methylbutyryl] methyl esters.

3.2.10 Kinetic Analysis.

(2*S*)-styryl-α-alanine, the amine donor was varied from 100 μM to 1 mM, at fixed concentrations of each epoxide enantiomer (100 μM, 500 μM, 1 mM, and 2.5 mM) in triplicate assays containing *Tc*PAM (100 μg/mL) to calculate the steady-state enzyme kinetic constants. The reactions were terminated with 10% formic acid (pH 3.0), and 3'-bromo-α-phenylalanine (50 nM) was added as an internal standard. This reaction mixture was analyzed using a liquid chromatography-electrospray ionization-multiple reaction monitoring (LC/ESI-MRM) method without further chemical derivatization. The apparent kinetic parameters ($K_{\mathrm{M}}^{app}$and k_{cat}^{app}) were calculated by non-linear regression with Origin Pro 9.0 software (Northampton, MA), using a modified Michaelis-Menten equation (Eq. (1), See Supporting Information). A secondary plot of V_{max}^{app} vs the concentration of 3-phenylglycidate enantiomers (Eq. (4) See Supporting Information) was used to calculate the true kinetic parameters (K_{M} and k_{cat}) of each enantiomer.

3.3 Results and Discussion

3.3.1 Synthesis of and Characterization of Enantioenriched 3-Phenylglycidate Substrates (14aa and 14ab).

The enantiomeric potassium 3-phenylglycidates were made by oxidizing cinnamyl alcohol with the Sharpless asymmetric epoxidation catalyst using a (–)–DET or (+)-DET ligand to make (2*R*,3*R*)-3-phenylglycidol (**21a**) or the (2*S*,3*S*)-isomer, respectively (**Scheme 3.1**). The absolute configuration of each 3-phenylglycidol enantiomer was confirmed by measuring the corresponding specific rotation in chloroform and comparing that with the reported literature.[37] Asymmetric Sharpless epoxidation employing (–)-DET resulted in (2*R*,3*R*)-3-phenylglycidol (**21a**), whereas the epoxidation with (+)-DET produced (2*S*,3*S*)-3-phenylglycidol (**21b**). Enantiopurity of each glycidol enantiomer was calculated by measuring the relative peak areas of the glycidols separated on a HPLC fitted with a chiral column. Glycidol **21b** eluted at 7.42 min (90% *ee*) followed by its enantiomer **21a** (8.42 min, 92% *ee*) (**Figure. 3.2**).

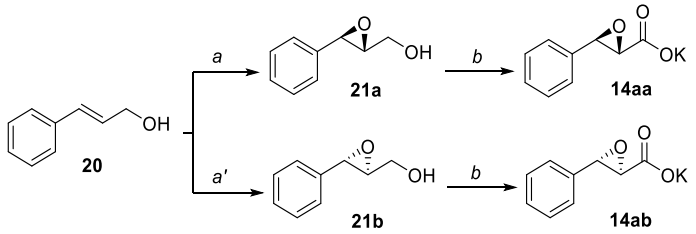

Scheme 3.1. Synthesis of (2*S*,3*R*)-3-phenylglycidate (**14aa**) and (2*R*,3*S*)-3-phenylglycidate (**14ab**). a) (–)-DET, Ti(O*i*-Pr)$_4$, *t*-BuOOH, 4 Å MS, CH_2Cl_2, 16 h, –30 °C; a′) (+)-DET, Ti(O*i*-Pr)$_4$, *t*-BuOOH, 4 Å MS, CH_2Cl_2, 16 h, –30 °C; b) *i*) $RuCl_3$, $NaIO_4$, $NaHCO_3$, $CH_3CN/CCl_4/H_2O$, rt, 72 h.; *ii*) $KHCO_3$, acetone/H_2O, 0 °C, 1h.

Glycidols **21a** and **21b** were was oxidized to their carboxylic acids using a $RuCl_3/NaIO_4$-based oxidation protocol (**Scheme 3.1**)[36] under basic ($NaHCO_3$) conditions to facilitate the deprotonation of the carboxylic acid and prevent any potential decomposition due to spontaneous decarboxylation. Oxidation (2*R*,3*R*)-3-phenylglycidol (**21a**) gave potassium (2*S*,3*R*)-3-phenylglycidate (**14aa**) while the (2*S*,3*S*)-3-phenylglycidol (**21b**) produced potassium (2*R*,3*S*)-3-

phenylglycidate (**14ab**). In contrast to 43 h reaction time reported in the literature,[36] the oxidation reaction was run for 72 h to achieve complete oxidation to enantioenriched 3-phenylglycidates.

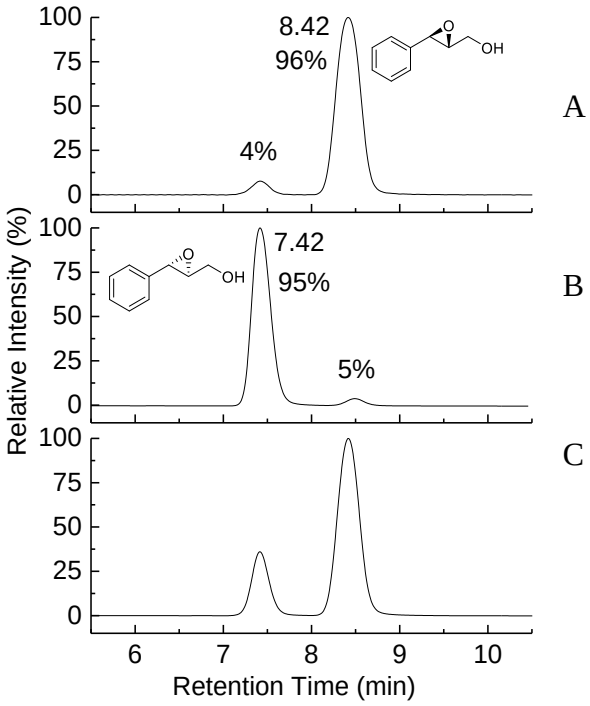

Figure. 3.2. Chiral HPLC separation of A). (2*R*,3*R*)-3-phenylglycidol (**21a**), 92% *e.e.*; B) .(2*S*,3*S*)-3-phenylglycidol (**21b**), 90% *e.e*; and C) a co-injection of enantioenriched samples of **21a** and **21b**.

3.3.2 Enantiopurity of the Synthesized 3-Phenylglycidate isomers (14aa and 14ab).

The enantiomeric excess (*ee*) of both (2*S*,3*R*)- and (2*R*,3*S*)-3-phenylglycidate potassium salts were measured by converting them to their corresponding methyl esters using CH_2N_2 and characterized by GC/EI-MS fitted with a chiral column. The retention times of the eluted peaks for the enantiopure methyl 3-phenylglycidate isomers were verified by comparing to the retention times of authentic racemic methyl 3-phenylglycidate standards characterized in my earlier work (Chapter 2:, section 2.3.2, **Figure. 3.3** and **Figure. 2.12**A).[29] Comparing the relative peak areas of the glycidate methyl esters analyzed by GC/EI-MS verified that the (2*S*,3*R*)-isomer was made at

92% *ee* and its (2*R*,3*S*)-antipode was prepared at 90% *ee*. The *ee* values of the glycidates tracked those of the corresponding glycidols from which they were synthesized.

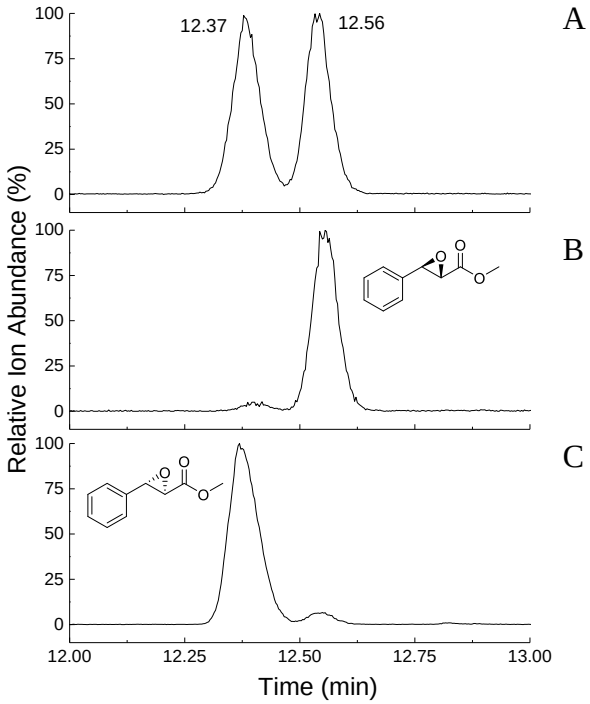

Figure. 3.3. Extracted ion (*m*/*z* 121) chromatogram of (A) racemic methyl 3-phenylglycidate (51:49), (B) methyl (2*S*,3*R*)-3-Phenylglycidate (4:96, 12.56 min), and (C) methyl (2*R*,3*S*)-3-Phenylglycidate (95:5, 12.37 min).

3.3.3 Glycidate Ring-Opening by *Tc*PAM Catalysis and Analysis of its Stereoselectivity.

In our previous work,[29] we reported that *Tc*PAM could be repurposed to irreversibly biocatalyze an intermolecular amine transfer reaction from (2*S*)-styryl-α-alanine to racemic 3-arylglycidates to access arylserines and arylisoserines. Racemic glycidates were used to explore the enantioselectivity of *Tc*PAM for the conversion of the glycidates to their corresponding hydroxy amino acid products. Surprisingly, *Tc*PAM turned over the arylglycidate racemates to a mixture of *anti*-arylserine enantiomers as the major biocatalyzed products, with a modest stereopreference for the (2*R*)-*anti* isomer over its (2*S*)-*anti* antipode (**Figure. 3.4**). These results inspired us to examine whether the isomeric ratio of the (2*R*)-*anti*- and (2*S*)-*anti*-arylserine products resulted

from the stereospecificity *Tc*PAM for a particular arylglycidate in the racemic mixture and not from bond rotation within one of the glycidate substrate isomers during catalysis.

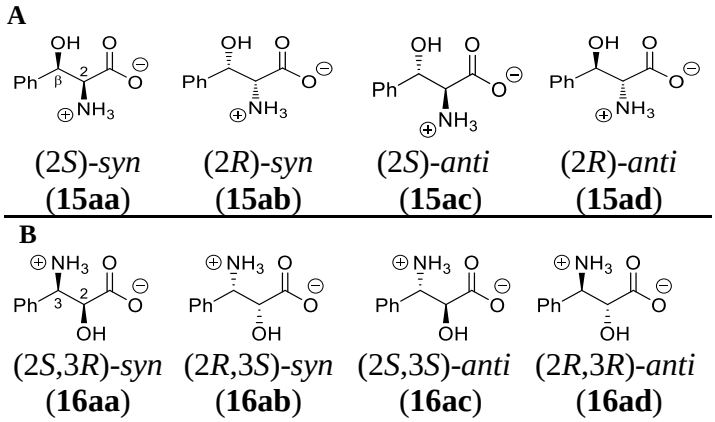

Figure. 3.4. Stereoisomerism convention for A) phenylserine, and B) phenylisoserine used herein.

The turnover (k_{cat}^{app}) of the *trans*-3-arylglycidate racemates ranged from 0.02 min^{-1} for 3-(4′-chlorophenyl)glycidate to 1.3 min^{-1} for 3-(3′-chlorophenyl)glycidate, and the turnover of the 3-phenylglycidate was in between at 0.4 min^{-1}. Thus, we chose to examine the turnover of each *trans*-3-phenylglycidate enantiomer by *Tc*PAM to gain further insight into its stereospecificity and stereoselectivity. *Tc*PAM was incubated separately with each enantioenriched 3-phenylglycidate (**14aa** or **14ab**) along with the amino group donor substrate (2*S*)-styryl-α-alanine. Noticeably, *Tc*PAM turned over **14aa** ~1.6-times faster than **14ab** to their *anti*-phenylserines (**15ac** and **15ad**, respectively) preferentially over the *syn*-isomers (**15aa** and **15ab**). *Tc*PAM-catalyzed the ring-opening of each 3-phenylglycidate preferentially at the C_α to produce phenylserine as the primary product. A small amount of *anti*-phenylisoserine (3%), resulting from amination at the C_β, was also made. 3-Phenylglycidates inherently stabilize a partial positive charge (δ^+) at the benzylic carbon, and this usually promotes nucleophilic attack at the C_β. For example, nucleophilic epoxide ring-opening by $InCl_3$-catalyzed thiolysis,[38] bromolysis and iodolysis,[39] copper-catalyzed azidolysis,[40] and *N*-alkyl-(hydroxylamines)[41] occurred at C_β of 3-phenylglycidates. In our study,

we observed a reversal of regioselectivity with *Tc*PAM as the biocatalyst and **12** as the amine-nucleophile donor where the 3-phenylglycidates were ring-opened by nucleophilic cleavage of the C_α-O bond to produce phenylserine as the major biocatalyzed product.

The relative and absolute stereoconfigurations of *O*-trimethylsilyl *N*-[(2*S*)-2-methylbutyryl] methyl esters derivatives of phenylserine and phenylisoserine biocatalyzed by *Tc*PAM were assessed. Authentic standards of phenylserine chiral derivatives (**Scheme 3.2**A) were synthesized and characterized (**Scheme 2.1**B) and analyzed by GC/EI-MS (Section **2.3.9** and **Figure. 3.5**A), as described in **Chapter 2** of this thesis.[29]

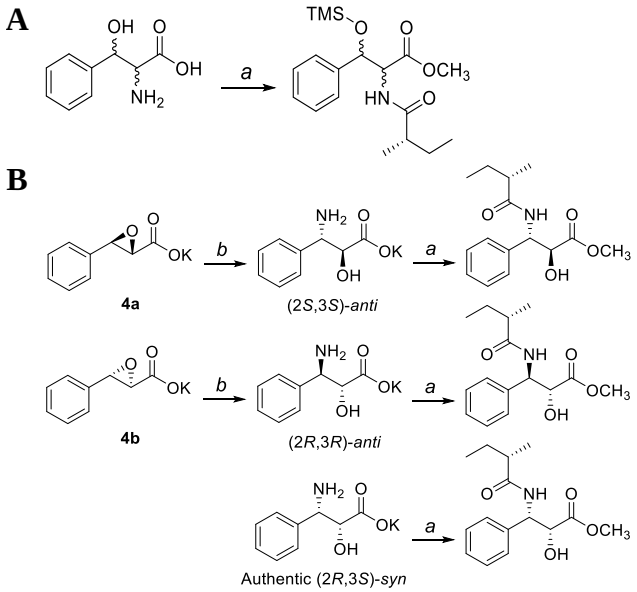

Scheme 3.2. Chiral auxiliary derivatization of A) authentic phenylserine diastereomers; and B) phenylisoserine diastereomers comprising (2*S*,3*S*)-*anti*-(**16ac**), (2*R*,3*R*)-*anti*-(**16ad**), and (2*R*,3*S*)-*syn*-phenylisoserine (**16ab**). Derivatization was performed using (a) (*i*) (2*S*)-2-Methylbutyric anhydride, pyridine, rt, 15 min; (*ii*) 6 M HCl, pH 2; (*iii*) CH_2N_2, EtOAc/MeOH (3:1 v/v), rt, 10 min; and (*iv*) chlorotrimethylsilane, pyridine,CH_2Cl_2, rt, 15 min.; and (b) 2 M aq. NH_4OH, rt, 1h.

The peak elution order of (2*S*)-*anti*- (**15ac**, 8.88 min) followed by (2*R*)-*anti*-phenylserine (**15ad**,8.93 min), and (2*S*)-*syn*- (**15aa**, 9.02 min) followed by (2*R*)-*syn*-phenylserine (**15ab**, 9.05 min) has previously been established (**Figure. 2.19** and **Figure. 3.5**).[29]

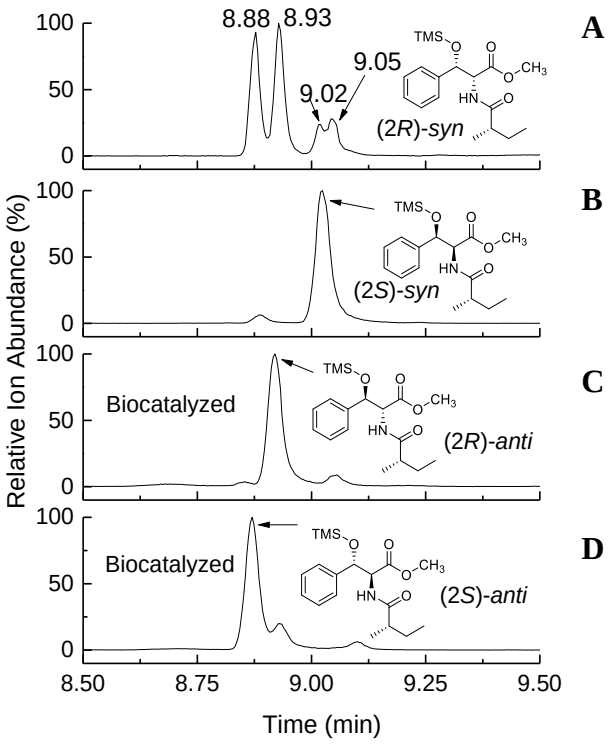

Figure. 3.5. GC/EI-MS extracted-ion chromatograms with *m*/*z* 179 ion monitoring of A) phenylserine stereoisomers derivatized with a chiral auxiliary (cf. **Scheme 3.2A**). An earlier study[29] involving enzymatic resolution with (2*S*)-threonine aldolase confirmed that peaks at 8.88 min and 8.93 min correspond to chiral derivatives of (2*S*)-*anti*- and (2*R*)-*anti*-phenylserine isomers, respectively, and peaks at 9.02 and 9.05 min correspond to the chiral derivatives of (2*S*)-*syn*- and (2*R*)-*syn*-phenylserine isomers (cf. **Figure. 2.19**). Chiral derivatives of B) authentic (2*S*)-*syn*-phenylserine (Bachem); C) biocatalyzed phenylserine made from (2*S*,3*R*)-3-phenylglycidate (the (2*S*)-*anti*:(2*R*)-*anti*:(2*S*)-*syn* isomers are abundant at a relative ratio of 2:90:8); and D) biocatalyzed phenylserine made from (2*R*,3*S*)-3-phenylglycidate (the (2*S*)-*anti*:(2*R*)-*anti*:(2*R*)-*syn* isomers are abundant at a relative ratio of 76:15:9).

Guided by accounts reported previously, [42,43] racemic 3-phenylglycidate was first treated with 2 M NH_4OH to make a mixture of *anti*-phenylisoserine enantiomers (**16ac** and **16ad**) *in situ* to establish the absolute stereoconfiguration of phenylisoserine diastereomers. Also, enantiopure **14aa** was treated with NH_4OH to invert the configuration at the C_β to make (2*S*,3*S*)-*anti*-phenylisoserine (**16ac**),[42,43] and enantioenriched **14ab** was treated similarly to make the (2*R*,3*R*)-*anti*-phenylisoserine (**16ad**) (**Scheme 3.2**B). These synthesized *anti*-phenylisoserine isomers and

commercial (2*R*,3*S*)-*syn*- (**16ab**) and (2*R*,3*R*)-*anti*-phenylisoserine (**16ad**) methyl esters were derivatized with chiral auxiliaries and analyzed by GC/EI-MS (**Figure. 3.12**).

The GC/EI-MS fragmentation patterns for the biocatalyzed phenylisoserines were identical to those for the chiral auxiliary derivatives of the commercial (2*R*,3*S*)-*syn*-, (2*R*,3*R*)-*anti*-, and synthesized (2*S*,3*S*)-*anti*- and (2*R*,3*R*)-*anti*-phenylisoserine isomers (**Figure. 3.19** and **Figure. 3.20**). The derivative of the commercial (2*R*,3*S*)-*syn*-phenylisoserine (**16ab**) and (2*R*,3*R*)-*anti*-phenylisoserine (**16ad**) eluted at 9.05 min and 9.33 min, respectively (**Figure. 3.6**A and B), whereas those of the *anti*-phenylisoserine racemate, prepared from 3-phenylglycidate racemate, eluted at 9.33 and 9.41 min (**Figure. 3.6**C). This data indicates that the peak eluting at 9.41 min corresponds to the derivatized (2*S*,3*S*)-anti-phenylisoserine (**16ac**). The retention times of the *anti*-phenylisoserines in the racemic mixture was identified by comparing them against the retention times of enantioenriched (2*S*,3*S*)-*anti*-phenylisoserine (**16ac**, 9.41 min) (**Figure. 3.6**D), and (2*R*,3*R*)-*anti*-phenylisoserine (**16ad**, 9.33 min) (**Figure. 3.6**E) derivatized identically.

GC/EI-MS analysis of the chiral derivatives of the products biocatalyzed by *Tc*PAM from (2*S*,3*R*)-3-phenylglycidate (**14aa**, 92% *ee*) in the amine transfer reaction showed that (2*R*)-*anti*-phenylserine was the major product (90%) with (2*S*)-*syn*-phenylserine as the minor product (8%). The (2*S*)-*syn*-phenylserine is believed to be formed when the carboxylate group of the glycidate substrate nucleophilically and intramolecularly opens the epoxy ring and forms a three-membered oxiranone intermediate, (*R*)-3-((*R*)-hydroxy(phenyl)methyl)oxiran-2-one (**22aa**), (**Figure. 3.7**C and **Figure. 3.8**B) before being aminated at the C_α by the MIO-NH_2 adduct in the *Tc*PAM active site. Also, trace amount of the (2*R*,3*S*)-3-phenylglycidate present at 4% in the substrate was converted to (2*S*)-*anti*-phenylserine at a relative abundance of 2% (**Figure. 3.5**C).

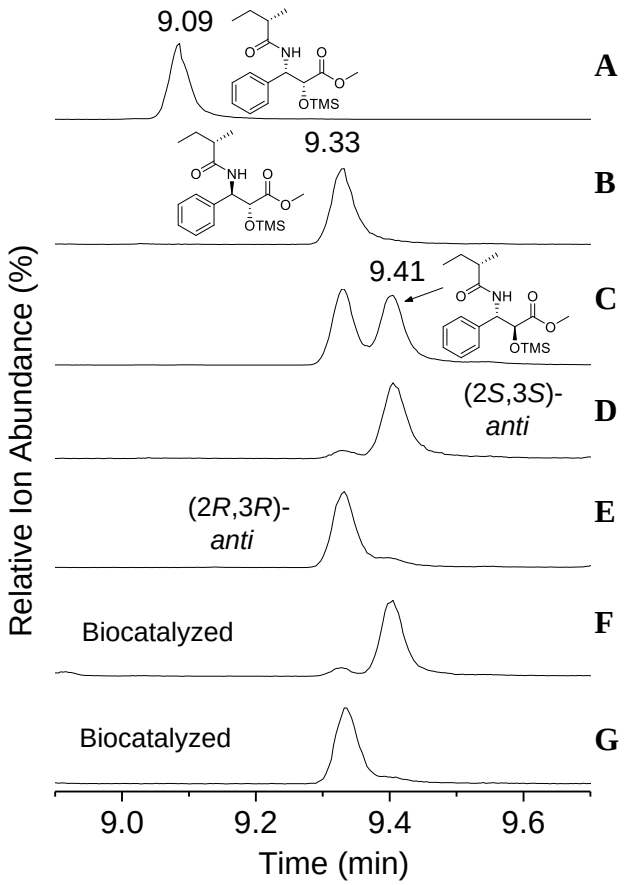

Figure. 3.6. GC/EI-MS extracted-ion chromatograms with *m*/*z* 106 ion monitoring of a chiral auxiliary derivative of A) authentic (2*R*,3*S*)-*syn*-phenylisoserine (Bachem); B) authentic (2*R*,3*R*)-*anti*-phenylisoserine (Chem Impex); C) *anti*-phenylisoserine enantiomers synthesized from authentic racemic 3-phenylglycidate;[42,43] D) (2*S*,3*S*)-*anti*-phenylisoserine synthesized from (2*S*,3*R*)-3-phenylglycidate (**14aa**); E) (2*R*,3*R*)-*anti*-phenylisoserine made from (2*R*,3*S*)-3-phenylglycidate (**14ab**); F) biocatalyzed (2*S*,3*S*)-*anti*-phenylisoserine made from (2*S*,3*R*)-3-phenylglycidate substrate (**14aa**); and G) biocatalyzed (2*R*,3*R*)-*anti*-phenylisoserine made from (2*R*,3*S*)-3-phenylglycidate substrate (**14ab**). Note, isoserines in *Panels C*, *D*, and *E*, were made from the corresponding glycidates by nucleophilic addition of NH_4OH.

By comparison, the chiral derivatives of the products biocatalyzed by *Tc*PAM from (2*R*,3*S*)-3-phenylglycidate (**14ab**, 90% *ee*) showed that (2*S*)-*anti*-phenylserine was the major product at only 76% relative abundance with the (2*R*)-*syn*-phenylserine present at 9% abundance (**Figure. 3.5**D). The (2*R*)-*syn*-phenylserine is formed from (2*R*,3*S*)-3-phenylglycidate (**14ab**) following a mechanism similar to that for the formation of the (2*S*)-*syn*-isomer via an oxiranone intermediate, (*S*)-3-((*S*)-hydroxy(phenyl)methyl)oxiran-2-one (**22ab**) before being aminated at the C_α (**Figure.**

3.7D and **Figure. 3.9**B). It was interesting to find that *Tc*PAM converted the 5% (2*S*,3*R*)-3-phenylglycidate impurity in the substrate to (2*R*)-*anti*-phenylserine at 15% relative abundance. The latter is compared to the 2% relative abundance of the (2*S*)-*anti*-phenylserine made from the 4% (2*R*,3*S*)-3-phenylglycidate impurity in the previous assay. These results suggested that *Tc*PAM has a stereospecific preference for (2*S*,3*R*)-3-phenylglycidate over the (2*R*,3*S*)-enantiomer.

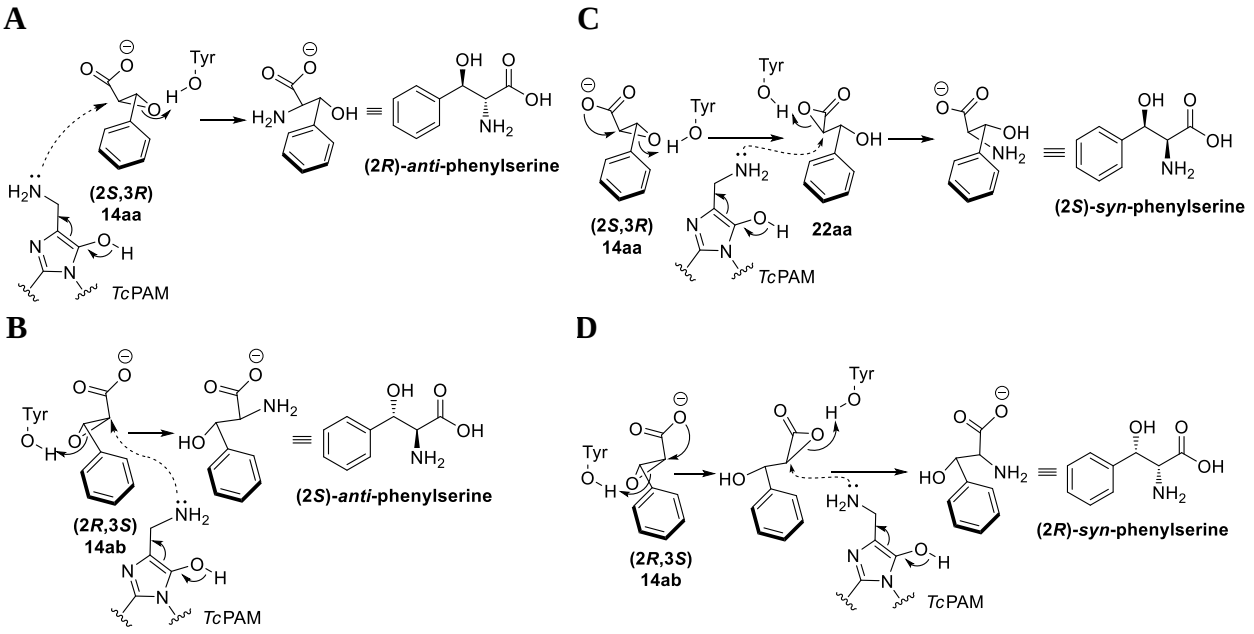

Figure. 3.7. Absolute stereoconfiguration of biocatalyzed phenylserine produced from A) (2*S*,3*R*)-3-phenylglycidate (**14aa**); and B) (2*R*,3*S*)-3-phenylglycidate (**14ab**). Proposed mechanism for the formation of C) (2*S*)-*syn*-phenylserine from **14aa**; and D) (2*R*)-*syn*-phenylserine from **14ab** through intramolecular carboxylate assisted oxiranone formation followed by amination at C_α by MIO-NH_2.

Incubating the enantioenriched 3-phenylglycidates with 2 M NH_4OH showed that nonenzymatic, regioselective ring-opening took place predominantly (82%) at the β-carbon (**Figure. 3.21**), producing phenylisoserine as the major product. This result demonstrated that nucleophilic attack on phenylglycidate occurs inherently at the more electropositive benzylic carbon (C_β). In contrast, *Tc*PAM used (2*S*)-styryl-α-alanine as an amine donor and catalyzed the amination of enantiopure 3-phenylglycidates predominantly at C_α to produce phenylserine. It is

worth noting, in its natural reaction, *Tc*PAM transfers the amino group from the NH_2-MIO adduct equally to both C_α and C_β of cinnamate to make α- and β-amino acids. However, with 3-phenylglycidates, amination is precluded at C_β, resulting in *Tc*PAM converting (2*S*,3*R*)-3-phenylglycidate (**14aa**) and (2*R*,3*S*)-3-phenylglycidate (**14ab**) to small amounts of (2*S*,3*S*)-*anti*-phenylisoserine (3%) (**Figure. 3.6**F), and (2*R*,3*R*)-*anti*-phenylisoserine (1%) (**Figure. 3.6**G), respectively.

3.3.4 Probing the Formation of the *Anti*- and *Syn*-Phenylserines using Computational Docking.

Protein-ligand computational docking studies were performed to explain the formation of *syn*-phenylserine isomers (minor product) biocatalyzed by *Tc*PAM. The crystal structure of *Tc*PAM in complex with cinnamate [PDB: 3NZ4] was used to model structures of (2*S*,3*R*)- (**14aa**) and (2*R*,3*S*)-3-phenylglycidate (**14ab**) and their oxiranones (*R*)-3-((*R*)-hydroxy(phenyl)methyl)oxiran-2-one (**22aa**) and (*S*)-3-((*S*)-hydroxy(phenyl)methyl)oxiran-2-one (**22ab**) into the *Tc*PAM active site using AutoDock Vina by the method described in Section **2.2.15** of this thesis.[44]

3.3.4.1 Computational Docking of Intermediates Leading to *Anti*-phenylserines.

Lowest energy docked conformations of 3-phenylglycidate enantiomers producing anti-phenylserines has been discussed in Section **2.3.11** of this thesis. The lowest energy docked conformation of the (2*S*,3*R*)-3-phenylglycidate (**14aa**) inside the active site of *Tc*PAM hinted that the carboxylate oxygen could adopt a bidentate salt-bridge with Arg 325 (**Figure. 3.8**A).[29] The glycidate oxygen was within a hydrogen bonding distance from the catalytic Tyr80 residue that usually functions as a general acid/base during the α/β-isomerization of phenylalanine catalyzed by *Tc*PAM. We hypothesize that Tyr80 acts as a general acid with the glycidates to promote

protonation-initiated ring opening of the epoxide during the amination at the C_α to produce the major biocatalyzed product, (2*R*)-*anti*-phenylserine. Notably, in the docking model, C_α of the glycidate substrate is positioned close to the NH_2-MIO nitrogen (**Figure. 3.8**A), and this modeled geometry is spatially consistent for S_N2 nucleophilic attack by the amino group at C_α of the glycidate.

Similarly, a low energy binding conformation of the (2*R*,3*S*)-3-phenylglycidate (**14ab**) substrate was calculated by AutoDock Vina limited to the active site cavity of *Tc*PAM.[29,44] As shown for the antipode (**14aa**) of **14ab** modelled within *Tc*PAM, the carboxylate purportedly can form a salt-bridge interaction with Arg325, and the glycidate oxygen of **14ab** is placed proximate to Tyr322 residue in a projected hydrogen bonding contact, facilitating epoxide ring-opening during the S_N2 amination step to produce (2*S*)-*anti*-phenylserine (**Figure. 3.9**A), in this case, as the major biocatalyzed product.

3.3.4.2 Computational Docking Intermediates on the Pathway to *Syn*-Phenylserines.

We hypothesized that the (2*S*)-*syn*-phenylserine was produced during *Tc*PAM catalysis through a (*R*)-3-((*R*)-hydroxy(phenyl)methyl)oxiran-2-one (**22aa**) intermediate made by an intramolecular carboxylate-assisted ring-opening of the glycidate. To provide some insight on this proposal, a low-energy docking conformation of the (*R*)-3-((*R*)-hydroxy(phenyl)methyl)oxiran-2-one (**22aa**) intermediate inside the *Tc*PAM active site was calculated using the AutoDock Vina program.[44] Similar to the other modelled phenylpropanoid structures shown herein, the oxiranone (O=C-O) functional group is placed into a salt-bridge complex with Arg325 (**Figure. 3.8**B). The calculated low-energy pose places the oxiranone oxygen and the hydroxyl group close to the Tyr80 residue (**Figure. 3.8**B) and C_α of the oxiranone close to the NH_2-MIO nitrogen. This docking pose suggests that the Tyr80 residue can potentially facilitate the transition of the hydroxy oxiranone

intermediate to access the (2*S*)-*syn*-phenylserine isomer directly from intermediate **22aa** through proton-transfer steps and S_N2 attack of the NH_2-MIO at the C_α (**Figure. 3.8**B).

Likewise, (*S*)-3-((*S*)-hydroxy(phenyl)methyl)oxiran-2-one (**22ab**) is proposed as an intermediate to the minor product (2*R*)-*syn*-phenylserine made analogous to **22aa**. AutoDock Vina[44] calculated a low-energy binding pose for **22ab** in complex with *Tc*PAM. While the antipode **22ab** was modeled in the active site as the mirror image, it made binding interactions similar to those made by **22aa**. The oxiranone formed a salt bridge with Arg325, an oxiranone oxygen is near Tyr80, and the hydroxyl group is positioned close to Tyr322, the latter two interactions likely indicating catalytic hydrogen-bonding interactions. The docked conformation also placed C_α near the nitrogen atom of the NH_2-MIO priming the mechanism for favorable S_N2 attack at the C_α thus forming the (2*R*)-*syn*-phenylserine(**Figure. 3.9B**).

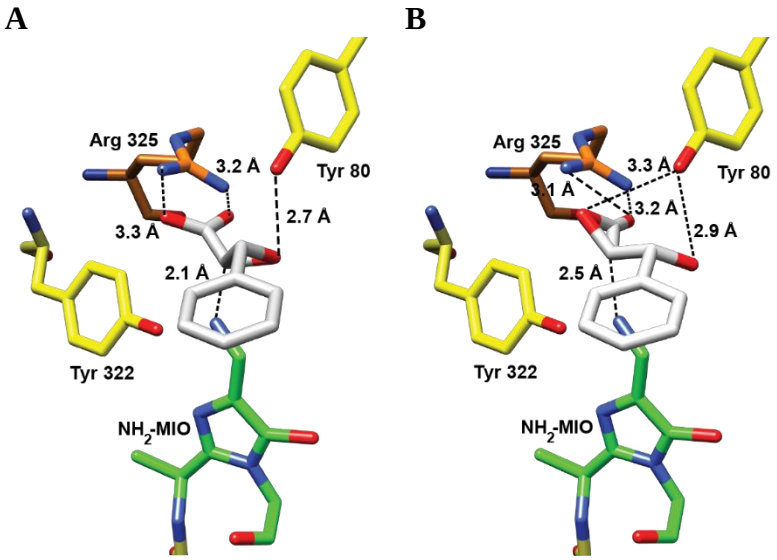

Figure. 3.8. A) Lowest energy binding conformations of A) (2*S*,3*R*)-3-phenylglycidate (**14aa**) (light-grey sticks); and B) (*R*)-3-((*R*)-hydroxy(phenyl)methyl)oxiran-2-one (**22aa**) (light grey sticks) are shown at the center of the image inside the *Tc*PAM active site. The residues shown here include a catalytic Tyr80 (yellow sticks), a putative catalytic Tyr322 (yellow sticks), binding contact Arg325 (orange sticks), and the methylidene imidazolone (MIO) moiety (green sticks). Heteroatoms are colored red for oxygen and blue for nitrogen. The images were produced with UCSF Chimera,[45] and the docking conformations were generated with AutoDock Vina[44] from *Tc*PAM crystal structure (PDB code 3NZ4).

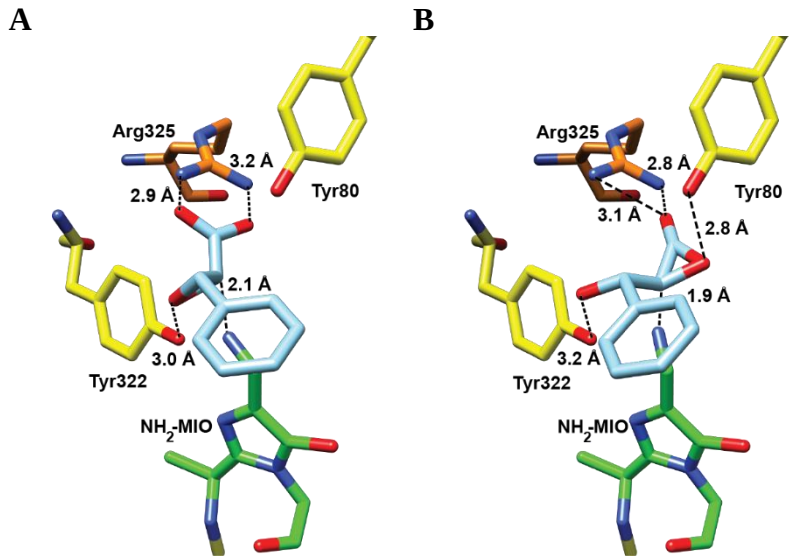

Figure. 3.9. A) Lowest energy binding conformations of A) (2*R*,3*S*)-3-phenylglycidate (**14ab**) (light-grey sticks); and B) (*R*)-3-((*R*)-hydroxy(phenyl)methyl)oxiran-2-one (**22ab**) (light grey sticks) are shown at the center of the image inside the *Tc*PAM active site. The residues shown here include a catalytic Tyr80 (yellow sticks), a putative catalytic Tyr322 (yellow sticks), binding contact Arg325 (orange sticks), and the methylidene imidazolone (MIO) moiety (green sticks). Heteroatoms are colored red for oxygen and blue for nitrogen. The images were produced with UCSF Chimera,[45] and the docking conformations were generated with AutoDock Vina[44] from *Tc*PAM crystal structure (PDB code 3NZ4).

3.3.5 Proposed Mechanism and Derivation of the Kinetic Equation.

A two-substrate ping-pong mechanism was proposed for *Tc*PAM to biocatalyze phenylserine from a glycidate and (2*S*)-styryl-α-alanine. In a typical ping-pong mechanism (**Scheme 3.3**, *inset 1*), substrate 1 ($\mathbf{S_1}$) binds to the enzyme (**E**) forming an enzyme-substrate complex ($\mathbf{ES_1}$). This is followed by subsequent release of product 1 ($\mathbf{P_1}$), which is usually a fragment of $\mathbf{S_1}$. The remainder of $\mathbf{S_1}$ stays covalently attached to the enzyme, resulting in a modified enzyme ($\mathbf{E^*}$). Next, substrate 2 ($\mathbf{S_2}$) binds and reacts with $\mathbf{E^*}$ and forms a modified enzyme-substrate complex ($\mathbf{E^*S_2}$) before releasing the product 2 ($\mathbf{P_2}$). The release of $\mathbf{P_2}$ restores $\mathbf{E^*}$ to **E**.[46] This is a non-sequential mechanism, thus $\mathbf{S_1}$ and $\mathbf{S_2}$ do not have to bind **E** before releasing $\mathbf{P_1}$. The name "ping-pong" refers to how the enzyme bounces back and forth from an $\mathbf{E^{(*)}S_n}$ state to its standard state ($\mathbf{E^*}$ or **E**).[47]

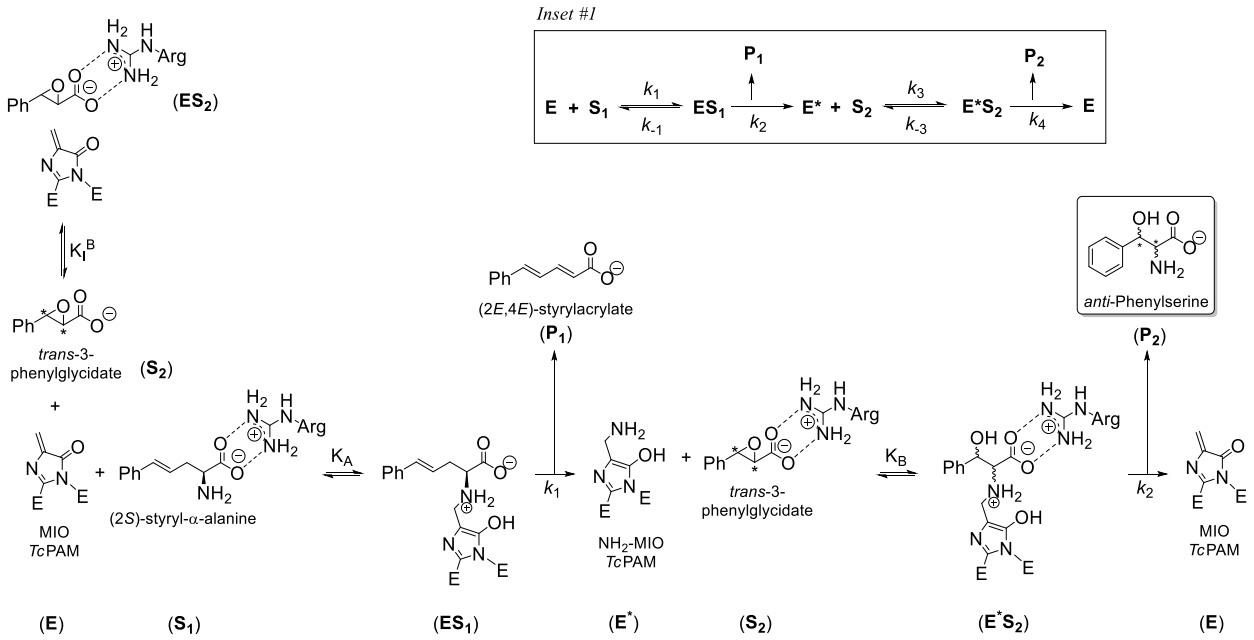

Scheme 3.3. Proposed mechanism of phenylserine biocatalysis. The pathway constituting E→Q depicts the two-substrate ping-pong mechanism where (2*S*)-styryl-α-alanine acts as the amino group donor. The pathway involving E→EB shows the competitive substrate inhibition at higher concentration (>1000 μM) of 3-phenylglycidate. *Inset 1* shows the scheme of a typical ping-pong mechanism.

Biocatalysis of phenylserine from 3-phenylglycidate, similarly, involves two substrates, (2*S*)-styryl-α-alanine (**S1**) and *trans*-3-phenylglycidate (**S2**) that bind the enzyme forming separate enzyme-substrate complexes to ultimately transfer an amino group from **S1** to **S2**. We hypothesized that the amino donor substrate, (2*S*)-styryl-α-alanine (**S1**) transfers its amino group to the MIO of *Tc*PAM (**E**) to form a covalent *N*-alkylated adduct (**ES1**). Crystal structures of analogous *N*-alkylated complexes of both α- and β-phenylalanine have been previously reported in a mechanistically similar *Tch*PAM (PDB:4C5R),[48] and a bacterial PAM (PDB:3UNV),[31] suggesting a common covalent mechanism for other MIO-enzymes, including *Tc*PAM. The nucleophilic α- or β-amino group of the substrate is found to attack the electrophilic methylene carbon of MIO to form this *N*-alkylated adduct. The enzyme-substrate complex (**ES1**) is proposed to proceed through an elimination step, removing H_β and the NH_2-MIO group (**E***) to release the first product, (2*E*,4*E*)-

styrylacrylate (**P₁**). In an earlier burst-phase kinetic study, the formation of **P₁** was monitored where the lifetime of the aminated *Tc*PAM (NH_2-MIO, **E***) was found to be long enough to transfer the amine group to exogenously supplied acceptor substrates.[32]

After the release of product **P₁**, **S₂** (*trans*-3-phenylglycidate) likely binds covalently to *Tc*PAM through an NH_2-MIO (**E*S₂**) adduct that ring-opens the glycidate regioselectively. This proposed covalent adduct is based on a previously reported crystal structure of a homologous MIO-AM (*Sg*TAM from *Streptomyces globisporus,* PDB:2RJR). *Sg*TAM formed a covalent *N*-alkyl bond between the MIO moiety and an intermediate derived from 3-(4′-fluorophenyl)glycidate analogous to that proposed for **E*S₂** (**Figure. 2.6**A).[49] To continue, our proposed mechanism proceeds through proton-transfer steps and deamination of the MIO releases the major biocatalyzed product *anti*-phenylserine (**P₂**) to regenerate the apo-enzyme **E** (**Scheme 3.3**). Assembly of this rational mechanistic pathway led us to derive a modified Michaelis-Menten kinetic equation to support the hypothesis (**Eq. 3.2**). The following rate equations were derived from the ping-pong mechanism.

$$V = \frac{E_t}{\frac{1}{f_1 k_1} + \frac{1}{f_2 k_2}} \qquad \text{Eq (3.1)}$$

where $f_1 = \frac{[ES_1]}{[E]+[ES_1]+[ES_2]}$ and $f_2 = \frac{[E^*S_2]}{[E^*]+[E^*S_2]}$

$$f_1 = \frac{\frac{[E][S_1]}{K_{S_1}}}{[E]+\frac{[E][S_2]}{K_I^{S_2}}+\frac{[E][S_1]}{K_{S_1}}} \qquad f_2 = \frac{\frac{[E^*][S_2]}{K_{S_2}}}{[E^*]+\frac{[E^*][S_2]}{K_{S_2}}}$$

$$f_1 = \frac{[S_1]}{K_{S_1}\left(1+\frac{[S_2]}{K_I^{S_2}}\right)+[S_1]} \qquad f_2 = \frac{[S_2]}{K_{S_2}+[S_2]}$$

Substituting f_1 and f_2 in Eq (3.1),

$$V = \frac{E_t}{\frac{\frac{1}{[S_1]k_1}}{K_{S_1}\left(1+\frac{[S_2]}{K_I^{S_2}}\right)+[S_1]} + \frac{\frac{1}{[S_2]k_2}}{K_{S_2}+[S_2]}}$$

$$V=\frac{E_t}{\frac{K_{S_1}\left(1+\frac{[S_2]}{K_I^{S_2}}\right)+[S_1]}{[S_1]k_1}+\frac{K_{S_2}+[S_2]}{[S_2]k_2}}$$

$$V=\frac{k_1k_2[S_1][S_2]E_t}{[S_2]k_2\left(K_{S_1}\left(1+\frac{[S_2]}{K_I^{S_2}}\right)+[S_1]\right)+k_1[S_1](K_{S_2}+[S_2])}$$

$$V=\frac{k_1k_2[S_1][S_2]E_t}{K_{S_1}\left(1+\frac{[S_2]}{K_I^{S_2}}\right)k_2[S_2]+K_{S_2}k_1[S_1]+(k_1+k_2)[S_1][S_2]}$$

$$V=\frac{\frac{k_1k_2}{k_1+k_2}[S_1][S_2]E_t}{K_{S_1}\left(1+\frac{[S_2]}{K_I^{S_2}}\right)\frac{k_2}{k_1+k_2}[S_2]+\frac{K_{S_2}k_1}{k_1+k_2}[S_1]+[S_1][S_2]}$$

$$V=\frac{V_{max}[S_1][S_2]}{K_M^{S_1}\left(1+\frac{[S_2]}{K_I^{S_2}}\right)[S_2]+K_M^{S_2}[S_1]+[S_1][S_2]}$$ …………………………………… Eq. (3.2)

where, $V_{max}=\frac{k_1k_2}{k_1+k_2}E_t$, $K_M^{S_1}=\frac{k_2K_A}{k_1+k_2}$ and $K_M^{S_2}=\frac{k_2K_{S_2}}{k_1+k_2}$.

Under the condition of constant $[S_2]$, $V=\frac{V_{max}[S_1]}{K_M^{S_1}\left(1+\frac{[S_2]}{K_I^{S_2}}\right)+\frac{K_M^{S_2}}{[S_2]}[S_1]+[S_1]}$

$$V=\frac{V_{max}[S_1]}{K_M^{S_1}\left(1+\frac{[S_2]}{K_I^{S_2}}\right)+\left(1+\frac{K_M^{S_2}}{[S_2]}\right)[S_1]}$$

$$V=\frac{V_{max}[S_1]/\left(1+\frac{K_M^{S_2}}{[S_2]}\right)}{K_M^{S_1}\left(1+\frac{[S_2]}{K_I^{S_2}}\right)\Big/\left(1+\frac{K_M^{S_2}}{[S_2]}\right)+[S_1]}$$

$$V=\frac{V_{max}^{app}[S_1]}{K_M^{app}+[S_1]}$$ ………………………………………………………………... Eq. (3.3)

Where $V_{max}^{app}=V_{max}\Big/\left(1+\frac{K_M^{S_2}}{[S_2]}\right)$ ………………………………………… Eq. (3.4)

and $K_M^{app}=K_M^{S_1}\left(1+\frac{[S_2]}{K_I^{S_2}}\right)\Big/\left(1+\frac{K_M^{S_2}}{[S_2]}\right)$ …………………………………… Eq. (3.5)

3.3.6 Kinetic Analyses.

The Michaelis-Menten kinetic parameters of *Tc*PAM for converting 3-phenylglycidate stereoisomers to phenylserine isomers were facilitated by a quantitative LC-ESI-MRM method following the derived rate equations (**Eq. 3.3** to **Eq. 3.5**). The rate of phenylserine production was measured against the concentration of the amino donor substrate, (2*S*)-styryl-α-alanine, at different fixed concentrations of the 3-phenylglycidate substrate (**14aa** or **14ab**). To dissect the mechanism of this sequential catalytic reaction pathway, the concentrations of both substrates, (2*S*)-styryl-α-alanine and phenylglycidate, were independently varied to evaluate their effects on the turnover rate of *Tc*PAM to make phenylserine. The concentration of (2*S*)-styryl-α-alanine was varied from 100 µM to 1mM for each of the four fixed concentrations of the 3-phenylglycidate (**14aa** or **14ab**) (100 µM, 500 µM, 1 mM, and 2 mM). For each particular concentration of the (2*S*,3*R*)-3-phenylglycidate (**14aa**), the V_{max}^{app} of *Tc*PAM was calculated at ~1 mM for (2*S*)-styryl-α-alanine (**Figure. 3.10**A and **Eq. 3.3**). The phenylserine production rate increased with increasing (2*S*,3*R*)-3-phenylglycidate (**14aa**) up to 1 mM, following a traditional two substrate ping-pong mechanism.[50,51] The phenylserine production was significantly reduced when the glycidate **14aa** was at 2.5 mM (**Figure. 3.10**A), suggesting a competitive substrate inhibition. Evidence of 3-phenylglycidate inhibition on *Tc*PAM catalysis was also supported by a Lineweaver-Burk plot showing convergent Y-intercepts for concentrations of **14aa** at 0.5 mM, 1 mM and 2.5 mM that indicates an unchanged V_{max}^{app} and increased K_{M}^{app} (**Figure. 3.10**C**)**, a hallmark of competitive inhibition.

A similar kinetic trend was observed for substrate **14ab**, where the V_{max}^{app} for *Tc*PAM was calculated at ~1 mM of (2*S*)-styryl-α-alanine for each of the four different concentrations of **14ab** (**Figure. 3.10**B**)**. **14ab** also inhibited the rate of phenylserine production at 2.5 mM (**Figure.**

3.10D). V_{max}^{app} of *Tc*PAM for (2*S*)-styryl-α-alanine (**S₂**), calculated from each kinetics plot measured at various fixed glycidate (**S₁**) concentrations, were plotted against the concentration of **S₁** (**14aa** or **14ab**) to calculate the intrinsic K_M and k_{cat} of *Tc*PAM for **14aa** or **14ab** at steady state (**Eq. 3.4**) (**Table 3.1**). The catalytic efficiency (k_{cat}/K_M) of *Tc*PAM for **14aa** appeared to be 1.3-fold higher than that for **14ab** largely due to the 1.5-fold higher k_{cat} for **14aa** over that for **14ab**. The inhibition constant (K_I) for each of the glycidate substrates were calculated from **Eq. 3.5** using a previously reported K_M value of (2*S*)-styryl-α-alanine (105 μM).[32] (2*S*,3*R*)-3-phenylglycidate (**14aa**) was found to have a K_I value lower than its (2*R*,3*S*)-enantiomer (**14ab**), indicating that **14aa** binds *Tc*PAM better than **14ab** during the phenylserine production, and likely affects the reaction turnover at higher concentrations by precluding the binding of the amino donor (2*S*)-styryl-α-alanine (**S₁**) to the active site.

In our previous study with racemic 3-phenylglycidate as the substrate, *Tc*PAM made a mixture of (2*R*)-*anti*- and (2*S*)-*anti*-phenylserine products, with the 2*R*-isomer predominating (68:32, >2 times more abundant), suggesting modest enantioselectivity. In this study, we wanted to assess whether the observed isomeric distribution of products resulted directly from enantioselectivity or was the stereoselectivity combined with enantiospecificity or other effects. Stereoisomeric phenylserines were made irreversibly by *Tc*PAM, which converted (2*S*,3*R*)-3-phenylglycidate to (2*R*)-*anti*-phenylserine as the primary product 1.3 times faster than it converted (2*R*,3*S*)-3-phenylglycidate to (2*S*)-*anti*-phenylserine. This moderate substrate specificity did not account fully for the ~2-fold enantioselectivity observed earlier for *Tc*PAM with the racemic 3-phenylglycidate substrate. Access to each glycidate enantiomer enabled us to calculate that the competitive inhibition constant (K_I) for (2*S*,3*R*)-3-phenylglycidate was 1.5-fold lower than that for the (2*R*,3*S*)-isomer. In this study, we revealed that a combination of kinetic (k_{cat}) and

thermodynamic (K_I) differences likely account for the 2-fold higher enantioselectivity for the (2*S*,3*R*)-glycidate substrate over its enantiomer in the racemate in the earlier study.

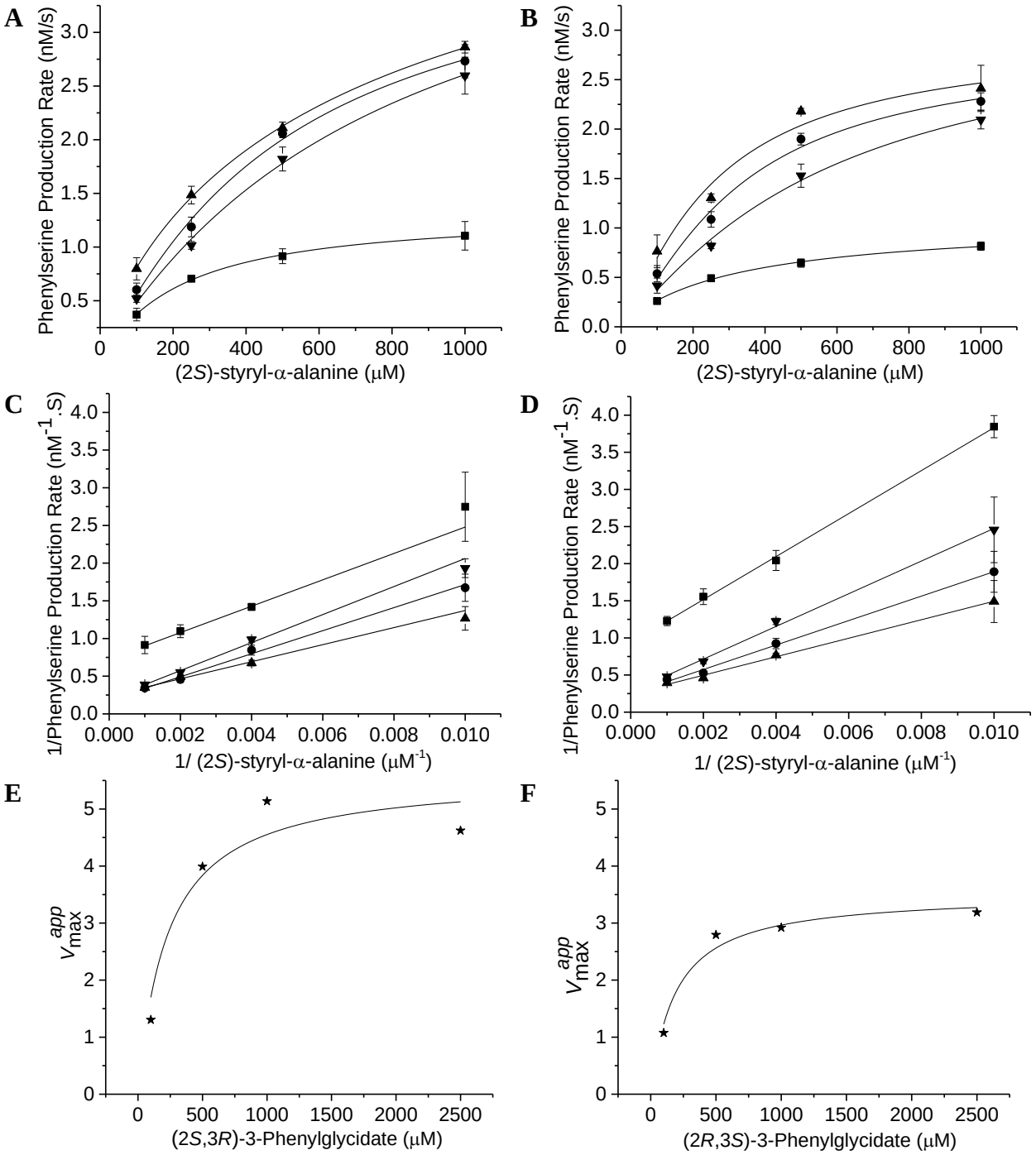

Figure. 3.10. Modified Michaelis-Menten plots for the turnover of A) (2*S*,3*R*)-3-phenylglycidate (**14aa**); and B) (2*R*,3*S*)-3-phenylglycidate (**14ab**) to their corresponding phenylserine at fixed concentration of the 3-phenylglycidate enantiomer. Double reciprocal Lineweaver-Burk plot of C) (2*S*,3*R*)-3-phenylglycidate (**14aa**); and D) (2*R*,3*S*)-3-phenylglycidate (**14ab**) to their corresponding phenylserine at fixed concentration of 3-phenylglycidate enantiomer [100 μM (■), 500 μM (●), 1000 μM (▲), and 2500 μM (▼)].E) Secondary plot of V_{max}^{app} (calculated from each plot of **Figure. 3.10**A vs [**14aa**]; and F) Secondary plot of v_{max}^{app} (calculated from each plot of **Figure. 3.10**B vs [**14ab**] to calculate the true K_M of the glycidate substrates.

Table 3.1. Kinetics of *Tc*PAM for turnover of 3-phenylglycidate enantiomers to phenylserine[a].

Entry	K_M (μM)	k_{cat} (min^{-1})	k_{cat}/K_M (M^{-1} s^{-1})	K_I[c] (μM)
14aa	230 (127)[b]	0.31 (0.04)	22.8	350
14ab	190 (54)	0.20 (0.01)	17.5	520

[a]In addition to phenylserine, **14aa** forms 3% phenylisoserine and **14ab** produces 1% phenylisoserine. [b]Standard deviation in parenthesis (n = 3). [c]Inhibition was observed at 2500 μM of **14aa** or **14ab**.

3.4 Conclusion

*Tc*PAM catalyzed the stereoselective amination of 3-phenylglycidate enantiomers through a sequential ping-pong aminotransfer reaction using (2*S*)-styryl-α-alanine as the amine donor and (2*S*,3*R*)- and (2*R*,3*S*)-3-phenylglycidate substrates as the amino group acceptors. Under non-enzymatic conditions, amine nucleophiles intrinsically cleave 3-phenylglycidates at the electropositive C_β-O bond to make phenylisoserine more abundantly over the phenylserine isomer.[42,43] In this study, the constraints of the *Tc*PAM catalytic environment forced the amino nucleophile resourced from (2*S*)-styryl-α-alanine to preferentially cleave the C_α-O bond of each *trans*-3-phenylglycidate enantiomer to produce a single antipode of *anti*-phenylserine preferentially. Nucleophilic attack at the C_β-O bond of the glycidates was prevented by *Tc*PAM, and only between 1% and 3%, relative abundance, of *anti*-phenylisoserines from each of the *trans*-3-phenylglycidate enantiomers was made. *Tc*PAM also turned over each *trans*-enantiomers of phenylglycidate to a single antipode *syn*-phenylserine (~10% relative abundance), which were evident as a mixture in an earlier study when racemic phenylglycidates were used as substrates.[29] Computational modeling of a proposed oxiranone intermediate, formed from an intramolecular carboxylate-assisted oxirane-cleavage, showed that the intermediate made binding contacts with active site residues similar to those made in other MIO enzymes with their natural substrates. The modeled structures were poised for amination by the NH_2-MIO to yield the *syn*-phenylserines.

This work provides an alternative biocatalytic route to access single antipode of *anti*-phenylserine starting from each enantiomer of *trans*-3-phenylglycidates. This work extends the transaminase activity of MIO-aminomutases to a new class of acceptor molecules to produce bi-functionalized hydroxy amino acids. This biocatalytic approach provides an easier access to the (2*R*)-*anti*-enantiomer of β-hydroxy-α-amino acids, which is difficult to obtain in large quantities otherwise and is highly expensive.[52] It also lays the foundation for further exploration into active site mutagenesis of the enzyme to achieve better enantioselectivity, and to accommodate structurally more complex aryl and aliphatic glycidates as well as expansion into other three membered heterocycles in the future.

3.5 Future Studies.

Wild-type *Tc*PAM was used to biocatalyze the production of arylserines and arylisoserines from 3-arylglycidate and (2*S*)-styryl-α-alanine in Assay Buffer. *Tc*PAM efficiently utilized (2*S*)-styryl-α-alanine as a sacrificial amino group donor to ring-open the arylglycidate substrate regioselectively at the C_α to produce arylserine predominantly. After the amino group transfer, (2*S*)-styryl-α-alanine is converted to (2*E*,4*E*)-styrylacrylate. Future studies will focus on these aspects.

Active Site Mutagenesis: Low-energy docking conformations suggested that (2*S*,3*R*)-3-phenylglycidate possibly forms a hydrogen bonding interaction with Tyr80 residue during the amination reaction. Similarly, computational docking conformations indicated that (2*R*,3*S*)-3-phenylglycidate is within the hydrogen bonding distance of Tyr322 residue that possibly plays a vital role during the protonation assisted amination reaction. Tyr80 is also reported to be responsible for the H_β elimination of (2*S*)-styryl-α-alanine to (2*E*,4*E*)-styrylacrylate,[32,34] thus, forming the essential NH_2-MIO adduct for transaminase activity. We envision that using an Y322F

mutant of *Tc*PAM through active site mutagenesis and employing it in phenylserine biocatalysis would prevent the (2*R*,3*S*)-3-phenylglycidate from getting converted to (2*S*)-*anti*-phenylserine. Hence, (2*R*)-*anti*-phenylserine could be stereoselectively biocatalyzed from a racemic mixture 3-phenylglycidate by ring-opening only the (2*S*,3*R*)-isomer.

In an earlier report on a *Taxus chinensis* phenylalanine aminomutase (*Tch*PAM),[18,20] active site mutagenesis (Q319M) altered the regioselectivity of amination reaction of arylacrylates by destabilizing the binding contacts of the carboxylate group of the substrate. This mutagenesis helped in stabilizing the intermediate formed from β-amination. Thus, enantiopure β-amino acids were synthesized from arylacrylates through one-step ammonia addition. We hypothesize that such mutagenesis would also affect the amination of 3-arylglycidate moiety and promote more β-amination reaction, producing arylisoserines.

Expansion into cis-Glycidates to Biocatalyze syn-Phenylserines and syn-Phenylisoserines: Due to the "backside" attack of the incoming nucleophile during an S_N2 reaction catalyzed by *Tc*PAM, the ring-opened, aminated product generated from a *trans*-glycidate made the anti-stereoconfiguration of the hydroxyamino acid predominantly. However, the majority of the naturally occurring and medicinally important compounds with an arylserine motif (**Figure. 2.7**) and those with an arylisoserine moiety have relative *syn*-stereoisomerism (**Figure. 2.9**). Hence, future efforts will focus on engineering *Tc*PAM, using site directed mutagenesis and guided by low-energy docking conformations, to accommodate a cisoid glycidate substrate to produce *syn*-hydroxyamino acids.

Accessing aliphatic β-Hydroxy-α-Amino acids: Non-proteinogenic amino acids containing an aliphatic side chain show a wide range of biological activities such as, cytotoxicity, anti-tumor, anti-fungal, and anti-HIV.[53] (2*R*)-*anti*-threonine, as an example, is present in callipeltins,

PCM1206, and plipastatin which showed potent anti-HIV activity and/or cytotoxicity.[52,54] (2*S*)-*anti*-3-hydroxy-leucine is a key component of several natural peptide antibiotics that include telomycin, azinothricin, citropeptin, variapeptin, and A83586C.[53,55] These aliphatic hydroxy amino acids likely also be accessed via the *Tc*PAM catalyzed transamination reactions from the corresponding alkyl glycidates.

Regenerating (2S)-Styryl-α-alanine Enzymatically. (2*S*)-Styryl-α-alanine acts as a sacrificial amine donor in this biocatalysis reaction and gets converted to (2*E*,4*E*)-styrylacrylate. The styrylacrylate byproduct can be easily extracted out of the aqueous reaction buffer with organic solvent. Recent descriptions in the literature show that a mutated phenylalanine ammonia lyase from *Petroselinum crispum* (*Pc*PAL) can add ammonia to (2*E*,4*E*)-styrylacrylate and regenerate (2*S*)-styryl-α-alanine.[24] This recycling event will significantly increase the applicability and turnover efficiency of the *Tc*PAM-assisted amination of 3-arylglycidates.

Exploring Aziridines and Thiiranes as Amino Group Acceptors: This transaminase activity of *Tc*PAM employing (2*S*)-Styryl-α-alanine as the amino group donor can likely be extended also to other acceptor molecules, such as aziridines and thiiranes. Amination of 3-phenylaziridine-2-carboxylic acid will produce 2,3-diamino-3-phenylpropanoic acid. This class of α,β-diamino acids are important structural units found in natural products,[56] peptide antibiotics,[57] and in medicinally valuable compounds.[58] *Tc*PAM assisted amination of 3-phenylaziridine-2-carboxylic acid analogues will provide an entry point to access these α,β-diamino acids.

Similarly, *Tc*PAM catalyzed amination of 3-phenylthiirane-2-carboxylic acid will produce 2-amino-3-mercapto-3-phenylpropanoic acid (also known as phenylcysteine) or its regioisomer, phenylisocysteine depending on the regioselectivity of the thiirane ring-opening. Phenylcysteines are known as metabolic sequester of acetaldehyde derived from ethanol oxidation in the blood

stream of chronic alcoholics and thus, reducing acetaldehyde toxicity by diverting it to urinary excretion pathways.[59] They have been found to lower the amount of ethanol-derived acetaldehyde by 40-60% in mice models. Phenylcysteines are also effectively used in Native Chemical Ligation (NCL) for the synthetic preparation of therapeutic peptides and protein targets.[60]

APPENDIX

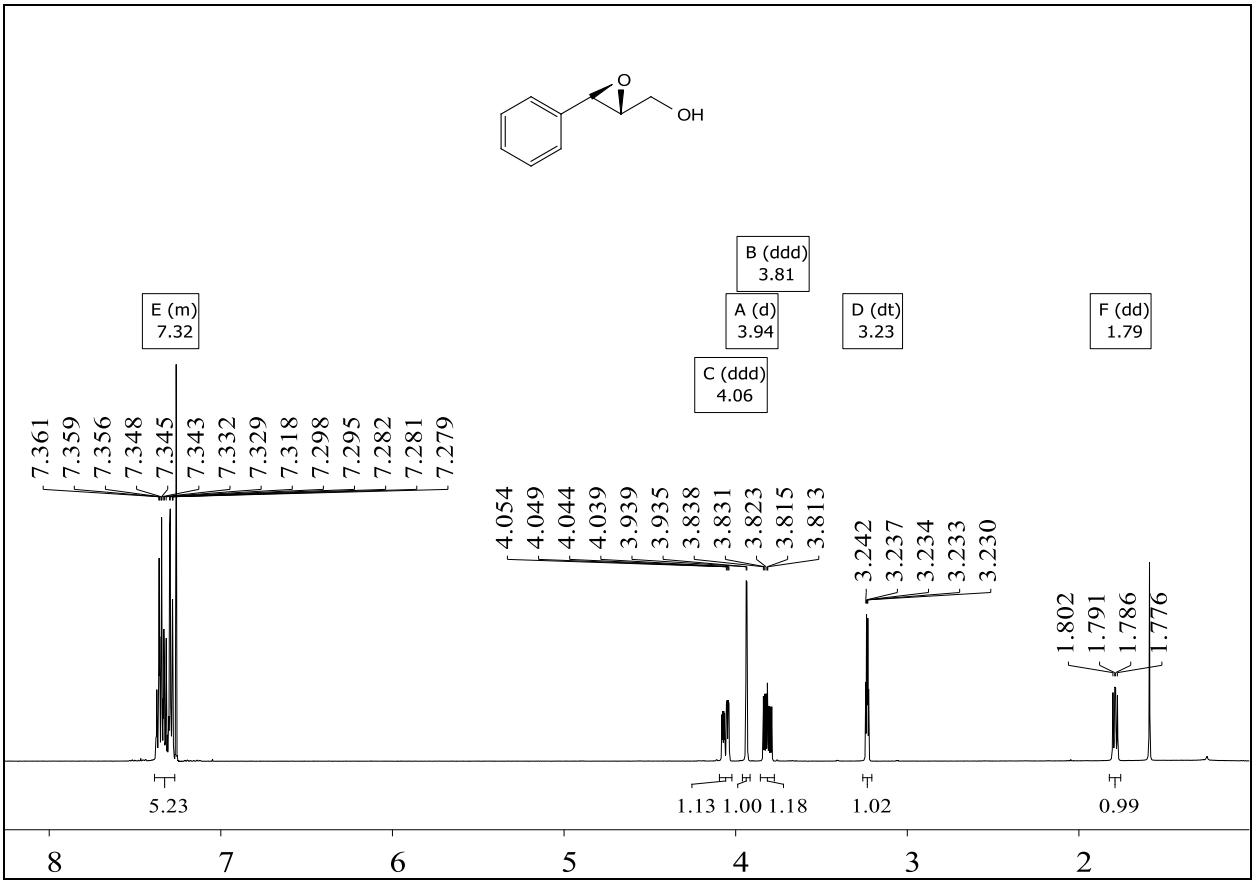

Figure. 3.11. Partial ^{1}H NMR (500 MHz, $CDCl_3$) spectra of (2*R*,3*R*)-3-Phenylglycidol (**21a**).

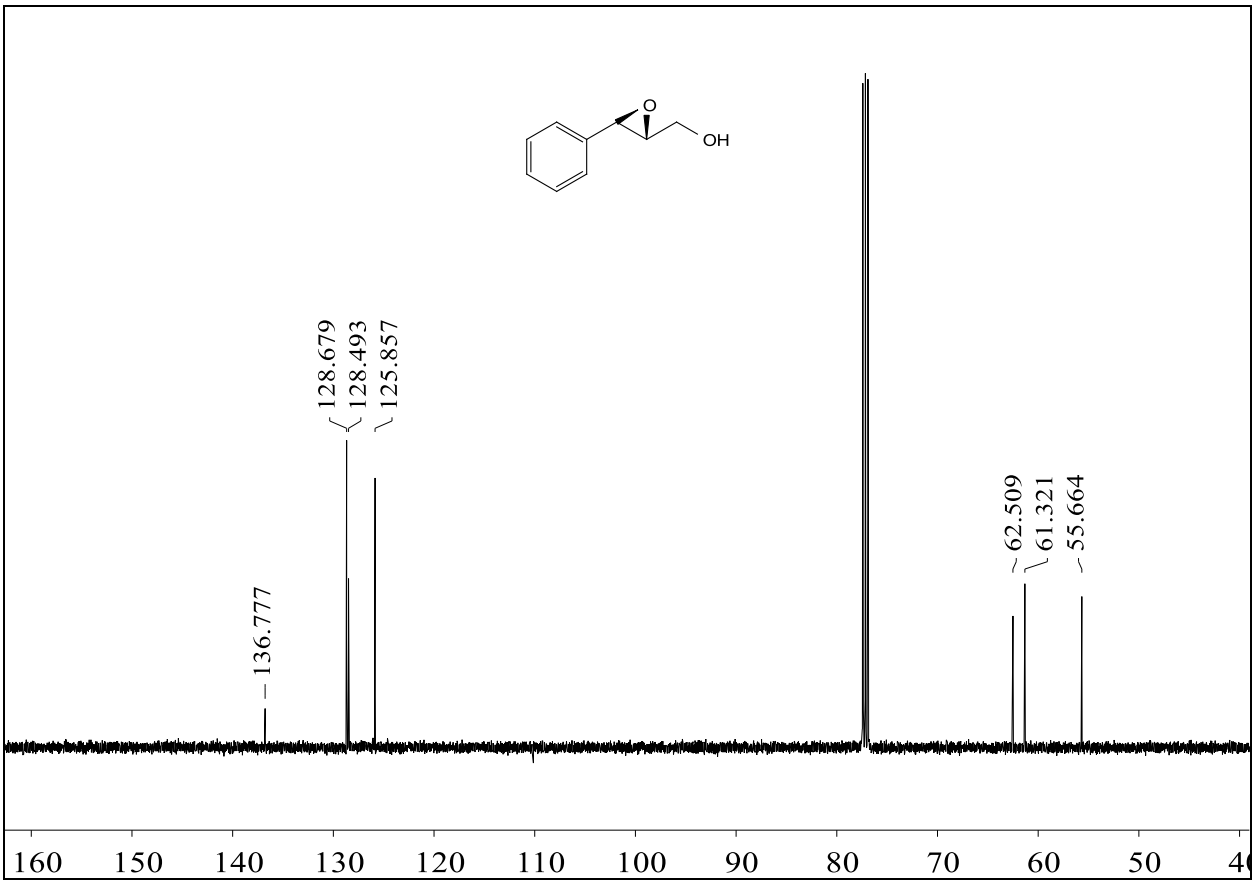

Figure. 3.12. Partial ^{13}C NMR (126 MHz, $CDCl_3$) spectra of (2*R*,3*R*)-3-Phenylglycidol (**21a**).

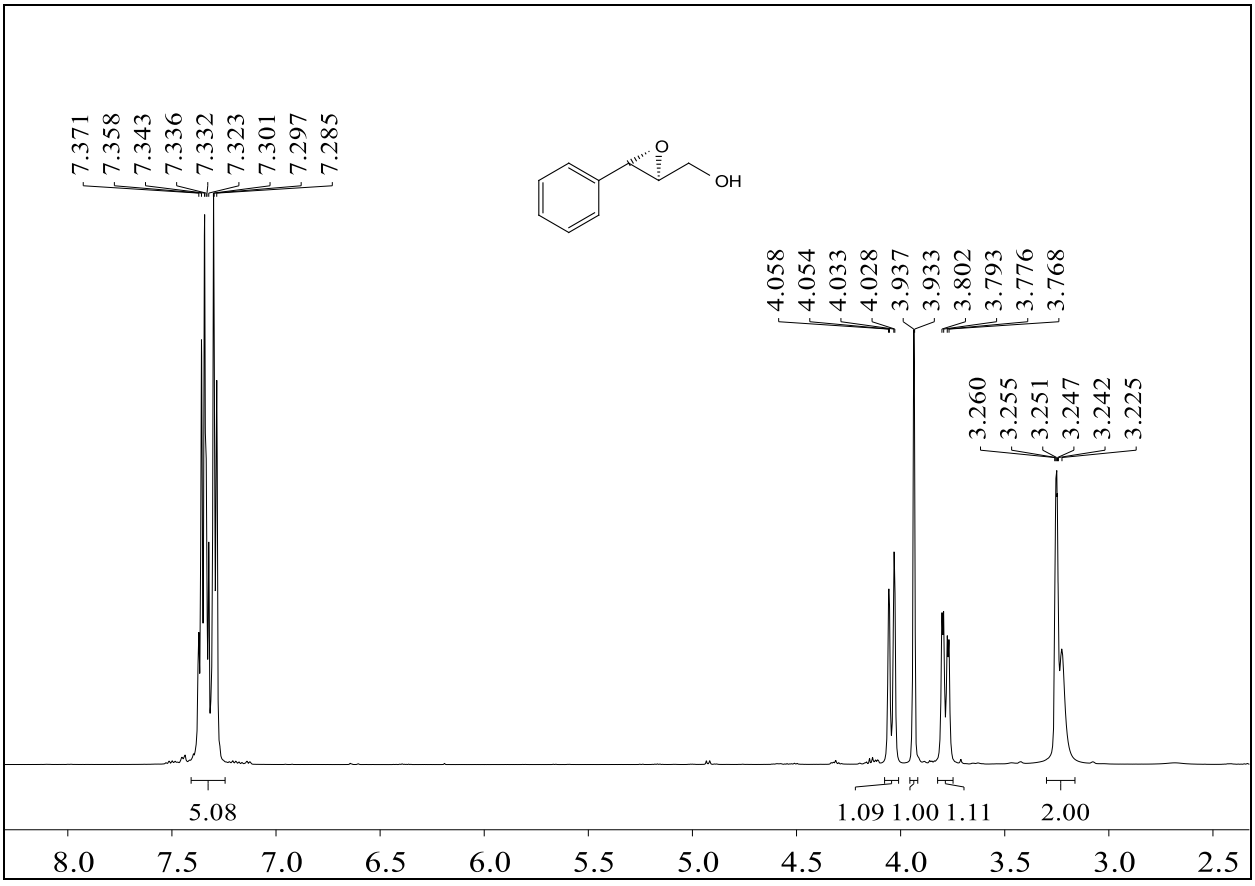

Figure. 3.13. Partial ^{1}H NMR (500 MHz, $CDCl_3$) spectra of (2*S*,3*S*)-3-Phenylglycidol (**21b**).

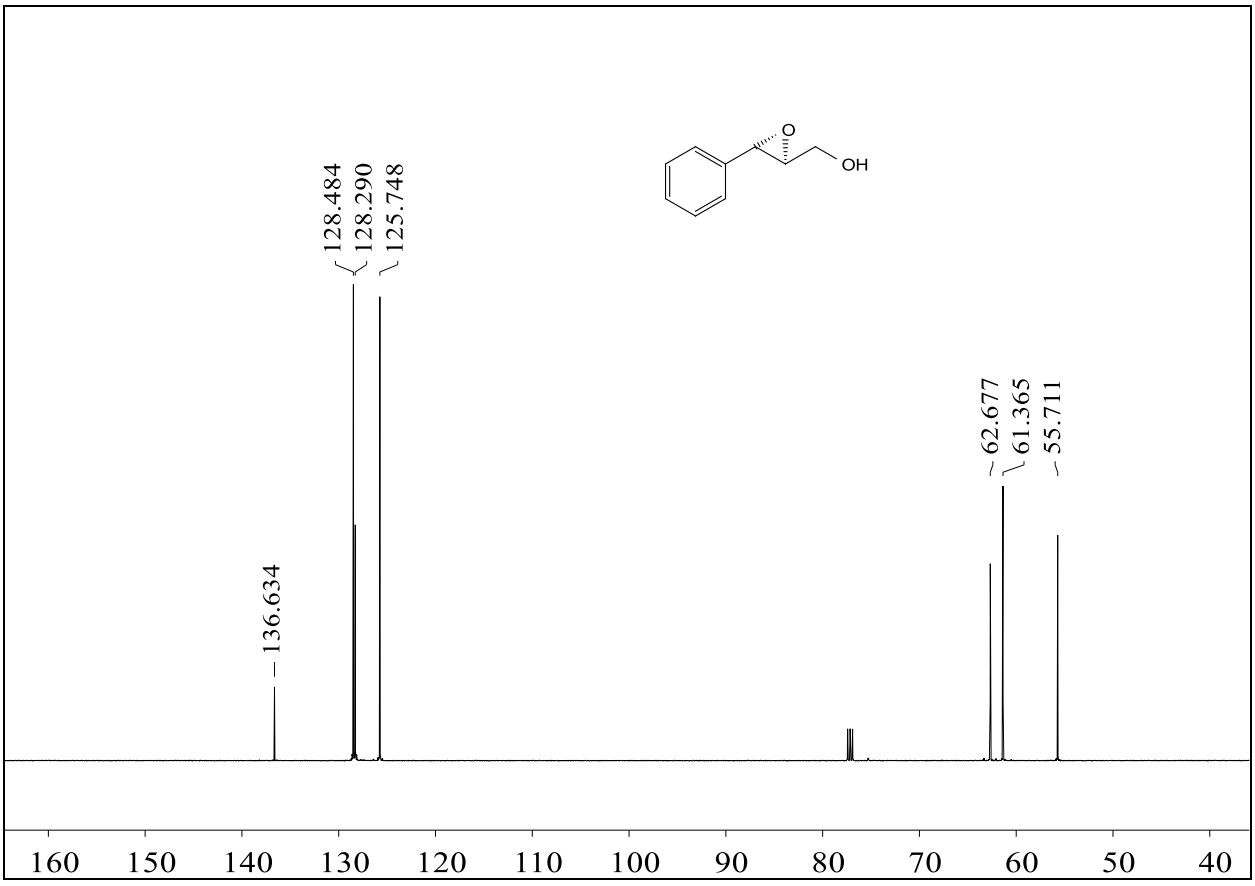

Figure. 3.14. Partial ^{13}C NMR (126 MHz, $CDCl_3$) spectra of (2*S*,3*S*)-3-Phenylglycidol (**21b**).

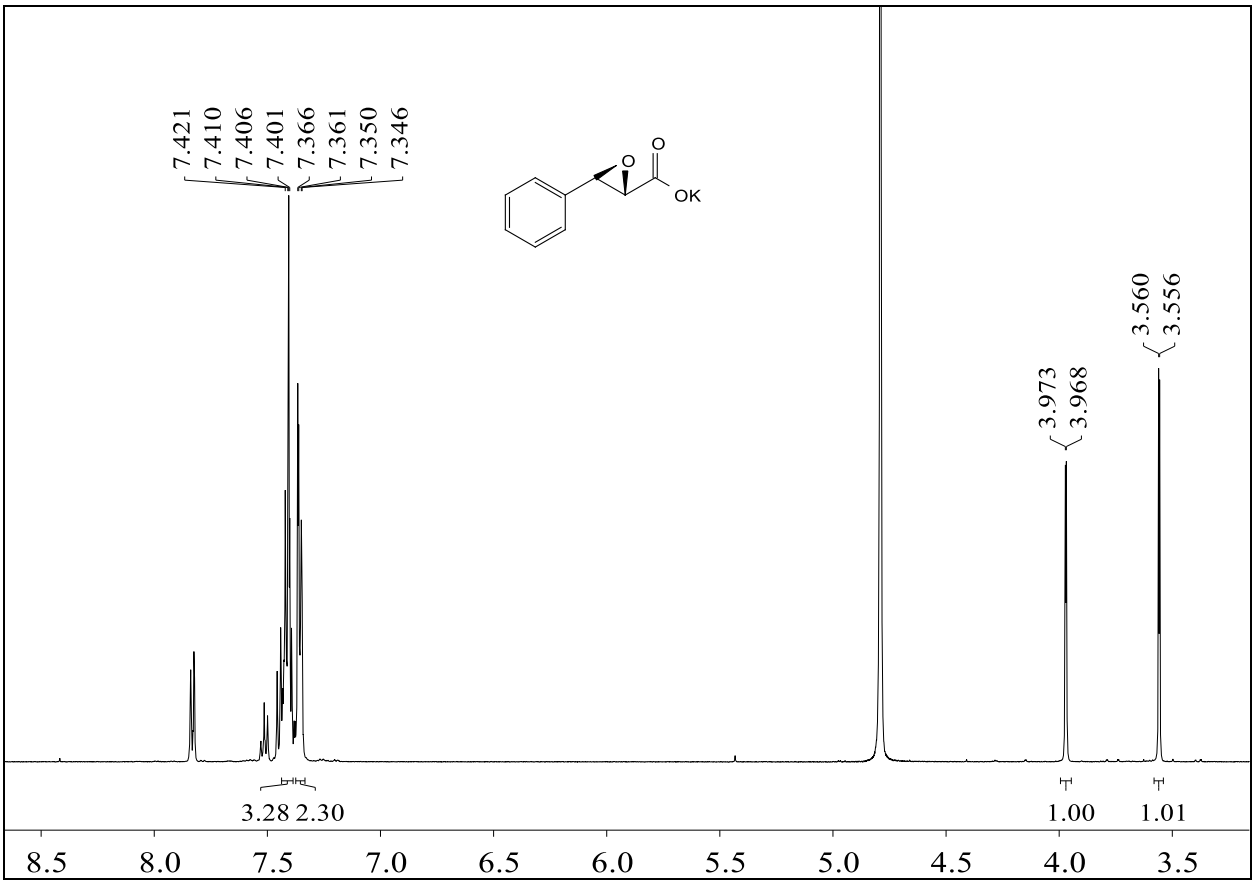

Figure. 3.15. Partial ^{1}H NMR (500 MHz, D_2O) spectra of Potassium (2*S*,3*R*)-3-Phenylglycidate (**14aa**).

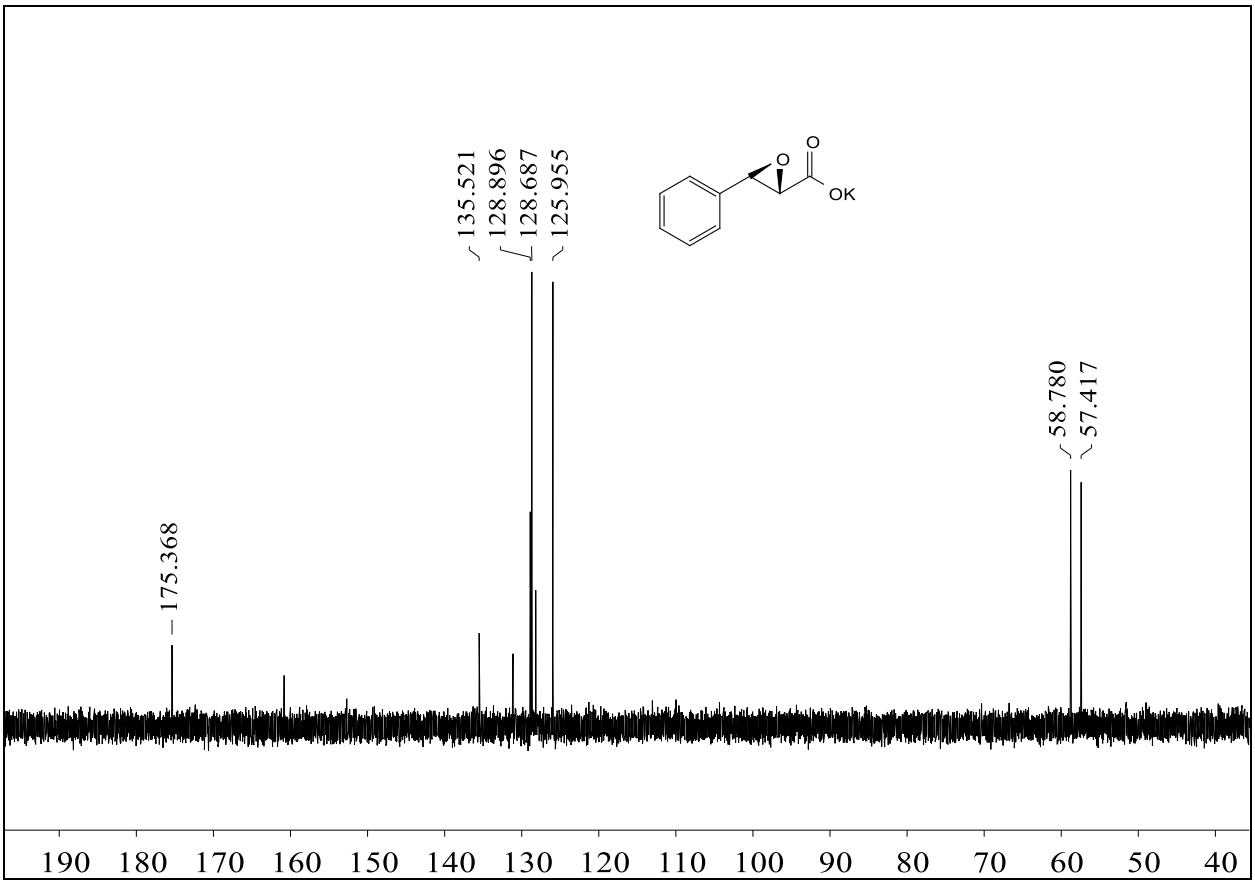

Figure. 3.16. Partial ^{13}C NMR (126 MHz, D_2O) spectra of Potassium (2*S*,3*R*)-3-Phenylglycidate (**14aa**).

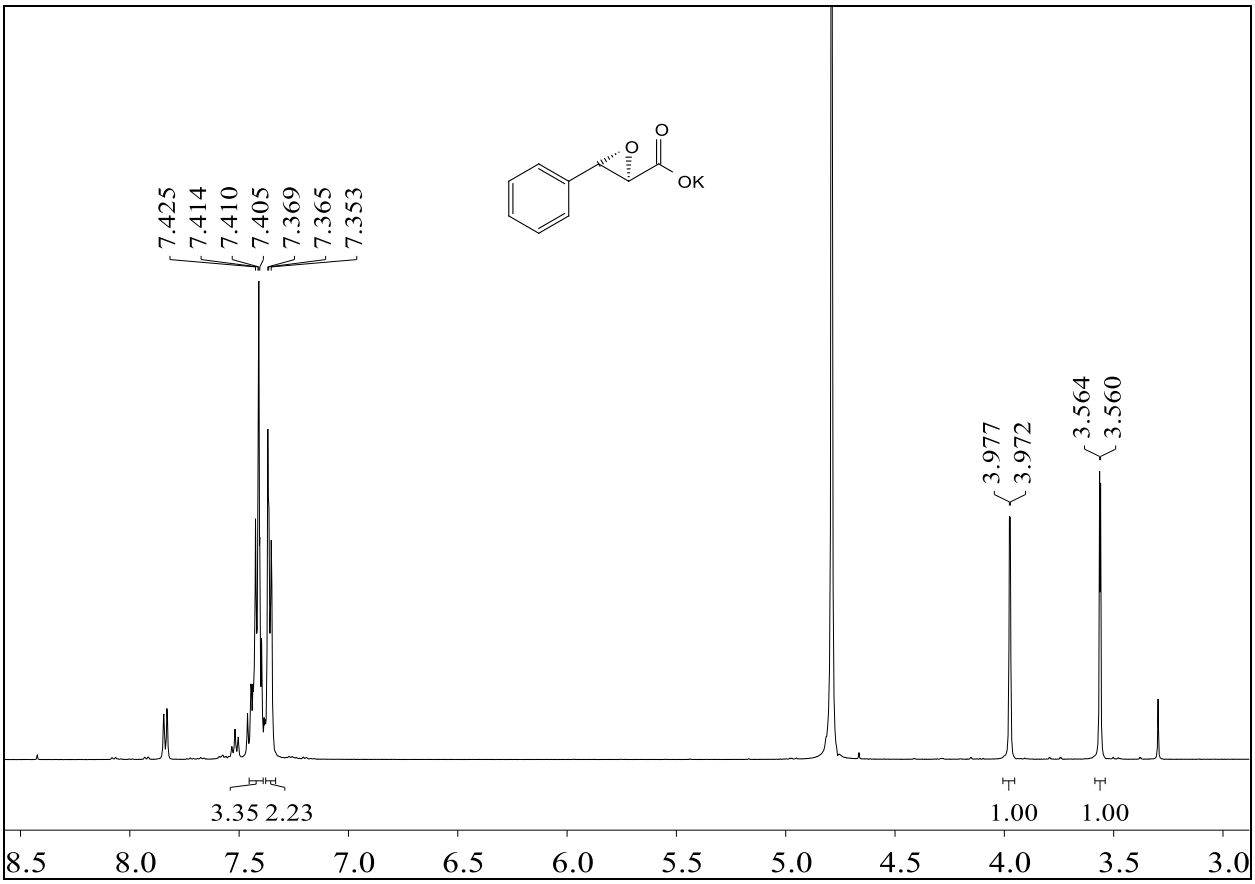

Figure. 3.17. Partial ^{1}H NMR (500 MHz, D_2O) spectra of Potassium (2*R*,3*S*)-3-Phenylglycidate (**14ab**).

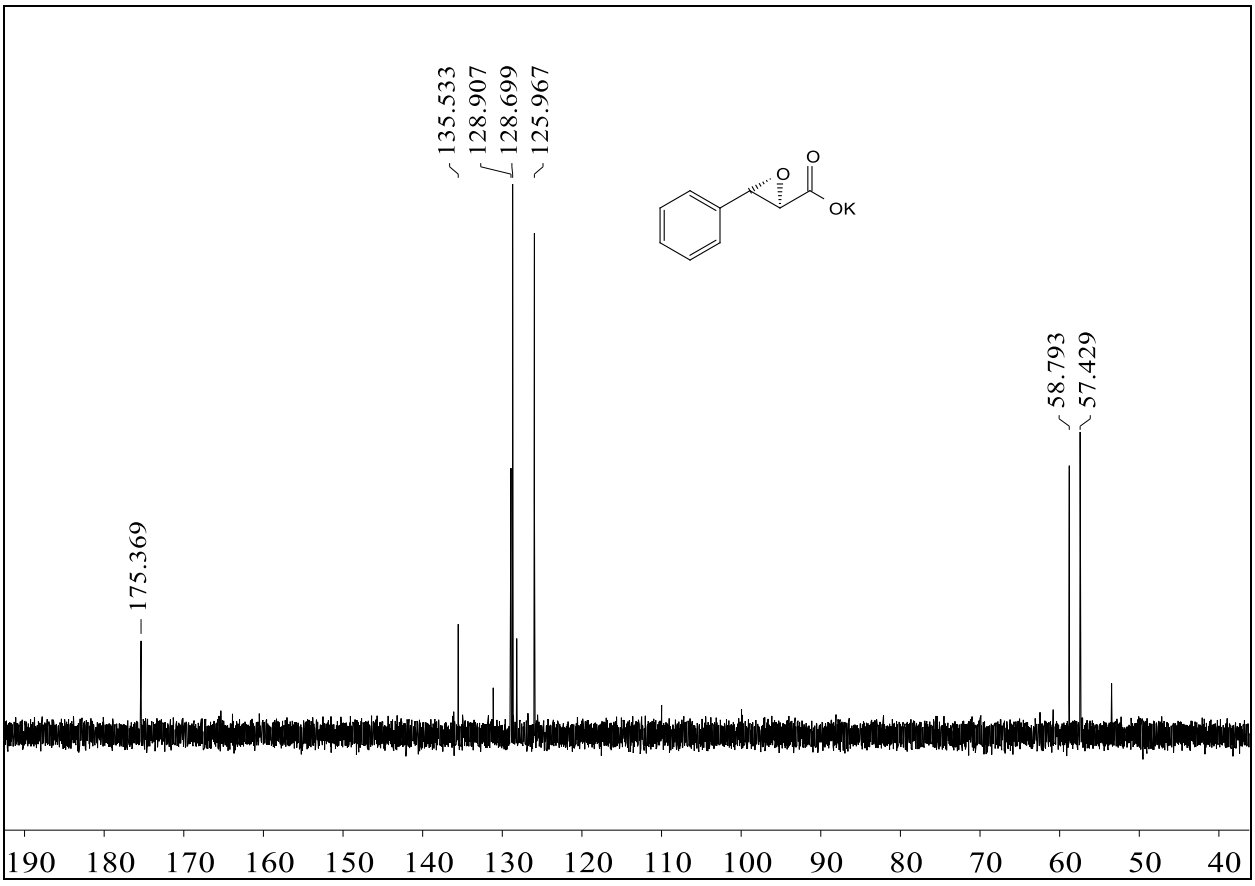

Figure. 3.18. Partial ^{13}C NMR (126 MHz, D_2O) spectra of Potassium (2*R*,3*S*)-3-Phenylglycidate (**14ab**).

GC/EI-MS Analysis of Phenylisoserine Diastereomers Derivatized as *O*-Trimethylsilyl *N*-[(2S)-2-Methylbutyryl] Methyl Esters

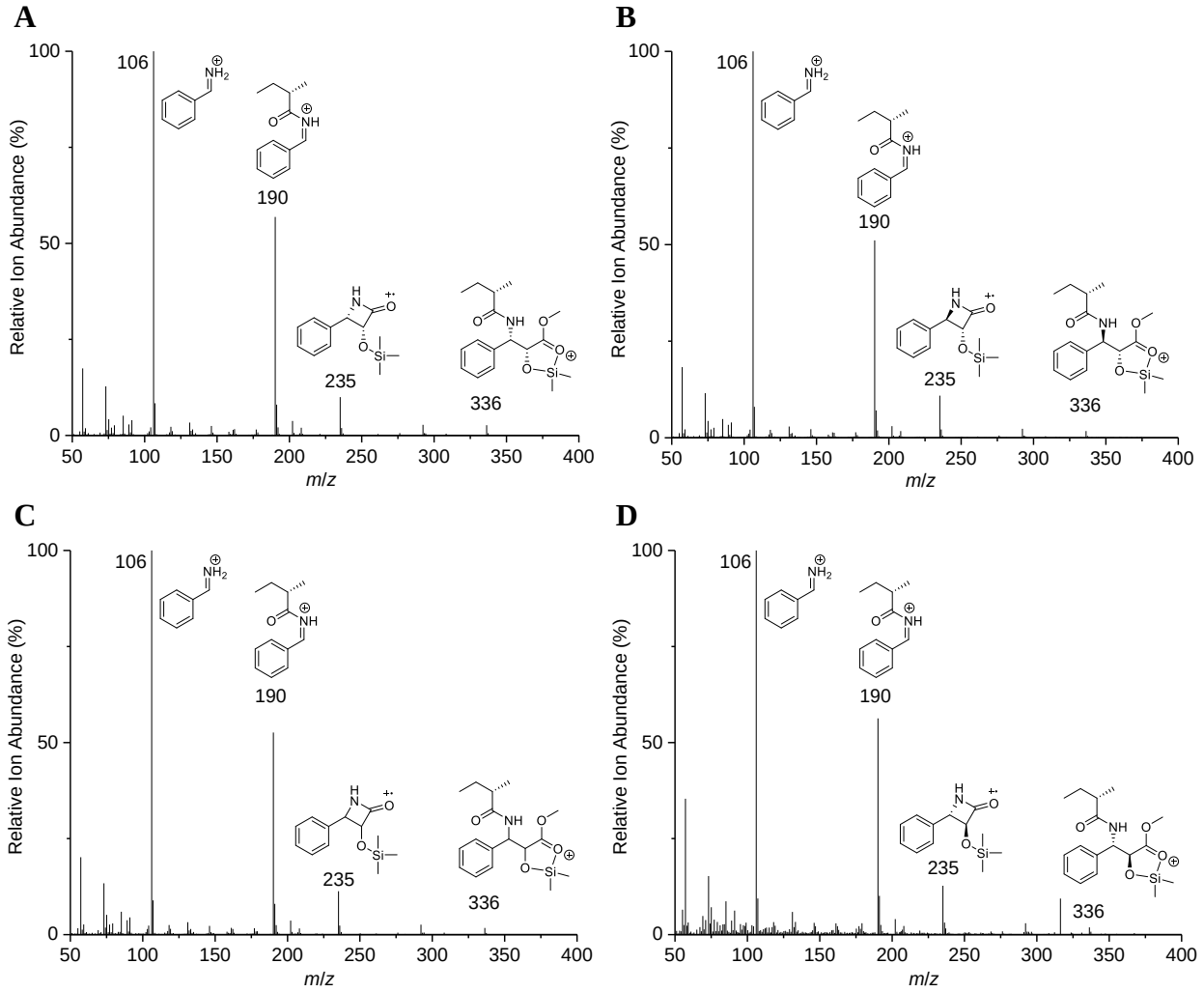

Figure. 3.19. GC/EI-MS spectra of A) authentic (2*R*,3*S*)-*syn*-phenylisoserine from Bachem (**6b**); B) authentic (2*R*,3*R*)-*anti*-phenylisoserine from ChemImpex C) derivatized *anti*-phenylisoserine enantiomers produced from authentic racemic 3-phenylglycidate; and D). derivatized (2*S*,3*S*)-*anti*-phenylisoserine (**16ac**) made from (2*S*,3*R*)-3-phenylglycidate (**14aa**) and NH_4OH. Each hydroxyamino acid was derivatized as their *O*-trimethylsilyl *N*-[(2*S*)-2-methylbutyryl] methyl ester. The molecular ion ($M^{\bullet+}$, *m*/*z* 351) was not observed.

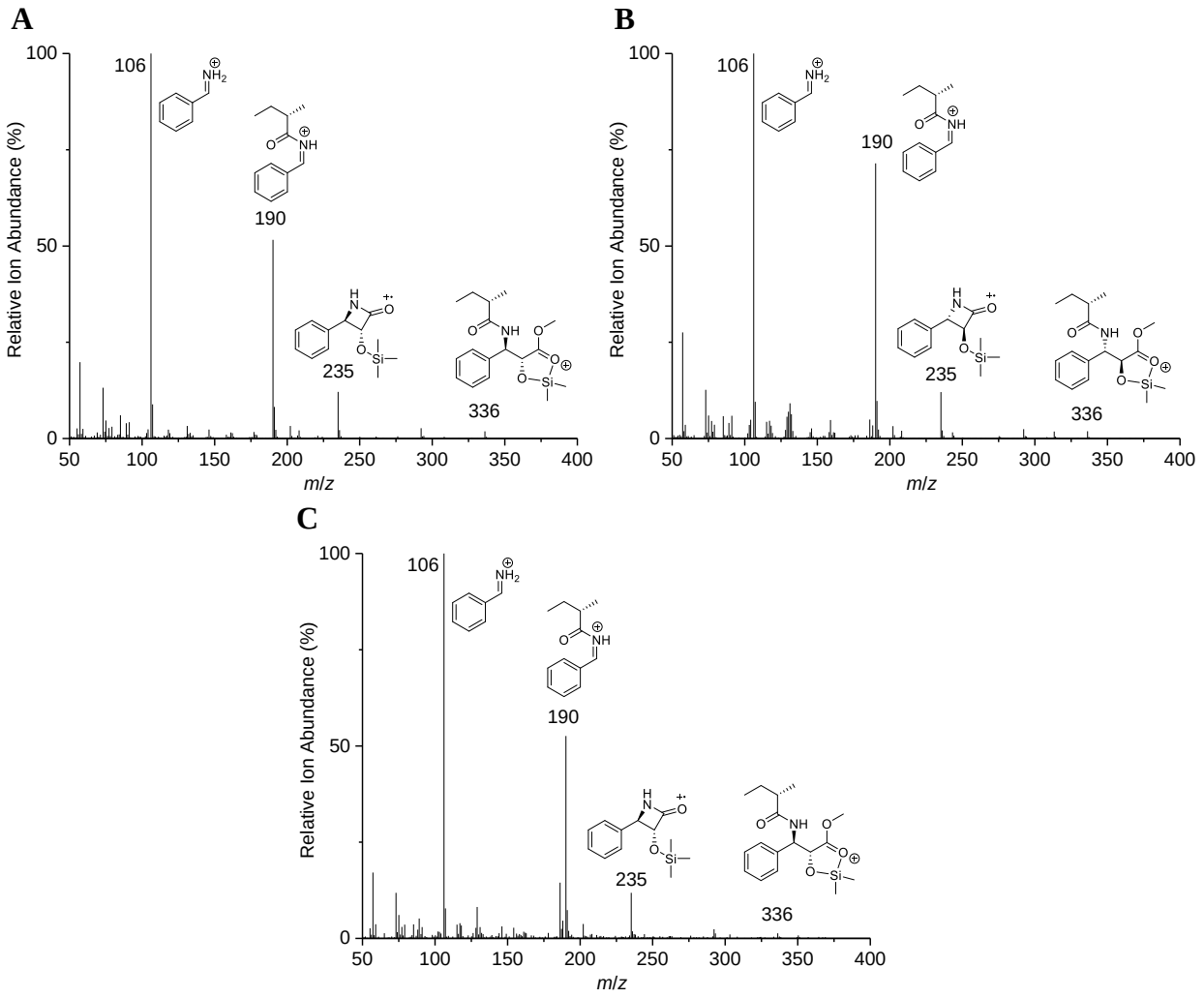

Figure. 3.20. GC/EI-MS spectra of A) derivatized (2*R*,3*R*)-*anti*-phenylisoserine (**16ad**) made from (2*R*,3*S*)-3-phenylglycidate (**14ab**) and NH_4OH B) biocatalyzed (2*S*,3*S*)-*anti*-phenylisoserine (**16ac**) made from (2*S*,3*R*)-3-phenylglycidate (**14aa**) by *Tc*PAM; and C) biocatalyzed (2*R*,3*R*)-*anti*-phenylisoserine (**16ad**) made from (2*R*,3*S*)-3-phenylglycidate (**14ab**) by *Tc*PAM. Each hydroxyamino acid was derivatized as their *O*-trimethylsilyl *N*-[(2*S*)-2-methylbutyryl] methyl ester. The molecular ion ($M^{\bullet+}$, *m*/*z* 351) was not observed.

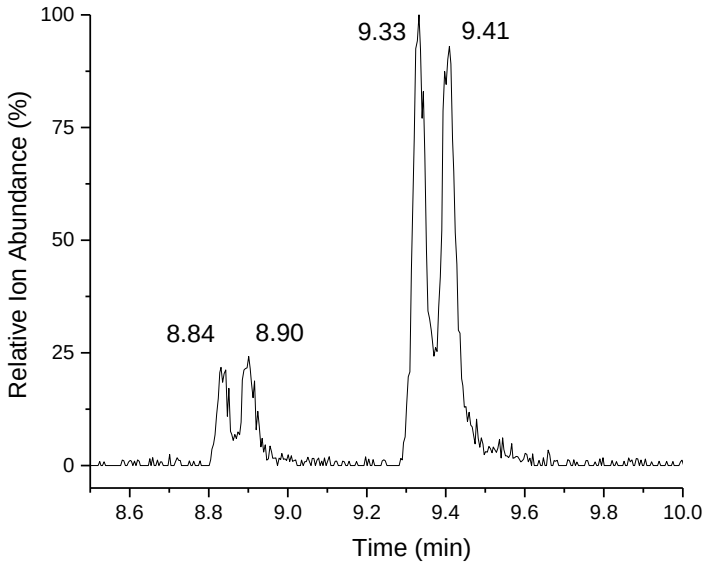

Figure. 3.21. Gas-chromatography/mass spectrometry extracted-ion chromatograms with *m*/*z* 336 ion monitoring of derivatized *anti*-phenylserine and *anti*-phenylisoserine enantiomers produced from NH_4OH assisted ring opening of authentic racemic 3-phenylglycidate. Peaks at 8.84 min and 8.90 min correspond to racemic *anti*-phenylserine (18%) produced from amination at the C_α, and peaks at 9.33 min and 9.41 min correspond to racemic *anti*-phenylisoserine produced from the amination at C_β.

REFERENCES

REFERENCES

1. Walker, K. D., and Floss, H. G. (1998) Detection of a Phenylalanine Aminomutase in Cell-Free Extracts of *Taxus brevifolia* and Preliminary Characterization of Its Reaction, *J. Am. Chem. Soc. 120*, 5333-5334.

2. Christenson, S. D., Liu, W., Toney, M. D., and Shen, B. (2003) A Novel 4-Methylideneimidazole-5-one-Containing Tyrosine Aminomutase in Enediyne Antitumor Antibiotic C-1027 Biosynthesis, *J. Am. Chem. Soc. 125*, 6062-6063.

3. Christianson, C. V., Montavon, T. J., Van Lanen, S. G., Shen, B., and Bruner, S. D. (2007) The Structure of L-Tyrosine 2,3-Aminomutase from the C-1027 Enediyne Antitumor Antibiotic Biosynthetic Pathway, *Biochemistry 46*, 7205-7214.

4. Huang, S.-X., Lohman, J. R., Huang, T., and Shen, B. (2013) A New Member of the 4-Methylideneimidazole-5-One-Containing Aminomutase Family From the Enediyne Kedarcidin Biosynthetic Pathway, *Proc. Natl. Acad. Sci. U S A 110*, 8069-8074.

5. Wanninayake, U., and Walker, K. D. (2013) A Bacterial Tyrosine Aminomutase Proceeds Through Retention or Inversion of Stereochemistry to Catalyze Its Isomerization Reaction, *J. Am. Chem. Soc. 135*, 11193-11204.

6. Yan, J., Aboshi, T., Teraishi, M., Strickler, S. R., Spindel, J. E., Tung, C.-W., Takata, R., Matsumoto, F., Maesaka, Y., McCouch, S. R., Okumoto, Y., Mori, N., and Jander, G. (2015) The Tyrosine Aminomutase TAM1 Is Required for β-Tyrosine Biosynthesis in Rice, *The Plant Cell 27*, 1265-1278.

7. Walter, T., King, Z., and Walker, K. D. (2016) A Tyrosine Aminomutase from Rice (*Oryza sativa*) Isomerizes (*S*)-α- to (*R*)-β-Tyrosine with Unique High Enantioselectivity and Retention of Configuration, *Biochemistry 55*, 1-4.

8. Davidson, V. L. (2010) 7.19 - Protein-Derived Cofactors In *Comprehensive Natural Products II* (Liu, H.-W., and Mander, L., Eds.), pp 675-710, Elsevier, Oxford.

9. Dressen, A., Hilberath, T., Mackfeld, U., Rudat, J., and Pohl, M. (2017) Phenylalanine Ammonia Lyase From *Arabidopsis thaliana* (*At*PAL2): A Potent MIO-Enzyme for the Synthesis of Non-Canonical Aromatic α-Amino Acids. Part II: Application in Different Reactor Concepts for the Production of (*S*)-2-Chloro-phenylalanine, *J. Biotechnol. 258*, 158-166.

10. Dressen, A., Hilberath, T., Mackfeld, U., Billmeier, A., Rudat, J., and Pohl, M. (2017) Phenylalanine Ammonia Lyase From *Arabidopsis thaliana* (*At*PAL2): A Potent MIO-Enzyme for the Synthesis of Non-Canonical Aromatic α-Amino Acids: Part I: Comparative Characterization to the Enzymes From *Petroselinum crispum* (*Pc*PAL1) and *Rhodosporidium toruloides* (*Rt*PAL), *J. Biotechnol. 258*, 148-157.

11. Lovelock, S. L., Lloyd, R. C., and Turner, N. J. (2014) Phenylalanine Ammonia Lyase Catalyzed Synthesis of Amino Acids by an MIO-Cofactor Independent Pathway, *Angew. Chem. Int. Ed. Engl. 53*, 4652-4656.

12. Langer, B., Langer, M., and Retey, J. (2001) Methylidene-Imidazolone (MIO) from Histidine and Phenylalanine Ammonia-Lyase, *Adv. Protein Chem. 58*, 175-214.

13. Jendresen, C. B., Stahlhut, S. G., Li, M., Gaspar, P., Siedler, S., Förster, J., Maury, J., Borodina, I., and Nielsen, A. T. (2015) Highly Active and Specific Tyrosine Ammonia-Lyases from Diverse Origins Enable Enhanced Production of Aromatic Compounds in Bacteria and *Saccharomyces cerevisiae*, *Appl. Environ. Microbiol. 81*, 4458.

14. Weise, N. J., Parmeggiani, F., Ahmed, S. T., and Turner, N. J. (2015) The Bacterial Ammonia Lyase EncP: A Tunable Biocatalyst for the Synthesis of Unnatural Amino Acids, *J. Am. Chem. Soc. 137*, 12977-12983.

15. Zhou, L., Wang, Y., Liu, H., Han, L., Zhang, W., Cui, W., Liu, Z., and Zhou, Z. (2019) Surface Engineering of a *Pantoea agglomerans*-Derived Phenylalanine Aminomutase for the Improvement of (*S*)-β-Phenylalanine Biosynthesis, *Biochem. Biophys. Res. Commun. 518*, 204-211.

16. Zhu, L., Feng, G., Ge, F., Tao, Y., and Song, P. (2018) Immobilized Phenylalanine Aminomutase and Application in Synthesis of β-Phenylalanine, Anhui Polytechnic University, Peop. Rep. China . CN108707597A.

17. Zhu, L., Ge, F., Li, W., Song, P., Tang, H., Tao, Y., Liu, Y., and Du, G. (2018) One Step Synthesis of Unnatural β-Arylalanines Using Mutant Phenylalanine Aminomutase From *Taxus chinensis* With High β-Regioselectivity, *Enzyme Microb. Technol. 114*, 22-28.

18. Wu, B., Szymański, W., Wybenga, G. G., Heberling, M. M., Bartsch, S., de Wildeman, S., Poelarends, G. J., Feringa, B. L., Dijkstra, B. W., and Janssen, D. B. (2012) Mechanism-Inspired Engineering of Phenylalanine Aminomutase for Enhanced β-Regioselective Asymmetric Amination of Cinnamates, *Angew. Chem. Int. Ed. 51*, 482-486.

19. Szymanski, W., Wu, B., Weiner, B., de Wildeman, S., Feringa, B. L., and Janssen, D. B. (2009) Phenylalanine Aminomutase-Catalyzed Addition of Ammonia to Substituted Cinnamic Acids: A Route to Enantiopure α- and β-Amino Acids, *J. Org. Chem. 74*, 9152-9157.

20. Wu, B., Szymanski, W., Wietzes, P., de Wildeman, S., Poelarends, G. J., Feringa, B. L., and Janssen, D. B. (2009) Enzymatic Synthesis of Enantiopure α- and β-Amino Acids by Phenylalanine Aminomutase-Catalysed Amination of Cinnamic Acid Derivatives, *ChemBioChem 10*, 338-344.

21. Wanninayake, U., Deporre, Y., Ondari, M., and Walker, K. D. (2011) (*S*)-Styryl-α-Alanine Used to Probe the Intermolecular Mechanism of an Intramolecular MIO-Aminomutase, *Biochemistry 50*, 10082-10090.

22. Ratnayake, N. D., Theisen, C., Walter, T., and Walker, K. D. (2016) Whole-Cell Biocatalytic Production of Variously Substituted β-Aryl- and β-Heteroaryl-β-Amino Acids, *J. Biotechnol. 217*, 12-21.

23. Parmeggiani, F., Lovelock, S. L., Weise, N. J., Ahmed, S. T., and Turner, N. J. (2015) Synthesis of D- and L-Phenylalanine Derivatives by Phenylalanine Ammonia Lyases: A Multienzymatic Cascade Process, *Angew. Chem. Int. Ed. 54*, 4608-4611.

24. Filip, A., Nagy, E. Z. A., Tork, S. D., Bánóczi, G., Toşa, M. I., Irimie, F. D., Poppe, L., Paizs, C., and Bencze, L. C. (2018) Tailored Mutants of Phenylalanine Ammonia-Lyase from *Petroselinum crispum* for the Synthesis of Bulky L- and D-Arylalanines, *ChemCatChem 10*, 2627-2633.

25. Raj, H., Weiner, B., Veetil, V. P., Reis, C. R., Quax, W. J., Janssen, D. B., Feringa, B. L., and Poelarends, G. J. (2009) Alteration of the Diastereoselectivity of 3-Methylaspartate Ammonia Lyase by Using Structure-Based Mutagenesis, *ChemBioChem 10*, 2236-2245.

26. Raj, H., Szymański, W., de Villiers, J., Rozeboom, H. J., Veetil, V. P., Reis, C. R., de Villiers, M., Dekker, F. J., de Wildeman, S., Quax, W. J., Thunnissen, A.-M. W. H., Feringa, B. L., Janssen, D. B., and Poelarends, G. J. (2012) Engineering Methylaspartate Ammonia Lyase for the Asymmetric Synthesis of Unnatural Amino Acids, *Nat. Chem. 4*, 478-484.

27. Weiser, D., Bencze, L. C., Bánóczi, G., Ender, F., Kiss, R., Kókai, E., Szilágyi, A., Vértessy, B. G., Farkas, Ö., Paizs, C., and Poppe, L. (2015) Phenylalanine Ammonia-Lyase-Catalyzed Deamination of an Acyclic Amino Acid: Enzyme Mechanistic Studies Aided by a Novel Microreactor Filled with Magnetic Nanoparticles, *ChemBioChem 16*, 2283-2288.

28. Bartsch, S., Wybenga, G. G., Jansen, M., Heberling, M. M., Wu, B., Dijkstra, B. W., and Janssen, D. B. (2013) Redesign of a Phenylalanine Aminomutase into a Phenylalanine Ammonia Lyase, *ChemCatChem 5*, 1797-1802.

29. Shee, P. K., Ratnayake, N. D., Walter, T., Goethe, O., Onyeozili, E. N., and Walker, K. D. (2019) Exploring the Scope of an α/β-Aminomutase for the Amination of Cinnamate Epoxides to Arylserines and Arylisoserines, *ACS Catal. 9*, 7418-7430.

30. Ratnayake, N. D., Wanninayake, U., Geiger, J. H., and Walker, K. D. (2011) Stereochemistry and Mechanism of a Microbial Phenylalanine Aminomutase, *J. Am. Chem. Soc. 133*, 8531-8533.

31. Strom, S., Wanninayake, U., Ratnayake, N. D., Walker, K. D., and Geiger, J. H. (2012) Insights into the Mechanistic Pathway of the *Pantoea agglomerans* Phenylalanine Aminomutase, *Angew. Chem. Int. Ed. 51*, 2898-2902.

32. Wanninayake, U., and Walker, K. D. (2012) Assessing the Deamination Rate of a Covalent Aminomutase Adduct by Burst Phase Analysis, *Biochemistry 51*, 5226-5228.

33. Walter, T., Wijewardena, D., and Walker, K. D. (2016) Mutation of Aryl Binding Pocket Residues Results in an Unexpected Activity Switch in an *Oryza sativa* Tyrosine Aminomutase, *Biochemistry 55*, 3497-3503.

34. Feng, L., Wanninayake, U., Strom, S., Geiger, J., and Walker, K. D. (2011) Mechanistic, Mutational, and Structural Evaluation of a *Taxus* Phenylalanine Aminomutase, *Biochemistry 50*, 2919-2930.

35. Yadav, J. S., Reddy, M. S., Rao, P. P., and Prasad, A. R. (2006) Enantioselective Synthesis of (+)-Sedamine and (-)-Allosedamine, *Synthesis 23*, 4005-4012.

36. Nandy, J. P., Prabhakaran, E. N., Kumar, S. K., Kunwar, A. C., and Iqbal, J. (2003) Reverse Turn Induced π-Facial Selectivity during Polyaniline-Supported Cobalt(II) Salen Catalyzed Aerobic Epoxidation of N-Cinnamoyl L-Proline Derived Peptides, *J. Org. Chem. 68*, 1679-1692.

37. Yadav, J. S., Raju, A. K., Rao, P. P., and Rajaiah, G. (2005) Highly Stereoselective Synthesis of Antitumor Agents: Both Enantiomers of Goniothales Diol, Altholactone, and Isoaltholactone, *Tetrahedron Asymmetry 16*, 3283-3290.

38. Fringuelli, F., Pizzo, F., Tortoioli, S., and Vaccaro, L. (2005) $InCl_3$-Catalyzed Regio- and Stereoselective Thiolysis of α,β-Epoxycarboxylic Acids in Water, *Org. Lett. 7*, 4411-4414.

39. Amantini, D., Fringuelli, F., Pizzo, F., and Vaccaro, L. (2001) Bromolysis and Iodolysis of α,β-Epoxycarboxylic Acids in Water Catalyzed by Indium Halides, *J. Org. Chem. 66*, 4463-4467.

40. Fringuelli, F., Pizzo, F., Rucci, M., and Vaccaro, L. (2003) First One-Pot Copper-Catalyzed Synthesis of α-Hydroxy-β-Amino Acids in Water. A New Protocol for Preparation of Optically Active Norstatines, *J. Org. Chem. 68*, 7041-7045.

41. Tabarki, M. A., and Besbes, R. (2014) Regioselective Ring Opening of β-Phenylglycidate and Aziridine-2-Carboxylates With N-Alkylhydroxylamines: Synthesis of Isoxazolidinones, *Tetrahedron 70*, 1060-1064.

42. Srivastava, R. P., and McChesney, J. D. (1995) A Practical and Inexpensive Synthesis of the Taxol C-13 Side Chain; N-Benzoyl-(2R,3S)-3-Phenylisoserine, *Nat. Prod. Lett. 6*, 147-152.

43. Wilding, B., Veselá, A. B., Perry, J. J. B., Black, G. W., Zhang, M., Martínková, L., and Klempier, N. (2015) An Investigation of Nitrile Transforming Enzymes in the Chemo-Enzymatic Synthesis of the Taxol Sidechain, *Org. Biomol. Chem. 13*, 7803-7812.

44. Trott, O., and Olson, A. J. (2010) AutoDock Vina: Improving the Speed and Accuracy of Docking with a New Scoring Function, Efficient Optimization, and Multithreading, *J. Comput. Chem. 31*, 455-461.

45. Pettersen, E. F., Goddard, T. D., Huang, C. C., Couch, G. S., Greenblatt, D. M., Meng, E. C., and Ferrin, T. E. (2004) UCSF Chimera—A Visualization System for Exploratory Research and Analysis, *J. Comput. Chem. 25*, 1605-1612.

46. Ulusu, N. N. (2015) Evolution of Enzyme Kinetic Mechanisms, *J. Mol. Evol. 80*, 251-257.

47. Segel, I. H. (1993) *Enzyme Kinetics: Behavior and Analysis of Rapid Equilibrium and Steady-State Enzyme Systems*, Wiley.

48. Wybenga, G. G., Szymanski, W., Wu, B., Feringa, B. L., Janssen, D. B., and Dijkstra, B. W. (2014) Structural Investigations into the Stereochemistry and Activity of a Phenylalanine-2,3-aminomutase from *Taxus chinensis*, *Biochemistry 53*, 3187-3198.

49. Montavon, T. J., Christianson, C. V., Festin, G. M., Shen, B., and Bruner, S. D. (2008) Design and Characterization of Mechanism-Based Inhibitors for the Tyrosine Aminomutase *Sg*TAM, *Bioorg. Med. Chem. Lett. 18*, 3099-3102.

50. Goodenough-Lashua, D. M., and Garcia, G. A. (2003) tRNA–Guanine Transglycosylase From *E. coli*: A Ping-Pong Kinetic Mechanism Is Consistent With Nucleophilic Catalysis, *Bioorg. Chem. 31*, 331-344.

51. Stein, R. L. Kinetics of Two-Substrate Enzymatic Reactions In *Kinetics of Enzyme Action*, pp 141-168.

52. Kikuchi, M., and Konno, H. (2013) Improved synthesis of D-allothreonine derivatives from L-threonine, *Tetrahedron 69*, 7098-7101.

53. Kimura, T., Vassilev, V. P., Shen, G.-J., and Wong, C.-H. (1997) Enzymatic Synthesis of β-Hydroxy-α-Amino Acids Based on Recombinant D- and L-Threonine Aldolases, *J. Am. Chem. Soc. 119*, 11734-11742.

54. Zampella, A., D'Auria, M. V., Gomez Paloma, L., Casapullo, A., Minale, L., Debitus, C., and Henin, Y. (1996) Callipeltin A, an anti-HIV cyclic depsipeptide from the new Caledonian lithistida sponge *Callipelta sp.*, *J. Am. Chem. Soc. 118*, 6202-6209.

55. J. Hale, K., Manaviazar, S., and M. Delisser, V. (1994) A Practical New Asymmetric Synthesis of (2*S*,3*S*)- and (2*R*,3*R*)-3-hydroxyleucine, *Tetrahedron 50*, 9181-9188.

56. Luo, Y., Blaskovich, M. A., and Lajoie, G. A. (1999) Stereoselective Synthesis of β-Substituted α,β-Diamino Acids from β-Hydroxy Amino Acids, *The Journal of Organic Chemistry 64*, 6106-6111.

57. Khan, J. K., Kuo, Y. H., Haque, A., and Lambein, F. (1995) Inhibitory and Excitatory Amino Acids in Cerebrospinal Fluid of Neurolathyrism Patients, a Highly Prevalent Motorneurone Disease, *Acta Neurol. Scand. 91*, 506-510.

58. Lucet, D., Le Gall, T., and Mioskowski, C. (1998) The Chemistry of Vicinal Diamines, *Angew. Chem. Int. Ed. 37*, 2580-2627.

59. Nagasawa, H. T., Elberling, J. A., and Roberts, J. C. (1987) β-Substituted Cysteines As Sequestering Agents for Ethanol-Derived Acetaldehyde *in Vivo*, *J. Med. Chem. 30*, 1373-1378.

60. Crich, D., and Banerjee, A. (2007) Native Chemical Ligation at Phenylalanine, *J. Am. Chem. Soc. 129*, 10064-10065.